5 RESULT ANALYSIS AND DISCUSSION

5.1 General

This chapter presents the findings from both experimental and numerical analyses. Section 5.2 discusses the definitions and evaluation of parameters from the results obtained. The analysis was carried out in light of these parameters and technical and scientific reasoning were discussed after the analysis. Section 5.3 presents the results and analysis. This further divided into subtopics. These subtopics include the load settlement characteristics of model unpiled raft (UPR), pile group (PG), and piled raft foundation (PRF) with different shapes of the raft, *L/d* ratio of piles, spacing between piles, configuration of piles, soil-pile friction angle, and shape of piles. This chapter also presents the contact pressure distribution beneath the raft in UPR and PRF, the load shared by the raft (*LSR*), and the load shared by the piles/pile group (*LSPG*). Lastly, we provide the results of the numerical analysis of prototype piled raft foundations with different configurations of piles. Section 5.4 presents discussions. Suggested design methodology for piled raft foundation is given in section 5.5, while in section 5.6 concluding remarks are written.

5.2 Definitions and Evaluation of Parameters

5.2.1 Initial Tangent Stiffness of Unpiled Raft UPR (k_{ri})

It is defined as the slope of initial portion of the load settlement curve of unpiled raft foundation (Figure 5-1) (Alsanabani, 2017, Garcia, 2019, and Clancy and Randolph, 1993)

$$k_{ri} = \frac{P_{ri}}{s_{ri}} \tag{5-1}$$

where, P_{ri} = load in kN applied on UPR within initial straight-line portion of the load settlement curve; s_{ri} = settlement in meter corresponding to load P_{ri}.

Some researchers have defined this as the applied uniformly distributed load (kN/m^2) at the top of raft divided by the average (arithmetic mean) of raft settlements at the center and at the corners. (Bhartiya, 2019).

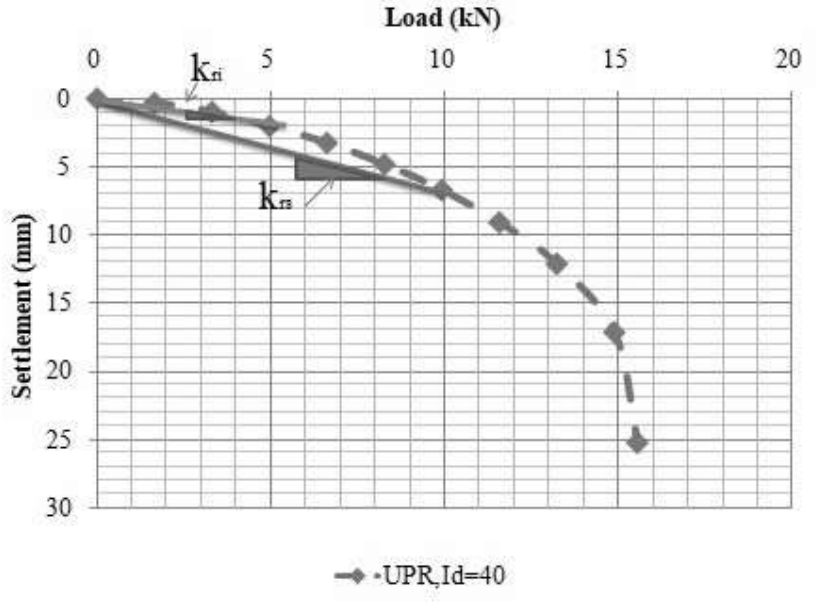

Figure 5-1 Load settlement curve of unpiled raft foundation to define Initial Tangent stiffness of Unpiled raft UPR(k_{ri}) and Secant stiffness of Unpiled raft UPR (k_{sr})

5.2.2 Secant Stiffness of Unpiled Raft UPR (k_{sr})

It is defined as the slope of a line joining origin with the point on a load settlement curve of unpiled raft foundation (Figure 5-1).

$$k_{sr} = \frac{P_{rs}}{s_{rs}} \qquad (5\text{-}2)$$

where, P_{rs} = load in kN applied on UPR; s_{rs}= settlement in meter corresponding to load P_{rs} from load settlement curve of UPR.

5.2.3 Initial Tangent Stiffness of Single Pile/Pile Group (k_{pi}) / ($(k_{pg})_i$)

It is defined as the slope of initial portion of the load settlement curve of single pile/pile group.

$$k_{pi} = \frac{P_{pi}}{s_{pi}} \tag{5-3}$$

where, P_{pi} = load in kN applied on single pile/pile group within initial straight-line portion of the load settlement curve; s_{pi}= settlement in meter corresponding to load P_{pi}

5.2.4 Settlement ratio (R_s)

It is defined as the ratio of settlement of pile group (s_g) at the same average load *P* per pile i.e. at the total pile group load of *nP* to the settlement of single pile (s_s) at load *P*.

$$R_s = \frac{s_g}{s_s} \tag{5-4}$$

5.2.5 Initial Yield Load (*IYL*) and Final Yield Load (*FYL*)

The load settlement characteristic of model piled raft foundation is shown in Figure 5-2. It can be shown that these characteristics will fall into tri-linear graph with point A resembles to initial Yield Load (*IYL*) and point B resembles to final Yield Load (*FYL*) Figure 5-3. Up to initial Yield load, pile + raft behave elastically. From point A to B the pile capacity is fully utilized with the increase in the load carried by the raft linearly up to point B. After reaching point B in many cases it is observed that significant amount of load is carried by piled raft in the residual part of the curve, i.e. part BC. The settlement corresponding to *IYL* is denoted by s_i and the load observed corresponding to s_i from the load settlement curve of the unpiled raft and that of a single pile was denoted by $(P_r)_{s_i}$ and $\left(P_{sp}\right)_{s_i}$ respectively (Figure 5-4).

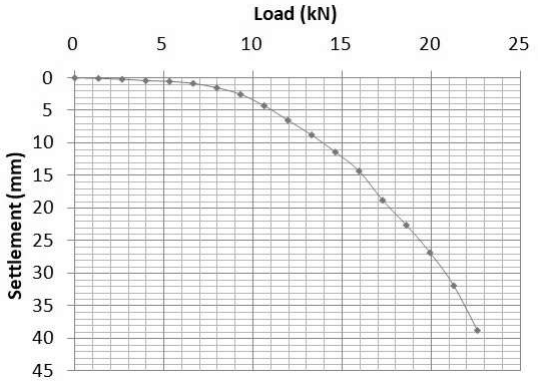

Figure 5-2 : Load-settlement characteristics of model piled raft foundation with trapezoidal raft at I_d = *40%*

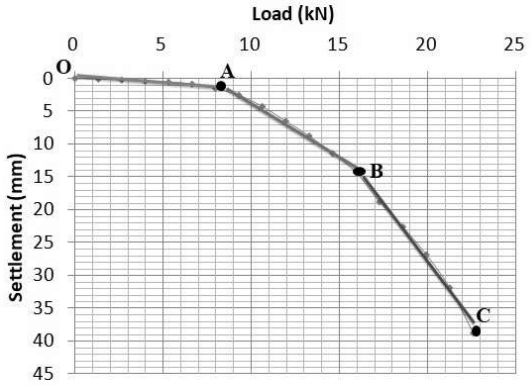

Figure 5-3 : Tri- linear Load-settlement characteristics of model piled raft foundation (MPRF) with trapezoidal raft at I_d = *40%*

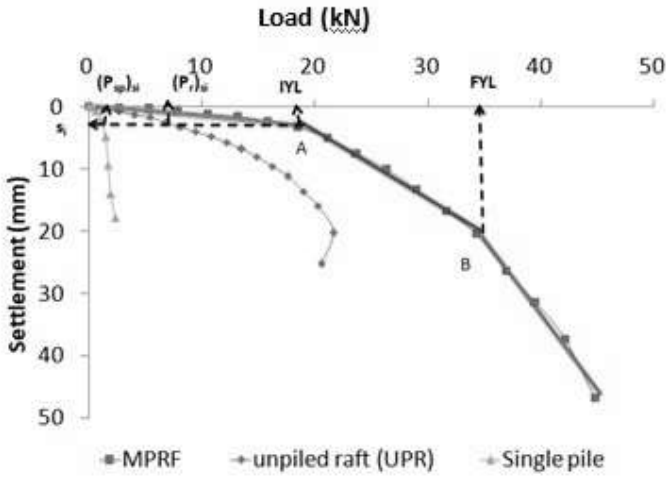

Figure 5-4 : Tri- linear Load-settlement characteristics of model piled raft foundation (MPRF), unpiled raft (UPR) with trapezoidal raft and single pile at I_d= *40%*

5.2.6 Primary Stiffness of Piled Raft $(k_{pr})_p$, Secondary Stiffness of Piled Raft $(k_{pr})_s$

The slope of load settlement curve of piled raft of the portion OA is referred to as primary stiffness of piled raft $(k_{pr})_p$, and the slope of the curve segment AB is referred to as secondary stiffness of piled raft $(k_{pr})_s$**(**Figure 5-3**).**

5.2.7 Load Shared by Raft (*LSR*) and Load Shared by Pile/Pile group (*LSP/LSPG*) in Loaded Piled Raft

Load shared by raft (*LSR*) and load shared by pile group (*LSPG*) in loaded piled raft foundation was calculated using the readings of earth pressure cells located beneath raft (or pile cap) and strain gauges attached on pile surface. The detailed procedure of this is explained below.

Earth pressure cells:

The earth pressure cells were kept below the raft (or pile cap) to measure the contact pressure distribution between the soil and the raft, and they were kept in such a way that their location resembles the symmetry of the zones below the raft. i.e., location 1 between the piles has the same pressure within area A_1 under the concentric load below the rigid raft as shown in Figure 5-5. Similarly, all the locations numbered 2 in Figure 5-5 have the same contact pressure within area A_2, and similarly for location 3. Since the total load is ultimately transferred by the raft (or pile cap) is divided into two parts: load shared by piles (i.e., contact area with the raft and piles) and load shared by rafts in the remaining major area of the raft (i.e., without the contact area with the piles). So multiplying readings of earth pressure cells with their influence area gives an idea of the load shared by the major portion of the raft, and deducting this load from the total load imposed on MPRF gives the load carried by piles.

The load shared by piles and rafts in the model piled raft foundation (SQ-5d (5 × 5 pile group)) was calculated as below using Figure 5-5.

Total load shared by model raft (or pile cap) (*LSR*) = $P_1+P_2+P_3$

Where,

P_1 = Load shared by symmetrical areas of raft A_1 = Reading of Earth pressure cell located at position 1 in kPa × A_1 × 4. (4 is a number of symmetric area A_1)

P_2 = Load shared by symmetrical areas of raft A_2 = Reading of Earth pressure cell located at position 2 in kPa × A_2 × 8. (8 is a number of symmetric area A_2)

P_3 = Load shared by symmetrical areas of raft A_3 = Reading of Earth pressure cell located at position 3 in kPa × A_3 × 4. (4 is a number of symmetric area A_3)

Total load shared by model piles (*LSPG*) = Total load imposed on model piled raft foundation – total load shared by model raft (or pile cap)

Strain gauges:

The strain gauges were attached at top, middle and bottom portion of pile to measure the axial strain developed in piles during loading on the piled raft. The piles on which strain gauges were attached were referred as instrumented pile and they were kept in such a way that their location resembles the symmetry of the location of piles. i.e., one of the piles located at corner of the pile group, one of the piles located at side of the pile group, and the pile located at the centre of the pile group were instrumented pile has the same axial strain under the concentric load below the rigid raft (Figure 5-6). The locations of strain gauges were provided in instrumented piles as shown in Figure 5-7. The readings of strain gauges attached near the top portion of the piles were used to calculate the load shared by pile/ pile group of model piled raft foundation (MPRF). So multiplying readings of strain gauges with cross sectional area of pile and modulus of elasticity of pile gives an idea of the load shared by the pile/ pile group (*LSPG*) , and deducting this load from the total load imposed on MPRF gives the load shared by raft (*LSR*) in PRF.

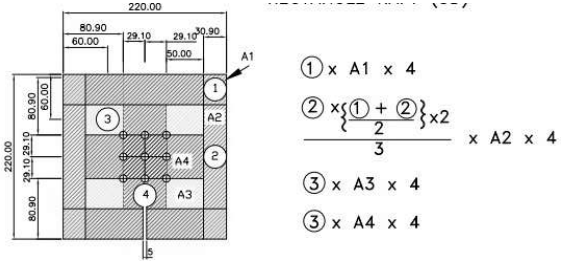

SQ-3d (3 x 3 pile group)

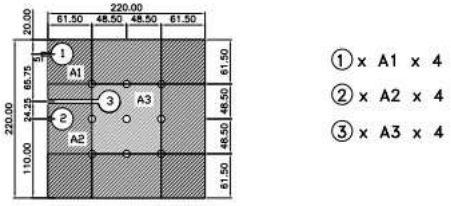

SQ-5d (3 x 3 pile group)

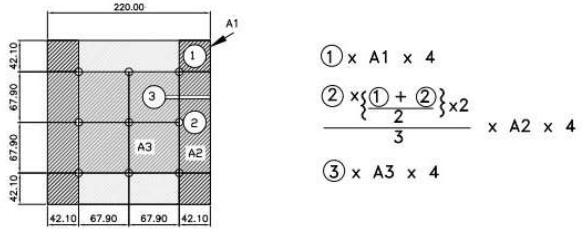

SQ-7d (3 x 3 pile group)

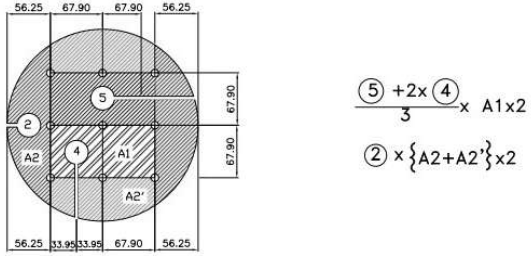

CIR-7d (3 x 3 pile group)

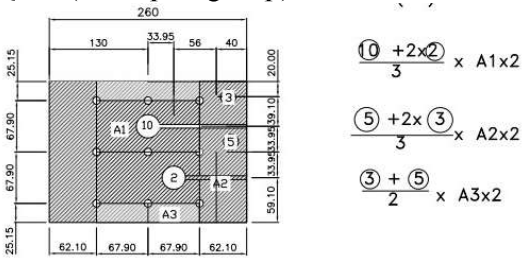

RECT-7d (3 x 3 pile group)

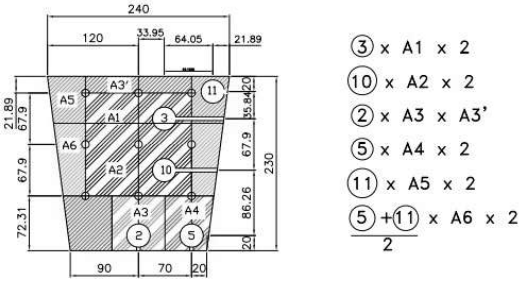

TRAP-7d (3 x 3 pile group)

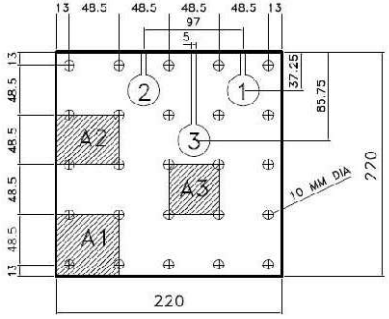

SQ-5d (5 x 5 pile group)

Figure 5-5 : Location of EPC and piles in model piled raft foundation (Not to scale, All dimensions are in mm)

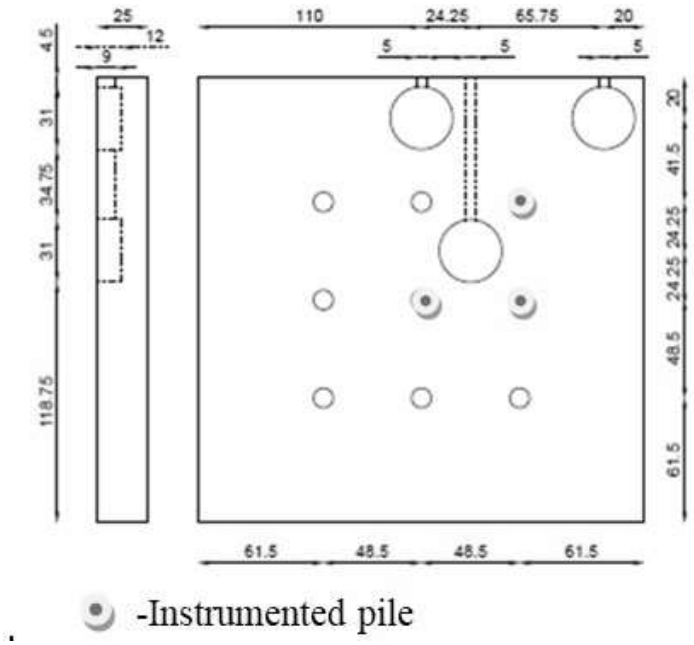

Figure 5-6 : Location of instrumented piles in MPRF

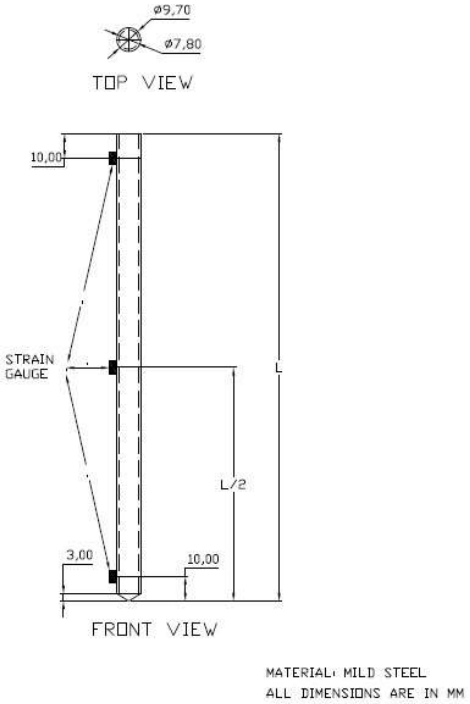

Figure 5-7 : Location of strain gauges in instrumented pile

The comparisons were made between load shared by piles and raft obtained from both methods and it was found in good correlation in the results. In present study, strain gauges were used in the *L/d* ratio of piles study. Later strain gauges were damaged during the experimentation and that idea was dropped and load sharing of raft and pile was determined based on readings of EPC and further analysis was carried out.

5.2.8 Piled Raft Coefficient (α_p)

The ratio of load shared by pile/pile group to the total load imposed on model piled raft foundation is referred as piled raft coefficient in this chapter.

$$\alpha_p = \frac{LSPG}{TL} \qquad (5\text{-}5)$$

where, $LSPG$ = Load shared by pile group of piled raft foundation

TL = Total load imposed on piled raft foundation

5.2.9 Load Improvement Ratio *(LIR)*

The ratio of load carried by piled raft foundation to the load carried by unpiled raft foundation at a particular settlement is referred as Load improvement ratio (*LIR*)

$$LIR = \frac{L_{PRF}}{L_{UPR}} \tag{5-6}$$

where, L_{PRF} = Load carried by piled raft foundation at a particular settlement

L_{UPR} = Load carried by unpiled raft foundation at a particular settlement

5.2.10 Settlement Reduction Ratio *(SRR)*

The ratio of settlement of piled raft foundation to the settlement of unpiled raft foundation at a particular load is referred as Settlement reduction ratio *(SRR).*

$$SRR = \frac{s_{UPR} - s_{PRF}}{s_{UPR}} X\ 100\ \% \tag{5-7}$$

where, s_{PRF}= Settlement of piled raft foundation at a particular load

s_{UPR} = Settlement of unpiled raft foundation at a particular load

5.2.11 Efficiency of piled raft at *IYL* (β_1), at *FYL* (β_2) , and at same settlement level (β)

The efficiency of piled raft at *IYL* (β_1) is defined as the ratio of load on piled raft to the sum of load of UPR and PG at same settlement corresponding to *IYL*. Whereas, the efficiency of piled raft at *FYL* (β_2) is defined as the ratio of *FYL* of piled raft foundation to the sum of ultimate load of UPR and PG.

$$\beta_1 = \frac{IYL}{(P_r)_{s_i} + (P_{pg})_{s_i}} \quad (5\text{-}8)$$

$$\beta_2 = \frac{FYL}{Qur + Qu{,}pg} \quad (5\text{-}9)$$

In study related to shape of piles, the efficiency of piled raft (β) is obtained as a ratio of load on piled raft to the sum of load of UPR and PG at same settlement.

5.3 Result and Analysis

5.3.1 Unpiled Raft Foundation (UPR)

5.3.1.1 Load Settlement Characteristics

The load settlement curves of a model unpiled raft (UPR) foundation with different shapes of rafts at different relative densities of sand bed are presented in Figure 5-8 to Figure 5-10. It can be observed that the load carrying capacity of circular rafts is lower than all other shapes at all relative densities. The load settlement characteristics of trapezoidal and rectangle shaped rafts were observed quite close to each other. Figure 5-11 represents the load settlement curves of a model unpiled raft foundation used in the study of shape of piles. The experimental results of load settlement of unpiled raft were validated with the results obtained from numerical method (using PLAXIS 3D) software which is based on finite element method (Figure 5-12).

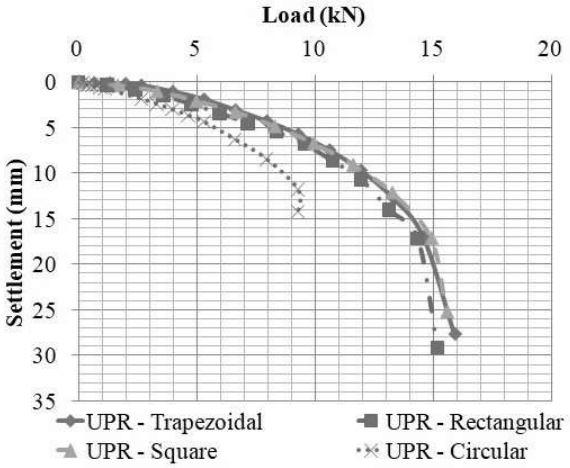

Figure 5-8 : Load settlement characteristics of unpiled raft foundation with different shape of raft *(I_d = 40%)*

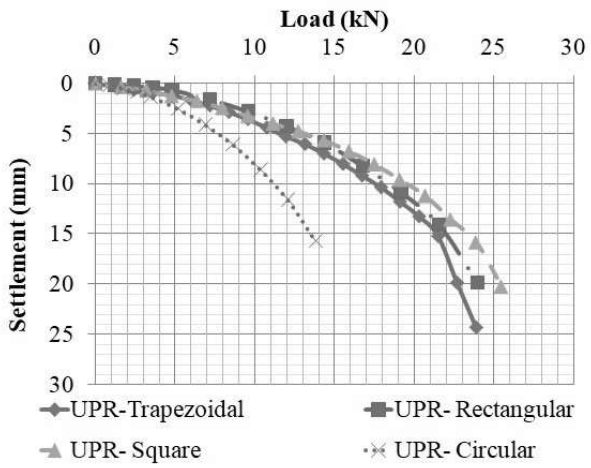

Figure 5-9 : Load settlement characteristics of unpiled raft foundation with different shape of raft *(I_d = 60%)*

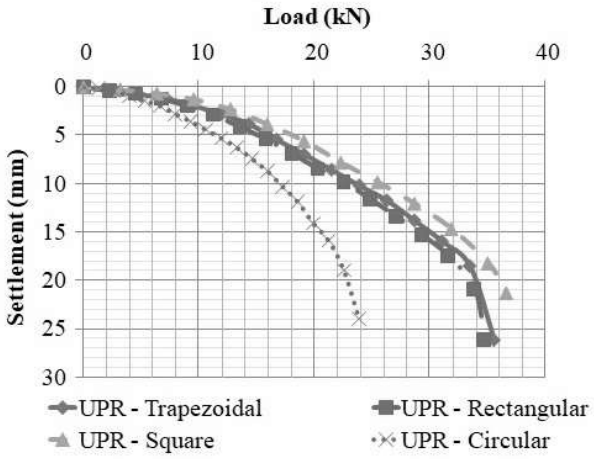

Figure 5-10 : Load settlement characteristics of unpiled raft foundation with different shape of raft *(I_d = 80%)*

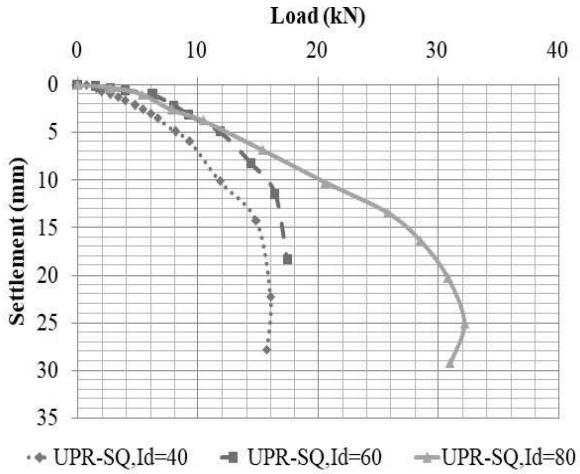

Figure 5-11 : Load settlement characteristics of unpiled raft foundation with square raft *(I_d = 40%, 60% and 80%; size of raft = 240mm × 240mm)*

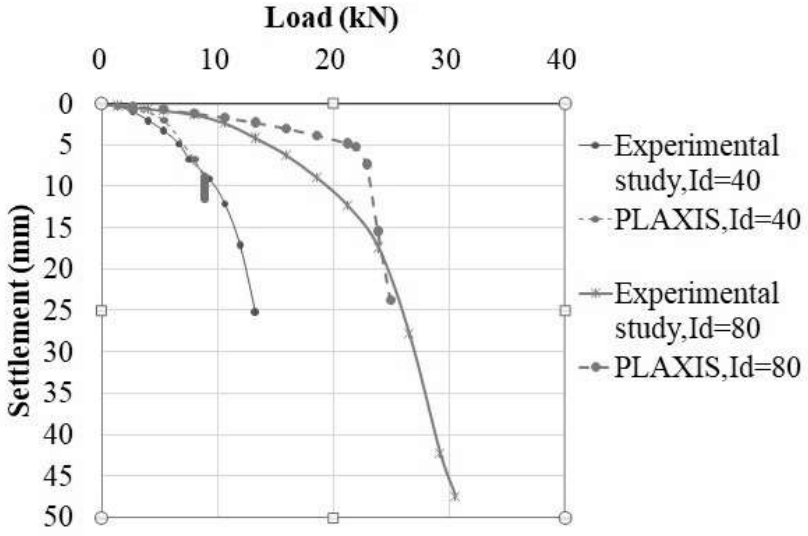

Figure 5-12 : Comparison of load settlement characteristics of square shaped unpiled raft foundation obtained from experimental study and PLAXIS 3D software

5.3.1.2 Ultimate Load of UPR

From Figure 5-13, it can be observed that the minimum and maximum ultimate loads of unpiled raft foundation (Q_{ur}) at all relative densities of Orsang river sand bed are obtained with a circular and a square raft, respectively. The above results are consistent with the theory. The range of percentage increment in Q_{ur} of square (SQ), rectangular (RECT), and trapezoidal (TRAP) rafts with respect to Q_{ur} of circular (CIR) rafts was found to be 36% to 96%, as shown in Table 5-1. The Q_{ur} of circular raft at 60% and 80% relative density (I_d) was found to be increased by 11% and 86% respectively as compared to $I_d = 40\%$. The increment in $Q_{ur}$of square raft at 60% and 80% relative density was found to be 53% and 117% respectively with respect to 40% relative density. As compared to $I_d = 40\%$, the Q_{ur} of trapezoidal and rectangular raft was found to be increased around 46% to 52% and 115% at $I_d = 60\%$ and $I_d = 80\%$ respectively.

Table 5-2 shows the ultimate load of unpiled raft (240 mm × 240 mm × 25 mm) used to study the effect of shape of pile at different relative density of Narmada river sand bed which shows

that the increment in Q_{ur} of raft at 60% and 80% relative density was found to be 11% and 119% respectively with respect to 40% relative density.

Table 5-3 and Table 5-4 show the ultimate bearing capacity of unpiled raft foundations (q_{ult}). The range of ultimate bearing capacity of circular, square, trapezoidal, and rectangular raft at 40% to 80% relative density was found to be 191.69 kN/m^2 to 356 kN/m^2, 273.76 kN/m^2 to 592.77 kN/m^2, 260.15 kN/m^2 to 559.92 kN/m^2, 271.11 kN/m^2 to 582.64 kN/m^2 respectively. The q_{ult} of square raft on Narmada river sand was found to be 255.21 kN/m^2 to 560.79 kN/m^2 at 40% to 80% relative density of sand. Since the higher relative density resembles closer packing of sand particles giving higher strength in the laterally confined condition.

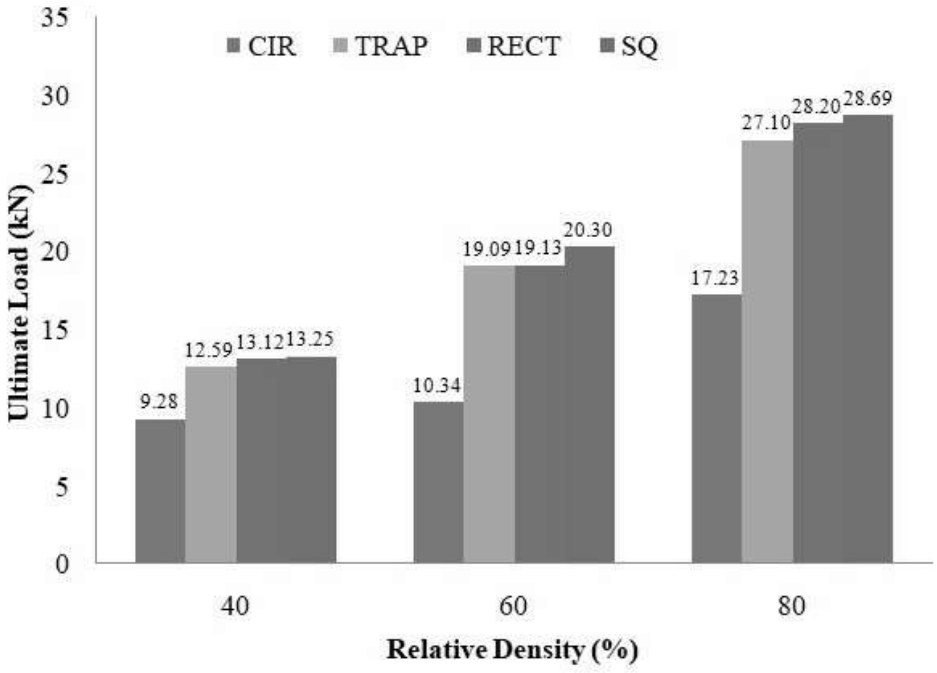

Figure 5-13 : Ultimate load of unpiled raft foundation (Q_{ur}) with different shape of raft and at different relative densities of sand bed

Table 5-1 Comparison of ultimate load of unpiled raft foundation (Q_{ur}) with different shape of raft and at different relative densities of sand bed

Shape of Raft ↓ / I_d (%) →	**Ultimate load of UPR (Q_{ur}) in kN at different I_d (%)**			**% increase in Q_{ur} w.r.t Q_{ur} of** CIR			**% increase in Q_{ur} w.r.t Q_{ur} of I_d = 40%**		
	40	60	80	40	60	80	40	60	80
CIR	9.28	10.34	17.23	**0**	**0**	**0**	**0**	**11**	**86**
SQ	13.25	20.30	28.69	**43**	**96**	**67**	**0**	**53**	**117**
TRAP	12.59	19.09	27.10	**36**	**85**	**57**	**0**	**52**	**115**
RECT	13.12	19.13	28.20	**41**	**85**	**64**	**0**	**46**	**115**

Table 5-2 Comparison of ultimate load of unpiled raft foundation (Q_{ur}) at different relative densities of sand bed

Shape of Raft ↓ / I_d (%) →	**Ultimate load of UPR (Q_{ur}) in kN at different I_d (%)**			**% increase in Q_{ur} w.r.t I_d = 40%**		
	40	60	80	40	60	80
SQ	14.7	16.3	32.3	**0**	**11**	**119**

Table 5-3 Ultimate bearing capacity of unpiled raft foundation (q_{ult}) with different shape of raft and at different relative densities of Orsang river sand bed

Shape of Raft	**Ultimate Bearing capacity (q_{ult}) of UPR in kN/m^2**		
	I_d=40%	***I_d=60%***	***I_d=80%***
CIR	191.69	213.60	356.00
SQ	273.76	419.42	592.77
TRAP	260.15	394.34	559.92
RECT	271.11	395.25	582.64

Table 5-4 Ultimate Bearing Capacity of unpiled raft foundation (q_{ult}) at different relative densities of Narmada river sand bed

Shape of Raft	**Ultimate Bearing capacity (q_{ult}) of UPR in kN/m^2**		
	I_d = 40%	***I_d = 60%***	***I_d = 80%***
SQ	255.21	282.99	560.79

5.3.1.3 Stiffness of UPR

5.3.1.3.1 Initial Tangent Stiffness of Unpiled Raft UPR (k_{ri})

The initial tangent stiffness of unpiled raft (k_{ri}) with different shapes of raft and at different relative density of Orsang river sand bed were found as shown in Table 5-5 and the same for Narmada river sand is shown in Table 5-6. It is observed that the k_{ri} increases as the relative density of sand bed increases and the amount of increment with respect to $I_d = 40\%$ is shown in Table 5-5 and Table 5-6. The range of increment in k_{ri} at 60% and 80% relative density as compared to 40% relative density was found to be 36% to 54% and 96% to 130% respectively. The increment in k_{ri} of raft (240 mm × 240 mm × 25mm) at 60% and 80% relative density as compared to 40% relative density was found to be 25% and 42% respectively. At 40%, 60%, and 80% relative densities of sand, the square raft's k_{ri} values were found to be 1038.33 kN/m, 1604.99 kN/m, and 2613.07 kN/m greater than those of the circular raft. i.e., 81%, 81%, and 96%, in percentage terms, respectively. The k_{ri} values of the trapezoidal raft were found to be 1055.63 kN/m, 1205.89 kN/m, and 1872.5 kN/m greater than those of the circular raft, or 82%, 61%, and 69%, in percentage terms, respectively, at 40%, 60%, and 80% relative densities of sand. At 40%, 60%, and 80% relative densities of sand, the k_{ri} values of the rectangular raft were found to be 691.50 kN/m, 1002.73 kN/m, and 1486.14 kN/m greater than those of the circular raft, or 54%, 51%, and 55%, in percentage terms, respectively. Because of greater strength and stiffness was achieved with densely packed sand particles, the initial tangent stiffness of the UPR was higher with higher relative density.

Table 5-5 Initial tangent stiffness of the unpiled raft (UPR) with different shape of raft and at different relative densities of the Orsang river sand bed

Shape of raft	**initial tangent stiffness of unpiled raft (k_{ri}) in kN/m**			**% increase in k_{ri} w.r.t I_d= 40%**	
	I_d = 40%	I_d = 60%	I_d = 80%	I_d = 60%	I_d = 80%
CIR	1283.11	1980.14	2718.29	**54**	**112**
SQ	2321.44	3585.12	5331.36	**54**	**130**
TRAP	1974.61	2982.86	4204.43	**51**	**113**
RECT	2338.74	3186.02	4590.79	**36**	**96**

Table 5-6 Initial tangent stiffness of the unpiled raft (UPR) at different relative densities of the Narmada river sand bed

Shape of raft	**Initial tangent stiffness of unpiled raft (k_{ri}) in kN/m**			**% increase in k_{ri} w.r.t I_d = 40%**	
	I_d = 40%	I_d = 60%	I_d = 80%	I_d = 60%	I_d = 80%
SQ	1796.42	2238.55	2558.44	25	42

5.3.1.3.2 Secant Stiffness of Unpiled Raft (k_{sr})

The secant stiffness of square raft and circular raft (k_{sr}) was calculated at 2, 4, 6, 8, 10, and 12 kN loads applied to UPR from experimental data, and the following equation was fitted for the same by rigorous analysis between the parameters mentioned in equation (5-10). Figure 5-14 and Figure 5-15 show the secant stiffness of square and circular rafts from experimental study and were calculated from the proposed equation (5-10) which is valid up to safe load on unpiled raft. From the work of Vakili (2015) on square UPR having 10 cm width on sand bed having 45% relative density of sand bed , the k_{sr} corresponding to 2.1 kN, 2.5 kN, 2.9 kN, 4 kN and 4.7 kN load was 2100 kN/m, 1667 kN/m, 1450 kN/m, 1143 kN/m, and 940 kN/m respectively. These values are calculated using equation (5-1) as 1711 kN/m, 1555 kN/m, 1433 kN/m, 1201 kN/m, and 1099 kN/m corresponding to 2.1 kN, 2.5 kN, 2.9 kN, 4 kN and 4.7 kN load respectively.

This shows that the k_{sr} calculated using equation (5-10) is matches with the values observed by Vakili (2015) with less than18% deviation.

$$k_{sr} = 7300 B_r S_c e^{(0.028 I_d)} P^{(-0.55)} \qquad (5\text{-}10)$$

where, k_{sr}= secant stiffness of unpiled raft foundation in kN/m; B_r= width/diameter of unpiled raft foundation in m; S_c= shape factor (1 for square and 0.55 for circular shape of unpiled raft foundation); I_d = relative density of foundation soil (%); P = load applied on unpiled raft foundation in kN.

Figure 5-14 and Figure 5-15 show the secant stiffness of square and circular rafts at different loads obtained from the experimental study, and the proposed equation is almost the same.

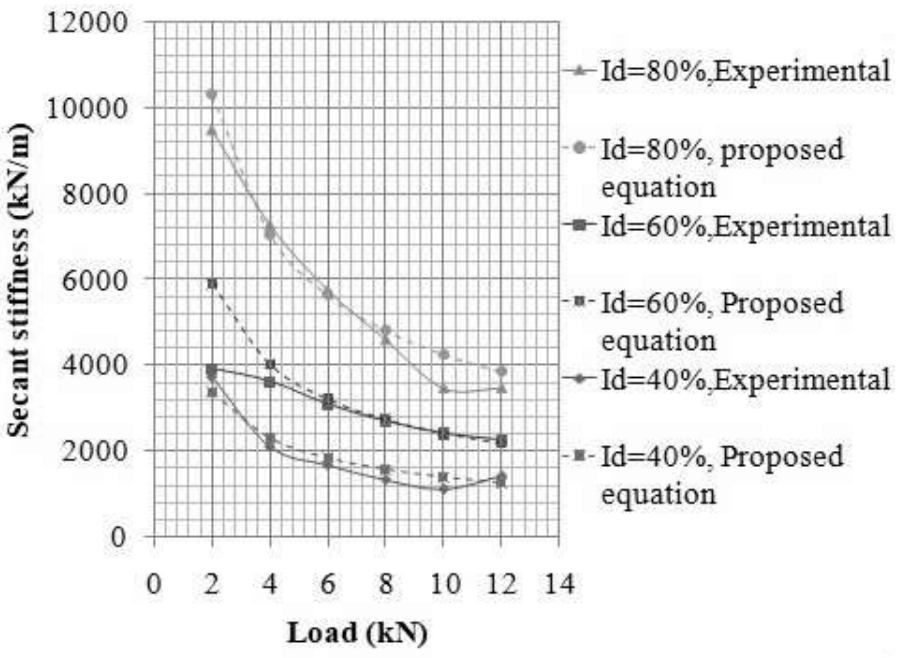

Figure 5-14 : Secant stiffness of square shaped unpiled raft from experimental study and proposed equation *(I_d = 40%, 60% and 80%; size of raft = 220 mm × 220 mm)*

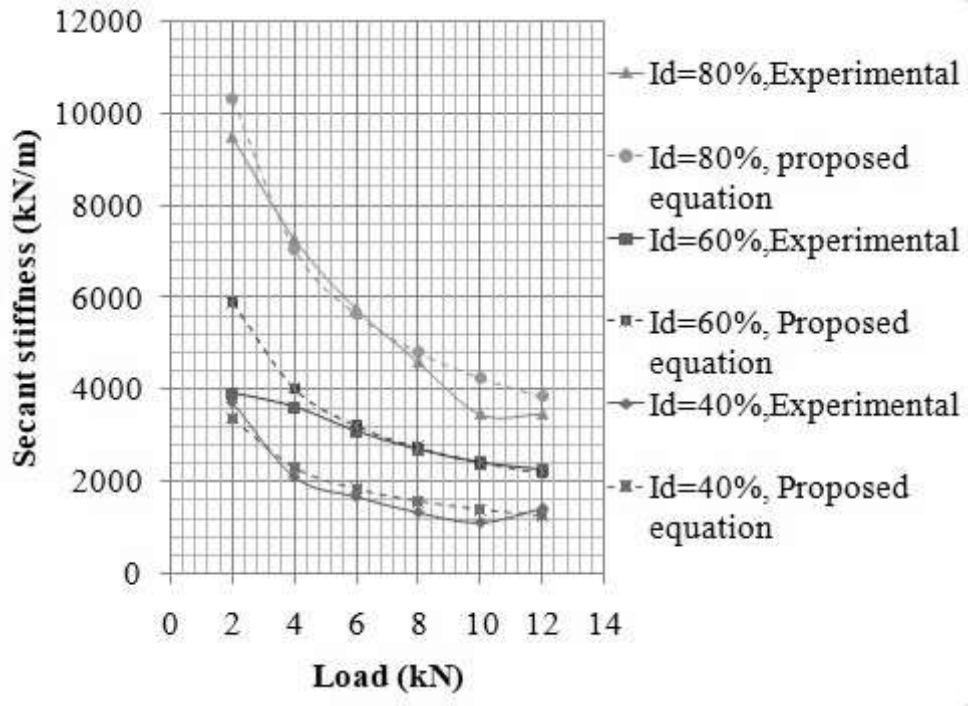

Figure 5-15 : Secant stiffness of circular shaped unpiled raft from experimental study and proposed equation *(I_d = 40%, 60% and 80%; diameter of raft = 248.3 mm)*

Figure 5-16 shows the comparison of load calculated from EPC readings as explained in Section 5.2.7 and actual applied load vs. relative settlement (s/B_r) characteristics of square raft foundation at 60% relative density of sand bed. It can be observed that the loads calculated from EPC readings are closer to the actual applied load.

The modulus of subgrade reaction was determined using a model plate load test, and the modulus of elasticity was determined using a basic triaxial test. The literature review revealed correlations between modulus of elasticity and modulus of subgrade reaction developed by various investigators, and it was discovered that the pattern of change of modulus of subgrade reaction with respect to change in relative density of sand obtained in the current study was closer to the correlation developed by **Vesic and Selvadurai**.

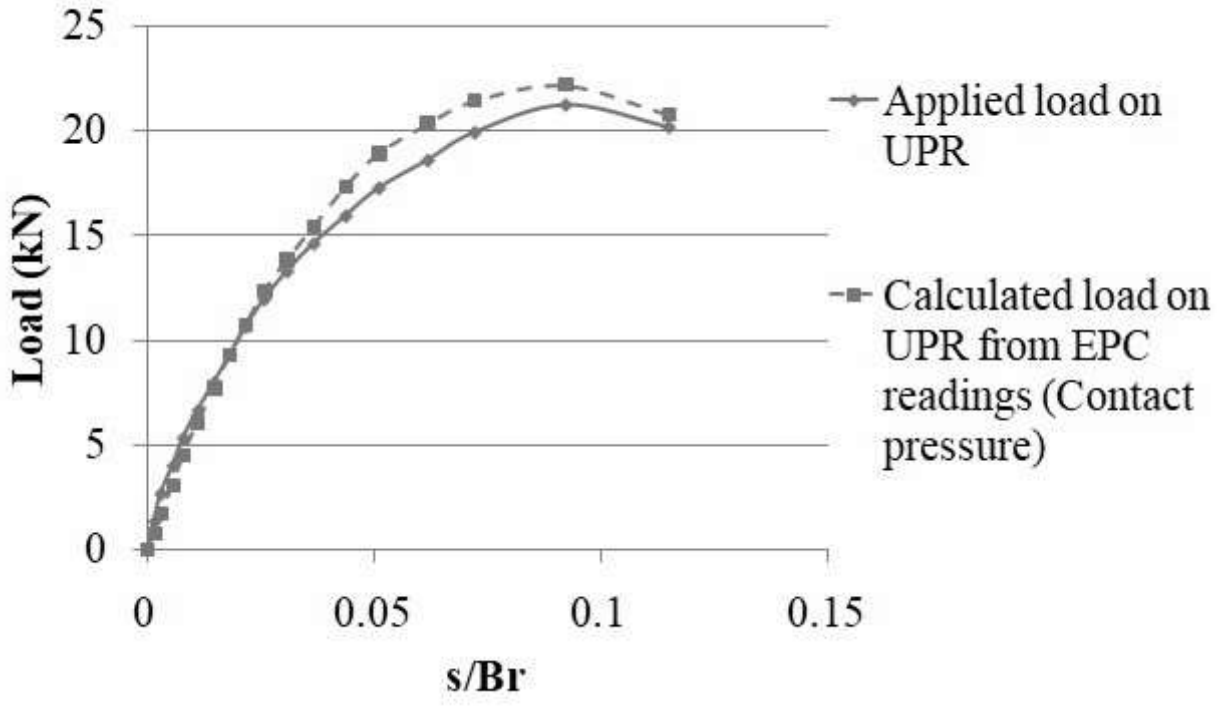

Figure 5-16 : comparison of Load calculated from EPC readings and actual applied load vs. relative settlement of unpiled raft foundation *(Square raft, I_d = 60%)*

5.3.2 Single Pile/ Pile Group (SP/PG)

5.3.2.1 Load Settlement Characteristics

Figure 5-17 to Figure 5-19 show the load settlement characteristics of a single pile with different *L/d* ratios at 40%, 60% and 80% relative densities of the sand bed, respectively. It can observe that as the *L/d* ratio of the pile increases, the load-carrying capacity of the single pile also increases. The percentage increment in the ultimate load of a single pile (considered at settlement = *10% of d*) with *L/d ratio = 10, 20, and 30* at 60% and 80% relative density of sand as compared to 40% relative density was found to be 27% and 327%, 169% and 241%, and 30% and 45%, respectively.

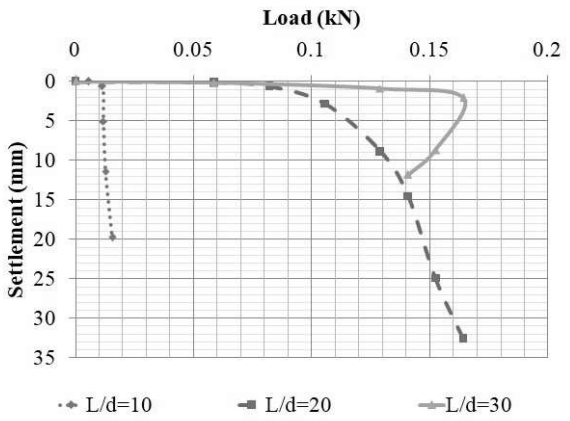

Figure 5-17 : Load settlement characteristics of single pile with different *L/d* ratio in sand *(I_d = 40%; d = 9.7 mm)*

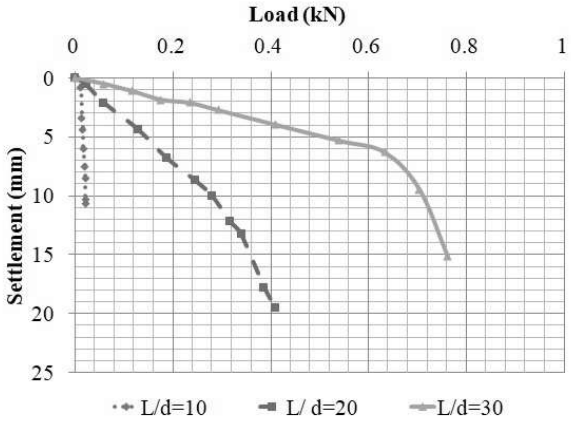

Figure 5-18 : Load settlement characteristics of single pile with different *L/d* ratio in sand *(I_d = 60%; d = 9.7 mm)*

Figure 5-20 to Figure 5-22 show the load settlement characteristics of the pile group with an *L/d* ratio of 30 and different spacing at 40%, 60%, and 80% relative densities of the sand bed, respectively. Table 5-7 shows the ultimate load of single pile $Q_{u,sp}$ and ultimate load of pile group $Q_{u,pg}$ with different spacing of piles at different relative density of sand bed. The $Q_{u,sp}$, and $Q_{u,pg}$ increased with an increase in the relative density of the sand bed.

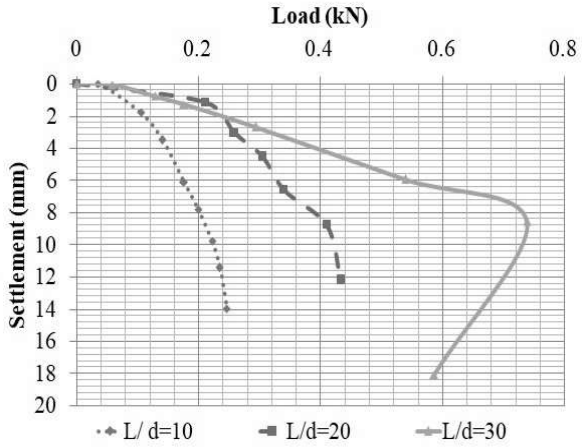

Figure 5-19 : Load settlement characteristics of single pile with different *L/d* ratio in sand *(I_d = 80%; d = 9.7 mm)*

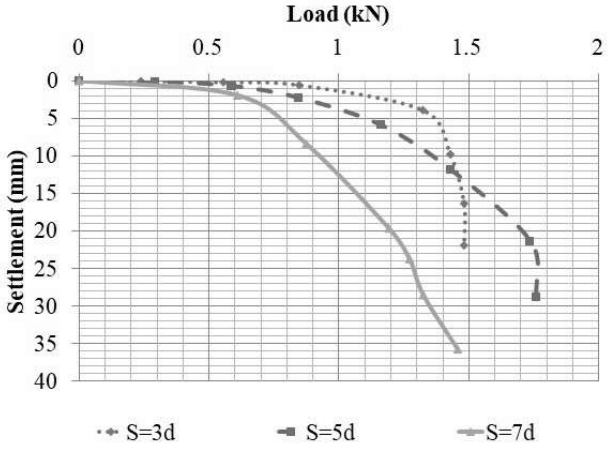

Figure 5-20 : Load settlement characteristics of pile group with different spacing between piles in sand *(L/d ratio of pile=30; I_d = 40%; d = 9.7 mm; Square uare pile group with 3 × 3 pile arrangement)*

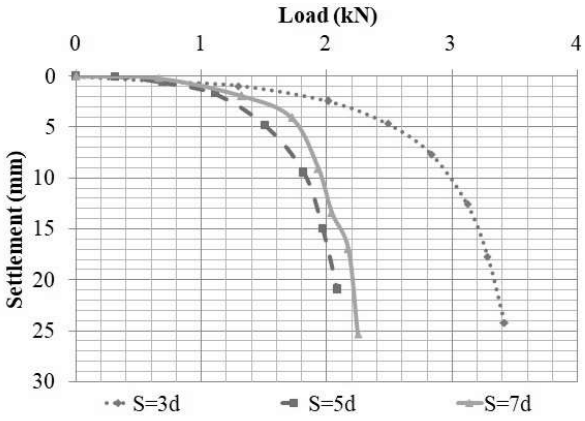

Figure 5-21: Load settlement characteristics of pile group with different spacing between piles in sand *(L/d ratio of pile = 30; I_d = 60%; d = 9.7 mm; Square pile group with 3 × 3 pile arrangement)*

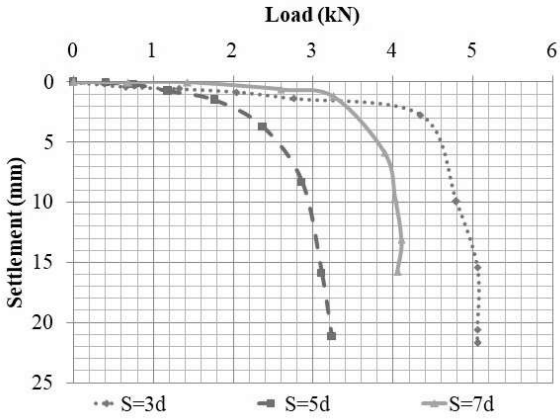

Figure 5-22 : Load settlement characteristics of pile group with different spacing between piles in sand *(L/d ratio of pile = 30; I_d = 80%; d = 9.7 mm; Square pile group with 3 × 3 pile arrangement)*

Table 5-7 Ultimate load of single pile $Q_{u,sp}$ and pile group $Q_{u,pg}$ with different spacing of piles at different relative density of sand bed

Spacing of piles (*S*)	**Relative Density of sand bed , I_d (%)**	**Ultimate load of single pile $Q_{u,sp}$ (kN)**	**Ultimate load of pile group $Q_{u,pg}$ (kN) (3x3)**	**Efficiency of pile group (η)**
3d	40	0.101	1.375	1.51
	60	0.131	2.736	2.32
	80	0.145	4.599	3.52
5d	40	0.101	1.379	1.52
	60	0.131	2.038	1.73
	80	0.145	2.938	2.25
7d	40	0.101	1.048	1.15
	60	0.131	2.081	1.77
	80	0.145	4.080	3.13

Figure 5-23 to Figure 5-25 show the load settlement characteristics of the 5×5 pile group with spacing = *5d* and different *L/d* ratios of the pile at 40%, 60% and 80% relative densities of the sand bed respectively. It was observed that as the *L/d* ratio of the pile increased, the load-carrying capacity of the pile group also increased.

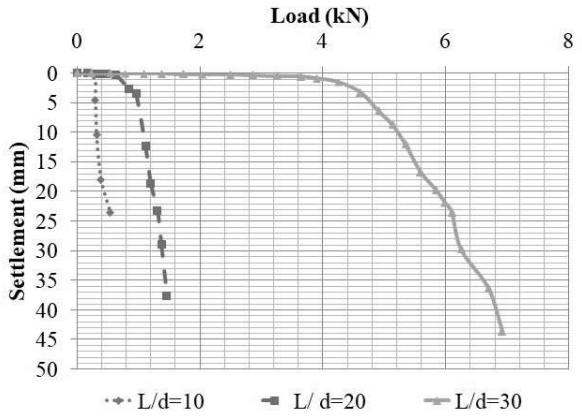

Figure 5-23 : Load settlement characteristics of pile group with different *L/d* ratio of piles in sand *(S = 5d; I_d = 40%; d = 9.7 mm; pile group = 5 × 5)*

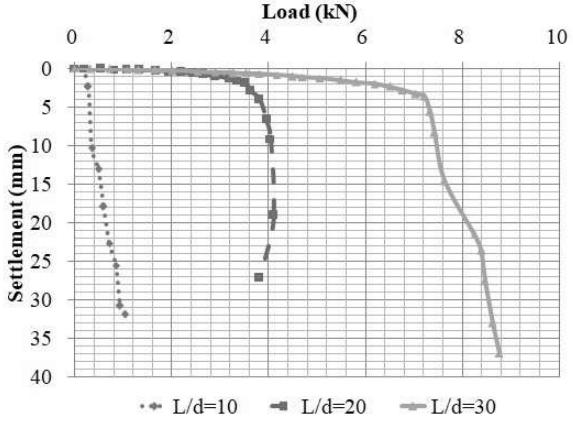

Figure 5-24 : Load settlement characteristics of pile group with *L/d* ratio of piles in sand *(S = 5d; I_d = 60%; d = 9.7 mm; pile group = 5 × 5)*

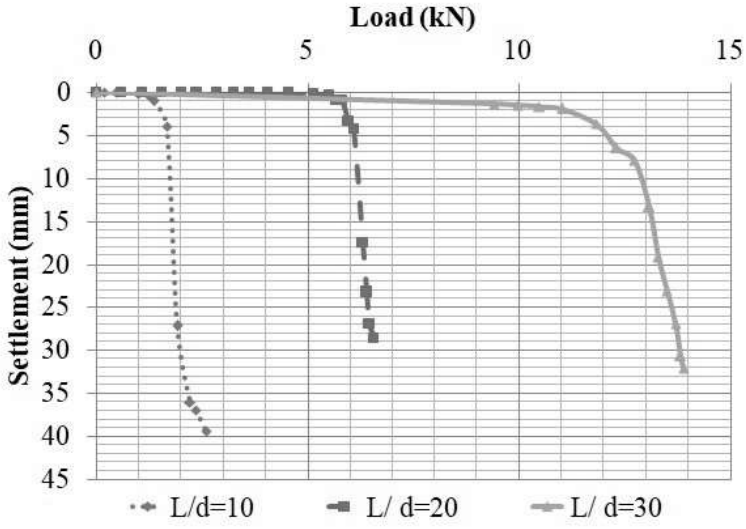

Figure 5-25 : Load settlement characteristics of pile group with different *L/d* ratio of piles in sand *(S = 5d; I_d = 80%; d = 9.7 mm; pile group = 5 × 5)*

Table 5-8 Ultimate load of single pile $Q_{u,sp}$ and pile group $Q_{u,pg}$ with different *L/d* ratios at different relative densities of the sand bed

***L/d* ratio of pile**	**Relative Density of sand bed, I_d (%)**	**Ultimate load of single pile $Q_{u,sp}$ (kN)**	**Ultimate load of pile group $Q_{u,pg}$ (kN) (5 × 5)**	**Efficiency of pile group (η)**
10	40	0.011	0.293	1.04
	60	0.012	0.422	1.36
	80	0.047	1.678	1.43
20	40	0.032	0.962	1.20
	60	0.086	3.355	1.56
	80	0.109	6.100	2.24
30	40	0.101	4.610	1.83
	60	0.131	7.332	2.24
	80	0.145	11.033	3.03

Figure 5-26 to Figure 5-28 illustrate the load settlement characteristics of a pile group with a spacing of *5d* and different pile shapes at relative densities of 40%, 60%, and 80% of the Narmada river sand bed. It was observed that the pile group with hollow circular (HC) piles carried less load compared to the other shapes of piles, such as hollow square (HSQ) and H-shaped piles, at the same settlement level of the pile group for all relative densities of the sand bed. At 40% relative density, the pile group with H-shaped piles can carry a higher load, while at 60% and 80% relative densities, the pile group with HSQ piles can carry more load as compared to the other two shapes of piles.

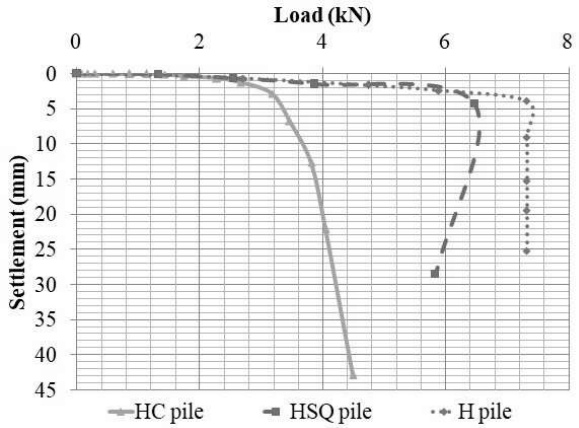

Figure 5-26 : Load settlement characteristics of pile group with different shape of piles in sand *(S = 5d; I_d = 40%; pile group = 3 × 3)*

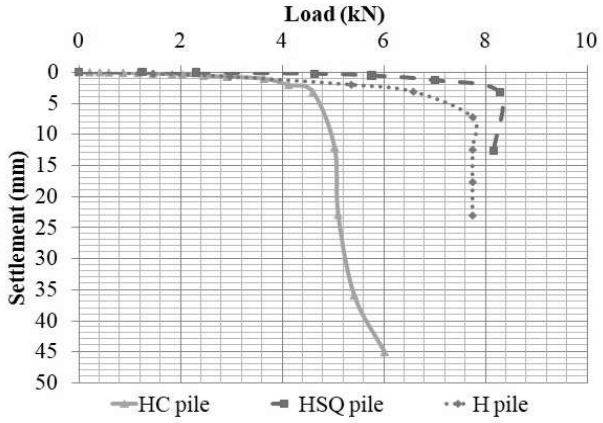

Figure 5-27 : Load settlement characteristics of pile group with different shape of piles in sand *(S = 5d; I_d = 60%; pile group = 3 × 3)*

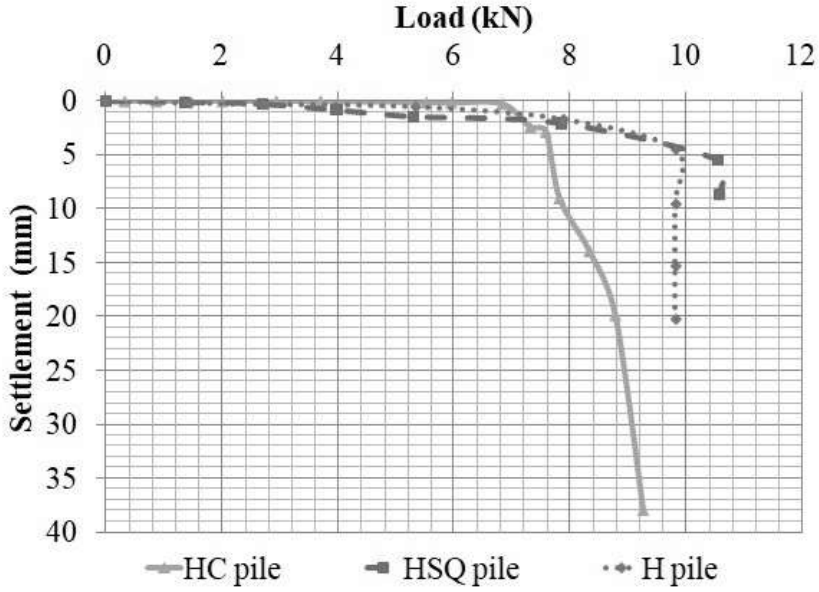

Figure 5-28 : Load settlement characteristics of pile group with different shape of piles in sand *(S = 5d; I_d = 80%; pile group = 3 × 3)*

5.3.2.2 Ultimate Load Carrying Capacity of Single Pile / Pile Group

Table 5-7 and Table 5-8 shows the ultimate load of single pile $Q_{u,sp}$ and pile group $Q_{u,pg}$ with different spacing of piles and *L/d* ratios respectively at different relative density of sand bed. It

was observed that as the relative density of sand increases the ultimate load carrying capacity of single pile and pile group increases. It was also noticed that at *3d* spacing of piles, the pile group carries more load as compared to *5d* and *7d* spacing. The reason behind this behaviour may be the block action of the pile group at *3d* spacing.

The percentage increment in the ultimate load of a pile group $Q_{u,pg}$ (3×3 with $L/d = 30$) with *3d* spacing was found to be 99% and 234% at 60% and 80% relative density, respectively, as compared to 40% relative density. The percentage increment in the ultimate load of a pile group $Q_{u,pg}$ (3×3 with $L/d = 30$) with *5d* spacing was found to be 48% and 113% at 60% and 80% relative density, respectively, as compared to 40% relative density. The percentage increment in $Q_{u,pg}$ of 3×3 pile group with *7d* spacing was found to be 99% and 289% at 60% and 80% relative density, respectively, as compared to 40% relative density. Due to block action, the load carrying capacity of pile group with *3d* spacing has maximum load carrying capacity amongst *3d, 5d* and *7d* spacing. At 40% relative density, the load carrying capacity was decreased as the spacing of pile increased. At 60% and 80% relative density, the load carrying capacity of pile group was decreased as the spacing of pile increased from *3d* to *5d* and after that it was increased at *7d* spacing. This is attributed to block action at *3d* spacing, individual pile pressure bulb overlapping at *5d* spacing and full individual action of piles at *7d* spacing.The ultimate load-carrying capacity of the pile group with *5d* and *7d* spacing was decreased by 0% and 24%, 26% and 24%, and 36% and 11% as compared to *3d* spacing at 40%, 60%, and 80% relative densities of sand, respectively.

In the case of the *L/d* ratio, the ultimate load of single piles $Q_{u,sp}$ and pile groups $Q_{u,pg}$ was observed to increase with an increase in the *L/d* ratio of piles in the pile group and relative density of sand.

The percentage increment in the ultimate load of a pile group (5×5 with *5d* spacing) with *L/d* ratios of 10, 20, and 30 at 60% and 80% relative density of sand as compared to 40% relative density found 44% and 473%, 249% and 534%, and 59% and 139%, respectively.

When the *L/d* ratio was increased from 10 to 20, the pile group's ultimate load-carrying capacity increased by 0.67 kN, 2.93 kN, and 4.42 kN at 40%, 60%, and 80% relative sand densities respectively. Similarly, when the *L/d* ratio was increased from 20 to 30, the ultimate load-carrying capacity increased by 3.65 kN, 3.98 kN, and 4.93 kN at the same relative densities. Compared to the *L/d* ratio of 10, the load-carrying capacity of the pile group with an *L/d* ratio of 20 increased by 228%, 695%, and 264% at 40%, 60%, and 80% relative densities respectively. For the *L/d* ratio of 30, the increase was 1473%, 1637%, and 558% at the same relative densities.

Table 5-9 shows the ultimate load capacity of pile group $Q_{u,pg}$ with various pile shapes at different relative densities of the sand bed. The results indicate that as the relative density of the sand bed increased, the ultimate load-carrying capacity of the pile group also increased. The increase in $Q_{u,pg}$ for HC pile, HSQ pile, and *H* pile at 60% and 80% relative density, compared to 40% relative density, was 1.43 kN and 4.14 kN, 1.81 kN and 4.08 kN, and 0.42 kN and 2.49 kN, respectively. This represents a percentage increase of 45% and 131%, 28% and 63%, and 6% and 34%, respectively. Based on Table 5-9, it was observed that the $Q_{u,pg}$ of the HC pile was lower compared to other types of piles at 40%, 60%, and 80% relative density. At 40%, 60%, and 80% relative density, the increase in $Q_{u,pg}$ for HSQ pile and *H* pile, when compared to HC pile, was 3.3 kN, 3.68 kN, and 3.24 kN; 4.15 kN, 3.14 kN, and 2.5 kN, respectively. This represents a percentage increase of 104%, 80%, and 44%; 131%, 68%, and 34%, respectively.The HC pile consist least surface area and base area (assuming soil plug has formed) giving least capacity and HSQ pile has higher total surface area (inside and outside surface area) compared to H pile and vise versa for base area so the highest load carrying capacity was found with HSQ pile and the capacity of H and HSQ pile are close.

Table 5-9 Ultimate load of pile group $Q_{u,pg}$ with different shape of piles at different relative density of sand bed

Relative Density of Sand bed (I_d)	**Ultimate load of pile group $Q_{u,pg}$ (kN) (3×3)**		
	Hollow circular pile (HC)	**Hollow Square pile (HSQ)**	**H pile (H)**
40%	3.17	6.47	7.32
60%	4.60	8.28	7.74
80%	7.31	10.55	9.81

5.3.2.3 Initial Tangent Stiffness of Single Pile k_{p1} and Pile Group $(k_{pg})_i$

Table 5-10 and Table 5-11 shows the initial tangent stiffness of single pile k_{p1} and pile group $(k_{pg})_i$ with different spacing of pile and different *L/d* ratios of pile respectively at different relative density of sand bed. The initial tangent stiffness of pile group $(k_{pg})_i$ obtained from experimental results and same value calculated using Fleming's relation are coming nearer to same except in spacing criteria at $I_d = 80\%$. The k_{p1} and $(k_{pg})_i$ was increased with increase in relative density of sand as at higher relative density the denseness of soil increased which tends to go increase in skin friction and unit base resistance of pile/ pile group.

Table 5-10 Initial tangent stiffness of single pile k_{p1} and pile group $(k_{pg})_i$ with different spacing of pile at different relative density of sand bed (Experimental and calculated using Fleming's relation)

Spacing of pile	**Relative Density of sand bed, I_d (%)**	**Initial Tangent Stiffness of single pile k_{p1} (kN/m)**	**Initial Tangent stiffness of pile group $(k_{pg})_i$ (kN/m)**	**Number of piles**	**Initial Tangent stiffness of pile group $(k_{pg})_i$ (kN/m)**
		(Experimental)	**(Experimental)**	***n***	**(Fleming)**
3d	40	72.54	266.59	9	217.61
	60	100.95	493.64	9	469.98
	80	103.56	1564.45	9	482.13
5d	40	72.54	315.72	9	337.69
	60	100.95	630.79	9	469.98
	80	103.56	1048.71	9	482.13
7d	40	72.54	315.01	9	337.69
	60	100.95	367.17	9	469.98
	80	103.56	2260.30	9	482.13

Table 5-11 Initial tangent stiffness of single pile k_{p1} and pile group $(k_{pg})_i$ with different *L/d* ratios of pile at different relative density of sand bed (Experimental and calculated using Fleming's relation)

L/d **ratio of pile**	**Relative Density of sand bed (I_d) (%)**	**Initial Tangent Stiffness of single pile k_{p1} (kN/m)**	**Initial Tangent stiffness of pile group $(k_{pg})_i$ (kN/m)**	**Number of piles**	**Initial Tangent stiffness of pile group $(k_{pg})_i$ (kN/m)**
		(Experimental)	**(Experimental)**	***n***	**(Fleming)**
10	40	2.05	19.51	25	19.51
	60	2.70	25.66	25	25.66
	80	45.06	319.38	25	428.91
20	40	25.57	203.16	25	243.40
	60	29.98	388.60	25	285.39
	80	39.40	414.79	25	375.02
30	40	72.54	686.11	25	690.41
	60	100.95	954.81	25	960.88
	80	103.56	1029.84	25	985.72

Table 5-12 Settlement of pile group with different *L/d* ratio (Experimental, calculated using Skempton and Meyerhof equation)Table 5-12 and Table 5-13 display the settlement of pile groups based on experimental results and calculated using the Skempton and Meyerhof equations with different *L/d* ratios and pile spacing, respectively. Most of the experimental values of settlement of pile groups are close to the values of settlement of pile groups calculated using the Skempton equation compared to Meyerhof equations.

Table 5-12 Settlement of pile group with different *L/d* ratio (Experimental, calculated using Skempton and Meyerhof equation)

L/d	I_d **(%)**	$Q_{u,sp}$ **(kN)**	$Q_{safe,sp}$ **(kN)**	***n***	$n*Q_{safe,sp}$ **(kN)**	s_s **(mm)**	R_s **(Skempton)**	R_s **(Meyerhof)**	s_g **(mm) (Skempton)**	s_g **(mm) (Meyerhof)**	s_g **(mm) (Exp)**
10	40	0.01	0.005	25	0.113	0.00	3.7	11.6	0.00	0.00	0.00
	60	0.01	0.005	25	0.124	0.00	3.7	11.6	0.00	0.00	0.00
	80	0.05	0.019	25	0.469	0.01	3.7	11.6	0.05	0.17	0.09
20	40	0.03	0.013	25	0.320	0.31	3.7	11.6	1.15	3.60	0.07
	60	0.09	0.034	25	0.860	0.04	3.7	11.6	0.15	0.48	0.14
	80	0.11	0.044	25	1.089	0.24	3.7	11.6	0.89	2.79	0.01
30	40	0.10	0.040	25	1.010	0.13	3.7	11.6	0.47	1.47	0.06
	60	0.13	0.052	25	1.310	0.48	3.7	11.6	1.79	5.58	0.18
	80	0.15	0.058	25	1.454	0.09	3.7	11.6	0.33	1.03	0.21

Table 5-13 Settlement of pile group with different spacing of piles (Experimental, calculated using Skempton and Meyerhof equation)

S	I_d (%)	$Q_{u,sp}$ (kN)	$Q_{safe,sp}$ (kN)	n	$n*Q_{safe,sp}$ (kN)	s_s (mm)	R_s (Meyerhof)	s_g (mm) (Skempton)	s_g (mm) (Meyerhof)	s_s (mm)
3d	40	0.10	0.04	9	0.36	0.13	6.75	0.20	0.86	0.10
	60	0.13	0.05	9	0.47	0.48	6.75	0.77	3.26	0.35
	80	0.15	0.06	9	0.52	0.09	6.75	0.14	0.60	0.32
5d	40	0.10	0.04	9	0.36	0.13	9.38	0.28	1.19	0.21
	60	0.13	0.05	9	0.47	0.48	9.38	1.08	4.52	0.20
	80	0.15	0.06	9	0.52	0.09	9.38	0.20	0.84	0.10
7d	40	0.10	0.04	9	0.36	0.13	10.50	0.36	1.34	1.15
	60	0.13	0.05	9	0.47	0.48	10.50	1.37	5.07	0.11
	80	0.15	0.06	9	0.52	0.09	10.50	0.25	0.94	0.01

5.3.3 Piled Raft Foundation (PRF)

5.3.3.1 Effect of Shape of Raft with Equal Contact Area

5.3.3.1.1 Load Settlement Characteristics

The load-settlement curve of a model piled raft foundation was plotted based on experiment readings and found to be tri-linear, as mentioned in clause 5.2.5. Figure 5-29 to Figure 5-32 show the load-settlement characteristics of PRF with different shapes of raft. These load-settlement curves exhibit tri-linear behaviour and are represented with different coloured lines. The load corresponding to the point where the initial and second linear portions of the load-settlement curve of PRF intersect is termed the initial yield load (*IYL*), and the load at the point where the second and third linear portions of the load-settlement curve of PRF intersect is termed the final yield load (*FYL*). It was observed that as the relative density of the sand bed increased, the load-carrying capacity of the model piled raft foundation also increased. For the model piled raft with different shapes of raft having the same contact area, the minimum and maximum load-carrying capacity of the piled raft was observed with circular raft and square raft, respectively.

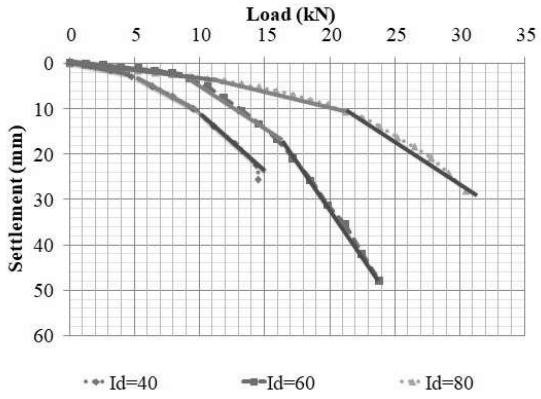

Figure 5-29 : Load settlement characteristics of model circular piled raft at different relative density of sand bed *(S = 7d; pile group = 3 × 3)*

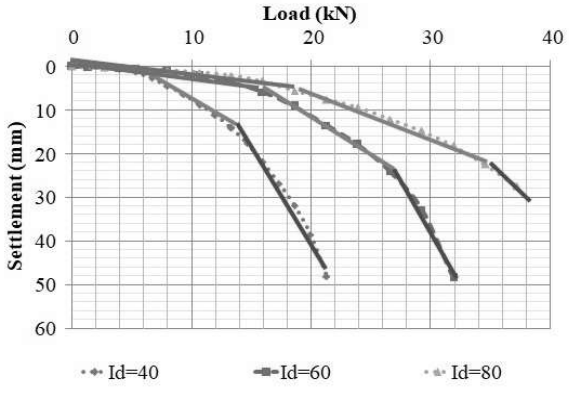

Figure 5-30 : Load settlement characteristics of model rectangular piled raft at different relative density of sand bed *(S = 7d; pile group = 3 × 3)*

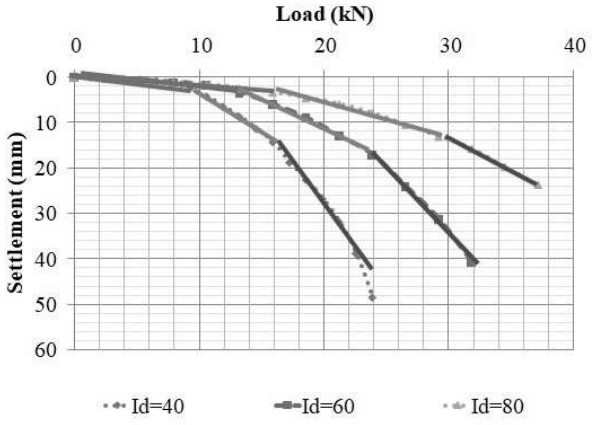

Figure 5-31 : Load settlement characteristics of model trapezoidal piled raft at different relative density of sand bed *(S = 7d; pile group = 3 × 3)*

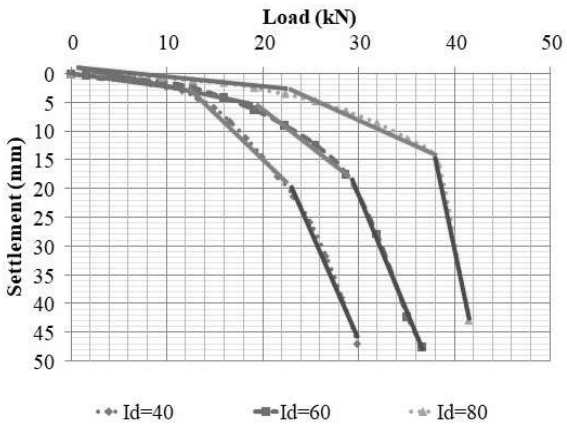

Figure 5-32 : Load settlement characteristics of model square piled raft at different relative density of sand bed *(S = 7d; pile group = 3 × 3)*

Figure 5-33 to Figure 5-36 represents the load settlement curves of only pile group (PG), unpiled raft (UPR), and piled raft (PRF) with circular, rectangular, trapezoidal, and square shape raft, respectively. It can be observed that at the same settlement level, the ascending order of load-carrying capacity is PG, UPR, and PRF. It is noticed that at the initial stage of loading, the load settlement behaviour of UPR and PRF are very close to each other, and in the later stage of loading, it is distiguised for UPR and PRF. i.e., UPR reached its maximum capacity at a lower settlement level and PRF at a higher settlement level. At the *IYL* level of PRF, the carrying capacity of **only** the pile group reached its ultimate level.

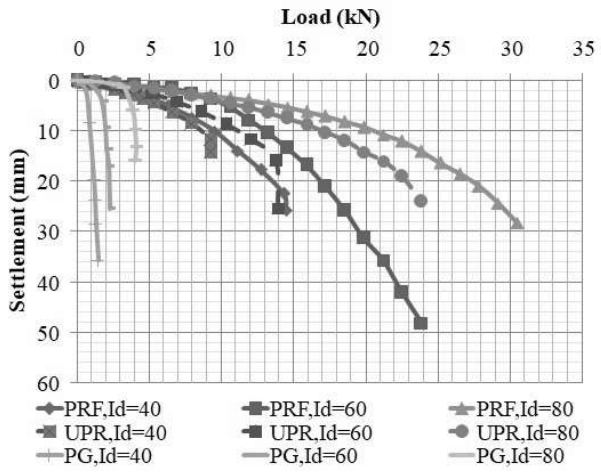

Figure 5-33 : Load settlement characteristics of only pile group, unpiled raft, and piled raft with circular shape of raft at different relative density of sand *(S = 7d; d = 9.7 mm; pile group = 3 × 3)*

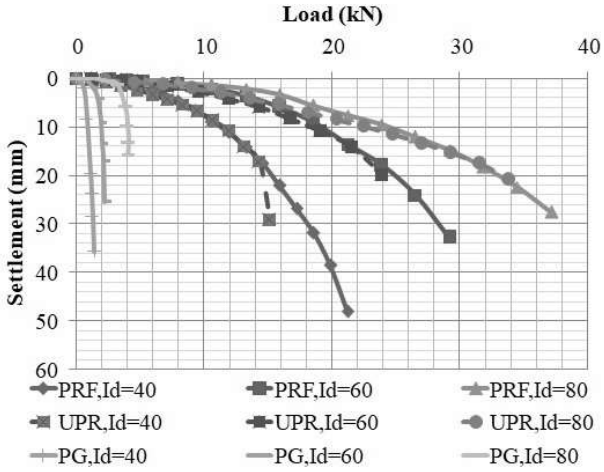

Figure 5-34 : Load settlement characteristics of only pile group, unpiled raft, and piled raft with rectangular shape of raft at different relative density of sand *(S = 7d; d = 9.7 mm; pile group = 3 × 3)*

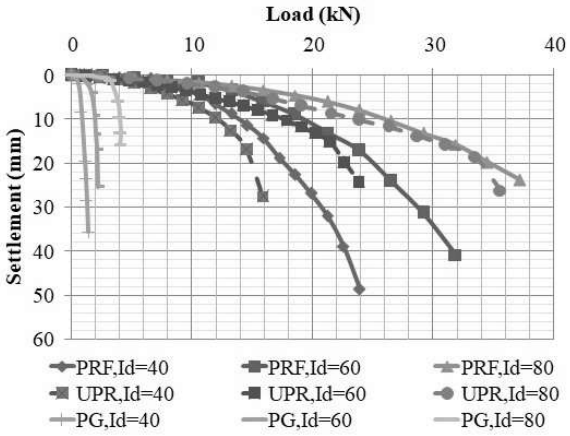

Figure 5-35 : Load settlement characteristics of only pile group, unpiled raft, and piled raft with trapezoidal shape of raft at different relative density of sand *(S = 7d; d = 9.7 mm; pile group = 3 × 3)*

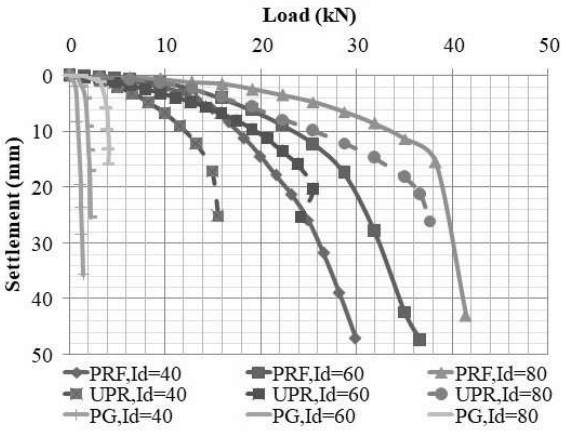

Figure 5-36 : Load settlement characteristics of only pile group, unpiled raft, and piled raft with square shape of raft at different relative density of sand *(S = 7d; d = 9.7 mm; pile group = 3 × 3)*

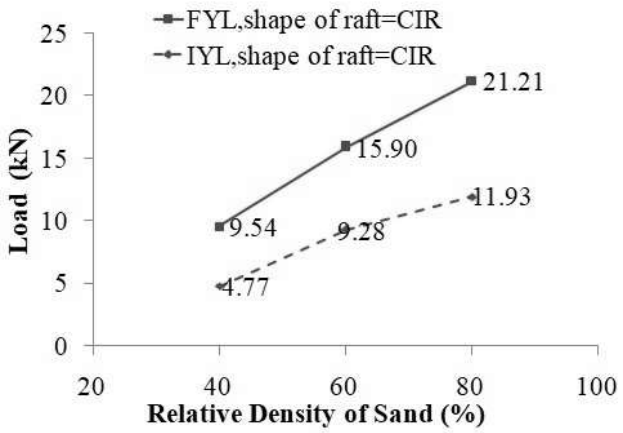

Figure 5-37 : Initial yield load (*IYL*) and Final yield load (*FYL*) of piled raft foundation at different relative density of sand bed *(S = 7d; d = 9.7 mm; pile group = 3 × 3; shape of raft = circular)*

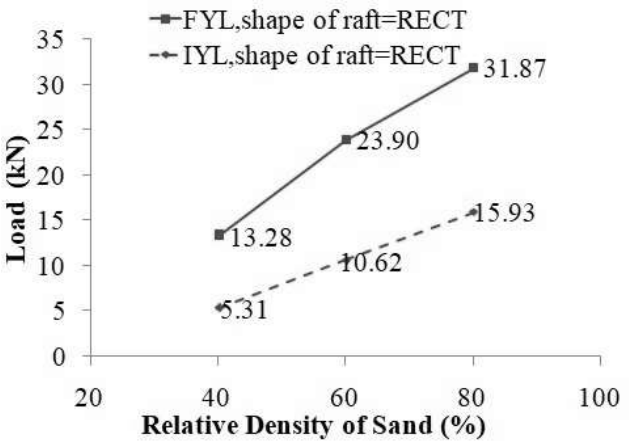

Figure 5-38 : Initial yield load (*IYL*) and Final yield load (*FYL*) of piled raft foundation at different relative density of sand bed *(S = 7d; d = 9.7 mm; pile group = 3 × 3; shape of raft = rectangular)*

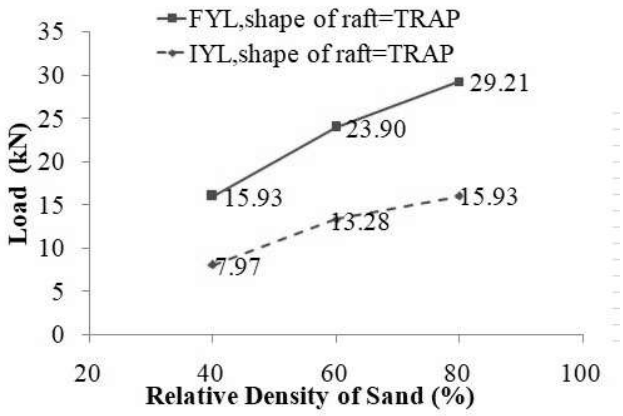

Figure 5-39 : Initial yield load (*IYL*) and Final yield load (*FYL*) of piled raft foundation at different relative density of sand bed *(S = 7d; d = 9.7 mm; pile group = 3 × 3; shape of raft = trapezoidal)*

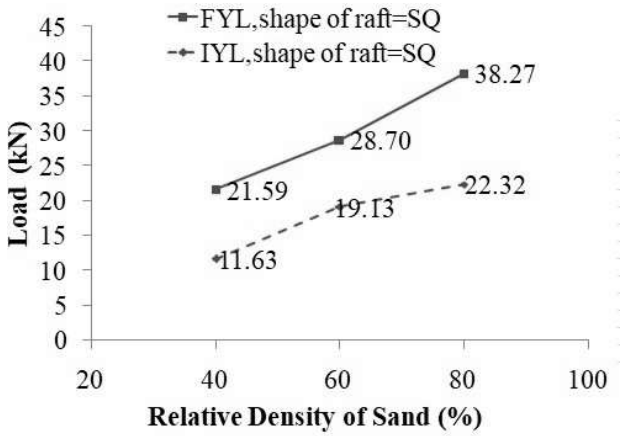

Figure 5-40 : Initial yield load (*IYL*) and Final yield load (*FYL*) of piled raft foundation at different relative density of sand bed *(S = 7d; d = 9.7 mm; pile group = 3 × 3; shape of raft = square)*

Figure 5-37 to Figure 5-40 show the value of *IYL* and *FYL* at different relative density obtained from the load settlement curve of model PRF with circular, rectangular , trapezoidal and square shape of raft respectively. It was observed that as the relative density of sand increased the *IYL* and *FYL* are also increased and the minumum and maximum values of *IYL* and *FYL* were found to be in PRF with circular raft and square raft respectively.The range of *IYL* of PRF with a circular raft was found to be 4.77 kN to 11.93 kN at 40% to 80% relative density of the sand bed. The value of *IYL* of PRF with a circular raft is increased by 4.51 kN and 7.16 kN at 60% and 80% relative densities, respectively, as compared to the 40% relative density of a sand bed. In the case of PRF with a circular raft, the range of *FYL* was found to be 9.54 kN to 21.21 kN for a 40% to 80% relative density of the sand bed. The increment in the value of *FYL* at 60% and 80% relative density as compared to 40% relative density was observed 6.36 kN and 11.66 kN, respectively.The increment in *FYL* as compared to *IYL* was observed to be 4.77 kN, 6.63 kN, and 9.28 kN at 40%, 60%, and 80% relative densities of the sand bed, respectively.

The values of *IYL* of PRF with a rectangular raft were observed to be 5.31 kN, 10.62 kN, and 15.93 kN at 40%, 60%, and 80% relative densities of the sand bed, respectively, i.e., they increased by 5.31 kN from 40% to 60% and 60% to 80% relative densities of the sand bed. The *FYL* of PRF with rectangular raft was found to be 13.28 kN, 23.90 kN, and 31.87 kN at 40%, 60%, and 80% relative densities of the sand bed, respectively, i.e., it increased by 10.62 kN and 18.59 kN at 60% and 80% relative densities as compared to 40% relative densities of the sand bed.The values of *FYL* were found to be 7.97 kN, 13.28 kN, and 15.93 kN higher than the *IYL* at 40%, 60%, and 80% relative densities, respectively.

The range of *IYL* and *FYL* of PRF with trapezoidal raft was found to be 7.97 kN to 15.93 kN and 15.93 kN to 29.21 kN, respectively, from 40% to 80% relative density of the sand bed. The increment in *IYL* at 60% and 80% relative densities as compared to 40% relative density was observed to be 5.31 kN and 7.97 kN, respectively, while in *FYL* it was found to be 7.97 kN and 13.28 kN. The values of *FYL* of PRF with trapezoidal raft as compared to *IYL* at 40%, 60%, and 80% relative densities were increased by 7.97 kN, 10.62 kN, and 13.28 kN, respectively.

The range of *IYL* and *FYL* of PRF with square raft was found to be 11.63 kN to 22.32 kN and 21.59 kN to 38.27 kN, respectively, from 40% to 80% relative density of the sand bed. The increment in *IYL* at 60% and 80% relative densities as compared to 40% relative density was observed to be 7.51 kN and 10.70 kN, respectively, while in *FYL* it was found to be 7.11 kN and 16.67 kN. The values of *FYL* of PRF with square raft as compared to *IYL* at 40%, 60%, and 80% relative densities were increased by 9.96 kN, 9.57 kN, and 15.94 kN, respectively.

It was found that the *IYL* of PRF with a rectangular raft was 11%, 15%, and 34% higher compared to the *IYL* of PRF with a circular raft at 40%, 60%, and 80% relative densities. On the other hand, the percentage increase in *IYL* of PRF with a trapezoidal raft was observed to be 67%, 43%, and 34% compared to the circular raft at I_d = 40%, 60%, and 80%, respectively. In addition, it was observed that the *IYL* of PRF with a square raft was 144%, 106%, and 87% higher than the *IYL* of PRF with a circular raft at 40%, 60%, and 80% relative densities, respectively. It was also noted that the ratio of *FYL* to *IYL* of PRF with a circular raft was 2, 1.7, and 1.8 at 40%, 60%, and 80% relative densities, respectively. Furthermore, the *FYL* was observed as 2.5, 2.3, and 2 times the *IYL* in the case of PRF with a rectangular raft at I_d of 40%, 60%, and 80%, respectively. Similarly, the *FYL* was observed as 2, 1.8, and 1.8 times the *IYL* in the case of PRF with a trapezoidal raft at I_d of 40%, 60%, and 80%, respectively. Finally, in the case of PRF with a square raft, the *FYL* was found to be 1.9, 1.5, and 1.7 times the *IYL* at 40%, 60%, and 80% relative densities, respectively.

5.3.3.1.2 Contact Pressure Distribution beneath UPR and PRF

The contact pressures were measured using miniature earth pressure cells (EPC) at the different symmetric locations of UPR and PRF. Figure 5-41 to Figure 5-46 show readings of EPC vs. relative settlements (s/B_r) of model foundations with circular rafts. The contact pressure in EPC-10 (located in one quadrant of 3 × 3 pile group) was higher than other locations in UPR and PRF at all relative densities. Readings of EPC-2 and EPC-5 were nearly the same in most of the cases of UPR and PRF, except in PRF at 40% relative density. At 40% relative density of the sand bed, the readings of contact pressures at *IYL* of circular PRF in EPC-2, EPC-5, and EPC-10 were 21

kPa, 0 kPa, and 139 kPa, respectively, while at *FYL* they were 92 kPa, 29 kPa, and 328 kPa, respectively. The readings of contact pressure in EPC-2, EPC-5, and EPC-10 were 62 kPa, 128 kPa, and 196 kPa, respectively, at 60% relative density of the sand bed, while at *FYL*, they were observed at 62 kPa, 286 kPa, and 344 kPa, respectively. At I_d = 80%, the readings in EPC-2, EPC-5, and EPC-10 were observed at 18 kPa, 9 kPa, and 421 kPa, respectively, while at *FYL*, they were 14 kPa, 9 kPa, and 948 kPa, respectively.

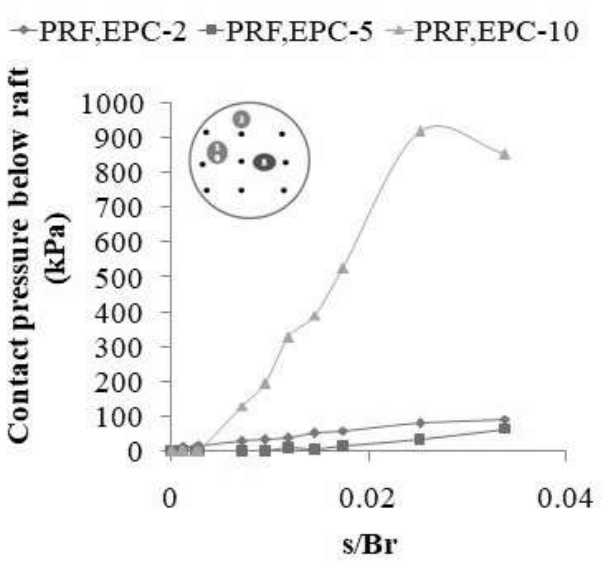

Figure 5-41 : Contact pressure distribution below unpiled raft for different location of earth pressure cells vs. relative settlement characteristics *(I_d = 40%; shape of raft = circular)*

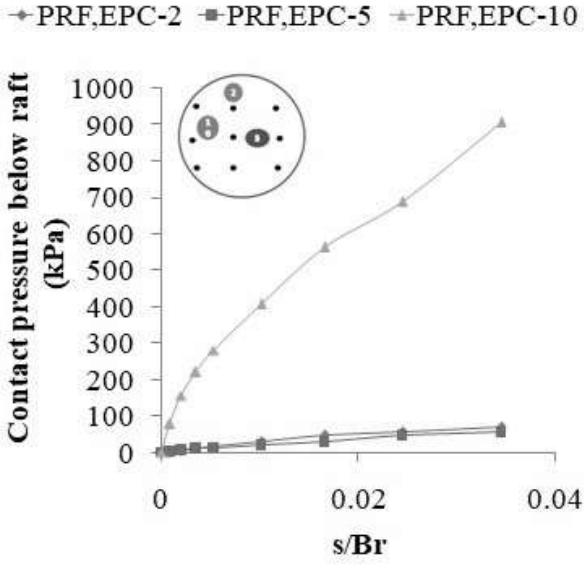

Figure 5-42 : Contact pressure distribution below unpiled raft for different location of earth pressure cells vs. relative settlement characteristics *(I_d = 60%; shape of raft = circular)*

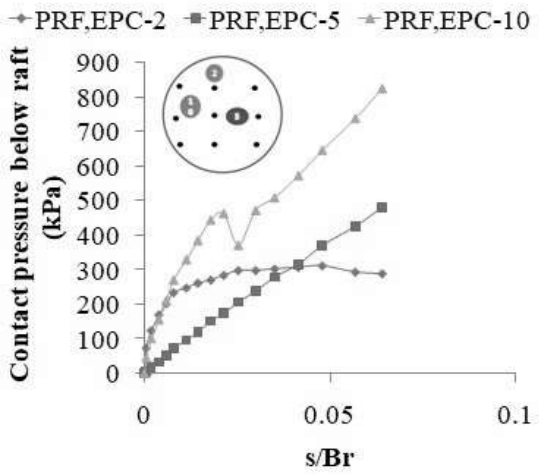

Figure 5-43 : Contact pressure distribution below unpiled raft for different location of earth pressure cells vs. relative settlement characteristics *(I_d = 80%; shape of raft = circular)*

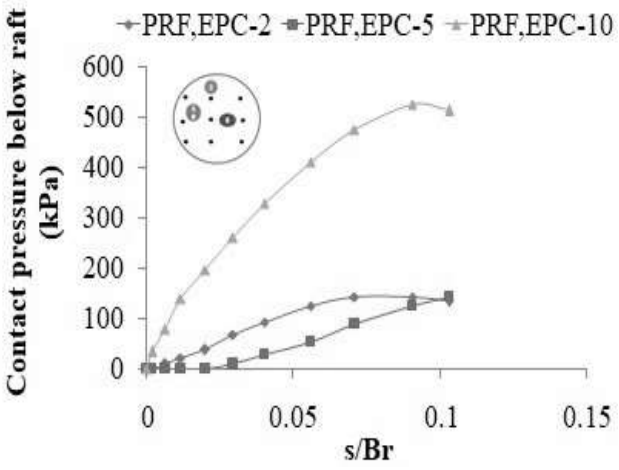

Figure 5-44 : Contact pressure distribution below raft for different location of earth pressure cells in PRF vs. relative settlement characteristics *(I_d = 40%; S = 7d; L/d ratio of pile = 30; d = 9.7 mm; pile group = 3 × 3; shape of raft = circular)*

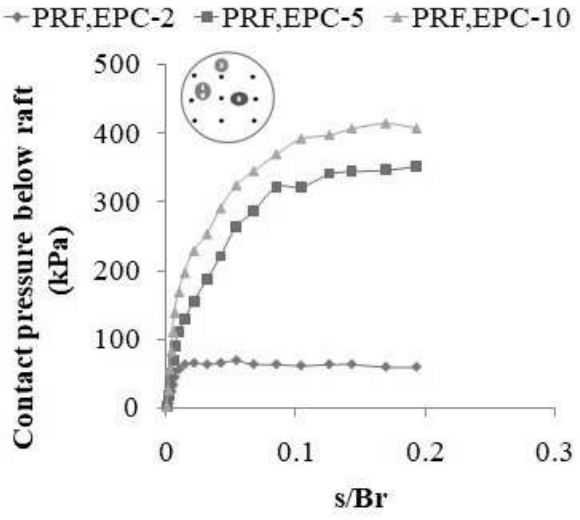

Figure 5-45 : Contact pressure distribution below raft for different location of earth pressure cells in PRF vs. relative settlement characteristics *(I_d = 60%; S = 7d; L/d ratio of pile = 30; d = 9.7 mm; pile group = 3 × 3; shape of raft = circular)*

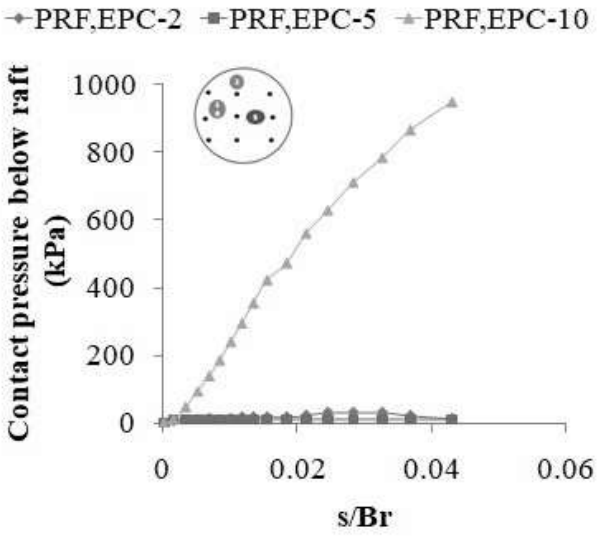

Figure 5-46 : Contact pressure distribution below raft for different location of earth pressure cells in PRF vs. relative settlement characteristics *(I_d = 80%; S = 7d; L/d ratio of pile = 30; d = 9.7 mm; pile group = 3 × 3; shape of raft = circular)*

Figure 5-47 to Figure 5-52 display the contact pressure at different locations in the UPR and PRF with a rectangular raft. The earth pressure cells (EPC-2 and EPC-10) situated closer to the central part of the model foundation show higher readings. Meanwhile, EPC-3 displays lower readings at the corners. At 40% relative density of the sand bed, the readings of EPC-2, EPC-3, EPC-5, and EPC-10 were 52 kPa, 29 kPa, 81 kPa, and 235 kPa, respectively, at *IYL*. At *FYL*, the readings were 206 kPa, 81 kPa, 142 kPa, and 713 kPa, respectively. At 60% relative density of the sand bed, the readings of EPC-2, EPC-3, EPC-5, and EPC-10 were 325 kPa, 185 kPa, 161 kPa, and 49 kPa, respectively, at *IYL*. At *FYL*, the readings were 642 kPa, 136 kPa, 237 kPa, and 384 kPa, respectively. At 80% relative density of sand, the readings of EPC-2, EPC-3, EPC-5, and EPC-10 were 255 kPa, 74 kPa, 204 kPa, and 923 kPa, respectively, at *IYL*. At *FYL*, the readings were 688 kPa, 150 kPa, 275 kPa, and 1052 kPa, respectively.

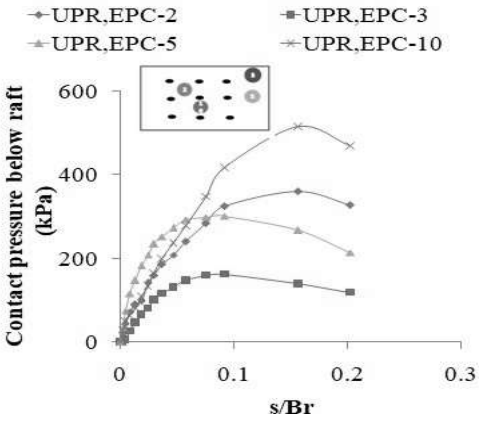

Figure 5-47 : Contact pressure distribution below unpiled raft for different location of earth pressure cells vs. relative settlement characteristics *(I_d = 40%; shape of raft = rectangular)*

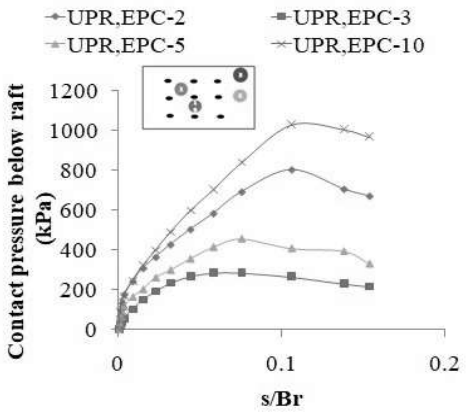

Figure 5-48 : Contact pressure distribution below unpiled raft for different location of earth pressure cells vs. relative settlement characteristics *(I_d = 60%; shape of raft = rectangular)*

Figure 5-53 to Figure 5-58 depicts the contact pressure distribution beneath the trapezoidal raft at various locations in UPR and PRF. In UPR, the maximum contact pressure was found in EPC-10, which is situated closer to the central region of the raft, while the pressure was lower in other EPCs (EPC-2, EPC-5, EPC-11) located near the sides and corners of the trapezoidal raft.

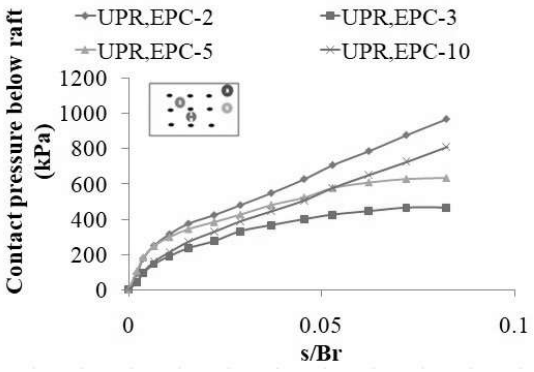

Figure 5-49 : Contact pressure distribution below unpiled raft for different location of earth pressure cells vs. relative settlement characteristics *(I_d = 80%; shape of raft = rectangular)*

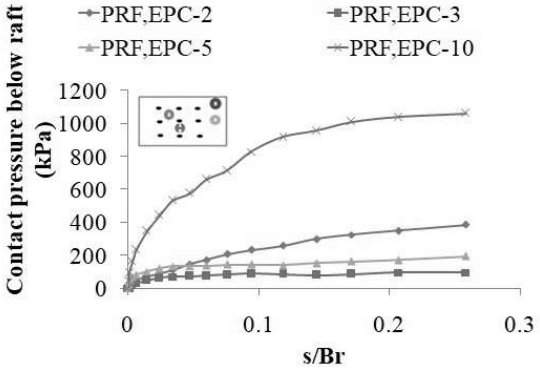

Figure 5-50 : Contact pressure distribution below raft for different location of earth pressure cells in PRF vs. relative settlement characteristics *(I_d = 40%; S = 7d; L/d ratio of pile = 30; d = 9.7 mm; pile group = 3 × 3; shape of raft = rectangular)*

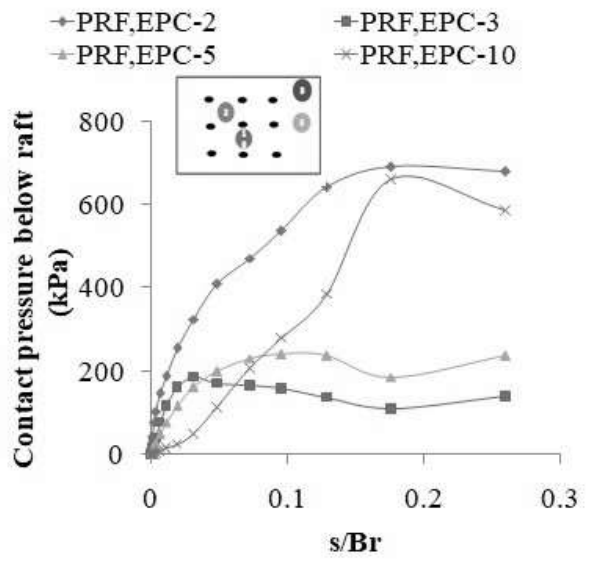

Figure 5-51 : Contact pressure distribution below raft for different location of earth pressure cells in PRF vs. relative settlement characteristics *(I_d = 60%; S = 7d; L/d ratio of pile = 30; d = 9.7 mm; pile group = 3 × 3; shape of raft = rectangular)*

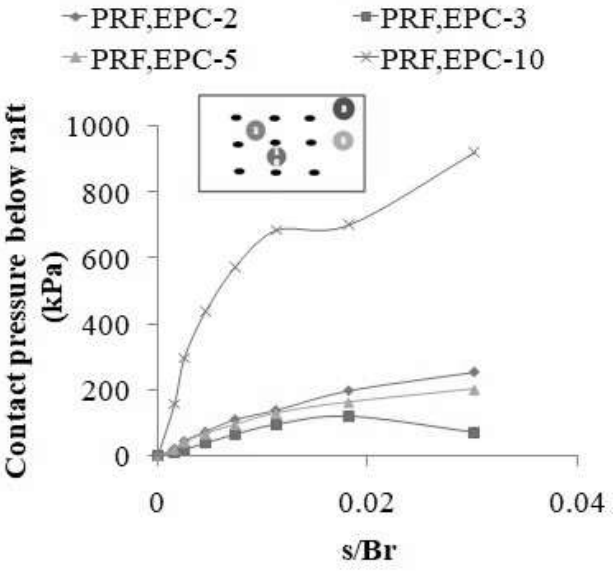

Figure 5-52 : Contact pressure distribution below raft for different location of earth pressure cells in PRF vs. relative settlement characteristics *(I_d = 80%; S = 7d; L/d ratio of pile = 30; d = 9.7 mm; pile group = 3 × 3; shape of raft = rectangular)*

Similarly, in trapezoidal PRF, the maximum contact pressure was found in EPC-3, located closer to the central region of the raft, while it was lower in other EPCs (EPC-2, EPC-5, EPC-11) located near the sides and corners of the trapezoidal raft, at higher relative settlements. At 40% relative density of the sand bed, the contact pressures observed were 123 kPa, 85 kPa, 68 kPa, 4 kPa, and 119 kPa, respectively, in EPC-2, EPC-3, EPC-5, EPC-10, and EPC-11 at *IYL* of the trapezoidal PRF. At *FYL*, the contact pressures were 217 kPa, 510 kPa, 153 kPa, 136 kPa, and 200 kPa, respectively. Similarly, at 60% relative density of the sand bed, the contact pressures in EPC-2, EPC-3, EPC-5, EPC-10, and EPC-11 were observed as 94 kPa, 26 kPa, 175 kPa, 4 kPa, and 163 kPa, respectively, while at *FYL*, they were observed as 210 kPa, 479 kPa, 270 kPa, 98 kPa, and 197 kPa, respectively. Finally, at 80% relative density of the sand bed, the contact pressure in EPC-2, EPC-3, EPC-5, EPC-10, and EPC-11 were observed as 0 kPa, 464 kPa, 19 kPa, 84 kPa, and 145 kPa, respectively, while at *FYL*, the contact pressures were 127 kPa, 877 kPa, 145 kPa, 436 kPa, and 206 kPa, respectively.

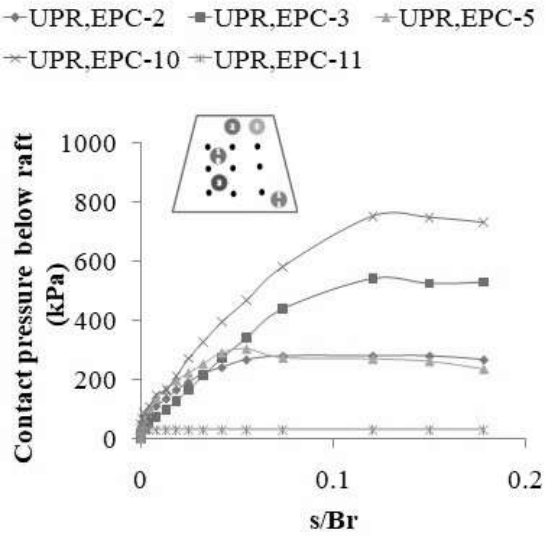

Figure 5-53 : Contact pressure distribution below unpiled raft for different location of earth pressure cells vs. relative settlement characteristics *(I_d = 40%; shape of raft = trapezoidal)*

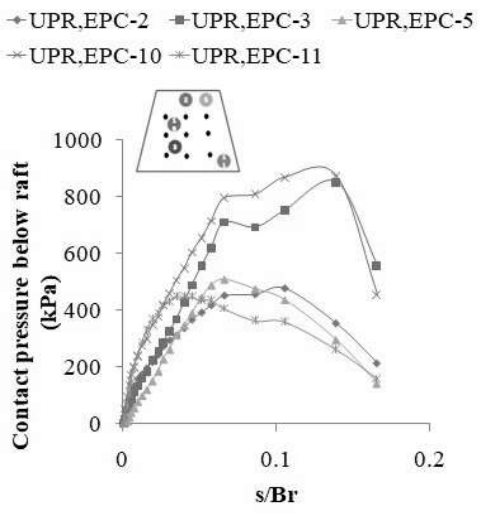

Figure 5-54 : Contact pressure distribution below unpiled raft for different location of earth pressure cells vs. relative settlement characteristics *(I_d = 60%; shape of raft = trapezoidal)*

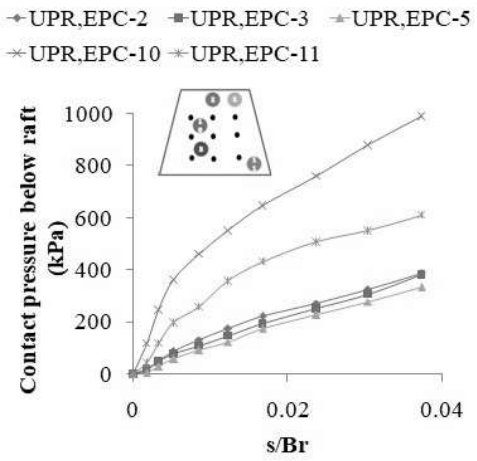

Figure 5-55 : Contact pressure distribution below unpiled raft for different location of earth pressure cells vs. relative settlement characteristics *(I_d = 80%; shape of raft = trapezoidal)*

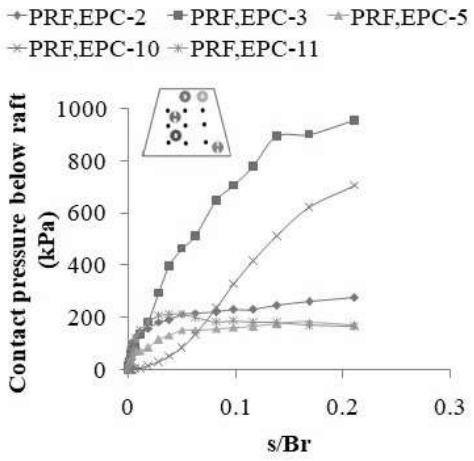

Figure 5-56 : Contact pressure distribution below raft for different location of earth pressure cells in PRF vs. relative settlement characteristics *(I_d = 40%; S = 7d; L/d ratio of pile = 30; d = 9.7 mm; pile group = 3 × 3; shape of raft = trapezoidal)*

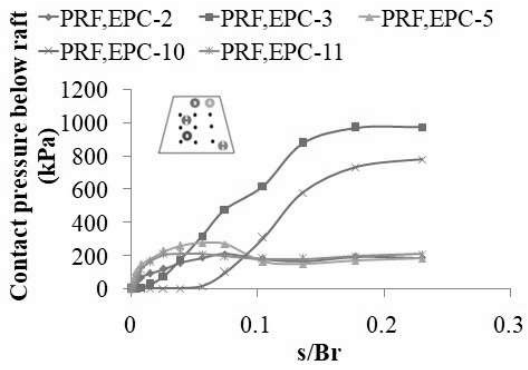

Figure 5-57 : Contact pressure distribution below raft for different location of earth pressure cells in PRF vs. relative settlement characteristics *(I_d = 60%; S = 7d; L/d ratio of pile = 30; d = 9.7 mm; pile group = 3 × 3; shape of raft = trapezoidal)*

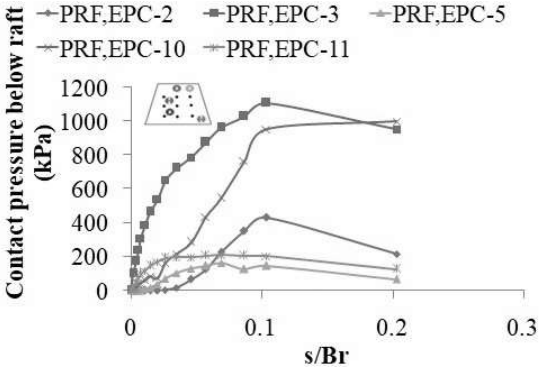

Figure 5-58 : Contact pressure distribution below raft for different location of earth pressure cells in PRF vs. relative settlement characteristics *(I_d = 80%; S = 7d; L/d ratio of pile = 30; d = 9.7 mm; pile group = 3 × 3; shape of raft = trapezoidal)*

Figure 5-59 to Figure 5-64 depicts the contact pressure beneath the square raft of UPR and PRF at different locations. It was observed that in almost all cases, the increase in rate of contact pressure with s/B_r was higher for EPC located nearer to the central portion of the raft and, in some cases, for EPC located nearer to the side of the raft. EPC-2, EPC-5, and EPC-10 readings at I_d = 40% were 153 kPa, 54 kPa, and 35 kPa, respectively, while at *FYL* they were 178 kPa, 70 kPa, and 202 kPa. EPC-2, EPC-5, and EPC-10 readings at I_d = 60% were 172 kPa, 235 kPa, and 151 kPa, respectively, while at *FYL* they were 273 kPa, 265 kPa, and 424 kPa. EPC-2, EPC-5, and EPC-10 readings at I_d = 80% were 71 kPa, 50 kPa, and 637 kPa, respectively, while at *FYL* they were 210 kPa, 251 kPa, and 1232 kPa.

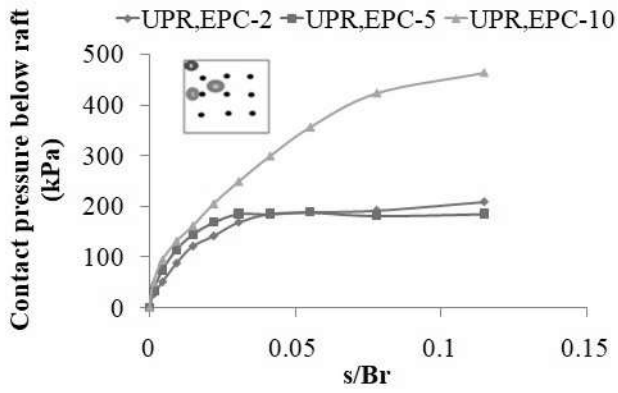

Figure 5-59 : Contact pressure distribution below unpiled raft for different location of earth pressure cells vs. relative settlement characteristics *(I_d = 40%; shape of raft = square)*

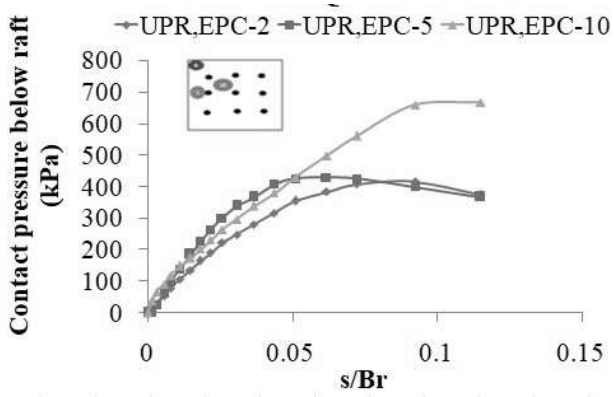

Figure 5-60 : Contact pressure distribution below unpiled raft for different location of earth pressure cells vs. relative settlement characteristics *(I_d = 60%; shape of raft = square)*

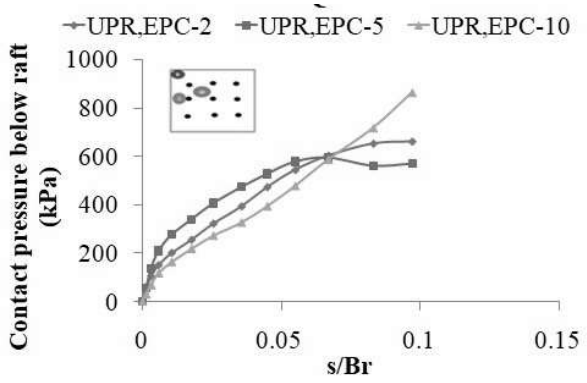

Figure 5-61 : Contact pressure distribution below unpiled raft for different location of earth pressure cells vs. relative settlement characteristics *(I_d = 80%; shape of raft = square)*

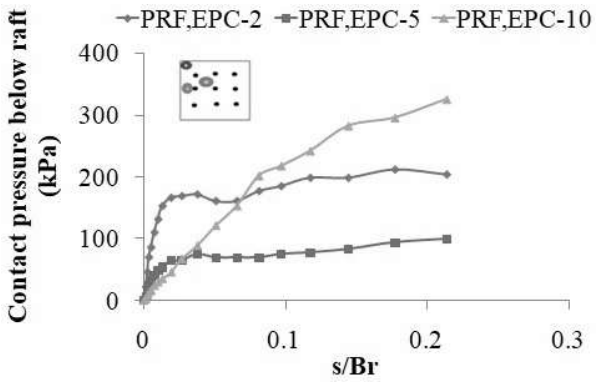

Figure 5-62 : Contact pressure distribution below raft for different location of earth pressure cells in PRF vs. relative settlement characteristics *(I_d = 40%; S = 7d; L/d ratio of pile = 30; d = 9.7 mm; pile group = 3 × 3; shape of raft = square)*

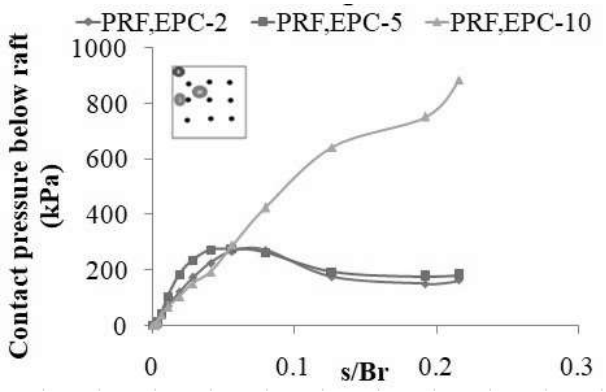

Figure 5-63 : Contact pressure distribution below raft for different location of earth pressure cells in PRF vs. relative settlement characteristics *(I_d = 60%; S = 7d; L/d ratio of pile = 30; d = 9.7 mm; pile group = 3 × 3; shape of raft = square)*

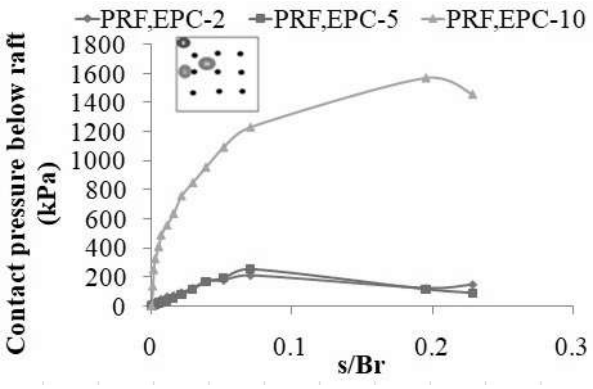

Figure 5-64 : Contact pressure distribution below raft for different location of earth pressure cells in PRF vs. relative settlement characteristics *(I_d = 80%; S = 7d; L/d ratio of pile = 30; d = 9.7 mm; pile group = 3 × 3; shape of raft = square)*

5.3.3.1.3 Load Sharing Mechanism

The load shared by pile groups and rafts in the model piled raft foundation has been calculated as discussed inclause 5.2.7. Figure 5-65 to Figure 5-68 show the load shared by pile group (*LSPG*), load shared by raft (*LSR*), and the total load on model piled raft (PRF) with the circular, rectangular, trapezoidal, and square shape of raft, respectively, at different relative densities of the sand bed. In almost all cases, the *LSPG* is higher in the initial stages of loading, and later on, it becomes smaller compared to the *LSR* at all relative densities of the sand bed. These basic graphs have been further analyzed given the percentage load shared by pile groups and rafts at various relative settlements.

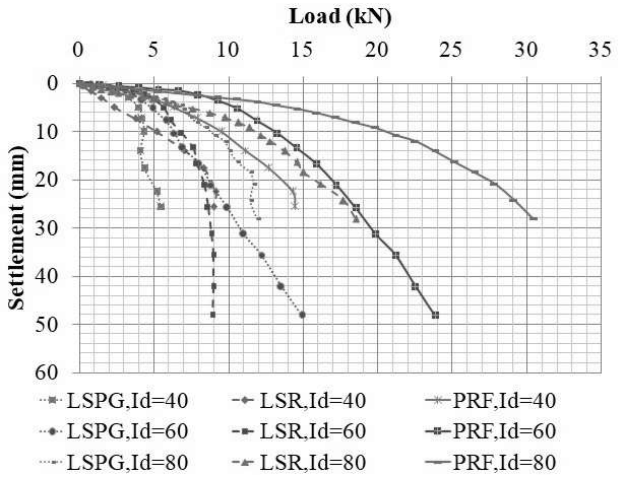

Figure 5-65 : Load settlement characteristics of piled raft and load shared by pile group and raft at different relative densities of sand *(S = 7d; d = 9.7 mm; pile group = 3 × 3; shape of raft = circular)*

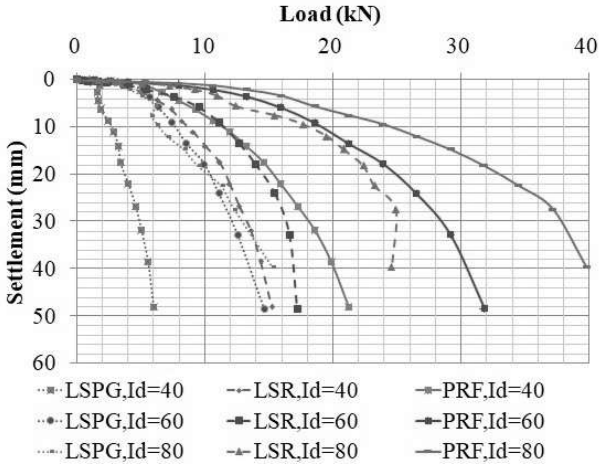

Figure 5-66 : Load settlement characteristics of piled raft and load shared by pile group and raft at different relative densities of sand *(S = 7d; d = 9.7 mm; pile group = 3 × 3; shape of raft = rectangular)*

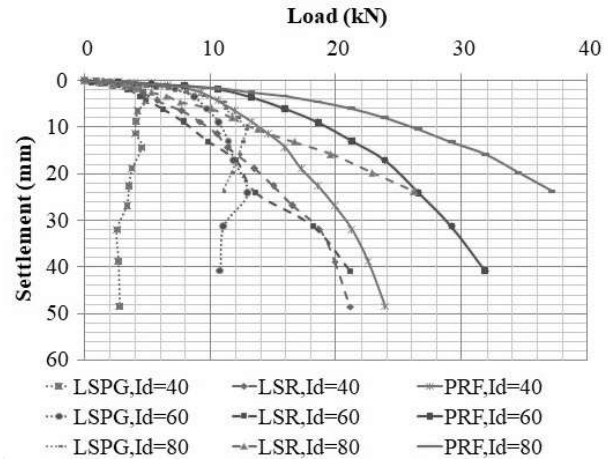

Figure 5-67 : Load settlement characteristics of piled raft and load shared by pile group and raft at different relative densities of sand *(S = 7d; d = 9.7 mm; pile group = 3 × 3; shape of raft = trapezoidal)*

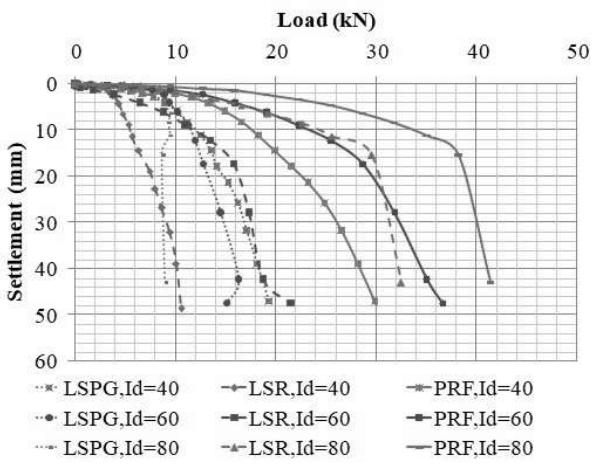

Figure 5-68 : Load settlement characteristics of piled raft and Load sharing by pile group and raft at different relative densities of sand *(S = 7d; d = 9.7 mm; pile group = 3 × 3; shape of raft = square)*

Figure 5-69 to Figure 5-71 demonstrate the percentage load shared by raft (% *LSR*) and pile groups (% *LSPG*) in circular PRF with respect to the relative settlement (s/B_r) for different relative densities. It is observed that at I_d = 40% and 80%, the percentage load shared by the pile group (% *LSPG*) was higher than % *LSR* up to a relative settlement range of s/B_r = 0 to 0.034, and it gradually decreased beyond that point. A similar trend was observed at 60% relative density, where % *LSPG* was higher up to *s/Br* = 0.01, after which it decreased up to *s/Br* = 0.067, and after that increased again compared to %*LSR*. The percentage load shared by the pile group (% *LSPG*) and raft (% *LSR*) was found to be equal (i.e., 50%) at s/B_r = 0.034, 0.01 and 0.067, and 0.02 for 40%, 60%, and 80% relative densities, respectively.

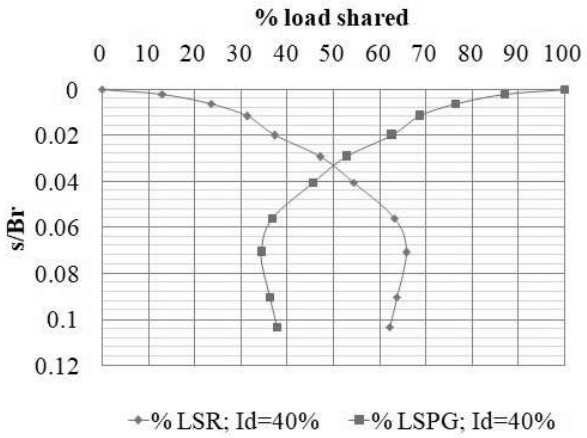

Figure 5-69 : Percentage load shared by pile group (% *LSPG*) and raft (% *LSR*) in circular piled raft vs. relative settlement at 40% relative density of sand bed *(S = 7d; d = 9.7mm; L/d ratio of pile = 30; pile group = 3 × 3)*

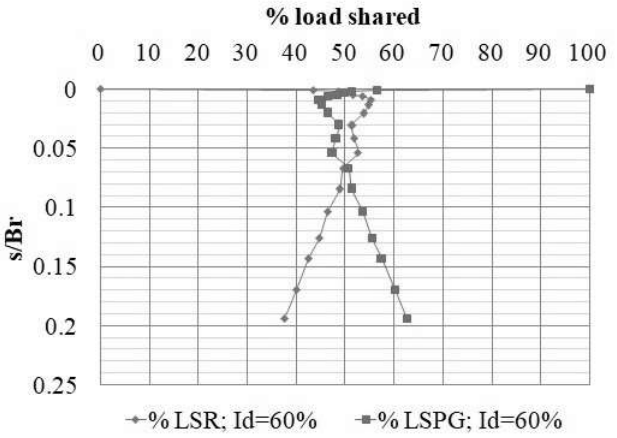

Figure 5-70 : Percentage load shared by pile group (% *LSPG*) and raft (% *LSR*) in circular piled raft vs. relative settlement at 60% relative density of sand bed *(S=7d; d = 9.7mm; L/d ratio of pile = 30; pile group = 3 × 3)*

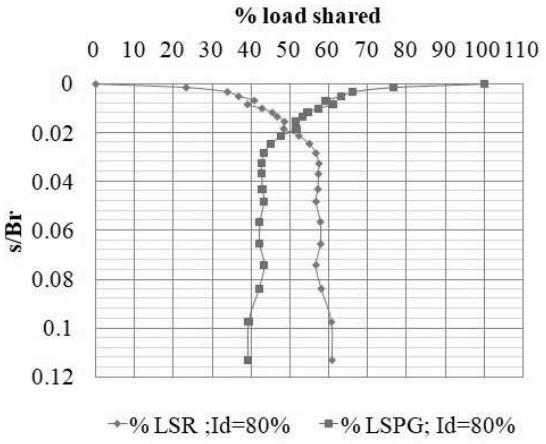

Figure 5-71 : Percentage load shared by pile group(% *LSPG*) and raft (% *LSR*) in circular piled raft vs. relative settlement at 80% relative density of sand bed *(S = 7d; d = 9.7 mm; L/d ratio of pile = 30; pile group = 3 × 3)*

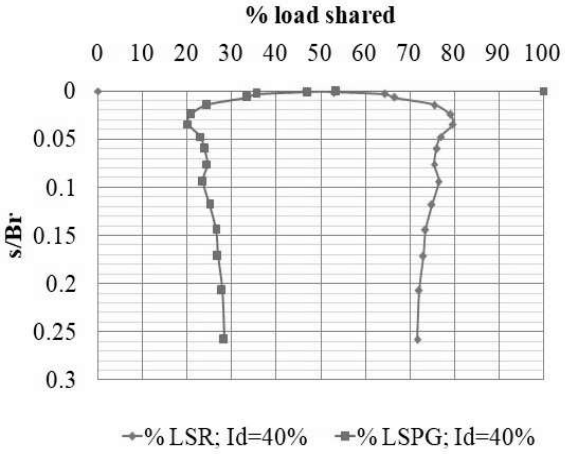

Figure 5-72 : Percentage load shared by pile group (% *LSPG*) and raft (% *LSR*) in rectangular piled raft vs. relative settlement at 40% relative density of sand bed *(S = 7d; d = 9.7 mm; L/d ratio of pile = 30; pile group = 3 × 3)*

Figure 5-72 to Figure 5-74 depict the variation in percentage load shared by the raft and pile groups in rectangular PRF based on relative settlement (s/B_r) at 40%, 60%, and 80% relative densities, respectively. It can be observed that the percentage load shared by the pile group (% *LSPG*) is higher at the very initial range of relative settlement (s/B_r = 0 to 0.02) and gradually decreases at all relative densities. The % load shared by the pile group (% *LSPG*) and raft (% *LSR*) was equal (i.e., 50%) at s/B_r = 0.001, 0.02, and 0.001 for I_d = 40%, 60%, and 80%, respectively.

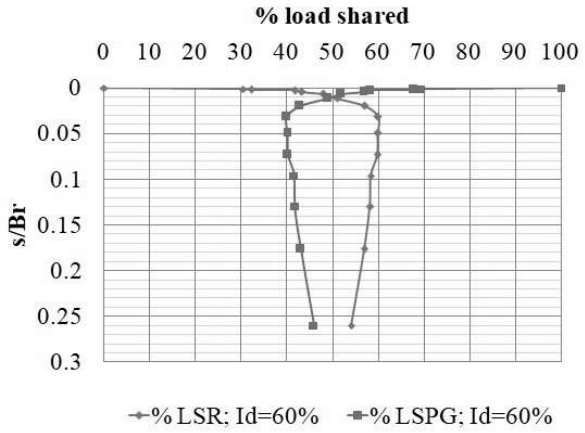

Figure 5-73 : Percentage load shared by pile group(% *LSPG*) and raft (% *LSR*) in rectangular piled raft vs. relative settlement at 60% relative density of sand bed *(S = 7d; d = 9.7 mm; L/d ratio of pile = 30; pile group = 3 × 3)*

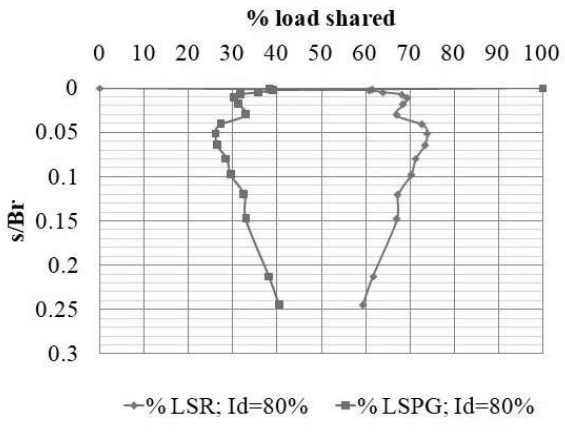

Figure 5-74 : Percentage load shared by pile group(% *LSPG*) and raft (% *LSR*) in rectangular piled raft vs. relative settlement at 80% relative density of sand bed *(S = 7d; d = 9.7 mm; L/d ratio of pile = 30; pile group = 3 × 3)*

Figure 5-75 to Figure 5-77 show the variation in percentage load shared by raft and pile groups in trapezoidal PRF with respect to relative settlement (s/B_r) at 40%, 60%, and 80% relative densities of the sand bed, respectively. It observed that at all relative densities of the sand bed, the % load shared by the pile group (% *LSPG*) was higher than % *LSR* at the initial range of relative settlement (up to s/B_r = 0.01, 0.07, and 0.04 for I_d = 40%, 60%, and 80%, respectively), and gradually it decreased.

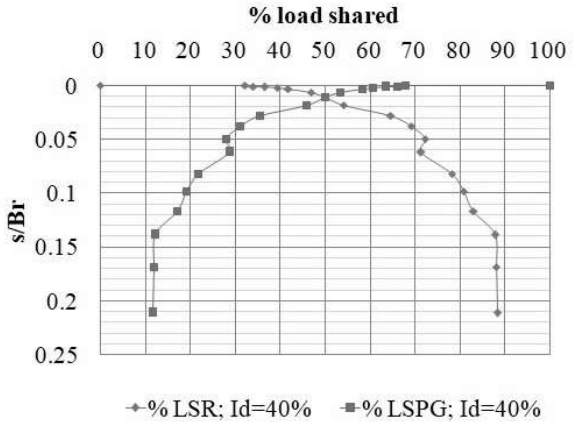

Figure 5-75 : Percentage load shared by pile group (% *LSPG*) and raft (% *LSR*) in trapezoidal piled raft vs. relative settlement at 40% relative density of sand bed *(S = 7d; d = 9.7mm; L/d ratio of pile = 30; pile group = 3 × 3)*

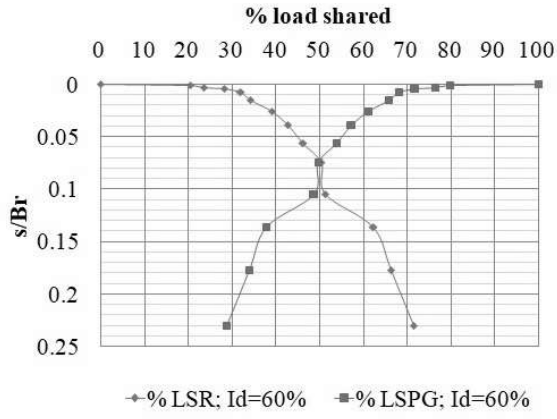

Figure 5-76 : Percentage load shared by pile group (% *LSPG*) and raft (% *LSR*) in trapezoidal piled raft vs. relative settlement at 60% relative density of sand bed *(S = 7d; d = 9.7mm; L/d ratio of pile = 30; pile group = 3 × 3)*

Figure 5-78 to Figure 5-80 illustrate the percentage of load shared by raft and pile groups in a square PRF with respect to the relative settlement (s/B_r) at I_d = 40%, 60%, and 80%. It was observed that at I_d = 40%, the pile group shared a higher percentage of the load (% *LSPG*) than the raft (% *LSR*) at all relative settlements. At I_d = 60%, the % *LSPG* ranged from 100% to 50% for s/B_r = 0 to 0.04, and then from 50% to 45% for s/B_r = 0.04 to 0.08, and after that, it remained almost constant for further relative settlement. When I_d = 80%, the % *LSPG* was less than the % *LSR* at all relative settlements, ranging from 15% to 40% for s/B_r = 0 to 0.02. The % *LSPG* decreased from 40% to 22% within the range of s/B_r = 0.02 to 0.07 and then remained almost constant for further relative settlement.

The *LSR* and *LSPG* at *IYL* and *FYL* of PRF with the circular, rectangular, trapezoidal, and square shape of the raft at different relative densities are demonstrated in Figure 5-81 to Figure 5-88, respectively.The *LSR* at *IYL* and *FYL* increased as the relative density of the sand bed increased. At *IYL*, the value of *LSPG* was higher than the *LSR* in all shapes of PRF at all relative densities, except in rectangular and square-piled rafts at 80% relative density. The *IYL* of PRF with a circular raft was the lowest among all the shapes considered in this study.

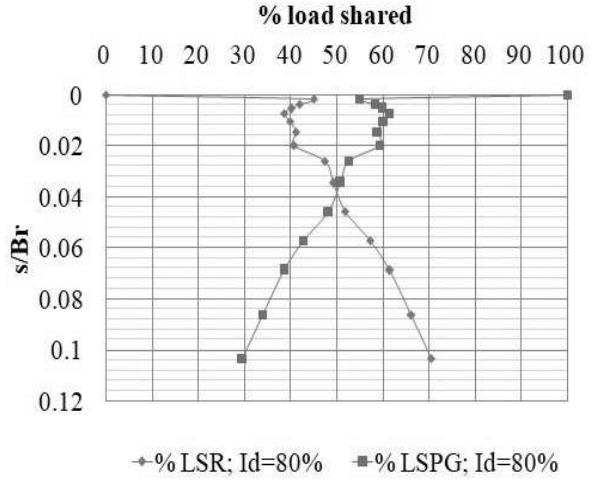

Figure 5-77 : Percentage load shared by pile group (% *LSPG*) and raft (% *LSR*) in trapezoidal piled raft vs. relative settlement at 80% relative density of sand bed *(S = 7d; d = 9.7 mm; L/d ratio of pile = 30; pile group = 3 × 3)*

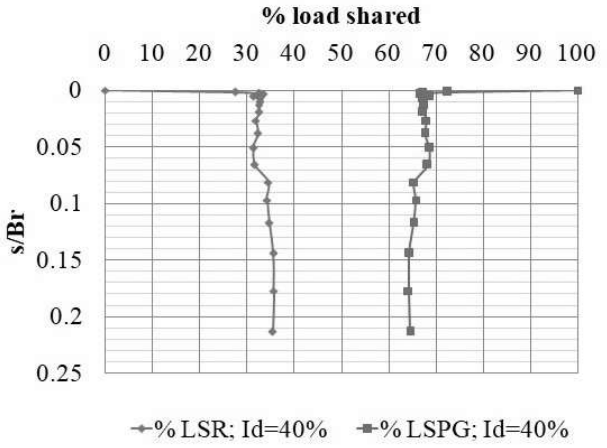

Figure 5-78 : Percentage load shared by pile group (% *LSPG*) and raft (% *LSR*) in square piled raft vs. relative settlement at 40% relative density of sand bed *(S = 7d; d = 9.7mm; L/d ratio of pile = 30; pile group = 3 × 3)*

The *LSR* at *IYL* of circular PRF increased by 3.84 kN and 4.55 kN at 60% and 80% relative densities of sand, respectively, compared to 40% relative density. i.e., in percentage, 309% and 366%, respectively. At the *IYL* of rectangular PRF, the values of *LSR* at 60% and 80% relative density were 1.89 kN and 7.38 kN higher than the *LSR* at 40% relative density of the sand bed, i.e., in percentages of 53% and 209%, respectively. The values of *LSR* of trapezoidal PRF at 60% and 80% relative densities of sand beds were 0.81 kN and 2.82 kN higher than the *LSR* at 40% relative densities of sand beds, respectively. i.e., in percentages of 22% and 76%, respectively. In the case of square PRF, the values of *LSR* at *IYL* for 60% and 80% relative densities were found to be 5.1 kN and 9.8 kN higher than the values at 40% relative density of the sand bed, i.e., in percentages of 135% and 260%, respectively.

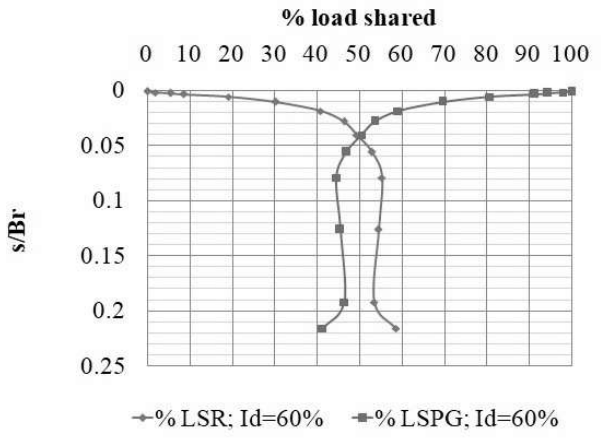

Figure 5-79 : Percentage load shared by pile group (% *LSPG*) and raft (% *LSR*) in square piled raft vs. relative settlement at 60% relative density of sand bed *(S = 7d; d = 9.7mm; L/d ratio of pile = 30; pile group = 3 × 3)*

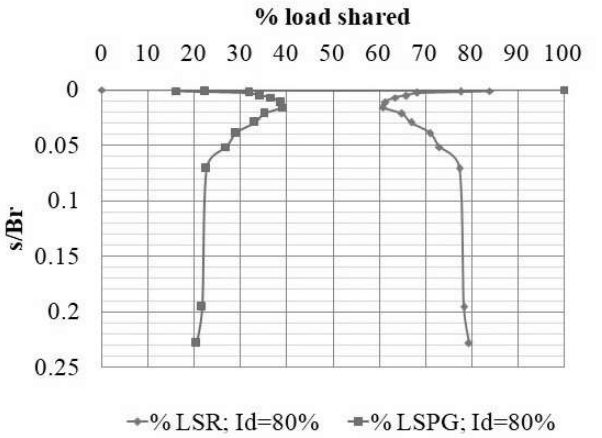

Figure 5-80 : Percentage load shared by pile group (% *LSPG*) and raft (% *LSR*) in square piled raft vs. relative settlement at 80% relative density of sand bed *(S = 7d; d = 9.7mm; L/d ratio of pile = 30; pile group = 3 × 3)*

The *LSR* at *FYL* of circular PRF increased by 3.55 kN and 7.81 kN at 60% and 80% relative densities of sand, respectively, compared to 40% relative density. i.e., in percentage, 82% and 180%, respectively. At *FYL* of rectangular PRF, the values of *LSR* at 60% and 80% relative density were found to be 3.93 kN and 12.39 kN higher than the *LSR* at 40% relative density of the sand bed. i.e., in percentages of 39% and 124%, respectively. The values of *LSR* of trapezoidal PRF at 60% and 80% relative densities of sand beds were 0.66 kN and 5.34 kN higher than the *LSR* at 40% relative densities of sand beds, respectively. i.e., in percentages of 6% and 47%, respectively. In the case of square PRF, the values of *LSR* at *IYL* for 60% and 80% relative densities were found to be 8.42 kN and 22.15 kN higher than the values at 40% relative density of the sand bed. i.e., in percentages of 113% and 297%, respectively.

As the relative density of sand increased, The *LSPG* at *IYL* of circular and trapezoidal PRF also increased. The *LSPG* at *IYL* of circular PRF increased by 0.67 kN and 2.61 kN at 60% and 80% relative densities of sand, respectively, compared to 40% relative density, i.e., in percentage, 19%, and 74%. The *LSPG* at *IYL* of trapezoidal PRF increased by 4.5 kN and 5.15 kN at 60% and 80% relative densities of sand, respectively, compared to 40% relative density, i.e., in

percentage, 106% and 121%. The *LSPG* at *IYL* of square and rectangular PRF increased at 60% relative density compared to 40% relative density and decreased at 80% relative density compared to 60% relative density of sand. The *LSPG* at *IYL* of square PRF increased by 2.41 kN and 0.9 kN at 60% and 80% relative densities of sand, respectively, compared to 40% relative density, i.e., in percentage, 31%, and 11%. The *LSPG* at *IYL* of rectangular PRF increased by 3.42 kN and 3.24 kN at 60% and 80% relative densities of sand, respectively, compared to 40% relative density, i.e., in percentage, 193% and 182%.

As the relative density of sand increased, the *LSPG* at *FYL* of circular and trapezoidal PRF also increased. The *LSPG* at *FYL* of circular PRF increased by 2.81 kN and 3.86 kN at 60% and 80% relative densities of sand, respectively, compared to 40% relative density. i.e., in percentage, 54% and 74%, respectively. The *LSPG* at *FYL* of trapezoidal PRF increased by 7.3 kN and 7.94 kN at 60% and 80% relative densities of sand, respectively, compared to 40% relative density. i.e., in percentage, 160% and 174%, respectively. The *LSPG* at *FYL* of square PRF decreased with an increase in the relative density of sand. The *LSPG* at *FYL* of square PRF decreased by 1.31 kN and 5.48 kN at 60% and 80% relative densities of sand, respectively, compared to 40% relative density. i.e., in percentage, 9% and 39%, respectively. The *LSPG* at *FYL* of rectangular PRF increased at 60% relative density compared to 40% relative density, while it decreased at 80% relative density compared to 60% relative density of sand. The *LSPG* at *FYL* of rectangular PRF increased by 6.69 kN and 6.2 kN at 60% and 80% relative densities of sand, respectively, compared to 40% relative density. i.e., in percentage, 206% and 191%, respectively.

At 40% relative density of the sand bed, we found that the *LSR* at *IYL* of square, rectangular, and trapezoidal PRF was 203%, 184%, and 199% higher than the *LSR* at *IYL* of circular PRF. At 40% relative density of the sand bed, the *LSPG* at *IYL* of square and trapezoidal PRF was123% and 20% more than the *LSPG* at *IYL* of circular PRF, respectively, while for rectangular PRF, it was 50% less than the circular PRF. At 40% relative density of the sand bed, the *LSR* at *FYL* of square, rectangular, and trapezoidal PRF was 72%, 132%, and 163% higher than the *LSR* at *FYL* of circular PRF. At 40% relative density of the sand bed, the *LSPG* at *FYL* of square PRF was

171% more than the *LSPG* at *FYL* of circular PRF, while for rectangular and trapezoidal PRF, it was 38% and 12% less than the circular PRF, respectively.

At 60% relative density of sand bed, the *LSR* at *IYL* of square and rectangular PRF was 75% and 7% more than the *LSR* at *IYL* of circular PRF, respectively, while for trapezoidal PRF, it was 11% less than the circular PRF.The *LSPG* at *IYL* of square, rectangular, and trapezoidal PRF was 144%, 24%, and 108% more than the *LSPG* at *IYL* of circular PRF at a relative density of 60% in the sand bed. The *LSR* at *FYL* of square, rectangular, and trapezoidal PRF was 102%, 77%, and 53% more than the *LSR* at *FYL* of circular PRF at a relative density of 60% in the sand bed. The *LSPG* at *FYL* of square, rectangular, and trapezoidal PRF was 60%, 24%, and 48% more than the *LSPG* at *IYL* of circular PRF at a relative density of 60% in the sand bed.

At 80% relative density of the sand bed, we found that the *LSR* at *IYL* of square, rectangular, and trapezoidal PRF was 134%, 88%, and 13% higher than the *LSR* at *IYL* of circular PRF. At 80% relative density of the sand bed, the *LSPG* at *IYL* of square and trapezoidal PRF was 43% and 53% more than the *LSPG* at *IYL* of circular PRF, respectively, while for rectangular PRF, it was 18% less than the circular PRF. At 80% relative density of the sand bed, the *LSR* at *FYL* of square, rectangular, and trapezoidal PRF was 144%, 85%, and 38% higher than the *LSR* at *FYL* of circular PRF. At 80% relative density of the sand bed, the *LSPG* at *FYL* of square PRF was 5% less than the *LSPG* at *FYL* of circular PRF, while for rectangular and trapezoidal PRF, it was 4% and 38% more than the circular PRF, respectively.

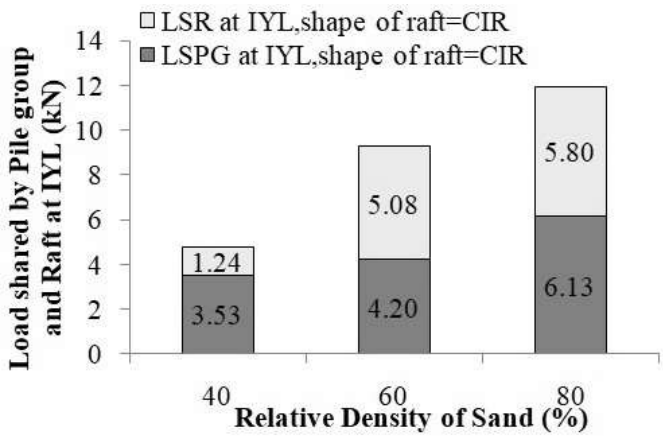

Figure 5-81 : Load shared by pile group and raft at *IYL* of piled raft foundation for configuration of piles at different relative densities of sand bed *(S = 7d; d = 9.7 mm; pile group = 3 × 3; shape of raft = circular)*

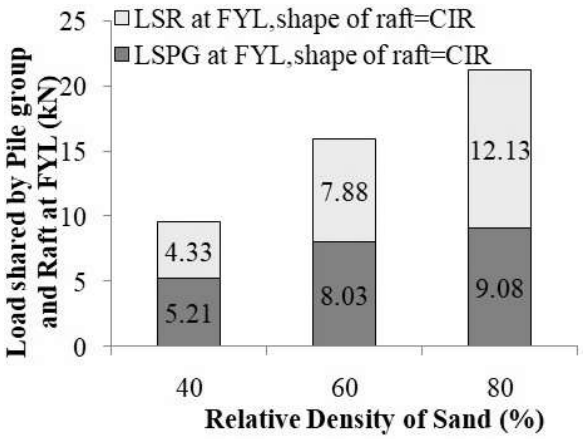

Figure 5-82 : Load shared by pile group and raft at *FYL* of piled raft foundation for configuration of piles at different relative densities of sand bed *(S = 7d; d = 9.7 mm; pile group = 3 × 3; shape of raft = circular*)

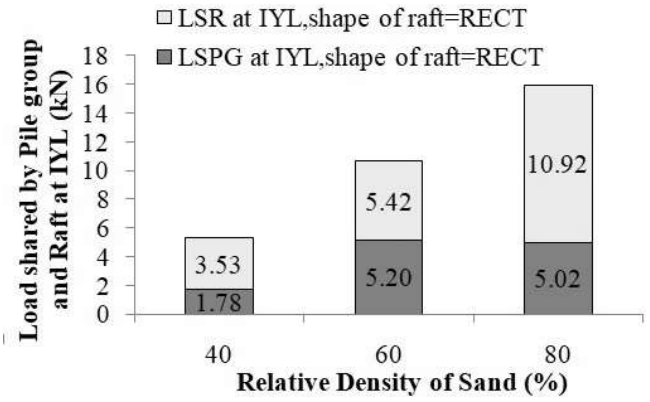

Figure 5-83 : Load shared by pile group and raft at *IYL* of piled raft foundation for configuration of piles at different relative densities of sand bed *(S = 7d;d = 9.7 mm; pile group = 3 × 3; shape of raft = rectangular)*

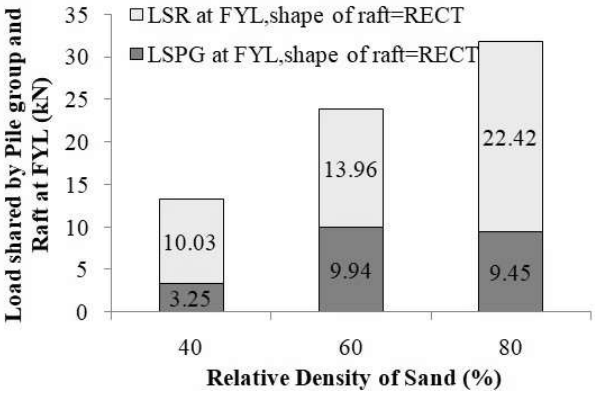

Figure 5-84 : Load shared by pile group and raft at *FYL* of piled raft foundation for configuration of piles at different relative densities of sand bed *(S = 7d; d = 9.7 mm; pile group = 3 × 3; shape of raft = rectangular)*

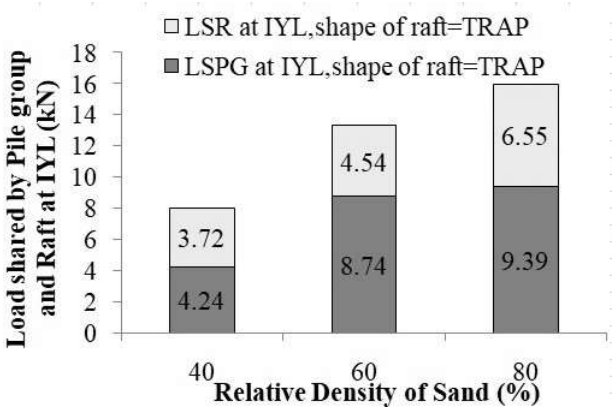

Figure 5-85 : Load shared by pile group and raft at *IYL* of piled raft foundation for configuration of piles at different relative densities of sand bed *(S = 7d; d = 9.7mm; pile group = 3 × 3; shape of raft = trapezoidal)*

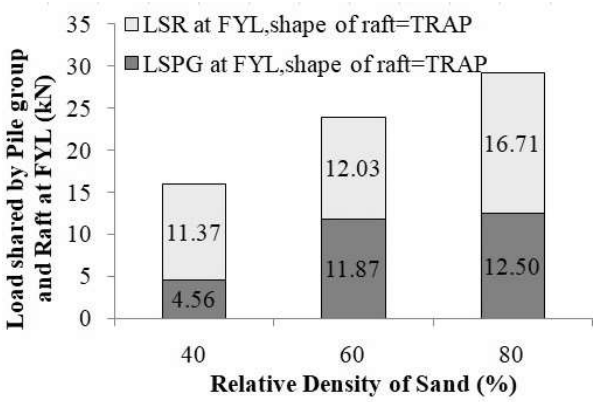

Figure 5-86 : Load shared by pile group and raft at *FYL* of piled raft foundation for configuration of piles at different relative densities of sand bed *(S = 7d; d = 9.7 mm; pile group = 3 × 3; shape of raft = trapezoidal)*

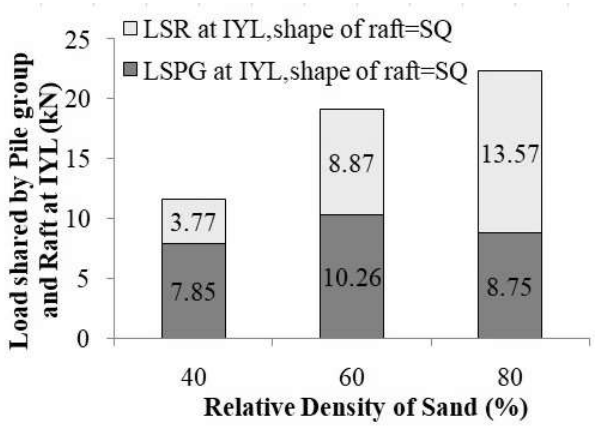

Figure 5-87 : Load shared by pile group and raft at *IYL* of piled raft foundation for configuration of piles at different relative densities of sand bed *(S = 7d; d = 9.7mm; pile group = 3 × 3; shape of raft = square)*

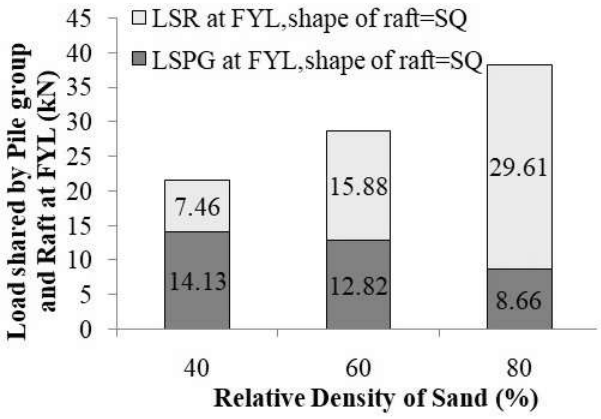

Figure 5-88 : Load shared by pile group and raft at *FYL* of piled raft foundation for configuration of piles at different relative densities of sand bed *(S = 7d; d = 9.7 mm; pile group = 3 × 3; shape of raft = square)*

5.3.3.1.4 Piled Raft Coefficient (α_p)

Figure 5-89 to Figure 5-92 depict the relationship between the Piled Raft Coefficient (α_p) and the relative settlement (s/B_r) characteristics of a piled raft foundation with various shapes of the raft, including circular, rectangular, trapezoidal, and square, at different relative densities of the sand bed. It was observed that α_p decreased with an increase in s/B_r. Additionally, it was noticed that the rate of change in α_p was more significant in the initial range of s/B_r, and after a certain value of s/B_r, this rate became very small. At I_d = 40%, the value of s/B_r after which the rate of change in α_p became very small was 0.05 for circular, 0.05 for rectangular, 0.14 for trapezoidal piled raft, and 0.01 for square piled raft. At I_d = 60%, the rate of change of α_p was more up to s/B_r = 0.02, 0.02, 0.05, and 0.05 in circular, rectangular, trapezoidal, and square PRF, respectively. At I_d = 80%, the rate of change of α_p was more up to s/B_r = 0.03, 0.05, 0.1, and 0.07 in circular, rectangular, trapezoidal, and square PRF, respectively.

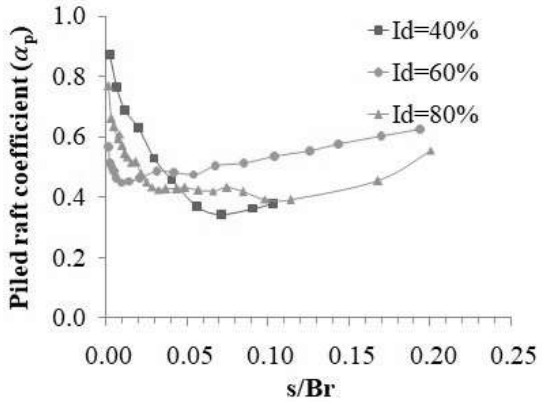

Figure 5-89 : Piled raft coefficient (α_p) vs. relative settlement characteristics of piled raft foundation at different relative densities of sand bed *(S = 7d; d = 9.7 mm; pile group = 3 × 3; shape of raft = Circular)*

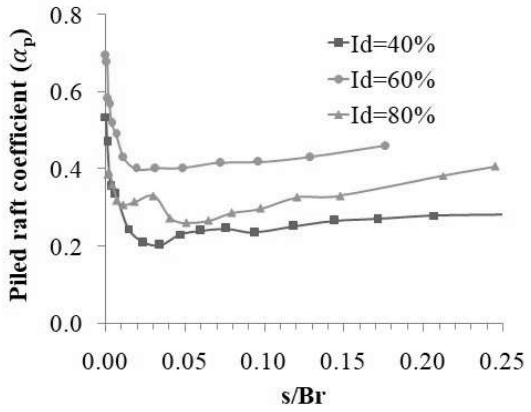

Figure 5-90 : Piled raft coefficient (α_p) vs. relative settlement characteristics of piled raft foundation at different relative densities of sand bed *(S = 7d; d = 9.7 mm; pile group = 3 × 3; shape of raft = Rectangular)*

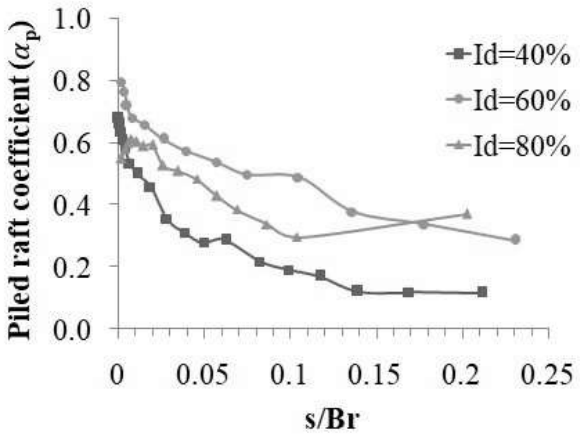

Figure 5-91 : Piled raft coefficient (α_p) vs. relative settlement characteristics of piled raft foundation at different relative densities of sand bed *(S = 7d; d = 9.7 mm; pile group = 3 × 3; shape of raft = Trapezoidal)*

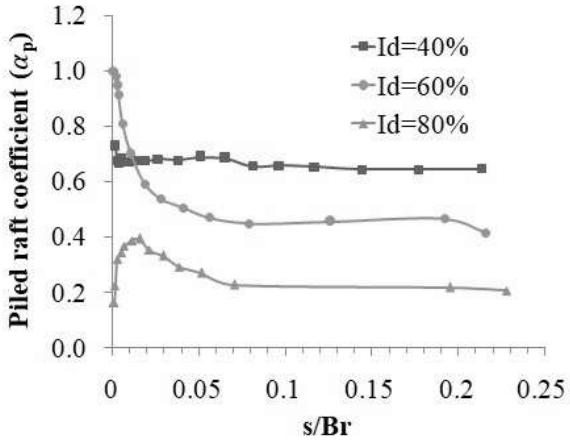

Figure 5-92 : Piled raft coefficient (α_p) vs. relative settlement characteristics of piled raft foundation at relative densities of sand bed *(S = 7d; d = 9.7 mm; pile group = 3 × 3; shape of raft = Square)*

5.3.3.1.5 Settlement Reduction Ratio (SRR) and Load Improvement Ratio (LIR)

Table 5-14 represents the settlement reduction ratio of PRF with a circular raft at different load levels and 40%, 60%, and 80% relative densities of the sand bed. It can observed that at 40% relative density, the range of settlement reduction in PRF as compared to UPR was 20% to 34% up to 5 kN load, and at 10 kN load, the UPR failed, so the *SRR* has not found at the higher load level. The range of *SRR* at 60% relative density was 30% to 52%, and at 80% relative density, it was 7% to 29%.

Table 5-14 Settlement reduction ratio of PRF with a circular raft at different load levels and relative densities of the sand bed

I_d	Load (kN)	Settlement (mm)		Settlement reduction ratio (%)
		UPR	PRF (CIR)	PRF (CIR)
40%	2.5	1.69	1.12	34
	5	4.01	3.21	20
	10	-	11.12	-
	12.5	-	17.08	-
	15	-	26.56	-
60%	2.5	0.82	0.50	39
	5	2.39	1.14	52
	10	8.09	4.40	46
	12.5	12.64	8.86	30
	15	27.26	14.42	47
80%	2.5	0.43	0.40	7
	5	1.35	1.24	8
	10	4.05	3.13	23
	12.5	5.74	4.15	28
	15	7.86	5.54	29

The load improvement ratio of PRF with a circular raft at various sand bed settlement levels and relative densities is shown in Table 5-15. At 40% relative density, it was found that as the settlement level increased, the load improvement ratio also increased, and the range of *LIR* was found to be 1.1 to 1.67. The range of *LIR* was found to be 1.15 to 1.36 and 1.21 to 2.31 at 60% and 80% relative densities of the sand bed, respectively.

Table 5-15 Load improvement ratio of PRF with a circular raft at different settlement levels and relative densities of the sand bed

I_d	Settlement (mm)	Load (kN)		Load improvement ratio
		UPR	PRF (CIR)	PRF (CIR)
40%	5.5	6.10	6.71	1.10
	11	8.97	9.95	1.11
	16.5	9.28	12.25	1.32
	22	9.28	14.17	1.53
	27.5	9.28	15.53	1.67
60%	5.5	8.11	10.76	1.33
	11	11.72	13.54	1.16
	16.5	13.80	15.83	1.15
	22	13.90	17.49	1.26
	27.5	13.90	18.97	1.36
80%	5.5	12.18	14.94	1.23
	11	17.80	21.51	1.21
	16.5	21.46	31.19	1.45
	22	23.33	39.55	1.70
	27.5	20.15	46.58	2.31

Table 5-16 represents the settlement reduction ratio of PRF with a rectangular raft at different load levels and relative densities of the sand bed. The range of *SRR* was 1% to 74%, 18% to 36%, and 36% to 47% at I_d = 40%, 60%, and 80%, respectively.

Table 5-16 Settlement reduction ratio of PRF with a rectangular raft at different load levels and relative densities of the sand bed

I_d	Load (kN)	Settlement (mm)		Settlement reduction ratio (%)
		UPR	PRF (RECT)	PRF (RECT)
40%	2.5	0.85	0.22	74
	5	2.58	1.06	59
	10	7.51	7.43	1
	12.5	12.28	12.00	2
	15	26.97	18.89	30
60%	2.5	0.23	0.19	18
	5	0.71	0.50	29
	10	3.03	1.94	36
	12.5	4.61	3.17	31
	15	6.54	5.07	22
80%	2.5	0.44	0.28	36
	5	0.82	0.45	45
	10	2.37	1.25	47
	12.5	3.55	1.89	47
	15	4.94	2.94	40

Table 5-17 represents the load improvement ratio of PRF with a rectangular raft at different settlement levels and relative densities of the sand bed. The range of *LIR* was 0.99 to 1.16, 1.02 to 1.37, and 1 to 1.85 at 40%, 60%, and 80% relative density of sand bed, respectively.

Table 5-17 Load improvement ratio of PRF with a rectangular raft at different settlement levels and relative densities of the sand bed

I_d	Settlement (mm)	Load (kN)		Load improvement ratio
		UPR	PRF (RECT)	PRF (RECT)
40%	5.5	8.41	8.68	1.03
	11	12.04	11.88	0.99
	16.5	14.07	14.19	1.01
	22	14.65	15.93	1.09
	27.5	15.04	17.44	1.16
60%	5.5	13.76	15.50	1.13
	11	19.27	19.72	1.02
	16.5	22.55	23.04	1.02
	22	15.05	25.67	1.71
	27.5	20.15	27.60	1.37
80%	5.5	15.97	18.44	1.15
	11	24.08	25.45	1.06
	16.5	30.60	30.55	1.00
	22	33.81	34.26	1.01
	27.5	20.15	37.19	1.85

Table 5-18 represents the settlement reduction ratio of PRF with a trapezoidal raft at different load levels and relative densities of the sand bed. The range of *SRR* was 27% to 69%, 32% to 57%, and 2 to 29% at 40%, 60% and 80% relative densities of sand bed, respectively.

Table 5-18 Settlement reduction ratio of PRF with a trapezoidal raft at different load levels and relative densities of the sand bed

I_d	Load (kN)	Settlement (mm)		Settlement reduction ratio (%)
		UPR	PRF (TRAP)	PRF (TRAP)
40%	2.5	0.28	0.20	27
	5	1.66	0.52	69
	10	6.63	3.47	48
	12.5	10.93	7.46	32
	15	20.35	12.28	40
60%	2.5	0.67	0.34	49
	5	1.25	0.69	45
	10	3.86	1.67	57
	12.5	5.62	3.00	47
	15	7.56	5.14	32
80%	2.5	0.40	0.35	12
	5	0.80	0.78	2
	10	2.10	1.58	24
	12.5	3.05	2.22	27
	15	4.28	3.04	29

Table 5-19 shows the load improvement ratio of PRF with a trapezoidal raft at different settlement levels and relative densities of the sand bed. The range of *LIR* was 1.15 to 1.26, 1.08 to 1.38, and 1.02 to 1.82 at 40%, 60%, and 80% relative density of sand bed, respectively.

Table 5-19 Load improvement ratio of PRF with a trapezoidal raft at different settlement levels and relative densities of the sand bed

I_d	Settlement (mm)	Load (kN)		Load improvement ratio
		UPR	PRF (TRAP)	PRF (TRAP)
40%	5.5	9.11	11.34	1.24
	11	12.53	14.40	1.15
	16.5	14.44	16.57	1.15
	22	15.20	18.36	1.21
	27.5	15.89	20.08	1.26
60%	5.5	12.30	15.37	1.25
	11	18.45	19.90	1.08
	16.5	21.81	23.49	1.08
	22	23.24	25.76	1.11
	27.5	20.15	27.81	1.38
80%	5.5	16.82	20.33	1.21
	11	25.14	27.05	1.08
	16.5	31.59	32.32	1.02
	22	33.59	35.98	1.07
	27.5	20.15	36.75	1.82

Table 5-20 represents the settlement reduction ratio of PRF with a square raft at different load levels and relative densities of the sand bed. The range of *SRR* was 50% to 86%,46% to 68%, and 30% to 66% at 40%, 60% and 80% relative density of sand bed, respectively.

Table 5-20 Settlement reduction ratio of PRF with a square raft at different load levels and relative densities of the sand bed

I_d	Load (kN)	Settlement (mm)		Settlement reduction ratio (%)
		UPR	PRF (SQ)	PRF (SQ)
40%	2.5	0.90	0.45	50
	5	2.97	0.79	74
	10	10.73	2.22	79
	12.5	25.30	3.60	86
	15	30.36	5.96	80
60%	2.5	0.62	0.33	46
	5	1.62	0.62	62
	10	4.42	1.43	68
	12.5	6.13	2.24	64
	15	8.54	3.58	58
80%	2.5	0.21	0.15	30
	5	0.50	0.27	46
	10	1.73	0.65	62
	12.5	2.85	1.09	62
	15	4.14	1.40	66

Table 5-21 shows the load improvement ratio of PRF with a square raft at different settlement levels and relative densities of the sand bed. The range of *LIR* was 1.78 to 2.05, 1.40 to 1.58, and 1.26 to 1.97 at 40%, 60%, and 80% relative density of sand bed, respectively.

Table 5-21 Load improvement ratio of PRF with a square raft at different settlement levels and relative densities of the sand bed

I_d	Settlement (mm)	Load(kN)		Load improvement ratio
		UPR	PRF (SQ)	PRF (SQ)
40%	5.5	7.11	14.56	2.05
	11	10.12	18.17	1.80
	16.5	11.76	20.93	1.78
	22	12.25	23.51	1.92
	27.5	13.59	25.38	1.87
60%	5.5	11.69	18.07	1.55
	11	17.06	24.27	1.42
	16.5	20.08	28.14	1.40
	22	20.84	30.11	1.44
	27.5	20.15	31.79	1.58
80%	5.5	17.23	26.93	1.56
	11	25.13	34.73	1.38
	16.5	30.45	38.38	1.26
	22	29.42	39.02	1.33
	27.5	20.15	39.66	1.97

5.3.3.1.6 Prediction of IYL and FYL

Interaction of the pile, soil, and raft is the key factor considered in designing the piled raft foundation. The efficient use of the interaction leads to end up with the economical design**.** The load settlement characteristic of raft in case of unpiled raft and piled raft foundation was found different and it is required to understand the pile-raft interaction which is responsible for this.

The load-carrying mechanism of piles causes variations in the load response of rafts in PRF by the pile-raft interaction. To reduce the contact pressure between rafts and underlying soils with lower load-carrying capacities, the mobilization of pile skin friction causes the surrounding soils to shift downward. The load capacity of rafts in PRF (LSR) can be expressed in terms of the load capacity of UPR (P_r) at same settlement as follows, introducing the Pile - Raft interaction effect by introducing efficiency factor of raft in PRF(C) :

$$(LSR) = C * (P_r) \qquad (5\text{-}11)$$

Liu et al. (1985) and Long (1993) suggested that the coefficient value C for sandy soils is close to one. However, in their centrifuge test results, Fioravante and Giretti (2010) discovered that the value of C is less than one, and that the load capacity of rafts is less than that of UPR. This implies that utilizing C without being cautious may lead to an unconservative approach. In present study this efficiency factor of raft in PRF at *IYL* has been denoted by C_1 and at *FYL* by C_3.

The load capacity of piles in PRF $(LSPG)$ can be obtained from the load capacity of PG $\left(P_{pg}\right)$ considering the raft-pile interaction effect by introducing efficiency factor of pile group in PRF C' as follows:

$$(LSPG) = C' * \left(P_{pg}\right) \qquad (5\text{-}12)$$

According to Katzenbach et al. (2000), the raft-pile interaction has a positive and negative impact on the load response of piles concerning their load-carrying capacity. The rise in confining stress within the soil due to raft pressure is what causes the beneficial effect, which is an increase in pile skin friction (Long, 1993; Franke et al., 2000; and Katzenbach et al., 2000). Increasing confining stress may have different effects based on the position of piles and raft's stress level. Plastic flow happens, and the shear tension at the pile-soil interface may drop if the soil beneath the raft fails due to a high raft load. It is unlikely that the soil below the raft will completely fail under normal design loads, so the effects of increasing confining stress are still relevant. However, because the soil under the raft is forced to move downwards under load, there is less mobilization of pile skin friction due to reduced relative displacement between the piles and the surrounding soil (Han and Ye, 2006). In present study this efficiency factor of pile group in PRF at *IYL* has been denoted by C_2 and at *FYL* by C_4.

To develop a relation between load carrying capacity of PRF, UPR, and PG following steps has been followed.

1. The total load on PRF at a particular settlement is taken as sum of *LSR* and *LSPG* at that particular settlement (equation (5-13)). *IYL* can be taken as the addition of $(LSR)_{s_i}$ and $(LSPG)_{s_i}$ found at *IYL* ($where, s_i = settlement\ of\ PRF\ at\ IYL$).

2. To develop the relation between $(LSR)_{s_i}$ and load taken by UPR $(P_r)_{s_i}$, an efficiency factor of raft in PRF (C_1) has been calculated as the ratio of $(LSR)_{s_i}$ to the load of UPR at the same settlement s_i,$(P_r)_{s_i}$i.e. $\left[C_1 = \frac{(LSR)_{s_i}}{(P_r)_{s_i}}\right]$as shown in table 5-22.

3. To develop the relation between $(LSPG)_{s_i}$ and load taken by only pile group $\left(P_{pg}\right)_{s_i}$ at the same settlement ($s_i = settlement\ of\ PRF\ at\ IYL$), an efficiency factor of pile group in PRF

(C_2) has been calculated as the ratio of $(LSPG)_{s_i}$ to the load of only pile group at the same settlement s_i, $(P_{pg})_{s_i}$ i.e. $\left[C_2 = \frac{(LSPG)_{s_i}}{(P_{pg})_{s_i}}\right]$ as shown in table 5-22.

4. The C_1 and C_2 in step 2 and 3 has been calculated from the experimental results of model UPR, only pile group, and PRF. Several attempts were made to develop empirical equations (5-14) and (5-15), which show the relationship between C_1, C_2, and non dimensional variables considered in this study like number of piles, relative density of sand bed, ratio of spacing between piles to external diameter of pile, ratio of width to length of raft, ratio of length to diameter of piles, and relative settlement of piled raft (ratio of settlement of PRF to width of raft).

5. The range of relative settlement (s_i/Br) at *IYL* of PRF with all shapes of raft considered in this study is 0.01 to 0.03 (Table 5-22).

6. Table 5-23 shows the values of C_1 and C_2 calculated using equations (5-14) and (5-15).

7. The $(LSR)_{s_i}$ and $(LSPG)_{s_i}$ are converted in terms of load on unpiled raft $\left[(LSR)_{s_i} = C_1 * Prsi\right.$ and load on only pile group $(LSPG)si = C2*Ppgsi$ at the same settlement (si) which is found to be at *IYL* as represented in equation (5-16).

8. The values of *IYL* calculated using equation (5-16) are also shown in Table 5-23 and the comparison between values of *IYL* obtained from experimental data and the proposed equation (5-16) is shown in Figure 5-93 and Table 5-23, which are in good agreement with each other.

As per this study the *IYL* of PRF can also be predicted using equation (5-17) which is similar to the equation proposed by Polous (2001) with some modifications.

$$IYL = (LSR)_{s_i} + (LSPG)_{s_i} \qquad (5\text{-}13)$$

$$C_1 = 0.00033 * n * I_d * {}^{S}/_{d} * {}^{B_r}/_{L_r} * {}^{L}/_{d} * {}^{s_i}/_{B_r} \quad (5\text{-}14)$$

$$C_2 = 8.375 * e^{\left(-0.000175 * n * I_d * {}^{S}/_{d} * {}^{B_r}/_{L_r} * {}^{L}/_{d} * {}^{s_i}/_{B_r}\right)} \quad (5\text{-}15)$$

$$IYL = C_1 * (P_r)_{s_i} + C_2 * \left(P_{pg}\right)_{s_i} \quad (5\text{-}16)$$

$$IYL = 0.149 * \frac{Qu, pg}{1 - \frac{\left[k_r\left(1 - \alpha_{cp}\right)\right]}{k_p + k_r\left(1 - \alpha_{cp}\right)}} + 0.185 * I_d \quad (5\text{-}17)$$

where,

C_1 = Efficiency factor of raft in PRF at $IYL = (LSR)_{s_i}/(P_r)_{s_i}$

C_2 = Efficiency factor of pile group in PRFat $IYL = (LSPG)_{s_i}/\left(P_{pg}\right)_{s_i}$

$(P_r)_{s_i}$= Load taken by UPR at s_i in kN

$\left(P_{pg}\right)_{s_i}$ = Load taken by only pile group at s_i in kN

s_i= Settlement of PRF at IYL in mm

IYL = Initial yield load of PRF in kN

$(LSR)_{s_i}$ = Load shared by raft in PRF at IYL in kN

$(LSPG)_{s_i}$ = Load shared by pile group in PRF at IYL in kN

B_r= Width of raft or least lateral dimension of raft in m

I_d =Relative density of sand bed in percentage

L = Length of pile in m

n = Number of piles

S = Spacing between piles in m

d = External diameter of pile in m

For predicting final yield load of PRF, the load shared by raft in PRF at FYL $(LSR)_{fyl}$ and the load shared by pile groups in PRF at FYL $(LSPG)_{fyl}$ were converted in terms of ultimate load of UPR (Qur) and ultimate load of pile group (Qu,pg) by introducing efficiency factor of raft in PRF (C_3) and efficiency factor of pile group in PRF (C_4) respectively as shown in equation (5-18) and (5-19). According to de Sanctis and Mandolini (2006) C_3 varies as a function of raft and pile geometry conditions, indicating that values of C_3 equal to 0 and 1 represent conditions of block failure of piles and unpiled–raft failure, respectively. For piled rafts embedded in undrained clays, the load capacity efficiency factor C_4 for pile group was suggested to be equal to 1 for practical purposes (Sanctis and Mandolini, 2006). For sands, the values of C_4 can be smaller or greater than 1 depending on the type or magnitude of interactions that occur between raft and piles (Han and Ye SL, 2006; Phung, 1993). If loading on a piled raft results in increased confining stress within underlying soil near piles, C_4 would be greater than 1 due to increases in pile skin friction (Phung, 1993)). Factor C_4 can be smaller than 1 when downward movements of the raft reduce relative displacements between soil and the pile shaft, resulting in decreased pile skin frictions (Han and Ye SL, 2006). For the present study the efficiency factors $C_3 = \frac{(LSR)_{fyl}}{Qur}$ and $C_4 = \frac{(LSPG)_{fyl}}{Qu,pg}$ were calculated using experimental results. These factors can be predicted

from the proposed equations (5-20) and (5-21). Table 5-24 shows the percentage variations in *FYL* determined from proposed equations with respect to experimental *FYL*. Figure 5-94 shows comparison of *FYL* of piled raft foundation with different shape of raft at different relative density of sand bed found from experimental results and calculated from proposed equation (5-19).

$$FYL = (LSR)_{fyl} + (LSPG)_{fyl} \tag{5-18}$$

$$FYL = C_3 * Qur + C_4 * Qu,pg \tag{5-19}$$

$$C_3 = 0.119 * \frac{S}{d} * \frac{B_r}{L_r} * e^{\left(0.0083 * I_d * {}^{1}/_{n} * {}^{L}/_{d} * {}^{S}/_{B_r}\right)} \tag{5-20}$$

$$C_4 = 0.871 * \frac{S}{d} * \frac{B_r}{L_r} * e^{\left(-0.016 * I_d * {}^{1}/_{n} * {}^{L}/_{d} * {}^{S}/_{B_r}\right)} \tag{5-21}$$

where,

C_3 = Efficiency factor of raft in PRF at $FYL = (LSR)_{fyl}/Qur$

C_4 = Efficiency factor of pile group in PRF at $FYL = (LSPG)_{fyl}/Qu,pg$

$(LSR)_{fyl}$ = Load shared by raft in PRF at *FYL* in kN

$(LSPG)_{fyl}$ = Load shared by pile group in PRF at *IYL* in kN

Table 5-22 represents the efficiency factor of raft in PRF (C_1), efficiency factor of pile group in PRF (C_2), and efficiency of PRF at *IYL* (β_1) in PRF with different shapes of raft. The range of C_1 was found to be 0.317 to 0.9 in PRF with all shapes of raft except in rectangular PRF at 40% relative density of sand. The range of C_2 was found to be 1.387 to 5.659 in PRF with all shapes of raft except in square PRF at 40% relative density of sand. The range of the piled raft foundation (PRF) efficiency at the initial yield load (*IYL*) (β_1) with different shapes of the raft was found to be between 0.9 and 1.69, and at the final yield load (*FYL*), it $(i.e.\beta_2)$ was between 0.89 and 1.47. The efficiency of PRF at *IYL* and *FYL* was found to be lowest at 80% relative density of sand in most cases, indicating that the efficiency of PRF is lower in dense sand compared to medium-dense sand. In other words, the load-carrying capacity of PRF increases more than the combined load-carrying capacity of the unpiled raft (UPR) and pile group (PG) in medium dense sand.

Table 5-22 Efficiency factor of raft (C_1), efficiency factor of pile group (C_2), and efficiency of PRF at *IYL* (β_1) in PRF with different shape of raft

Shape of raft	I_d **(%)**	***IYL*** **(kN)**	***LSR*** **in PRF at *IYL* (kN)**	***LSPG*** **in PRF at *IYL* (kN)**	**Piled raft coefficient**	**Settlement s_i at *IYL* (mm)**	B_r **(mm)**	s/B_r	$(P_r)_{s_i}$ **(kN)**	$(P_{sp})_{s_i}$ **(kN)**	$(P_{pg})_{s_i}$ **(kN)**	C_1	C_2	β_1
Circular	40	4.77	1.24	3.53	0.74	2.92	248.30	0.01	3.92	0.16	0.65	0.317	5.428	1.04
	60	9.28	5.08	4.20	0.45	3.44	248.30	0.01	6.16	0.36	1.61	0.824	2.608	1.19
	80	11.93	5.80	6.13	0.51	3.83	248.30	0.02	9.66	0.38	3.62	0.600	1.696	0.90
Square	40	11.63	3.77	7.85	0.68	2.88	220.00	0.01	6.23	0.16	0.65	0.606	12.109	1.69
	60	19.13	8.87	10.26	0.54	6.20	220.00	0.02	15.09	0.42	1.81	0.588	5.659	1.13
	80	22.32	13.57	8.75	0.39	3.46	220.00	0.02	15.08	0.52	3.57	0.900	2.454	1.20
Rectangular	40	5.31	3.53	1.78	0.33	1.20	186.10	0.01	3.10	0.14	0.38	1.140	4.701	1.53
	60	15.93	5.42	5.20	0.49	2.15	186.10	0.03	14.29	0.59	1.80	0.380	2.889	0.99
	80	18.59	10.92	5.02	0.31	3.40	186.10	0.03	16.16	0.52	3.62	0.676	1.387	0.94
Trapezoidal	40	7.97	3.72	4.24	0.53	1.53	180.00	0.01	4.79	0.15	0.83	0.778	5.121	1.42
	60	13.28	4.54	8.74	0.66	3.49	180.00	0.02	9.46	0.37	1.70	0.480	5.146	1.19
	80	15.93	6.55	9.39	0.59	3.37	180.00	0.01	13.25	0.34	3.62	0.494	2.596	0.94

Table 5-23 Efficiency factor of raft (C_1), and efficiency factor of pile group (C_2) in PRF with different shape of raft calculated from proposed equations and percentage variations in *IYL* determined from proposed equations with respect to experimental *IYL*

Shape of raft	I_d **(%)**	***IYL*** **(kN)**	***S/d***	B_r/L_r	***L/d***	***n***	s/B_r	C_1	C_2	***IYL*-EXP (kN)**	***IYL*-PROPOSED EQUATION (kN)**	**% Variations in predicted *IYL* as compared to *IYL*-EXP**
Circular	40	4.77	7	1	30	9	0.01	0.294	5.503	4.77	4.73	-1
	60	9.28	7	1	30	9	0.01	0.521	3.989	9.28	9.63	4
	80	11.93	7	1	30	9	0.02	0.773	2.786	11.93	17.55	47
Square	40	11.63	7	1	30	9	0.01	0.328	5.245	11.63	5.44	-53
	60	19.13	7	1	30	9	0.02	1.058	1.859	19.13	19.34	1
	80	22.32	7	1	30	9	0.02	0.787	2.733	22.32	21.61	-3
Rectangular	40	5.31	7	0.716	30	9	0.01	0.116	7.091	5.31	3.04	-43
	60	15.93	7	0.716	30	9	0.03	0.311	5.374	15.93	14.11	-11
	80	18.59	7	0.716	30	9	0.03	0.654	3.299	18.59	22.51	21
Trapezoidal	40	7.97	7	0.783	30	9	0.01	0.166	6.600	7.97	6.26	-21
	60	13.28	7	0.783	30	9	0.02	0.570	3.718	13.28	11.71	-12
	80	15.93	7	0.783	30	9	0.01	0.735	2.943	15.93	20.38	28

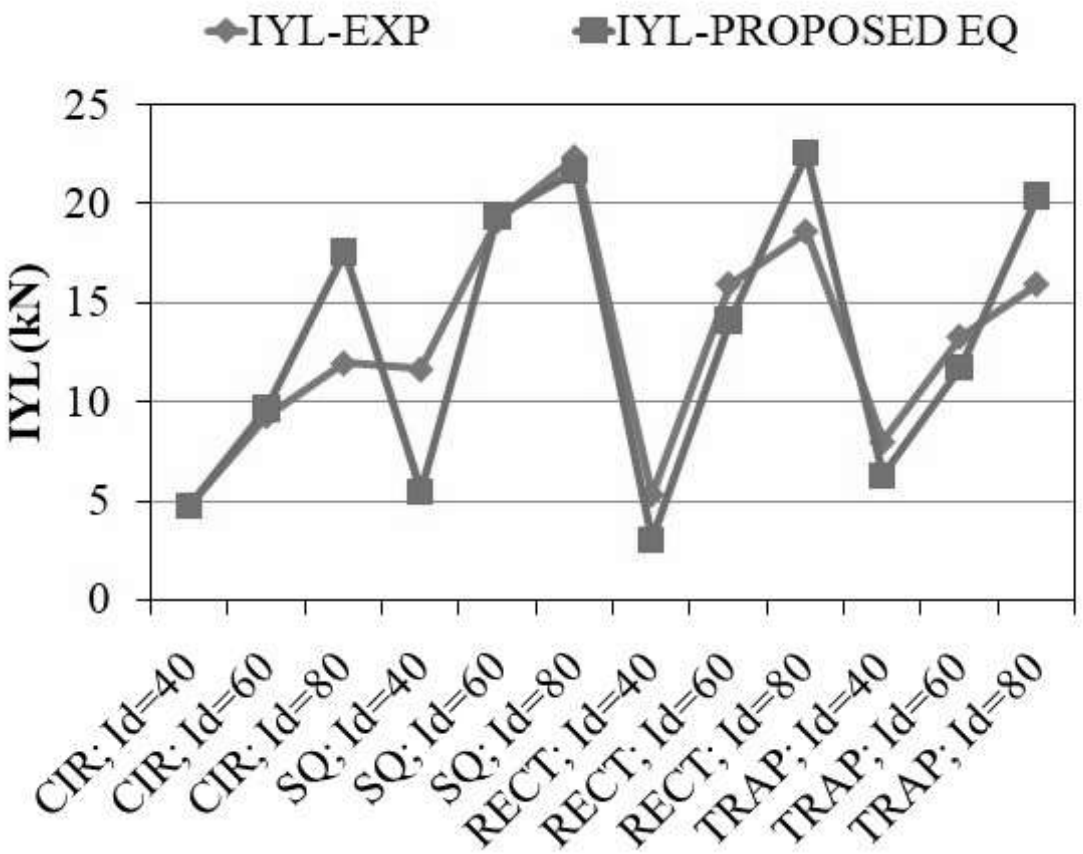

Figure 5-93 : Comparison of *IYL* of piled raft foundation with different shape of raft at different relative density of sand bed found from experimental results and calculated from proposed equation

Table 5-24 Efficiency of PRF at *FYL* (β_2) and percentage variations in *FYL* of PRF with different shape of raft determined from proposed equations with respect to experimental *FYL*

Shape of raft	I_d **(%)**	***FYL* (kN)**	***LSR* at FYL**	***LSP G* at FYL**	α_p	**Settlement (mm) at FYL**	B_r	s/B_r	C_3	C_4	Qur **(kN)**	Qu,pg **(kN)**	***FYL* (kN) -EXP**	***FYL* (kN) - PROPOSED EQUATION**	**% Variations in predicted *FYL* as compared to *FYL* - EXP**	(β_2)
Circular	40	9.54	4.33	5.21	0.55	10.02	248.3	0.040	0.871	5.594	9.28	1.48	9.54	16.39	72	0.89
	60	15.90	7.88	8.03	0.50	16.70	248.3	0.067	0.931	4.917	10.34	2.17	15.90	20.31	28	1.27
	80	21.21	12.13	9.08	0.43	10.71	248.3	0.043	0.916	5.072	17.23	4.11	21.21	36.63	73	0.99
Square	40	21.59	7.46	14.1	0.65	17.86	220	0.081	0.911	5.127	13.25	1.48	21.59	19.68	-9	1.47
	60	28.70	15.88	12.8	0.45	17.40	220	0.081	0.950	4.734	20.3	2.17	28.70	29.57	3	1.28
	80	38.27	29.61	8.66	0.23	15.50	220	0.070	0.974	4.514	28.69	4.11	38.27	46.48	21	1.17
Rectangular	40	13.28	10.03	3.25	0.25	14.13	186.1	0.076	0.648	3.711	13.12	1.48	13.28	14.02	6	0.91
	60	26.56	13.96	9.94	0.42	17.91	186.1	0.129	0.699	3.208	19.13	2.17	26.56	20.35	-23	1.25
	80	34.53	22.42	9.45	0.30	18.19	186.1	0.120	0.740	2.876	28.2	4.11	34.53	32.69	-5	1.07
Trapezoidal	40	15.93	11.37	4.56	0.29	14.33	180	0.080	0.712	4.026	12.59	1.48	15.93	14.94	-6	1.13
	60	23.90	12.03	11.8	0.50	17.14	180	0.068	0.764	3.519	19.09	2.17	23.90	22.22	-7	1.12
	80	29.21	16.71	12.5	0.43	13.16	180	0.073	0.766	3.493	27.1	4.11	29.21	35.12	20	0.94

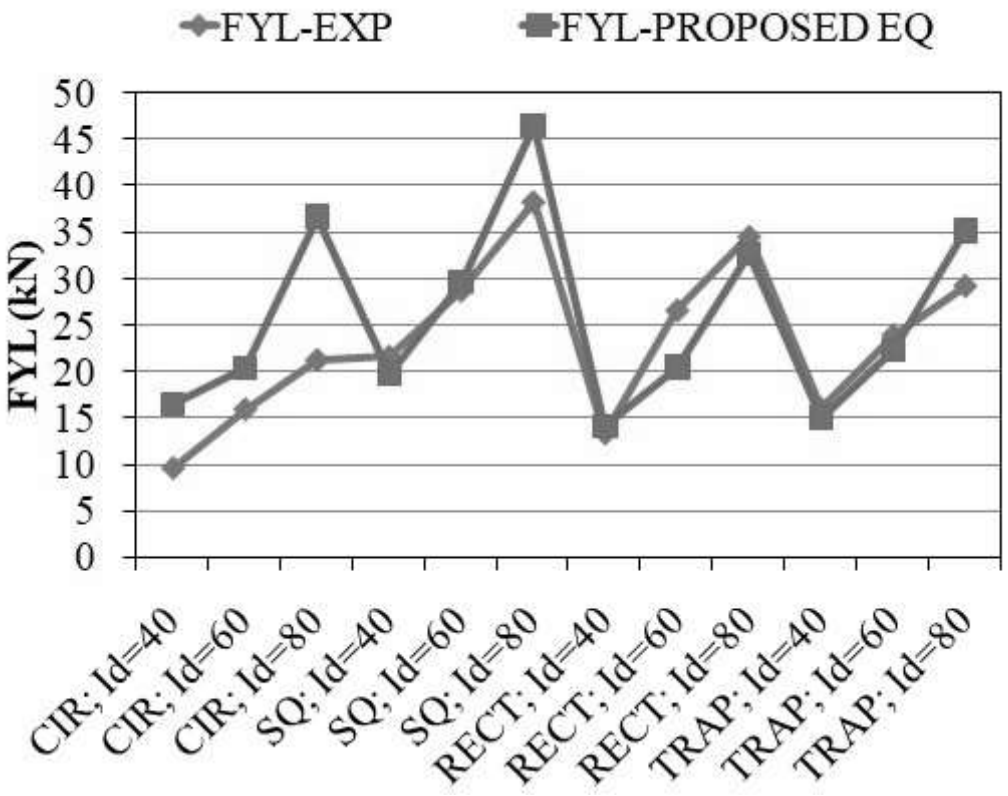

Figure 5-94 : Comparison of *FYL* of piled raft foundation with different shape of raft at different relative density of sand bed found from experimental results and calculated from proposed equation

5.3.3.1.7 Prediction of $(k_{pr})_p$

The values of primary stiffness of PRF $(k_{pr})_p$ in kN/m (experimental), secondary stiffness of PRF $(k_{pr})_s$ in kN/m, initial stiffness of UPR (k_{ri}) (kN/m), and initial stiffness of pile group (k_{pg}) obtained from experimental data for various shapes of raft are listed in Table 5-25. It observed that the $(k_{pr})_p$ and $(k_{pr})_s$ increased with the increment in the relative density of sand. The $(k_{pr})_p$ of circular piled raft foundations increased by 75% and 101% at 60% and 80% relative density, respectively, compared to I_d = 40%.The $(k_{pr})_p$ of square piled raft foundations increased by 42% and 88% at 60% and 80% relative density, respectively, compared to I_d = 40%. The $(k_{pr})_p$ of rectangular piled raft foundations increased by 24% and 56% at 60% and 80% relative density, respectively, compared to I_d = 40%. The $(k_{pr})_p$ of trapezoidal piled raft foundations increased by 72% and 83% at 60% and 80% relative density, respectively, compared to I_d = 40%. The lowest value of $(k_{pr})_p$ and $(k_{pr})_s$ were in circular piled rafts. The $(k_{pr})_p$ of square piled raft was 237%, 175%, and 215% more than the $(k_{pr})_p$ of circular piled raft at 40%, 60% and 80% relative density of sand, respectively. The $(k_{pr})_p$ of rectangular piled raft was 155%, 81%, and 99% more than the $(k_{pr})_p$ of circular piled raft at 40%, 60% and 80% relative density of sand, respectively. The $(k_{pr})_p$ of trapezoidal piled raft was 119%, 116%, and 99% more than the $(k_{pr})_p$ of circular piled raft at 40%, 60% and 80% relative density of sand, respectively.

The $(k_{pr})_s$ of circular piled raft foundations increased by 6% and 130% at 60% and 80% relative density, respectively, compared to I_d = 40%. The $(k_{pr})_s$ of square piled raft foundations was found to be increased by 121% and 170% at 60% and 80% relative density, respectively, compared to I_d = 40%. The $(k_{pr})_s$ of rectangular piled raft foundations increased by 36% and 88% at 60% and 80% relative density, respectively, compared to I_d = 40%. The $(k_{pr})_s$ of

trapezoidal piled raft foundations increased by 28% and 127% at 60% and 80% relative density, respectively, compared to I_d = 40%. The lowest value of $(k_{pr})_p$ and $(k_{pr})_s$ were found in circular piled rafts. The $(k_{pr})_s$ of square piled raft was 11%, 132%, and 31% more than the $(k_{pr})_s$ of circular piled raft at 40%, 60% and 80% relative density of sand, respectively. The $(k_{pr})_s$ of rectangular piled raft was 24%, 59%, and 1% more than the $(k_{pr})_s$ of circular piled raft at 40%, 60% and 80% relative density of sand, respectively. The $(k_{pr})_s$ of trapezoidal piled raft was 21%, 47%, and 20% more than the $(k_{pr})_s$ of circular piled raft at 40%, 60% and 80% relative density of sand, respectively.

To develop the relation between primary stiffness of PRF $(k_{pr})_p$ and variables considered in this study like relative density of sand (I_d), initial stiffness of UPR (k_{ri}) (kN/m), and initial stiffness of pile group $(k_{pg})_i$ (Experimental), rigorous analysis was done in Excel and finally equation (5-22) was derived. The variation in the values of $(k_{pr})_p$ determined from equation (5-22) and from tri-linear load settlement curve of PRF is shown in Table 5-25 and Figure 5-95, which show the good agreement between predicted values and experimental values of $(k_{pr})_p$.

$$(k_{pr})_p = 54.6I_d + 0.28k_{ri} + 0.86\,(k_{pg})_i \qquad (5\text{-}22)$$

Table 5-25 Variations in primary stiffness of PRF $(k_{pr})_p$ with different shapes of raft (experimental) and determined from the proposed equation

Shape of raft	**Relative density of sand (%)**	**B_r (m)**	**TLP (m)**	**Primary stiffness of PRF $(k_{pr})_p$ in kN/m (Experimental)**	**Secondary Stiffness of PRF $(k_{pr})_s$ in kN/m**	**Initial stiffness of UPR (k_{ri}) (kN/m)**	**Initial stiffness of PG $(k_{pg})_i$ (Experimental)**	**Primary stiffness of PRF $(k_{pr})_p$ in kN/m (Proposed equation)**	**% variation in $(k_{pr})_p$ calculated from proposed eq. and EXP.**
Circular	40	0.2483	2.619	1560.10	534.06	1283.11	315.01	2803.065	80
	60	0.2483	2.619	2723.14	566.45	1980.14	563.58	4145.629	52
	80	0.2483	2.619	3129.65	1226.04	2718.29	2260.30	6909.612	121
Square	40	0.22	2.619	5262.22	593.20	2321.44	315.01	3107.312	-41
	60	0.22	2.619	7489.01	1313.46	3585.12	563.58	4768.116	-36
	80	0.22	2.619	9873.06	1601.48	5331.36	2260.30	7809.436	-21
Rectangular	40	0.1861	2.619	3976.92	660.39	2338.74	315.01	2883.401	-27
	60	0.1861	2.619	4922.09	899.15	3186.02	563.58	4402.613	-11
	80	0.1861	2.619	6215.72	1243.46	4590.79	2260.30	7103.303	14
Trapezoidal	40	0.23	2.619	3411.18	647.98	1974.61	315.01	2881.651	-16
	60	0.23	2.619	5871.55	830.11	2982.86	563.58	4316.207	-26
	80	0.23	2.619	6235.71	1470.10	4204.43	2260.30	7051.733	13

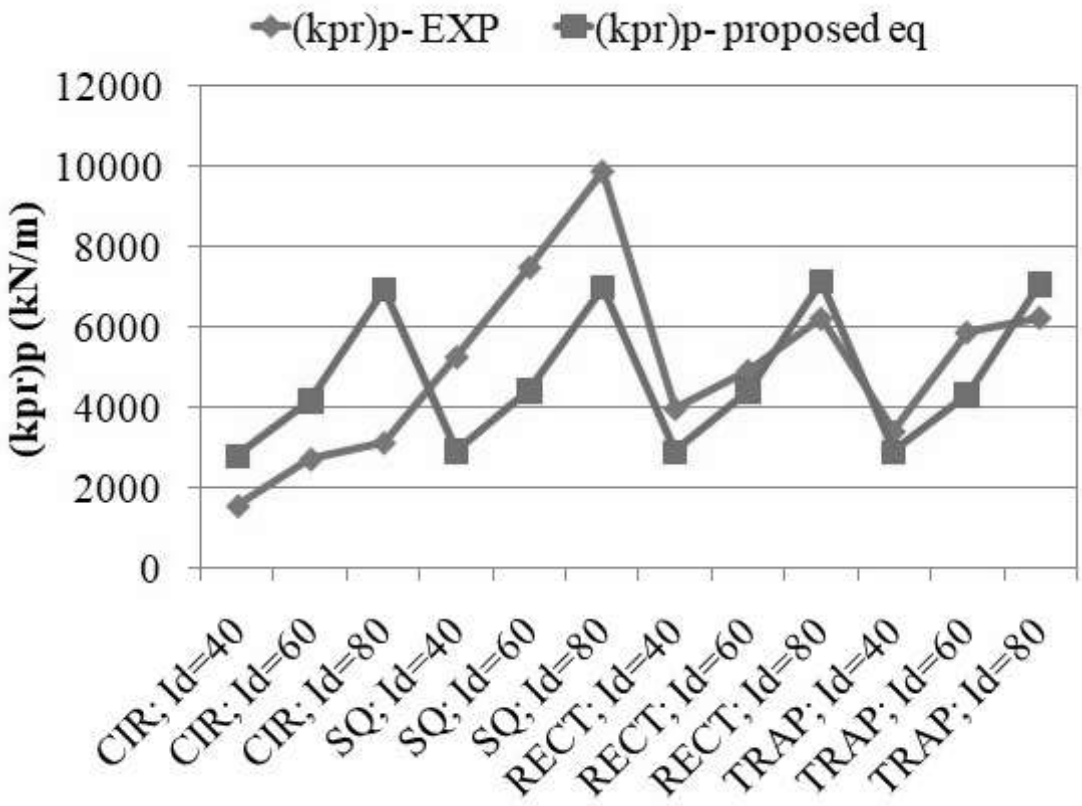

Figure 5-95 : Comparison of primary stiffness of PRF $\left(k_{pr}\right)_p$ (experimental) and determined from proposed equation

5.3.3.1.8 Prediction of $(k_{pr})_s$

As per Garcia et al. (2019), $(k_{pr})_s$ can be taken as k_r (stiffness of raft) (equation (2-30)). In present study $(k_{pr})_s$ is expressed in terms of initial stiffness of raft (k_{ri}) and relative density of sand bed (I_d) as shown in equation (5-23). This equation was derived from the experimental values of $(k_{pr})_s$ and (k_{ri}) in kN/m at different relative density of sand bed (I_d). The values of predicted $(k_{pr})_s$ and experimental values of $(k_{pr})_s$ are shown in Table 5-26.

$$(k_{pr})_s = 15.13I_d + 0.018k_{ri} \quad (5\text{-}23)$$

Table 5-26 Variations in secondary stiffness of PRF $(k_{pr})_s$ with different shapes of raft (experimental) and determined from the proposed equation

Shape of raft	I_d **(%)**	**Secondary Stiffness of Piled Raft** $(k_{pr})_s$ **- EXP in kN/m**	k_{ri} **(kN/m)**	$(k_{pr})_s$ **in kN/m predicted from eq. (5-23)**	**% variation in predicted** $(k_{pr})_s$ **from experimental** $(k_{pr})_s$**-EXP**
Circular	40	534.06	1283.11	628.30	18
	60	566.45	1980.14	943.44	67
	80	1226.04	2718.29	1259.33	3
Square	40	593.20	2321.44	646.99	9
	60	1313.46	3585.12	972.33	-26
	80	1601.48	5331.36	1306.36	-18
Rectangular	40	660.39	2338.74	647.30	-2
	60	899.15	3186.02	965.15	7
	80	1243.46	4590.79	1293.03	4
Trapezoidal	40	647.98	1974.61	640.74	-1
	60	830.11	2982.86	961.49	16
	80	1470.10	4204.43	1286.08	-13

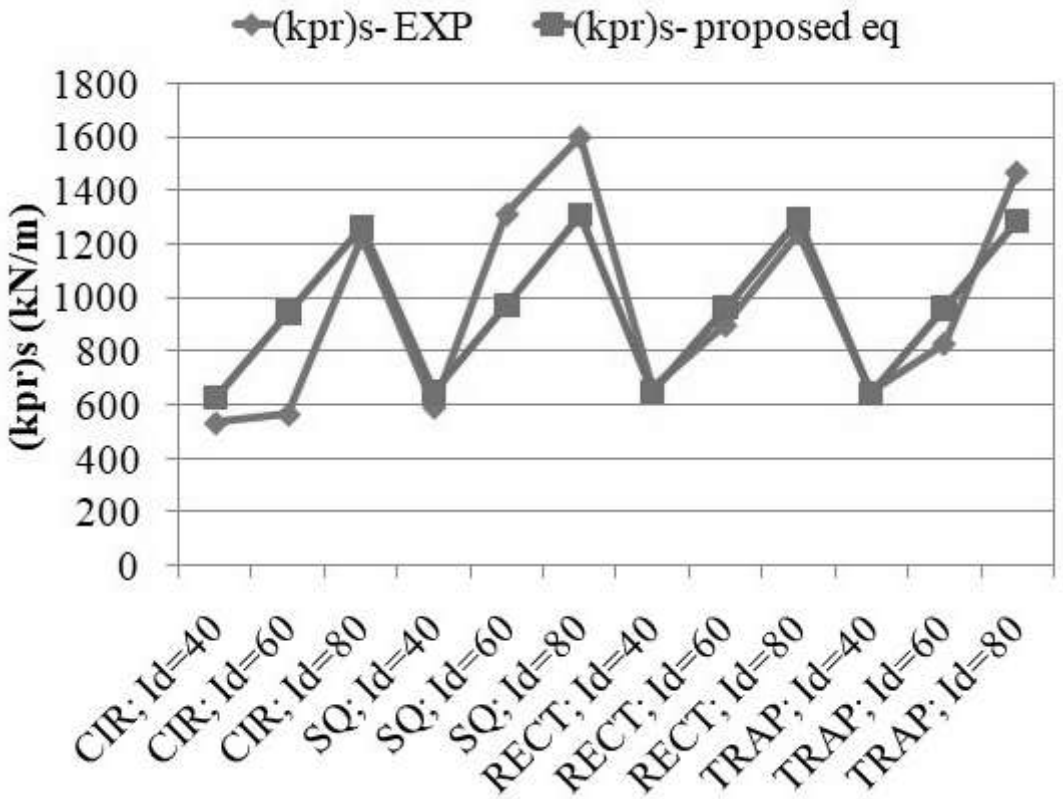

Figure 5-96 : Comparison of primary stiffness of PRF $\left(k_{pr}\right)_s$ (experimental) and determined from proposed equation

5.3.3.1.9 Comparison between Experimental Values of IYL and Predicted IYL from Poulos Method

The values of *IYL* obtained from the load settlement curve of model PRF with different shape of raft was compared with the values obtained from the equation (2- 27) $P_1 = \frac{P_{up}}{1-X}$ proposed by Poulos (2001) was modified as below in terms of the current study parameters (equation (5-24)).

$$IYL = \frac{Qu,pg}{1-X} \qquad (5\text{-}24)$$

The values of *IYL* obtained from experimental study and predicted from polous method using equation (5-24) were compared as shown in Table 5-27. FromTable 5-27, it can be observed that the values of *IYL* predicted from Polous method is underestimated by 5% to 55% of actual *IYL* i.e experimental *IYL*.The Poulos equation can be used in modified form as equation (5-17) for more precise value of *IYL*.

Table 5-27 Comparison of *IYL* obtained from experimental study and predicted from Poulos method

Shape of raft	**Relative density of sand bed (%)**	***IYL* – EXP (kN)**	Qu, pg **(Exp)**	k_{ri} **(kN/m)**	**Initial stiffness of pile group (Experimental)** $(k_{pg})_i$ **(kN/m)**	r_c	r_0	ν_s	r_m	α_{cp}	X	***IYL*-Predicted (Poulos)**	**% Variation in Predicted *IYL* from *IYL*-EXP**
Circular	40	4.77	1.048	1283.11	315.01	0.04	0.005	0.32	0.32	0.49	0.68	3.23	-32
	60	9.28	2.081	1980.13	563.58	0.04	0.005	0.30	0.33	0.49	0.64	5.81	-37
	80	11.93	4.08	2718.29	2260.30	0.04	0.005	0.27	0.33	0.49	0.38	6.57	-45
Square	40	11.63	1.048	2321.43	315.01	0.04	0.005	0.32	0.32	0.49	0.79	5.00	-57
	60	19.13	2.081	3585.12	563.58	0.04	0.005	0.30	0.33	0.49	0.76	8.83	-54
	80	22.32	4.08	5331.36	2260.30	0.04	0.005	0.27	0.33	0.49	0.54	8.96	-60
Rectangular	40	5.31	1.048	2338.73	315.01	0.04	0.005	0.32	0.32	0.49	0.79	5.03	-5
	60	15.93	2.081	3186.02	563.58	0.04	0.005	0.30	0.33	0.49	0.74	8.08	-49
	80	18.59	4.08	4590.79	2260.30	0.04	0.005	0.27	0.33	0.49	0.51	8.28	-55
Trapezoidal	40	7.97	1.048	1974.60	315.01	0.04	0.005	0.32	0.32	0.49	0.76	4.41	-45
	60	13.28	2.081	2982.86	563.58	0.04	0.005	0.30	0.33	0.49	0.73	7.69	-42
	80	15.93	4.08	4204.43	2260.30	0.04	0.005	0.27	0.33	0.49	0.49	7.93	-50

5.3.3.1.10 Comparision of Primary Stiffness of Piled Raft $(k_{pr})_p$ in kN/m obtained from Experimental Study and Predicted as per Omeman et al. (2012)

The Primary Stiffness of Piled Raft $(k_{pr})_p$ in kN/m obtained from experiments were compared with the values obtained from the equations (2-46), (2-49) and (2-50) suggested by omeman et al. (2012). The modification in the notations used in the mentioned equations were done as per the current study and these modifications are shown in eqations (5-25), (5-26) and (5-27). From Table 5-28, it can be observed that the values of $(k_{pr})_p$ predicted from Omeman method is varied by -18% to 57% of actual $(k_{pr})_p$ i.e experimental $(k_{pr})_p$. However, this method was not found suitable for piled rafts with a 5 × 5 pile group because it results in more than 100% variations.

$$(k_{pr})_p = \alpha_r k_{ri} + \alpha_p \, (k_{pg})_i \tag{5-25}$$

$$\alpha_r = -0.459 * ln\left({(k_{pg})_i}/{k_{ri}} \right) + \ 0.7967 \tag{5-26}$$

$$\alpha_p = -0.1818 * ln\left({(k_{pg})_i}/{k_{ri}} \right) + \ 0.7563 \tag{5-27}$$

Table 5-28 Comparison of $(k_{pr})_p$ obtained from experimental study and predicted from Omeman method

Shape of raft	**Relative density of sand bed (%)**	**Initial stiffness of pile group (Experimental) $(k_{pg})_i$ (kN/m)**	**k_{ri} (kN/m)**	**α_r**	**α_p**	**Primary Stiffness of Piled Raft $(k_{pr})_p$ in kN/m (Experimental)**	**$(k_{pr})_p$ in kN/m (Predicted as per Omeman)**	**% variation in predicted $(k_{pr})_p$ from $(k_{pr})_p$-EXP**
Circular	40	315.01	1283.11	1.44	1.01	1560.10	2168.07	39
	60	563.58	1980.14	1.37	0.98	2723.14	3274.67	20
	80	2260.30	2718.29	0.88	0.79	3129.65	4181.15	34
Square	40	315.01	2321.44	1.71	1.12	5262.22	4330.36	-18
	60	563.58	3585.12	1.65	1.09	7489.01	6516.76	-13
	80	2260.30	5331.36	1.19	0.91	9873.06	8409.45	-15
Rectangular	40	315.01	2338.74	1.72	1.12	3976.92	4368.39	10
	60	563.58	3186.02	1.59	1.07	4922.09	5675.19	15
	80	2260.30	4590.79	1.12	0.89	6215.72	7151.16	15
Trapezoidal	40	315.01	1974.61	1.64	1.09	3411.18	3580.14	5
	60	563.58	2982.86	1.56	1.06	5871.55	5254.84	-11
	80	2260.30	4204.43	1.08	0.87	6235.71	6511.91	4

5.3.3.2 Effect of L/d ratio of Pile

5.3.3.2.1 Load Settlement Characteristics

Figure 5-97 to Figure 5-99 represent the load settlement characteristics of a model piled raft with different *L/d* ratios of piles at 40%, 60%, and 80% relative density, respectively. The load settlement relation or curve of PRF was Tri-linear.

Figure 5-100 to Figure 5-102 show the variation in *IYL* and *FYL* of PRF with *L/d* ratios of 10, 20, and 30, respectively. It is evident from these figures that at the same relative density of the sand bed, the load-carrying capacity of PRF (*IYL* and *FYL*) increased as the *L/d* ratio of the pile increased. Additionally, the *IYL* and *FYL* of PRF with different *L/d* ratios increased as the relative density of the sand bed increased. Furthermore, the percentage increment of *FYL* was higher than the *IYL* with a relative density of the sand bed for all *L/d* ratios.

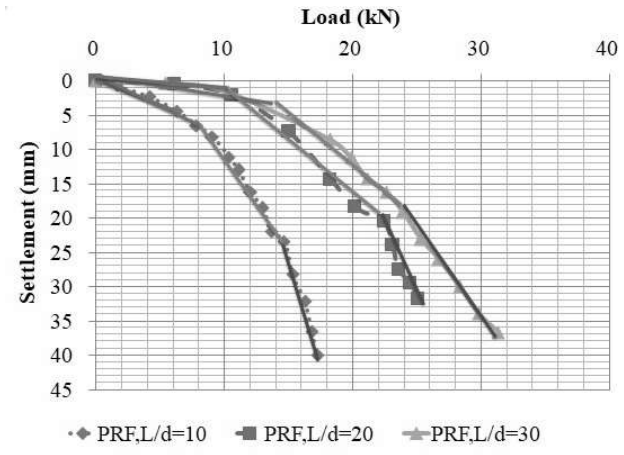

Figure 5-97 : Load settlement characteristics of model piled raft with different *L/d* ratio of piles *(S = 5d; pile group = 5 × 5; I_d = 40%)*

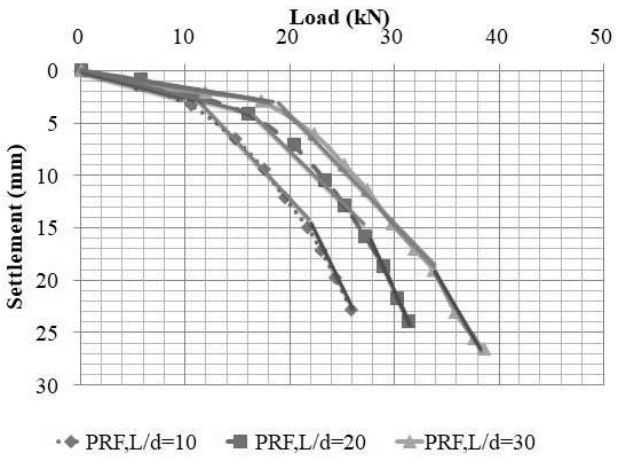

Figure 5-98 : Load settlement characteristics of model piled raft with different *L/d* ratio of piles *(S = 5d; pile group = 5 × 5; I_d = 60%)*

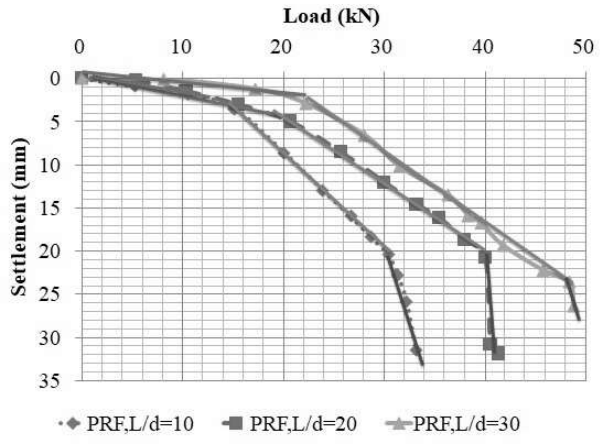

Figure 5-99 : Load settlement characteristics of model piled raft with different *L/d* ratio of piles *(S = 5d; pile group = 5 × 5; I_d = 80%)*

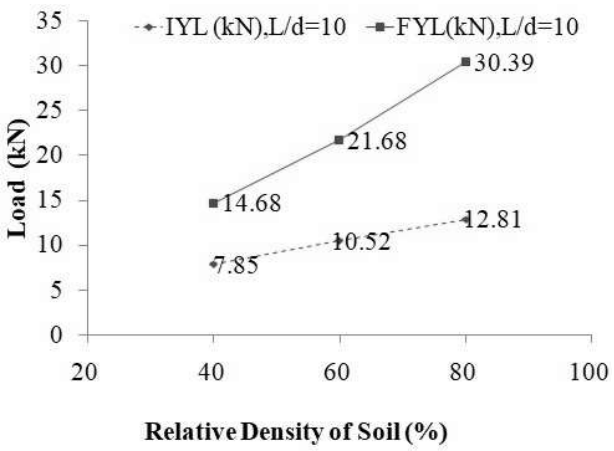

Figure 5-100 : Initial yield load (*IYL*) and Final yield load (*FYL*) of piled raft foundation at different relative density of sand bed *(S = 5d; L/d ratio of pile = 10; I_d = 40%, 60%, and 80%; pile group = 5 × 5)*

The range of *IYL* of PRF with *L/d* ratio = 10 was 7.85 kN to 12.81 kN at 40% to 80% relative density of the sand bed. The value of *IYL* of PRF with *L/d* ratio = 10 was increased by 2.67 kN and 4.95 kN at 60% and 80% relative densities, respectively, compared to 40% relative density of a sand bed. In the case of PRF with *L/d* ratio = 10, the range of *FYL* was 14.68 kN to 30.39 kN for 40% to 80% relative density of the sand bed. The increment in the value of *FYL* at 60% and 80% relative density compared to 40% relative density was observed as 7 kN and 15.7 kN, respectively. The increment in *FYL* as compared to *IYL* was 6.83 kN, 11.16 kN, and 17.58 kN at 40%, 60%, and 80% relative densities of the sand bed, respectively.

The percentage increase in *IYL* of PRF with *L/d* ratio = 10 at 60% and 80% relative density compared to 40% relative density was 34% and 63%, respectively. The percentage increase in *FYL* of square PRF with *L/d* ratio = 10 at 60% and 80% relative density compared to 40% relative density was 48% and 107%, respectively.

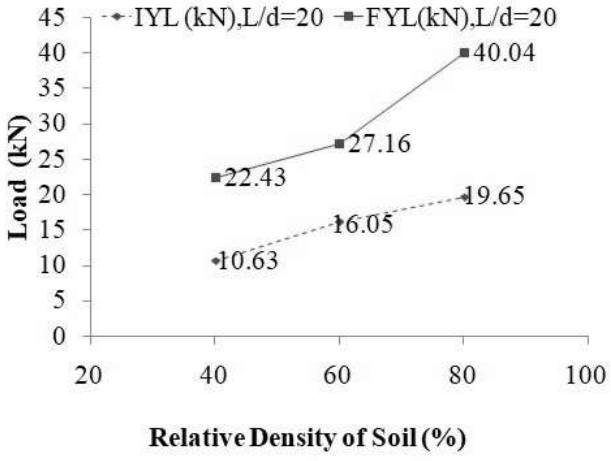

Figure 5-101 : Initial yield load (*IYL*) and Final yield load (*FYL*) of piled raft foundation at different relative density of sand bed *(S = 5d; I_d = 40%, 60%, and 80%; L/d ratio of pile = 20; pile group = 5 × 5)*

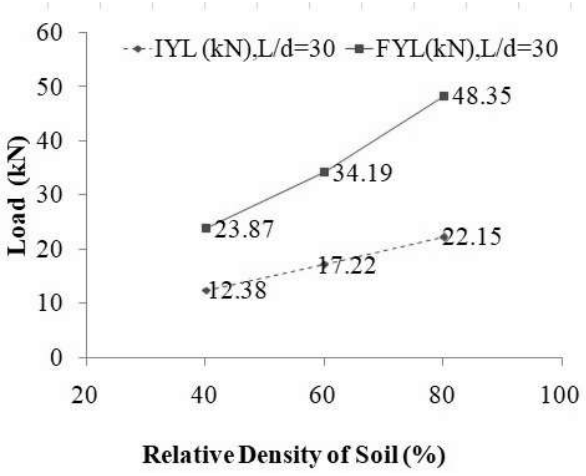

Figure 5-102 : Initial yield load (*IYL*) and Final yield load (*FYL*) of piled raft foundation at different relative density of sand bed *(S = 5d; I_d = 40%, 60%, and 80%; L/d ratio of pile = 30; pile group = 5 × 5)*

The range of *IYL* of PRF with an *L/d* ratio = 20 was 10.63 kN to 19.65 kN at a relative density of 40% to 80% of the sand bed. The value of *IYL* of PRF with an *L/d* ratio of 20 is increased by 5.42 kN and 9.03 kN at 60% and 80% relative densities, respectively, compared to 40% relative density of a sand bed. In the case of PRF with an *L/d* ratio of 20, the range of *FYL* was 22.43 kN to 40.04 kN for 40% to 80% relative density of the sand bed. The increment in the value of *FYL* at 60% and 80% relative densities compared to 40% relative densities was observed at 4.73 kN and 17.61 kN, respectively. The increment in *FYL* as compared to *IYL* was 11.81 kN, 11.11 kN, and 20.39 kN at 40%, 60%, and 80% relative densities of the sand bed, respectively.

The percentage increase in *IYL* of PRF with *L/d* ratio = 20 at 60% and 80% relative density compared to 40% relative density was 51% and 85%, respectively. The percentage increase in *FYL* of square PRF with *L/d* ratio = 20 at 60% and 80% relative density compared to 40% relative density was 21% and 78%, respectively.

The range of *IYL* of PRF with *L/d* ratio = 30 was 12.38 kN to 22.15 kN at a relative density of 40% to 80% in the sand bed. The value of *IYL* of PRF with *L/d* ratio = 30 is increased by 4.84 kN and 9.77 kN at 60% and 80% relative densities, respectively, compared to 40% relative density of a sand bed. In the case of PRF with *L/d* ratio = 30, the range of *FYL* was 23.87 kN to 48.35 kN for 40% to 80% relative density of the sand bed. The increment in the value of *FYL* at 60% and 80% relative densities compared to 40% relative densities was observed as 10.32 kN and 24.48 kN, respectively. The increment in *FYL* as compared to *IYL* was 11.49 kN, 16.96 kN, and 26.20 kN at 40%, 60%, and 80% relative densities of the sand bed, respectively.

The percentage increase in *IYL* of PRF with *L/d* ratio = 30, at 60% and 80% relative density compared to 40% relative density, was found to be 39% and 79%, respectively. The percentage increase in *FYL* of square PRF with *L/d* ratio = 30, at 60% and 80% relative density compared to 40% relative density, was found to be 43% and 103%, respectively.

At 40% relative density of the sand bed, the percentage increase in *IYL* of PRF with *L/d* ratios of 20 and 30 was 35% and 58%, respectively, compared to PRF with *L/d* ratios of 10, and in *FYL*, the same values were 53% and 63%.

At 60% relative density of sand bed, the percentage increase in *IYL* of PRF with *L/d* ratios of 20 and 30 was 53% and 64%, respectively, compared to PRF with *L/d* ratio of 10, and in *FYL*, it was 25% and 58%, respectively.

When the sand bed had a relative density of 80%, the increase in the percentage of initial yield load (*IYL*) for PRF with *L/d* ratios of 20 and 30 was 53% and 73%, respectively, compared to PRF with an *L/d* ratio of 10. In the final yield load (*FYL*), these values were 32% and 59%.

Figure5-103 to Figure 5-105 show the load-settlement characteristics of different foundation types: pile groups (PG), unpiled rafts (UPR), and piled rafts (PRF). These were tested with different *L/d* ratios (10, 20, and 30) for the piles. The results indicated that the carrying capacity of pile groups (PG) was significantly lower compared to unpiled rafts (UPR) and piled rafts (PRF). The carrying capacity of pile groups (PG) increased as the *L/d* ratio of the piles increased.

Additionally, the difference in load-carrying capacity between unpiled rafts (UPR) and piled rafts (PRF) was less significant with an *L/d* ratio of 10 compared to *L/d* ratios of 20 and 30. Moreover, the difference in load-carrying capacity between unpiled rafts (UPR) and piled rafts (PRF) was negligible at the settlement corresponding to the ultimate load of the pile groups (PG) but became significant at higher settlements. Finally, the difference in load-carrying capacity between unpiled rafts (UPR) and piled rafts (PRF) decreased as the relative density of the sand bed increased.

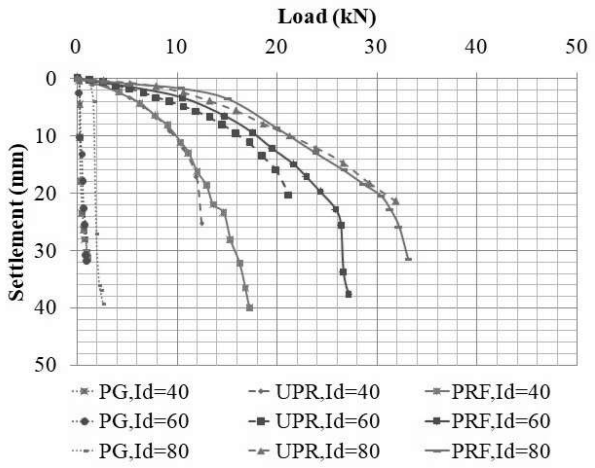

Figure5-103 : Load settlement characteristics of only pile group, unpiled raft, and piled raft with *L/d* ratio of pile = 10 *(S = 5d; d = 9.7 mm; pile group = 5 × 5)*

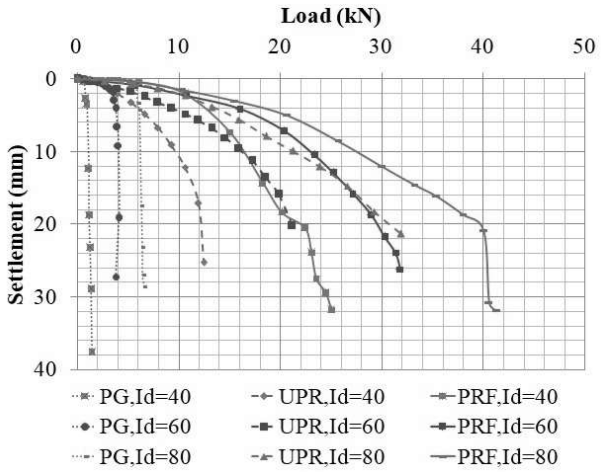

Figure 5-104 : Load settlement characteristics of only pile group, unpiled raft, and piled raft with *L/d* ratio of pile = 20 *(S = 5d; d = 9.7 mm; pile group = 5 ×5)*

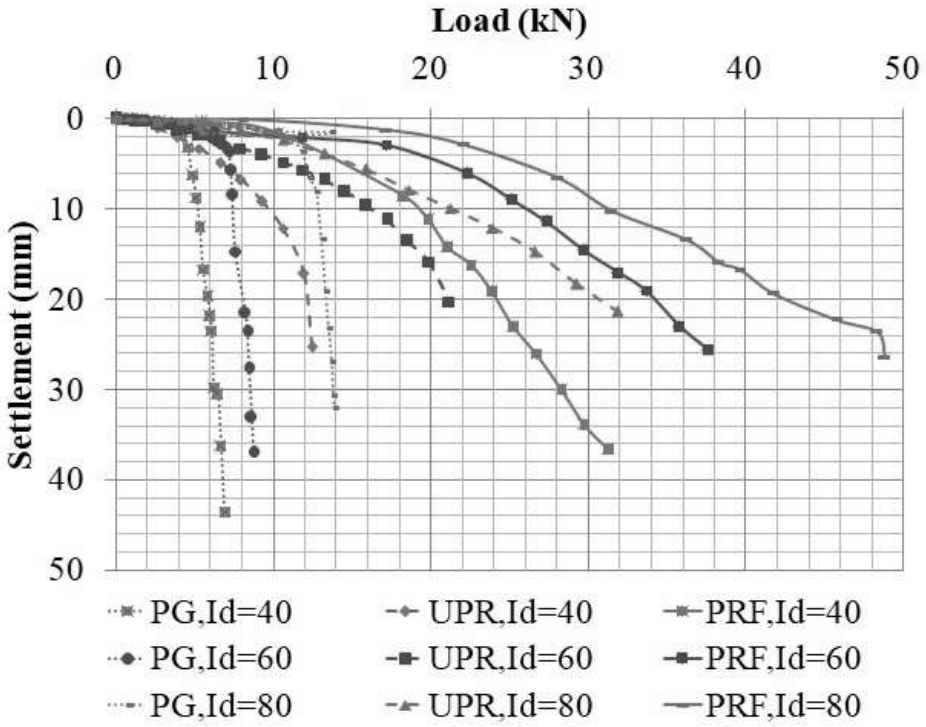

Figure 5-105 : Load settlement characteristics of only pile group, unpiled raft, and piled raft with *L/d* ratio of pile = 30 *(S = 5d; d = 9.7 mm; pile group = 5 × 5)*

5.3.3.2.2 Load Sharing Mechanism

Figure 5-106 to Figure 5-108 display the load settlement characteristics of piled rafts, load shared by pile group (*LSPG*), and load shared by raft (*LSR*) at varying relative densities of sand for PRF with *L/d* ratios of 10, 20, and 30 respectively. For *L/d* ratio of pile study the load shared by pile group was calculated using strain gauges readings and load shared by raft was calculated as discussed in section 5.2.7. In Figure 5-106, the load shared by the pile group (*LSPG*) with an *L/d* ratio of 10 remained almost the same at 60% and 80% relative densities. The *LSPG* was higher during the initial stages of loading on PRF, and the load shared by the raft (*LSR*) was higher than *LSPG* after a 2 kN to 4 kN load. In Figure 5-107, for PRF with an *L/d* ratio of 20, the *LSPG* was higher at I_d = 60% than at I_d = 40% and I_d = 80%. i.e., the *LSPG* increased as relative density increased from 40% to 60% and then decreased as relative density increased from 60% to 80%. Finally, Figure 5-108 shows that up to a 10 kN load, the *LSPG* in PRF with an *L/d* ratio of 30 was higher at I_d = 60%, and after a 10 kN load, it was higher at I_d = 80%.

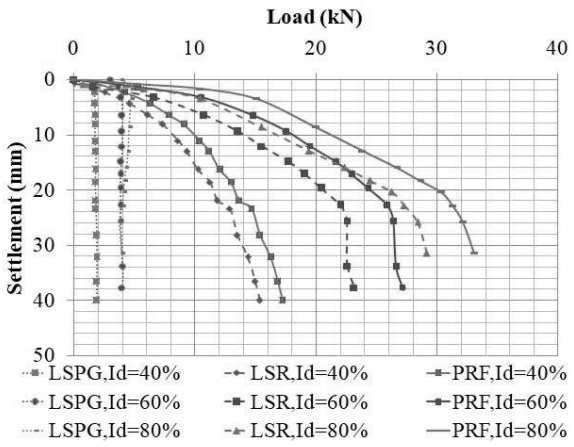

Figure 5-106 : Load settlement characteristics of piled raft and Load shared by pile group and raft at different relative densities of sand *(S = 5d; d = 9.7 mm; pile group = 5 × 5; L/d ratio = 10)*

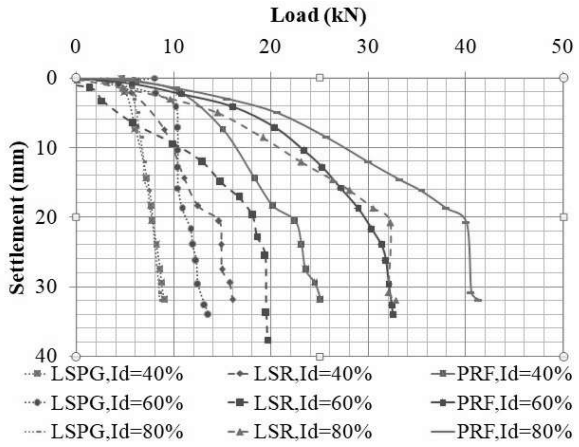

Figure 5-107 : Load settlement characteristics of piled raft and Load shared by pile group and raft at different relative densities of sand *(S = 5d; d = 9.7 mm; pile group = 5 × 5; L/d ratio = 20)*

Figure5-109 to Figure 5-111 illustrate the load settlement characteristics of piled rafts, load shared by pile group (*LSPG*), and load shared by raft (*LSR*) in PRF. These figures show the behaviour of PRF with varying *L/d* ratios of the pile at 40%, 60%, and 80% relative densities of sand. The load shared by the pile group (*LSPG*) of PRF increased when the *L/d* ratios of piles in PRF increased at all relative densities of sand. However, at 40% and 60% relative density of sand, the increase in *LSPG* of PRF with *L/d* = 30 was slight, compared to *L/d* = 20. An increase in *L/d* ratios of piles in PRF led to an increase in the *LSR* for all relative densities of sand. That could attributed to the increased confinement of sand caused by the higher *L/d* ratios of piles in PRF.

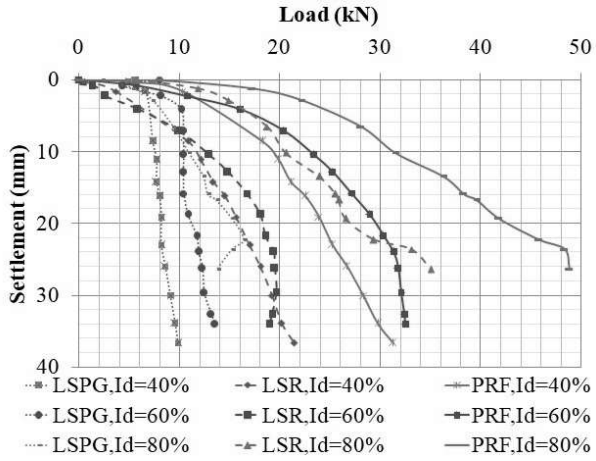

Figure 5-108 : Load settlement characteristics of piled raft and Load shared by pile group and raft at different relative densities of sand *(S = 5d; d = 9.7 mm; pile group = 5 × 5; L/d ratio = 30)*

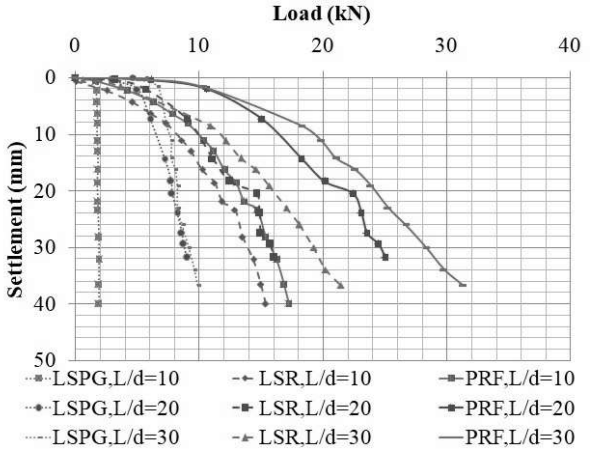

Figure5-109 : Load settlement characteristics of piled raft and Load shared by pile group and raft in PRF with different *L/d* ratios of pile at 40% relative density of sand *(S = 5d; d = 9.7 mm; pile group = 5 × 5)*

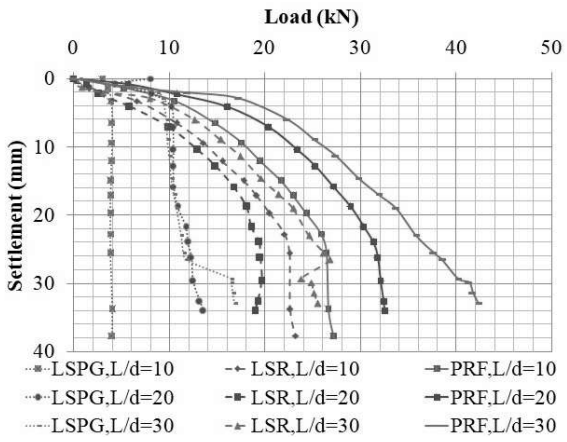

Figure 5-110 : Load settlement characteristics of piled raft and Load shared by pile group and raft in PRF with different *L/d* ratios of pile at 60% relative density of sand *(S = 5d; d = 9.7 mm; pile group = 5 × 5)*

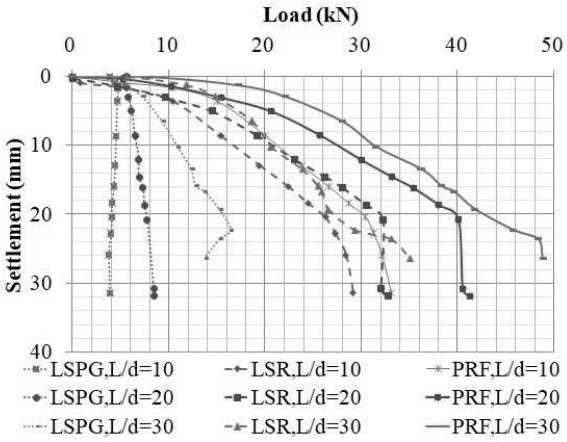

Figure 5-111 : Load settlement characteristics of piled raft and Load shared by pile group and raft in PRF with different *L/d* ratios of pile at 80% relative density of sand *(S = 5d; d = 9.7 mm; pile group = 5 × 5)*

Figure 5-112 to Figure 5-114 illustrate the percentage load shared by the pile group (% *LSPG*) and raft (% *LSR*) in a piled raft compared to the relative settlement (s/B_r) for PRF with *L/d* ratios of 10, 20, and 30 at I_d = 40%. The results indicate that at the initial relative settlement, the % *LSPG* was higher than the % *LSR*, and it decreased as the relative settlement increased. At I_d = 40%, the s/B_r values were 0.01, 0.008, and 0.022, respectively, at which the % *LSPG* and % *LSR* in the piled raft became equal (i.e., 50%) for PRF with *L/d* ratios of 10, 20, and 30. At I_d = 40%, the minimum value of % *LSPG* was 10%, 35%, and 32% in PRF with *L/d* ratios of 10, 20, and 30, respectively.

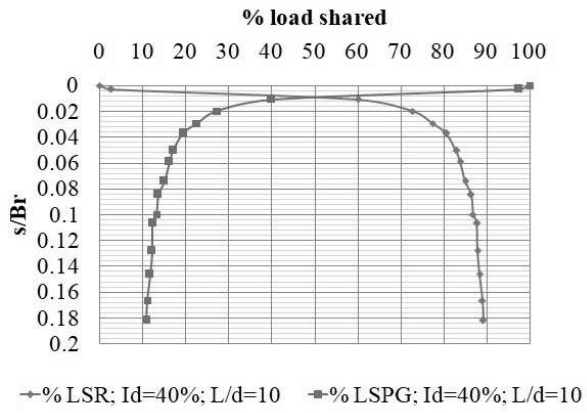

Figure 5-112 : Percentage load shared by pile group (%*LSPG*) and raft (%*LSR*) in piled raft at different relative settlement *(S = 5d; I_d = 40%; d = 9.7 mm; pile group = 5 × 5; L/d ratio = 10)*

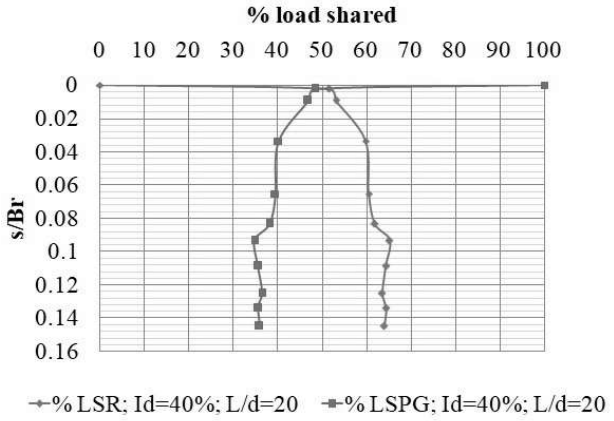

Figure 5-113 : Percentage load shared by pile group (%*LSPG*) and raft (%*LSR*) in piled raft at different relative settlement *(S = 5d; I_d = 40%; d = 9.7 mm; pile group = 5 × 5; L/d ratio = 20)*

Figure 5-115 to Figure 5-117depicts the percentage load shared by the pile group (% *LSPG*) and raft (% *LSR*) in a piled raft compared to the relative settlement (s/B_r) for PRF with *L/d* ratios of 10, 20, and 30 at I_d = 60%. The results show that at the initial relative settlement, the % *LSPG* was higher than the % *LSR*, and it decreased with an increase in relative settlement. At I_d = 60%, the s/B_r values were 0.012, 0.036, and 0.016, respectively, at which the % *LSPG* and % *LSR* in the piled raft became equal (i.e., 50%) for PRF with *L/d* ratios of 10, 20, and 30. At I_d = 60%, the minimum value of % *LSPG* was 15%, 38%, and 32% in PRF with *L/d* ratios of 10, 20, and 30, respectively.

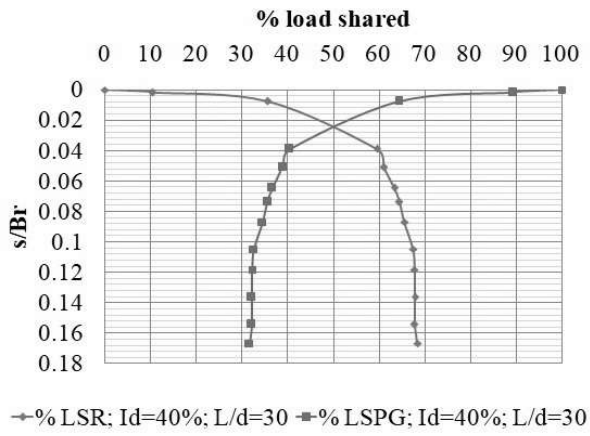

Figure 5-114 : Percentage load shared by pile group (% *LSPG*) and raft (% *LSR*) in piled raft at different relative settlement *(S = 5d; I_d = 40%; d = 9.7 mm; pile group = 5 × 5; L/d ratio = 30)*

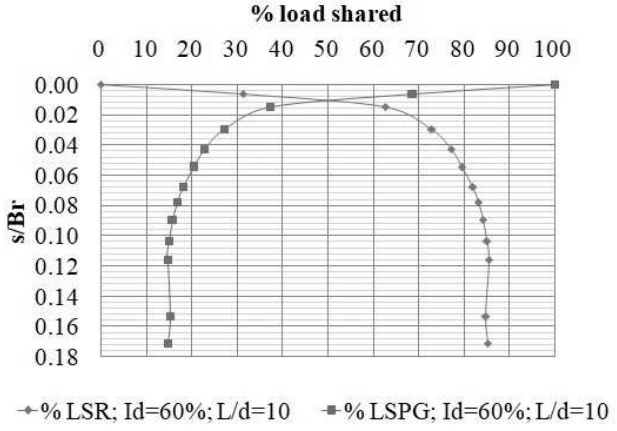

Figure 5-115 : Percentage load shared by pile group (% *LSPG*) and raft (% *LSR*) in piled raft at different relative settlement *(S = 5d; I_d = 60%; d = 9.7 mm; pile group = 5 × 5; L/d ratio = 10)*

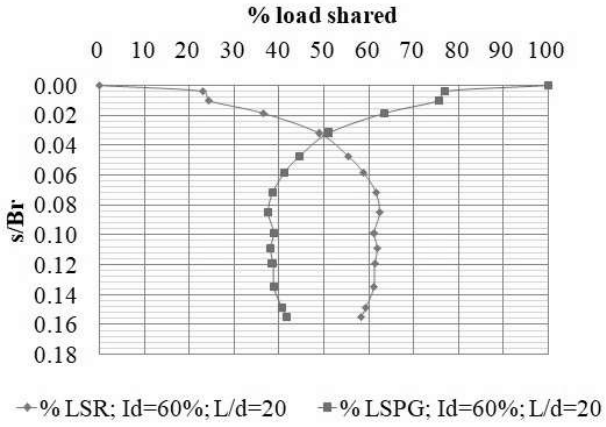

Figure 5-116 : Percentage load shared by pile group (% *LSPG*) and raft (% *LSR*) in piled raft at different relative settlement *(S = 5d; I_d = 60%; d = 9.7 mm; pile group = 5 × 5; L/d ratio = 20)*

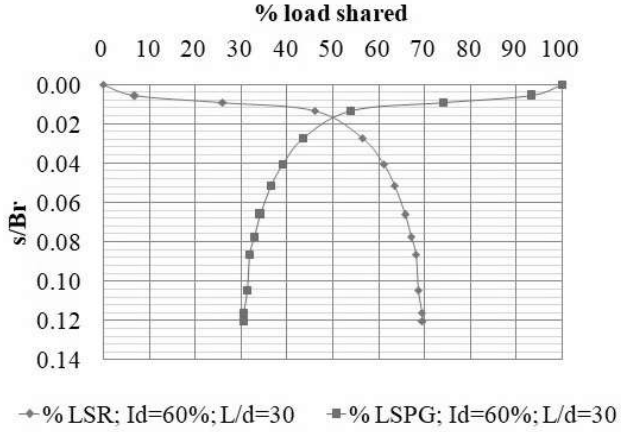

Figure 5-117 : Percentage load shared by pile group (% *LSPG*) and raft (% *LSR*) in piled raft at different relative settlement *(S = 5d; I_d = 60%; d = 9.7 mm; pile group = 5 × 5; L/d ratio = 30)*

Figure 5-118 to Figure 5-120 illustrates the percentage load shared by the pile group (% *LSPG*) and raft (% *LSR*) in a piled raft compared to the relative settlement (s/B_r) for PRF with *L/d* ratios of 10, 20, and 30 at I_d = 80%. The results show that at the initial relative settlement, the % *LSPG* was higher than the % *LSR*, and it decreased with relative settlement. At I_d = 80%, the s/B_r values were 0.008, 0.008, and 0.00, respectively, at which the % *LSPG* and % *LSR* in the piled raft became equal (i.e.50%) for PRF with *L/d* ratios of 10, 20, and 30. At I_d = 80%, the minimum value of % *LSPG* was 11%, 19%, and 29% in PRF with *L/d* ratios of 10, 20, and 30, respectively.

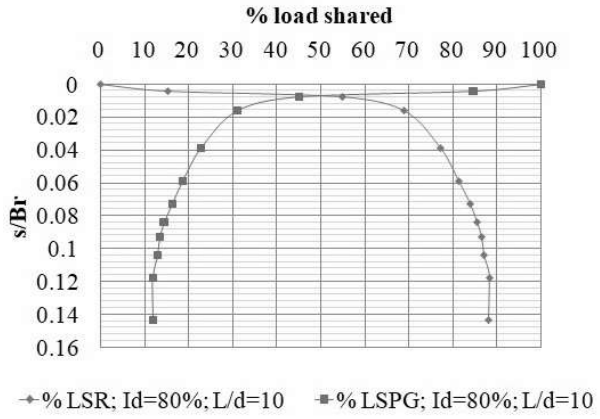

Figure 5-118 : Percentage load shared by pile group (% *LSPG*) and raft (% *LSR*) in piled raft at different relative settlement *(S = 5d; I_d = 80%; d = 9.7 mm; pile group = 5 × 5; L/d ratio = 10)*

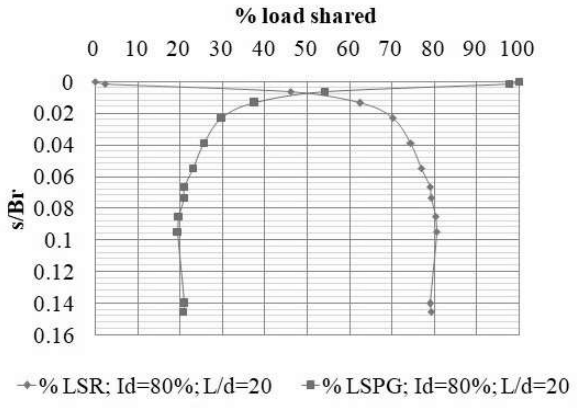

Figure 5-119 : Percentage load shared by pile group (% *LSPG*) and raft (% *LSR*) in piled raft at different relative settlement *(S = 5d; I_d = 80%; d = 9.7 mm; pile group = 5 × 5; L/d ratio = 20)*

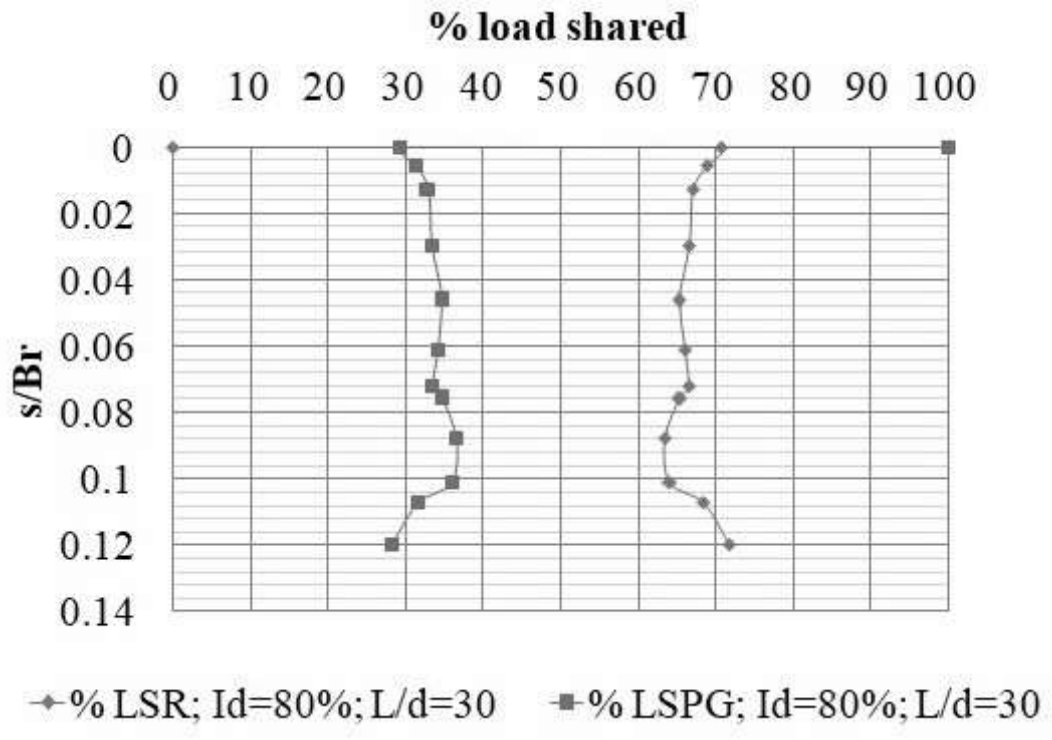

Figure 5-120 : Percentage load shared by pile group (% *LSPG*) and raft (% *LSR*) in piled raft at different relative settlement *(S = 5d; I_d = 80%; d = 9.7 mm; pile group = 5 × 5; L/d ratio = 30)*

Figure 5-121 to Figure 5-126 show how the load is shared between the pile group (*LSPG*) and raft (*LSR*) at *IYL* and *FYL* of a piled raft foundation, with different *L/d* ratios at different relative densities of the sand bed. It can be observed that in the case of PRF with an *L/d* ratio of pile = 10, the load shared by the pile group (*LSPG*) was almost the same at *IYL* and *FYL*. However, in the case of PRF with *L/d* ratios of pile = 20 and 30, there was a slight increase in *LSPG* at *FYL* compared to *IYL*. Nevertheless, the increment in *LSPG* of PRF with an *L/d* ratio of pile = 30 was higher at I_d = 80%. It is also observed that the *LSR* value at *FYL* was significantly higher than at *IYL* for all *L/d* ratios. This suggests that after *IYL*, the contribution of the pile group in sharing the load of PRF was less compared to the raft.

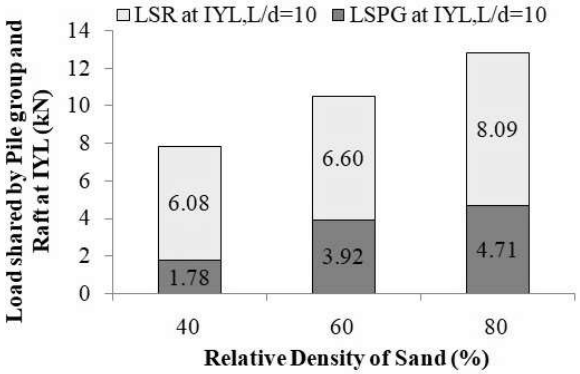

Figure 5-121 : Load shared by pile group and raft at *IYL* of piled raft foundation *(S = 5d; L/d ratio of pile =10; Pile group = 5 × 5)*

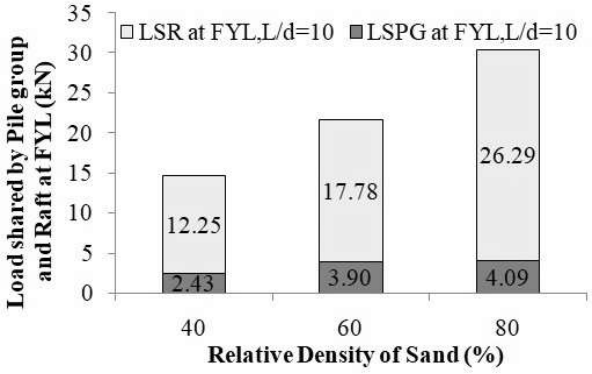

Figure 5-122 : Load shared by pile group and raft at *FYL* of piled raft foundation *(S = 5d; L/d ratio of pile =10; Pile group = 5 × 5)*

Compared to a relative density of 40%, the percentage increase in *LSR* at *IYL* of PRF with *L/d* = 10 was 9% and 33% at 60% and 80% relative density, respectively. Similarly, at *FYL*, the percentage increase in *LSR* was 45% and 115% at 60% and 80% relative density, respectively. For PRF with *L/d* = 10, the percentage increase in *LSPG* at 60% and 80% relative densities was 121% and 165%, respectively, compared to 40% relative density. The corresponding values for *FYL* were 60% and 68%, respectively.

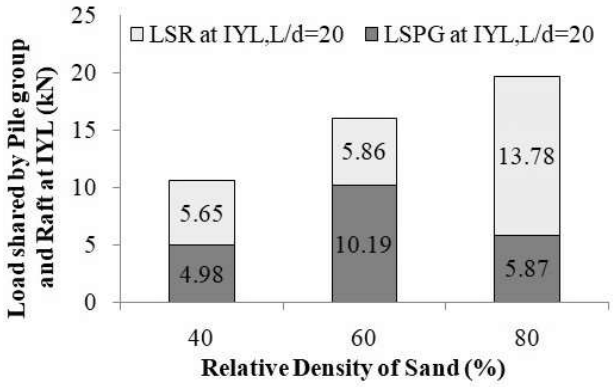

Figure 5-123 : Load shared by pile group and raft at *IYL* of piled raft foundation *(S = 5d; L/d ratio of pile = 20; Pile group = 5 × 5)*

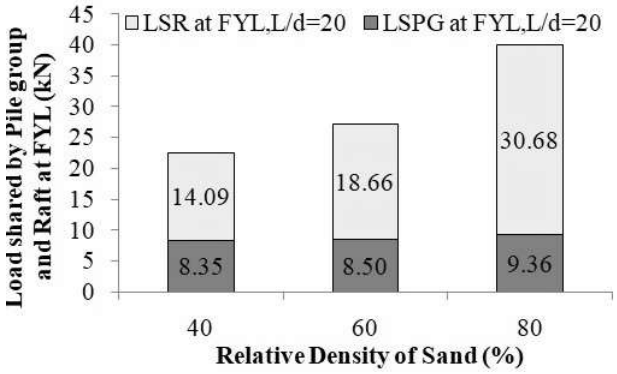

Figure 5-124 : Load shared by pile group and raft at *FYL* of piled raft foundation *(S = 5d; L/d ratio of pile = 20; Pile group = 5 × 5)*

As compared to 40% relative density, the percentage increase in *LSR* at *IYL* of PRF with *L/d* = 20 at 60% and 80% relative density were to be 4% and 144%, respectively, while the same values at *FYL* were to be 32% and 118% respectively. Compared to 40% relative density, the percentage increase in *LSPG* at *IYL* of PRF with *L/d* = 20 at 60% and 80% relative density was 105% and 18%, respectively, whereas the same values at *FYL* were 2% and 12%.

Compared to 40% relative density, the *LSR* at *IYL* of PRF with *L/d* = 30 was increased by 17% at 60% relative density and decreased by 8% at 80% relative density of sand. Compared to 40% relative density, the *LSR* at *FYL* of PRF with *L/d* = 30 at 60% and 80% relative density were increased by 149% and 235%, respectively.

In comparison to a 40% relative density, the *LSPG* at *IYL* of PRF with *L/d* = 30 increased by 17% at 60% relative density and decreased by 8% at 80% relative density. At *FYL*, the values decreased by 31% and increased by 9% at 60% and 80% relative densities, respectively.

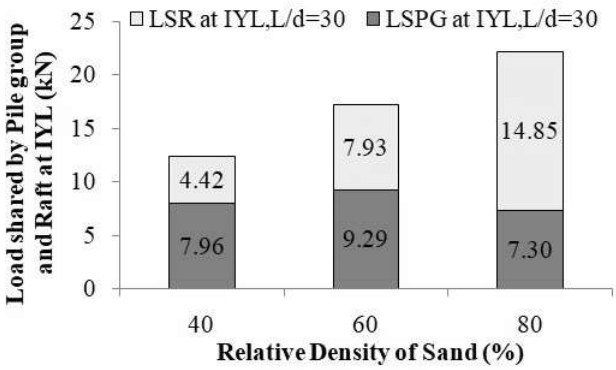

Figure 5-125 : Load shared by pile group and raft at *IYL* of piled raft foundation *(S = 5d; L/d ratio of pile =30; Pile group = 5 × 5)*

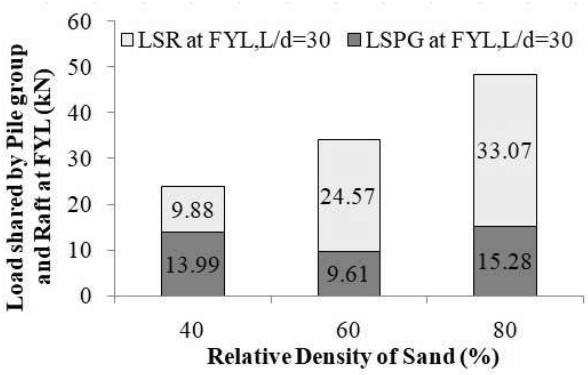

Figure 5-126 : Load shared by pile group and raft at *FYL* of piled raft foundation *(S = 5d; L/d ratio of pile =30; Pile group = 5 × 5)*

At I_d = 40%, the *LSR* at *IYL* of PRF with *L/d* = 20 and 30 decreased by 7% and 27%, respectively, compared to PRF with *L/d* = 10. the *LSR* at *FYL* of PRF with *L/d* = 20 and 30 were increased by 15% and decreased by 19%, respectively, compared to PRF with *L/d* = 10.

At I_d = 40%, the *LSPG* at *IYL* of PRF with *L/d* = 20 and 30 was increased by 180% and 348%, respectively, as compared to PRF with *L/d* = 10, while the same values were 243% and 475% at *FYL*.

At I_d = 60%, the *LSR* at *IYL* of PRF with *L/d* = 20 decreased by 11% as compared to *L/d* = 10, while the *LSR* at *IYL* of PRF with *L/d* = 30 was increased by 20% as compared to *L/d* = 10. At I_d = 60%, the *LSR* at *FYL* of PRF with *L/d* = 20 and 30 increased by 5% and 38% respectively, compared to *L/d* =10.

At I_d = 60%, the increase in *LSPG* at *IYL* of PRF with *L/d* = 20 and 30 was 160% and 137%, respectively, as compared to PRF with *L/d* = 10, while the same values were 118% and 146% at *FYL*.

At I_d = 80%, the increase in *LSR* at *IYL* of PRF with *L/d* = 20 and 30 was 70% and 84%, respectively, as compared to PRF with *L/d* = 10, while the same values were 17% and 26% at *FYL*.

At I_d = 80%, the increase in *LSPG* at *IYL* of PRF with *L/d* = 20 and 30 was 24% and 55%, respectively, as compared to PRF with *L/d* = 10, while the same values were 129% and 273% at *FYL*.

5.3.3.2.3 Piled Raft Coefficient (α_p)

Figure 5-127 to Figure 5-132 depicts the Piled raft coefficient (α_p) vs. relative settlement characteristics of piled raft foundation with different *L/d* ratios of the pile at different relative densities of the sand bed. It observed that for the *L/d* ratio of pile = 10, the α_p was decreased as relative settlement and relative density increased. The decrement in α_p was high at low relative settlement (s/B_r), and after s/B_r = 0.04, it decreased slowly in most of the cases of PRF considered in Figure 5-127 to Figure 5-132. so after s/B_r = 0.04, the contribution of the pile group in the piled raft foundation will be less as compared to the raft at all relative densities of the sand bed.

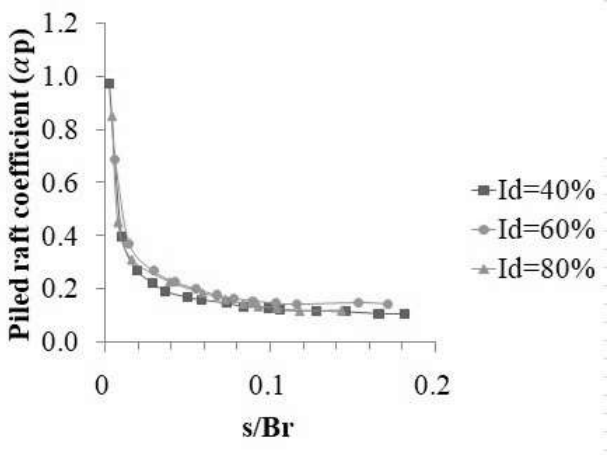

Figure 5-127 : Piled raft coefficient (α_p) vs. relative settlement characteristics of piled raft foundation at different relative densities of sand bed *(S = 5d; L/d ratio of pile = 10; Pile group = 5 × 5)*

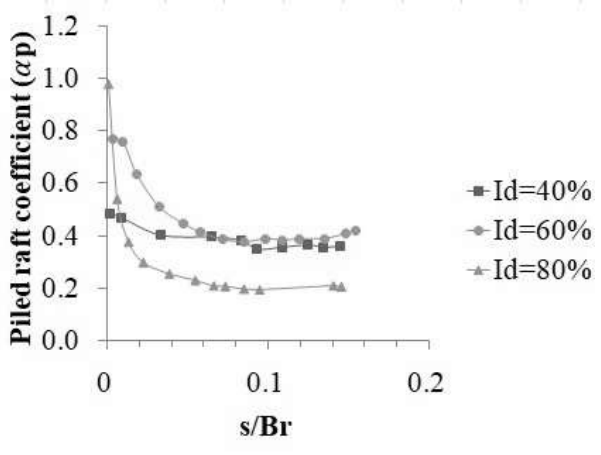

Figure 5-128 : Piled raft coefficient (α_p) vs. relative settlement characteristics of piled raft foundation at different relative densities of sand bed *(S = 5d; L/d ratio of pile = 20; Pile group = 5 × 5)*

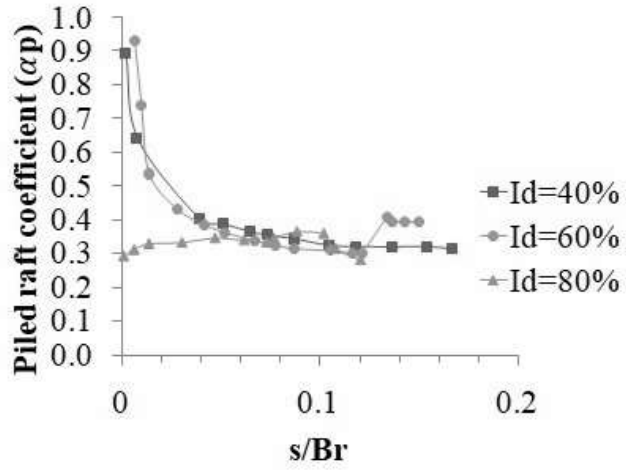

Figure 5-129 : Piled raft coefficient (α_p) vs. relative settlement characteristics of piled raft foundation at different relative densities of sand bed *(S = 5d; L/d ratio of pile = 30; Pile group = 5 × 5)*

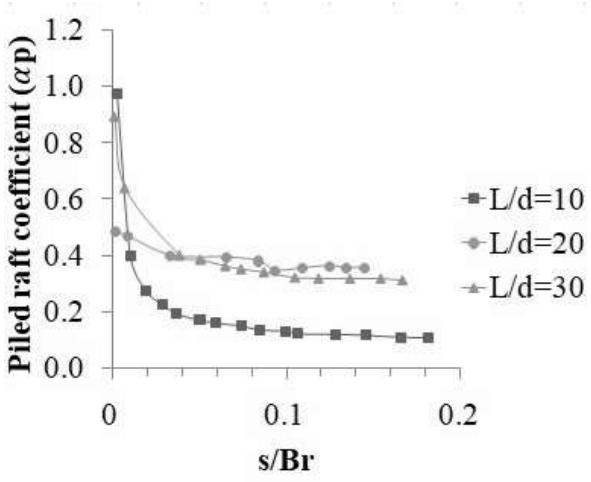

Figure 5-130 : Piled raft coefficient (α_p) vs. relative settlement characteristics of piled raft foundation at different *L/d* ratio of pile *(S = 5d; I_d = 40%; L/d ratio of pile =10, 20 and 30; Pile group = 5 × 5)*

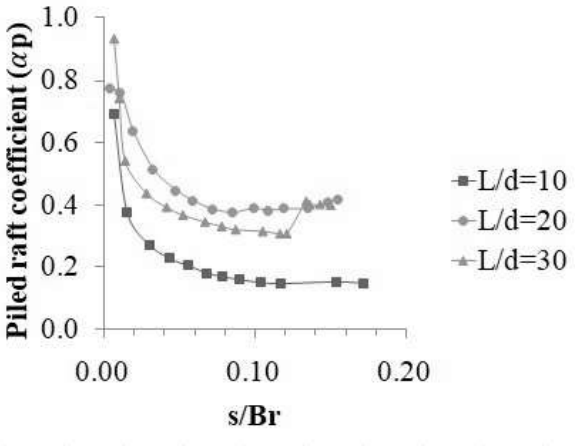

Figure 5-131 : Piled raft coefficient (α_p) vs. relative settlement characteristics of piled raft foundation at different *L/d* ratio of pile *(S = 5d; I_d = 60%; L/d ratio of pile = 10, 20 and 30; Pile group = 5 × 5)*

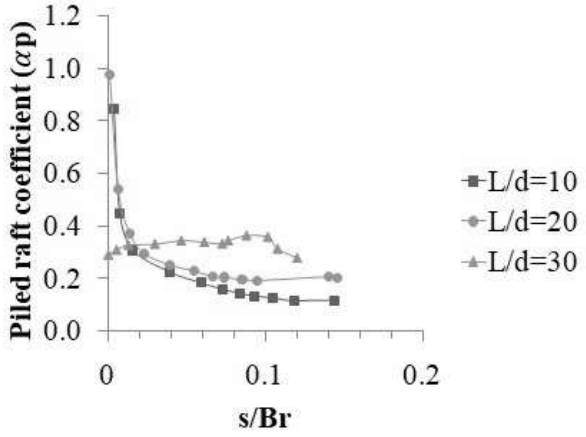

Figure 5-132 : Piled raft coefficient (α_p) vs. relative settlement characteristics of piled raft foundation at different *L/d* ratio of pile *(S = 5d; I_d = 80%; L/d ratio of pile = 10, 20 and 30; Pile group = 5 × 5)*

5.3.3.2.4 Settlement Reduction Ratio (SRR) and Load Improvement Ratio (LIR)

Table 5-29 to Table 5-31 represent the settlement reduction ratio of PRF with different *L/d* ratios of the pile at different load levels and 40%, 60%, and 80% relative densities of the sand bed, respectively. At 40% relative density, with an *L/d* ratio of 10, the settlement reduction ratio in PRF ranged from -58% to 5%, while for *L/d* ratios of 20 and 30, the range was approximately 73% to 88%. At 60% relative density of the sand bed, the range of settlement reduction ratio in PRF with an *L/d* ratio of 10, 20, and 30 was -6% to 21%, 39% to 56%, and 17% to 70%, respectively. Finally, the range of settlement reduction ratio for PRF with an *L/d* ratio of 10, 20, and 30 was -53% to 30%, 38% to 54%, and 81% to 93%, respectively at I_d = 80% .

Table 5-29 Settlement reduction ratio of PRF with different *L/d* ratios of pile at different load levels and 40% relative densities of the sand bed

I_d (%)	Load (kN)	Settlement (mm)				Settlement reduction ratio (%)		
		UPR	PRF *(L/d=10)*	PRF *(L/d=20)*	PRF *(L/d=30)*	PRF *(L/d=10)*	PRF *(L/d=20)*	PRF *(L/d=30)*
40	2.5	0.77	1.21	0.19	0.15	-58	75	81
	5	2.48	3.07	0.38	0.30	-24	85	88
	10	8.45	10.23	1.82	1.53	-21	78	82
	12.5	14.22	17.36	4.30	3.51	-22	70	75
	15	27.11	25.68	7.31	5.69	5	73	79

Table 5-30 Settlement reduction ratio of PRF with different *L/d* ratios of pile at different load levels and 60% relative densities of the sand bed

I_d (%)	Load(kN)	Settlement (mm)				Settlement reduction ratio (%)		
		UPR	PRF *(L/d=10)*	PRF *(L/d=20)*	PRF *(L/d=30)*	PRF *(L/d=10)*	PRF *(L/d=20)*	PRF *(L/d=30)*
60	2.5	0.62	0.66	0.38	0.51	-6	39	17
	5	1.62	1.31	0.75	1.02	19	54	37
	10	4.42	3.09	2.06	1.79	30	53	59
	12.5	6.13	4.79	2.88	2.15	22	53	65
	15	8.54	6.76	3.75	2.55	21	56	70

Table 5-31 Settlement reduction ratio of PRF with different *L/d* ratios of pile at different load levels and 80% relative densities of the sand bed

I_d (%)	Load (kN)	Settlement (mm)				Settlement reduction ratio (%)		
		UPR	PRF *(L/d=10)*	PRF *(L/d=20)*	PRF *(L/d=30)*	PRF *(L/d=10)*	PRF *(L/d=20)*	PRF *(L/d=30)*
80	2.5	0.28	0.43	0.13	0.02	-53	54	92
	5	0.65	0.86	0.26	0.04	-34	59	93
	10	2.07	1.62	1.38	0.31	21	34	85
	12.5	3.41	2.50	2.10	0.62	27	38	82
	15	4.99	3.48	2.85	0.93	30	43	81

Table 5-32 to Table 5-34 represent the load improvement ratio of PRF with different *L/d* ratios of the pile at different load levels and 40%, 60%, and 80% relative densities of the sand bed, respectively. It observed that at 40% relative density, the range of load improvement ratio in PRF with an *L/d* ratio of 10 was 0.9 to 1, while with an *L/d* ratio of 20 and 30, it was around 1.48 to 1.70 and 1.72 to 1.86 respectively. At 60% relative density of the sand bed, the range of load improvement ratio in PRF with an *L/d* ratio of pile equal to 10, 20, and 30 was 1.10 to 1.31, 1.37 to 1.58, and 1.57 to 1.94, respectively. The range of load improvement ratio of PRF with an *L/d* ratio of pile equal to 10, 20, and 30 was 0.98 to 1.13, 1.27 to 1.47, and 1.41 to 1.67, respectively.

Table 5-32 Load improvement ratio of PRF with different *L/d* ratios of pile at different settlement levels and 40% relative densities of the sand bed

I_d (%)	Settlement (mm)	Load (kN)				Load improvement ratio		
		UPR	PRF (L/d=10)	PRF (L/d=20)	PRF (L/d=30)	PRF (L/d=10)	PRF (L/d=20)	PRF (L/d=30)
40	5.5	7.96	7.16	13.50	14.78	0.90	1.70	1.86
	11	11.33	10.33	16.73	19.78	0.91	1.48	1.75
	16.5	13.18	12.16	19.30	22.72	0.92	1.46	1.72
	22	13.72	13.69	22.72	24.89	1.00	1.66	1.81
	27.5	15.22	15.25	23.57	27.30	1.00	1.55	1.79

Table 5-33 Load improvement ratio of PRF with different *L/d* ratios of pile at different settlement levels and 60% relative densities of the sand bed

I_d (%)	Settlement (mm)	Load(kN)				Load improvement ratio		
		UPR	PRF (L/d=10)	PRF (L/d=20)	PRF (L/d=30)	PRF (L/d=10)	PRF (L/d=20)	PRF (L/d=30)
60	5.5	11.69	13.43	18.02	21.44	1.15	1.54	1.83
	11	17.06	18.70	23.81	27.05	1.10	1.40	1.59
	16.5	20.08	22.59	27.58	31.44	1.13	1.37	1.57
	22	20.84	25.49	30.43	35.26	1.22	1.46	1.69
	27.5	20.15	26.46	31.90	39.12	1.31	1.58	1.94

Table 5-34 Load improvement ratio of PRF with different *L/d* ratios of pile at different settlement levels and 80% relative densities of the sand bed

I_d (%)	Settlement (mm)	Load(kN)				Load improvement ratio		
		UPR	PRF (L/d=10)	PRF (L/d=20)	PRF (L/d=30)	PRF (L/d=10)	PRF (L/d=20)	PRF (L/d=30)
80	5.5	15.78	17.03	21.40	26.39	1.08	1.36	1.67
	11	22.62	22.15	28.72	32.71	0.98	1.27	1.45
	16.5	27.92	27.14	35.77	39.25	0.97	1.28	1.41
	22	27.36	30.98	40.10	45.40	1.13	1.47	1.66
	27.5	31.30	32.45	40.38	50.94	1.04	1.29	1.63

5.3.3.2.5 Comparison between Predicted and Experimental values of IYL and FYL

Table 5-35 represents the efficiency factor of raft (C_1) and pile group (C_2) in PRF with different *L/d* ratios of pile calculated as mentioned in 5.3.3.1.6. Table 5-36 represents the efficiency factors of the raft (C_1), and pile group (C_2) in PRF with different *L/d* ratios of pile calculated from the proposed equations (5-14) to (5-15) and percentage variations in *IYL* determined from proposed equation (5-16) with respect to experimental *IYL*.The percentage variations in the predicted *IYL* from experimental *IYL* are observed to be in the range of -54% to +37%, and in most of the cases, it is found to be less than 25%. Figure 5-133 represents the comparison of *IYL* of piled raft foundation with different *L/d* ratios of pile at different relative densities of sand bed found from experimental results and calculated from the proposed equation (5-16). Table 5-37 shows the percentage variations in *FYL* of PRF with different *L/d* ratios of pile determined from the proposed equation (5-19) with respect to experimental *FYL*. The range of percentage variation in predicted *FYL* as compared to experimental *FYL* is found to be less than 30% in most cases. Figure 5-134 represents the comparison of *FYL* of piled raft foundation with different *L/d* ratios of pile at different relative densities of sand bed found from experimental results and calculated from the proposed equation.

Table 5-35 Efficiency factor of raft (C_1), efficiency factor of pile group (C_2), and efficiency of PRF at *IYL* (β_1) with different *L/d* ratios of pile

L/d **ratio of piles**	I_d **(%)**	***IYL*** **(kN)**	***LSR*** **in PRF at *IYL* (kN)**	***LSP*** ***G*** **in PRF at *IYL* (kN)**	**Piled raft coefficient (α_p)**	**Settlement s_i at *IYL* (mm)**	B_r **(mm)**	s/B_r	$(P_r)_{s_i}$ **(kN)**	$(P_{sp})_{s_i}$ **(kN)**	$(P_{pg})_{s_i}$ **(kN)**	C_1	C_2	(β_1)
10	40	7.85	6.08	1.78	0.23	6.45	220	0.03	8.71	0.01	0.30	0.70	5.91	0.87
	60	10.52	6.60	3.92	0.37	3.28	220	0.01	8.04	0.01	0.35	0.82	11.20	1.25
	80	12.81	8.09	4.71	0.37	2.62	220	0.01	11.15	0.06	1.43	0.73	3.30	1.02
20	40	10.63	5.65	4.98	0.47	2.04	220	0.01	4.46	0.06	0.79	1.27	6.32	2.02
	60	16.05	5.86	10.19	0.63	4.12	220	0.02	9.48	0.11	3.82	0.62	2.67	1.21
	80	19.65	13.78	5.87	0.30	4.75	220	0.02	14.63	0.31	6.11	0.94	0.96	0.95
30	40	12.38	4.42	7.96	0.64	1.94	220	0.01	4.32	0.16	4.34	1.02	1.83	1.43
	60	17.22	7.93	9.29	0.54	2.90	220	0.01	7.39	0.31	6.79	1.07	1.37	1.21
	80	22.15	14.85	7.30	0.33	2.86	220	0.01	11.56	0.31	11.42	1.29	0.64	0.96

Table 5-36 Efficiency factor of raft (C_1), and efficiency factor of pile group (C_2) in PRF with different *L/d* ratios of pile calculated from proposed equations and percentage variations in *IYL* determined from proposed equations with respect to experimental *IYL*

***L/d* ratio of piles**	**I_d (%)**	***IYL* (kN)**	***S/d***	**B_r/L_r**	***L/d***	***n***	**s/B_r**	**C_1**	**C_2**	***IYL*-EXP (kN)**	***IYL*-PROPOSED EQUATION (kN)**	**% Variations in predicted *IYL* as compared to *IYL*-EXP**
10	40	7.85	5	1	10	25	0.03	0.485	4.194	7.85	5.49	-30
	60	10.52	5	1	10	25	0.01	0.371	4.935	10.52	4.71	-55
	80	12.81	5	1	10	25	0.01	0.394	4.773	12.81	11.22	-12
20	40	10.63	5	1	20	25	0.01	0.306	5.407	10.63	5.63	-47
	60	16.05	5	1	20	25	0.02	0.930	2.231	16.05	17.33	8
	80	19.65	5	1	20	25	0.02	1.431	1.095	19.65	27.61	41
30	40	12.38	5	1	30	25	0.01	0.437	4.491	12.38	21.40	73
	60	17.22	5	1	30	25	0.01	0.984	2.066	17.22	21.30	24
	80	22.15	5	1	30	25	0.01	1.292	1.333	22.15	30.15	36

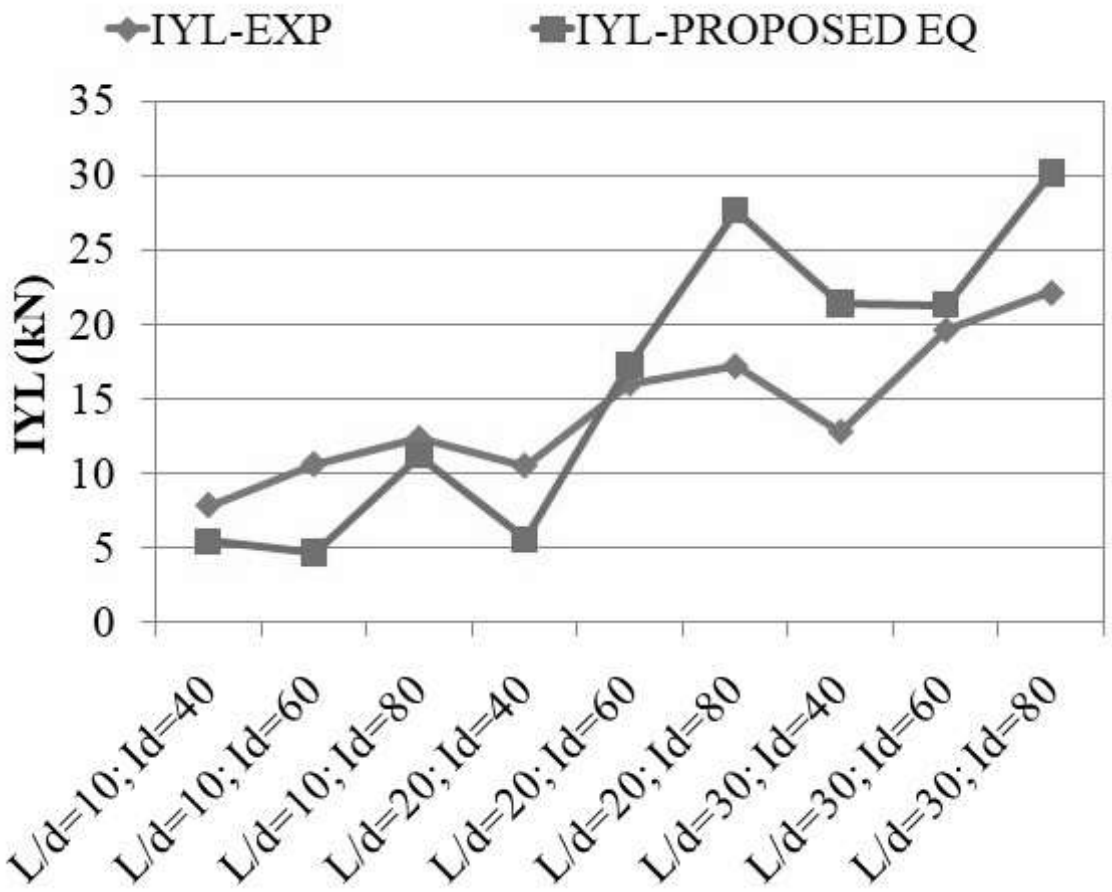

Figure 5-133 : Comparison of *IYL* of piled raft foundation with different *L/d* ratios of pile at different relative density of sand bed found from experimental results and calculated from proposed equation

The efficiency of the piled raft with different *L/d* ratios of piles at *IYL* (β_1) and at *FYL* (β_2) was found to be minimum at 80% relative density in most of the cases.

Table 5-37 Percentage variations in *FYL* of PRF with different *L/d* ratios of pile determined from proposed equations with respect to experimental *FYL* and efficiency of PRF at *FYL* (β_2)

***L/d* ratio of piles**	I_d **(%)**	***FYL* (kN)**	***LSR* at FYL**	***LSPG* at FYL**	α_p	**Settlement (mm) at FYL**	B_r	s/B_r	C_3	C_4	Qur **(kN)**	Qu,pg **(kN)**	***FYL*-EXP (kN)**	***FYL* - PROPOSED EQUATION (kN)**	**% Variations in predicted FYL as compared to FYL-EXP**	(β_2)
10	40	14.68	12.25	2.43	0.17	23.38	220	0.11	0.603	4.238	13.25	0.293	14.68	9.24	-37	1.08
	60	21.68	17.78	3.90	0.18	14.95	220	0.07	0.603	4.243	20.3	0.856	21.68	15.87	-27	1.02
	80	30.39	26.29	4.09	0.13	20.42	220	0.09	0.610	4.153	28.69	1.924	30.39	25.49	-16	0.99
20	40	22.43	14.09	8.35	0.37	20.51	220	0.09	0.610	4.152	13.25	1.302	22.43	13.49	-40	1.54
	60	27.16	18.66	8.50	0.31	15.82	220	0.07	0.612	4.121	20.3	3.965	27.16	28.77	6	1.12
	80	40.04	30.68	9.36	0.23	20.82	220	0.09	0.626	3.953	28.69	6.39	40.04	43.21	8	1.14
30	40	23.87	9.88	13.99	0.59	19.11	220	0.09	0.616	4.074	13.25	6.698	23.87	35.45	49	1.20
	60	34.19	24.57	9.61	0.28	25.55	220	0.12	0.638	3.810	20.3	7.026	34.19	39.71	16	1.25
	80	48.35	33.07	15.28	0.32	23.61	220	0.11	0.648	3.693	28.69	13.7	48.35	69.19	43	1.14

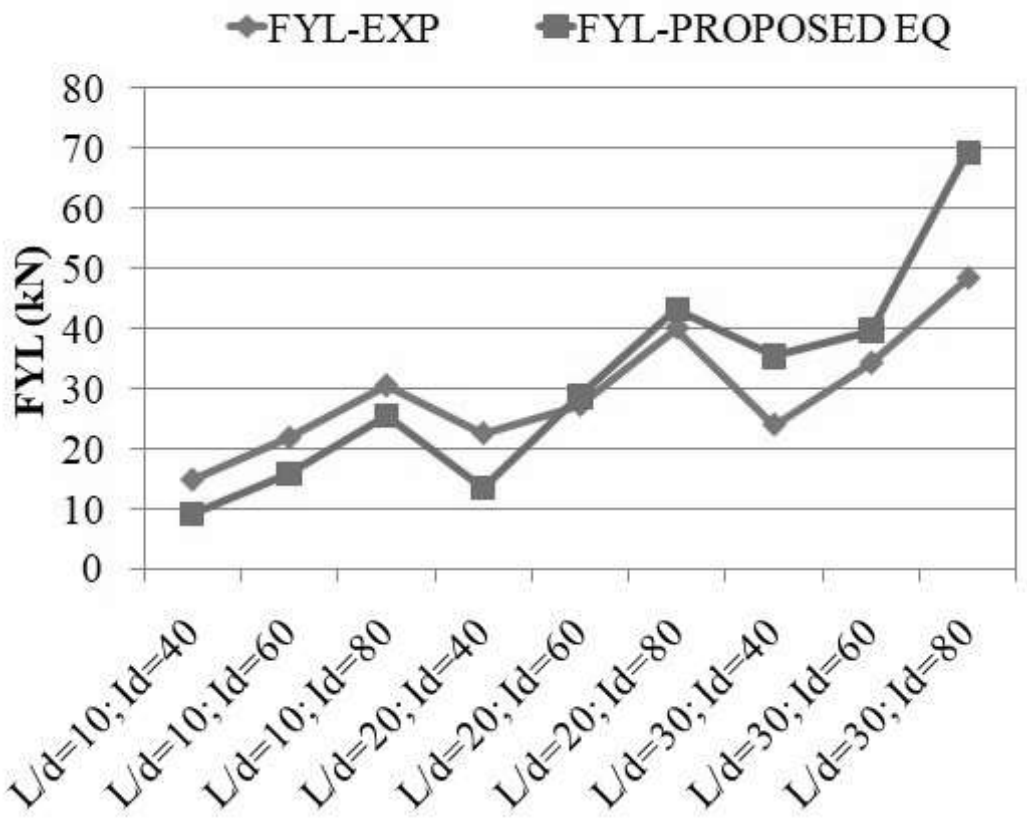

Figure 5-134 : Comparison of *FYL* of piled raft foundation with different *L/d* ratios of pile at different relative density of sand bed found from experimental results and calculated from proposed equation

5.3.3.2.6 Comparison between Predicted and Experimental values of $(k_{pr})_p$

Table 5-38 shows the variations in primary stiffness of PRF $(k_{pr})_p$ with different *L/d* ratios of pile (experimental) and determined from the proposed equation (5-22).The results show that the $(k_{pr})_p$ increased in all cases with an increase in the relative density of sand. The $(k_{pr})_p$ of PRF with *L/d* = 10 increased by 57% and 139% at 60% and 80% relative density, respectively, compared to 40% relative density of sand. The $(k_{pr})_p$ of PRF with *L/d* = 20 increased by 10% and 62% at 60% and 80% relative density, respectively, compared to 40% relative density. The

$(k_{pr})_p$ of PRF with *L/d* =30 increased by 59% and 77% at 60% and 80% relative density, respectively, compared to 40% relative density of sand. The $(k_{pr})_p$ of PRF with *L/d* = 20 increased by 63%, 14%, and 11% at I_d = 40%, I_d = 60%, and I_d = 80%, respectively, compared to *L/d* = 10. The $(k_{pr})_p$ of PRF with *L/d* = 30 increased by 113%, 116%, and 57% at I_d = 40%, I_d = 60%, and I_d = 80%, respectively, compared to *L/d* = 10.

Figure 5-135 shows the comparison of primary stiffness of PRF $(k_{pr})_p$ with different *L/d* ratios of pile determined from the proposed equation with respect to the experimental value.

5.3.3.2.7 Comparison between Predicted and Experimental values of $(k_{pr})_s$

The secondary stiffness $(k_{pr})_s$ of PRF with *L/d* = 10 increased by 10% and 23% at 60% and 80% relative density, respectively, compared to 40% relative density of sand. The secondary stiffness $(k_{pr})_s$ of PRF with *L/d* =20 increased by 3% and 40% at 60% and 80% relative density, respectively, compared to 40% relative density of sand. The secondary stiffness $(k_{pr})_s$ of PRF with *L/d* = 30 increased by 8% and 27% at 60% and 80% relative density, respectively, compared to 40% relative density of sand. The $(k_{pr})_s$ of PRF with *L/d* = 20 increased by 13%, 6%, and 29% at I_d = 40%, I_d = 60%, and I_d = 80%, respectively, compared to *L/d* = 10. The $(k_{pr})_s$ of PRF with *L/d* = 30 increased by 20%, 18%, and 24% at I_d = 40%, I_d = 60%, and I_d = 80%, respectively, compared to *L/d* = 10.

Table 5-39 and Figure 5-136 shows the comparison of secondary stiffness of PRF $(k_{pr})_s$ with different *L/d* ratios of pile determined from the proposed equation (5-23) with respect to the experimental value.

Table 5-38 Variations in primary stiffness of PRF $(k_{pr})_p$ with different *L/d* ratios of pile (experimental) and determined from the proposed equation

L/d **ratio of piles**	**Relative density of sand (%)**	***Br*** **(m)**	**TLP (m)**	**Primary stiffness of PRF** $(k_{pr})_p$ **in kN/m (Experimental)**	**Secondary Stiffness of PRF** $(k_{pr})_s$ **in kN/m**	**Initial stiffness of UPR** (k_{ri}) **(kN/m)**	**Initial stiffness of PG** $(k_{pg})_i$ **(Experimental)**	**Primary stiffness of PRF** $(k_{pr})_p$ **in kN/m (Proposed equation)**	**% variation in** $(k_{pr})_p$ **calculated from proposed eq. and** $(k_{pr})_p$ **- EXP.**
10	40	0.22	2.425	1765.02	734.98	2321.44	19.51	2853.18	62
	60	0.22	2.425	2769.20	811.40	3585.12	25.66	4305.51	55
	80	0.22	2.425	4226.81	902.57	5331.36	319.38	6140.25	45
20	40	0.22	4.85	2877.06	828.98	2321.44	203.16	3011.12	5
	60	0.22	4.85	3164.36	857.71	3585.12	388.60	4617.63	46
	80	0.22	4.85	4673.86	1162.15	5331.36	414.79	6222.30	33
30	40	0.22	7.275	3754.84	884.25	2321.44	686.11	3426.46	-9
	60	0.22	7.275	5981.83	954.38	3585.12	954.81	5104.57	-15
	80	0.22	7.275	6645.11	1122.42	5331.36	1029.84	6751.24	2

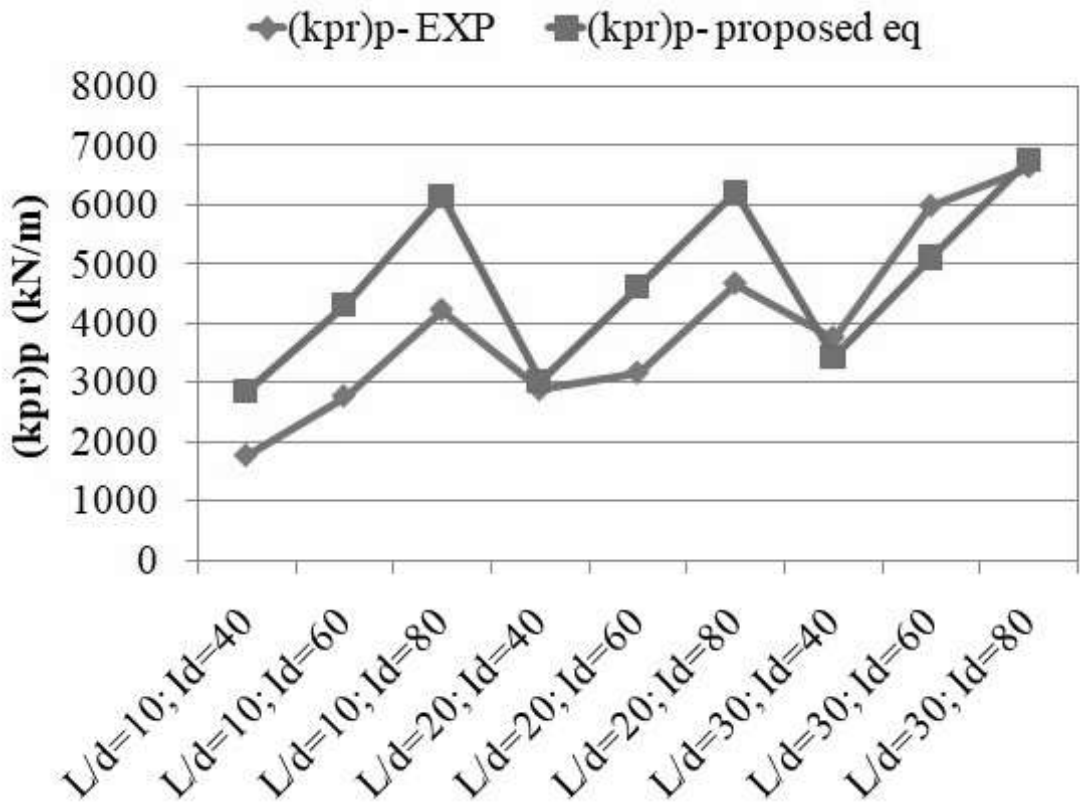

Figure 5-135 : Comparison of primary stiffness of PRF $(k_{pr})_p$ with different L/d ratios of pile (experimental) and determined from the proposed equation

Table 5-39 Variations in secondary stiffness of PRF $(k_{pr})_s$ with different *L/d* ratios of pile (experimental) and determined from the proposed equation

L/d **ratio of piles**	I_d **(%)**	**Secondary Stiffness of Piled Raft** $(k_{pr})_s$ **in kN/m**	k_{ri} **(kN/m)**	$(k_{pr})_s$ **in kN/m predicted from eq. (5-23)**	**% variation in predicted** $(k_{pr})_s$ **from experimental** $(k_{pr})_s$
10	40	734.98	2321.44	646.99	-12
	60	811.40	3585.12	972.33	20
	80	912.19	5331.36	1306.36	45
20	40	828.98	2321.44	646.99	-22
	60	857.71	3585.12	972.33	13
	80	1145.48	5331.36	1306.36	12
30	40	529.17	2321.44	646.99	-27
	60	873.55	3585.12	972.33	2
	80	1162.15	5331.36	1306.36	16

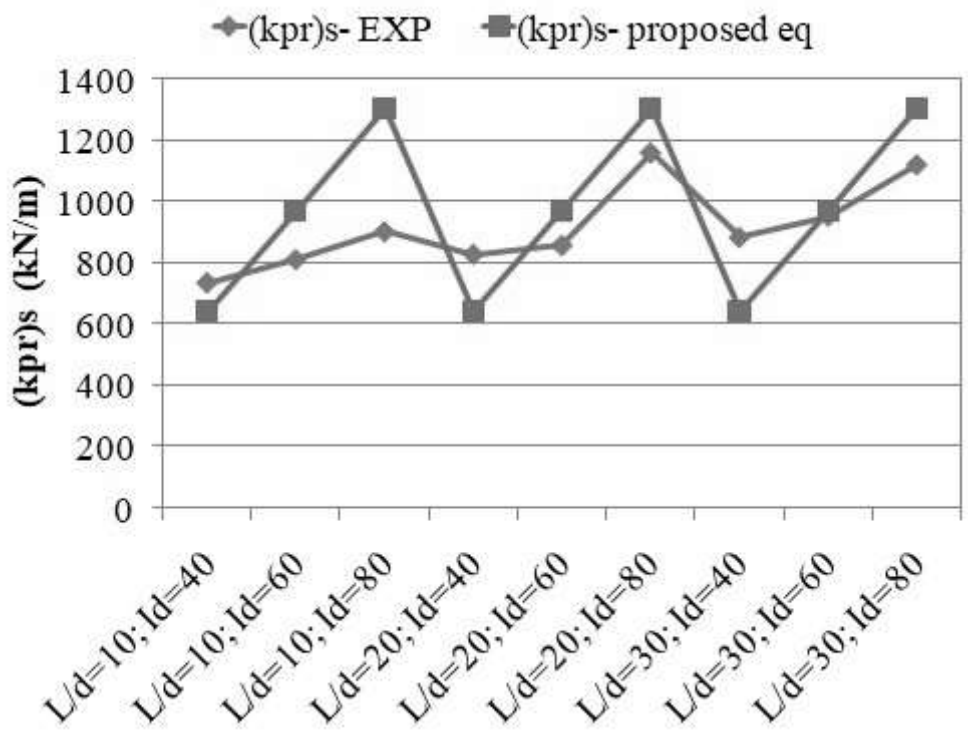

Figure 5-136 : Comparison of secondary stiffness of PRF $(k_{pr})_s$ with different *L/d* ratios of pile (experimental) and determined from the proposed equation

5.3.3.3 Spacing of piles

5.3.3.3.1 Load Settlement Characteristics

Figure 5-137 to Figure 5-139 display the load-settlement characteristics of a model square piled raft with *3d*, *5d*, and *7d* pile spacing, respectively, at different relative densities of the sand bed. The *IYL* and *FYL* obtained from the tri-linear behaviour are shown in Figure 5-140 to Figure 5-142. It was observed that the *IYL* and *FYL* increased as the relative density of the sand bed and the spacing between piles increased. The *IYL* of PRF with spacing = *3d* at 60% and 80% relative densities showed an increase of 2.77 kN and 5.87 kN, respectively, compared to the 40% relative density. This increment in percentage was 34% and 73%, respectively.

At 60% and 80% relative densities, the *IYL* (Initial Yield Load) of PRF with a spacing of *5d* was increased by 2.66 kN and 6.64 kN, respectively, compared to when the relative density was 40%. This represents a percentage increase of 29% and 71%, respectively. Similarly, compared to 40% relative density, the *IYL* of PRF with a spacing of *7d* increased by 7.51 kN and 10.70 kN at 60% and 80% relative densities, respectively. This represented a percentage increase of 65% and 92%, respectively.

Lastly, when comparing PRF with *5d* spacing to PRF with *3d* spacing, the *IYL* of PRF with *5d* spacing was found to increase by 1.23 kN, 1.12 kN, and 2.00 kN at 40%, 60%, and 80% relative densities of sand bed respectively. This represents a percentage increase of 15%, 10%, and 14% respectively.In comparison to PRF with *3d* spacing, the *IYL* of PRF with *7d* spacing increased by 3.55 kN, 8.29 kN, and 8.38 kN at 40%, 60%, and 80% relative densities of the sand bed, respectively. i.e., in percentage it was 44%, 76%, and 60% respectively.

The *FYL* of PRF with spacing = *3d* at 60% and 80% relative densities was increased by 6.96 kN and 15.61 kN, respectively, compared to a 40% relative density. i.e., the increment in percentage was 50% and 113%, respectively. The *FYL* of PRF with spacing = *5d* at 60% and 80% relative densities was increased by 5.31 kN and 15.94 kN, respectively, compared to a 40% relative density. i.e., the increment in percentage was 33% and 100%, respectively.The *FYL* of PRF with spacing = *7d* at 60% and 80% relative densities was increased by 7.11 kN and 16.67 kN, respectively, compared to 40% relative densities. i.e., the increment in percentage was 33% and 77%, respectively.

The *FYL* of PRF with *5d* spacing increased by 2.06 kN, 0.42 kN, and 2.39 kN at 40%, 60%, and 80% relative densities of the sand bed, respectively compared to PRF with *3d* spacing. i.e., the increment in percentage was 15%, 2%, and 8%, respectively.

In comparison to PRF with *3d* spacing, the *FYL* of PRF with *7d* spacing increased by 7.71 kN, 7.86 kN, and 8.77 kN at 40%, 60%, and 80% relative densities of the sand bed, respectively. i.e., the increment in percentage was 56%, 38%, and 30% respectively.

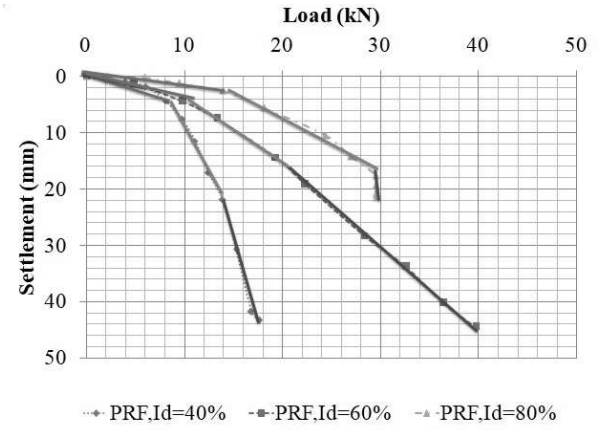

Figure 5-137 : Load settlement characteristics of model square piled raft at different relative density of sand bed *(S = 3d; pile group = 3 × 3; L/d ratio of pile = 30; d = 9.7 mm)*

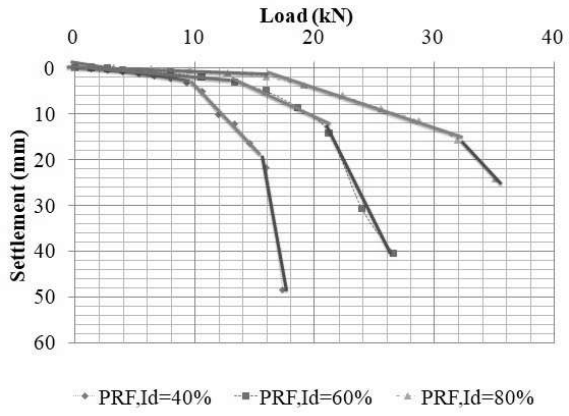

Figure 5-138 : Load settlement characteristics of model square piled raft at different relative density of sand bed *(S = 5d; pile group = 3 × 3; L/d ratio of pile = 30; d = 9.7 mm)*

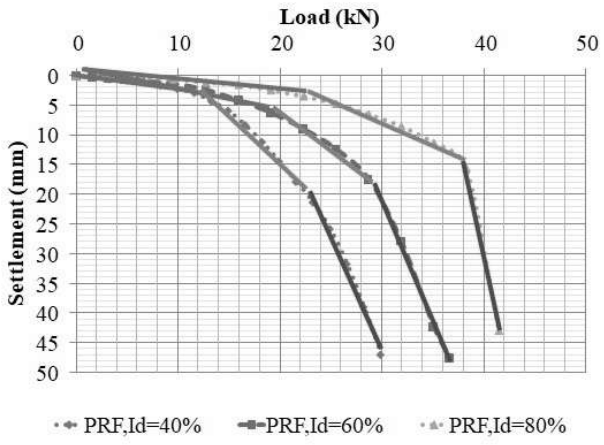

Figure 5-139 : Load settlement characteristics of model square piled raft at different relative density of sand bed *(S = 7d; pile group = 3 × 3; L/d ratio of pile = 30; d = 9.7 mm)*

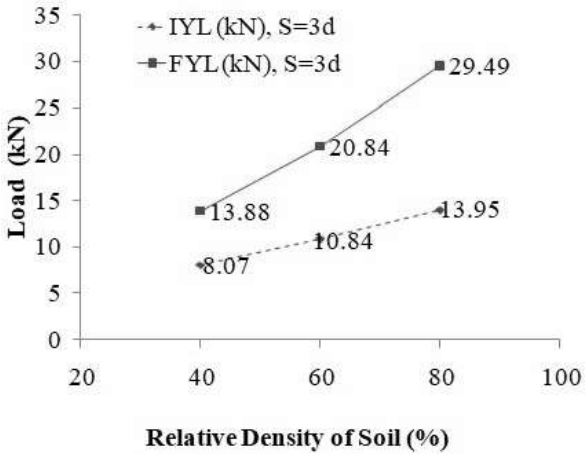

Figure 5-140 : Initial yield load (*IYL*) and Final yield load (*FYL*) of piled raft foundation at different relative density of sand bed *(S = 3d; pile group = 3 × 3; L/d ratio of pile = 30; d = 9.7 mm)*

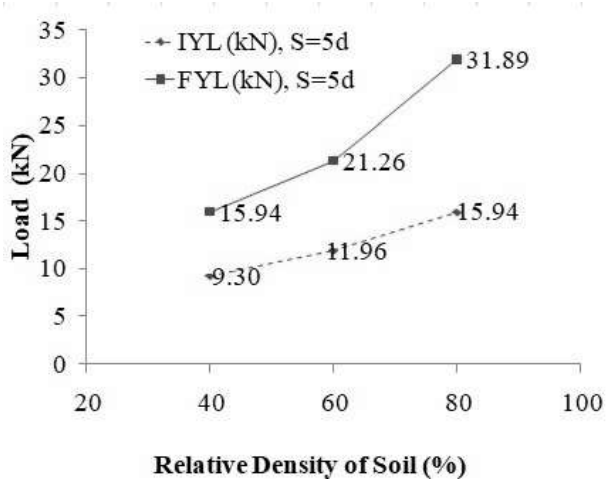

Figure 5-141 : Initial yield load (*IYL*) and Final yield load (*FYL*) of piled raft foundation at different relative density of sand bed *(S = 5d; pile group = 3 × 3; L/d ratio of pile = 30; d = 9.7 mm)*

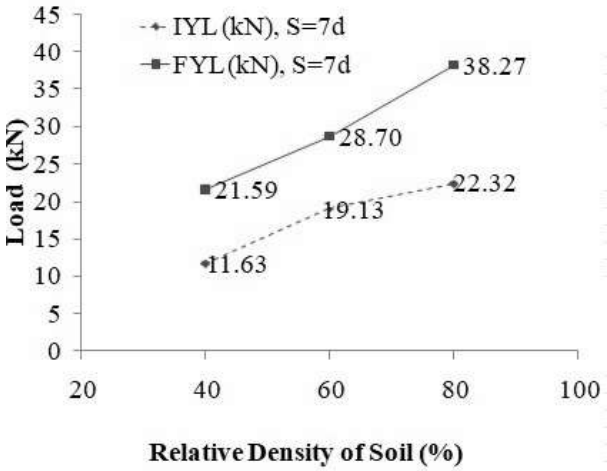

Figure 5-142 : Initial yield load (*IYL*) and Final yield load (*FYL*) of piled raft foundation at different relative density of sand bed *(S = 7d; pile group = 3 × 3; L/d ratio of pile = 30; d = 9.7 mm)*

The load settlement characteristics of only pile group (PG), unpiled raft (UPR), and piled raft (PRF) with *3d*, *5d*, and *7d* spacing between piles, respectively, are represented by Figure 5-143 to Figure 5-145. The load-carrying capacity of only the pile group was less than UPR and PRF with all spacing and at all relative densities. In the case of unpiled raft and piled raft with *3d* spacing, the difference in load-carrying capacity was much less at I_d = 40% and negligible at I_d = 60% and 80%. However, it was remarkable in the case of PRF with *5d* and *7d* spacing at all relative densities. It has been observed that PRF can take a load up to a large settlement (s/B_r = 0.15 to 0.2), while unpiled rafts can only take a load up to 15 to 25 mm in settlement (s/B_r = 0.068 to 0.11) and then collapse.

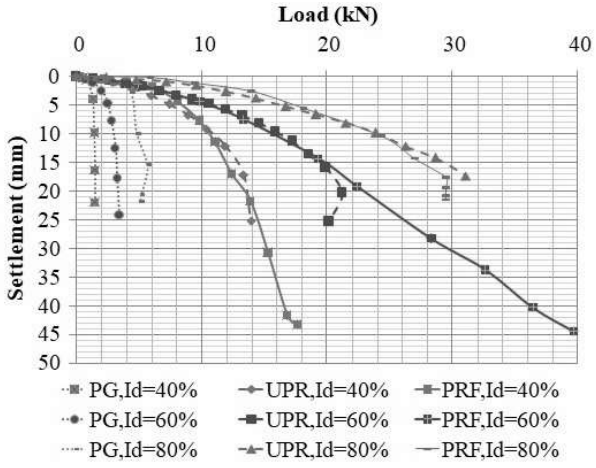

Figure 5-143 : Load settlement characteristics of only pile group, unpiled raft, and piled raft at different relative density of sand bed *(S = 3d; pile group = 3 × 3; L/d ratio of pile = 30; d = 9.7 mm)*

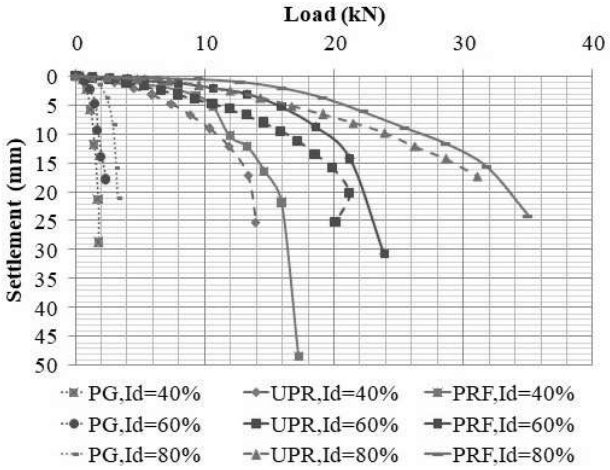

Figure 5-144 : Load settlement characteristics of only pile group, unpiled raft, and piled raft at different relative density of sand bed *(S = 5d; pile group = 3 × 3; L/d ratio of pile = 30; d = 9.7 mm)*

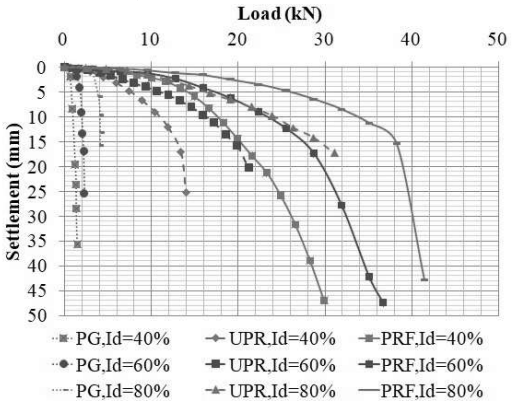

Figure 5-145 : Load settlement characteristics of only pile group, unpiled raft, and piled raft at different relative density of sand bed *(S = 7d; pile group = 3 × 3; L/d ratio of pile = 30; d = 9.7 mm)*

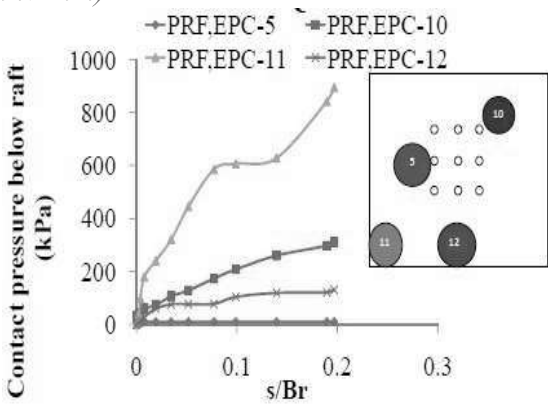

Figure 5-146 : Contact pressure distribution below raft for different location of earth pressure cells vs. relative settlement characteristics *(I_d = 40%; S = 3d; pile group = 3 × 3; L/d ratio of pile = 30; d = 9.7 mm)*

5.3.3.3.2 Contact Pressure Distribution Beneath Raft of PRF

Figure 5-146 to Figure 5-154 depict the contact pressure distribution below the raft for different locations of earth pressure cells vs. relative settlement characteristics of PRF with different spacing between piles at different relative densities of the sand bed. The contact pressure

increased as the relative settlement increased. The maximum contact pressure beneath the raft of PRF with *3d* spacing was at the corner, at the side, and nearer to the corner for 40%, 60%, and 80% relative density, respectively, while it was minimum nearer to the central portion of PRF. The maximum and minimum contact pressure beneath a raft of PRF with *5d* and 7*d* spacing was at the side and the corner, respectively, for all relative densities.

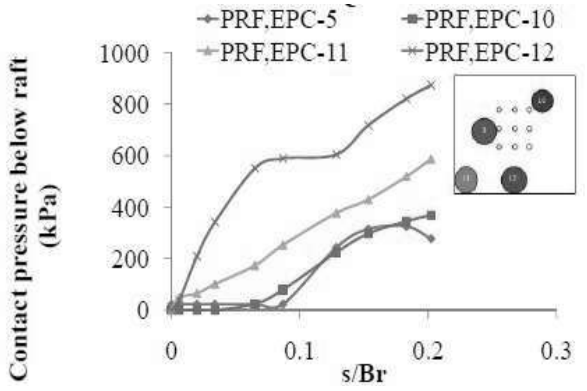

Figure 5-147: Contact pressure distribution below raft for different location of earth pressure cells vs. relative settlement characteristics *(I_d = 60%; S = 3d; pile group = 3 × 3; L/d ratio of pile = 30; d = 9.7 mm)*

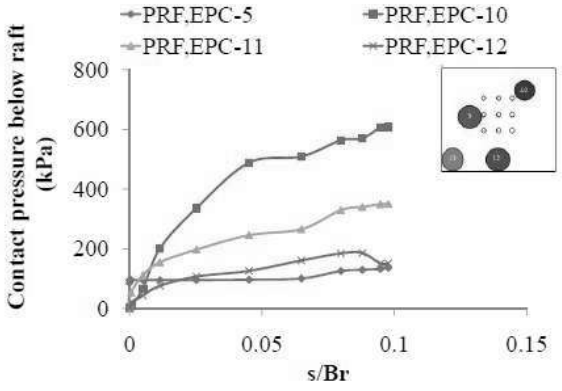

Figure 5-148 : Contact pressure distribution below raft for different location of earth pressure cells vs. relative settlement characteristics *(I_d = 80%; S = 3d; pile group = 3 × 3; L/d ratio of pile = 30; d = 9.7 mm)*

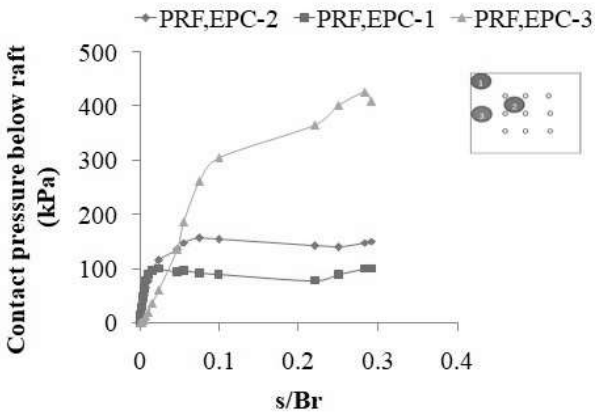

Figure 5-149 : Contact pressure distribution below raft for different location of earth pressure cells vs. relative settlement characteristics *(I_d = 40%; S = 5d; pile group = 3 × 3; L/d ratio of pile = 30; d = 9.7 mm)*

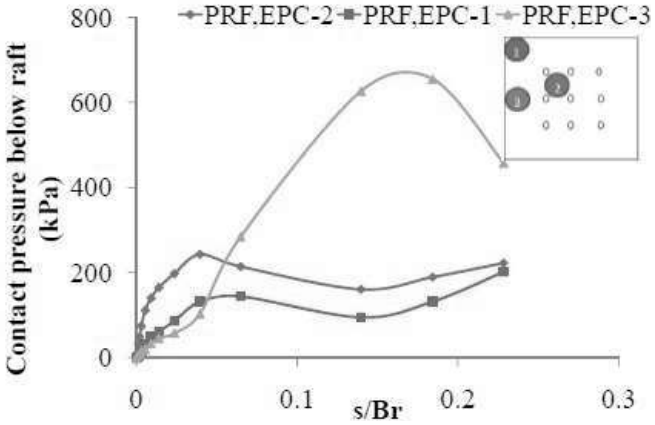

Figure 5-150 : Contact pressure distribution below raft for different location of earth pressure cells vs. relative settlement characteristics *(I_d = 60%; S = 5d; pile group = 3 × 3; L/d ratio of pile = 30; d = 9.7 mm)*

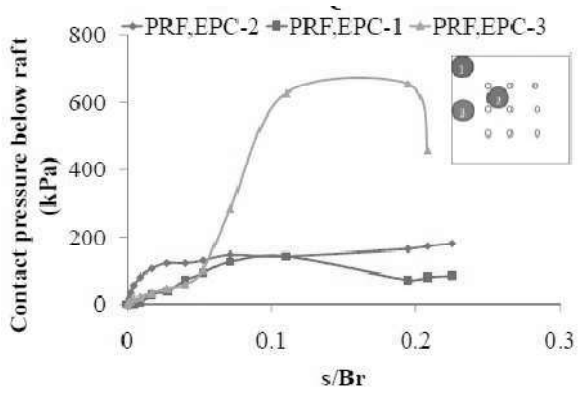

Figure 5-151 : Contact pressure distribution below raft for different location of earth pressure cells vs. relative settlement characteristics *(I_d = 80%; S = 5d; pile group = 3 × 3; L/d ratio of pile = 30; d = 9.7 mm)*

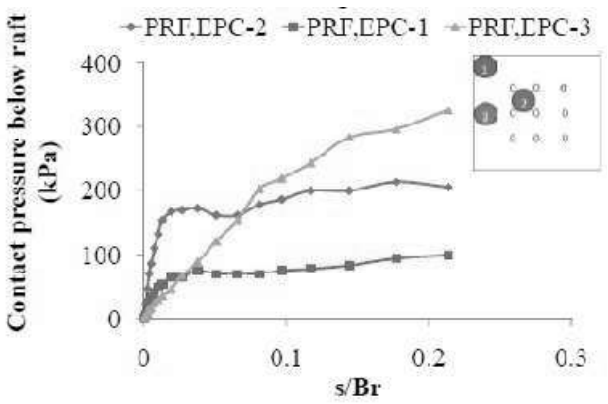

Figure 5-152 : Contact pressure distribution below raft for different location of earth pressure cells vs. relative settlement characteristics *(I_d = 40%; S = 7d; pile group = 3 × 3; L/d ratio of pile = 30; d = 9.7 mm)*

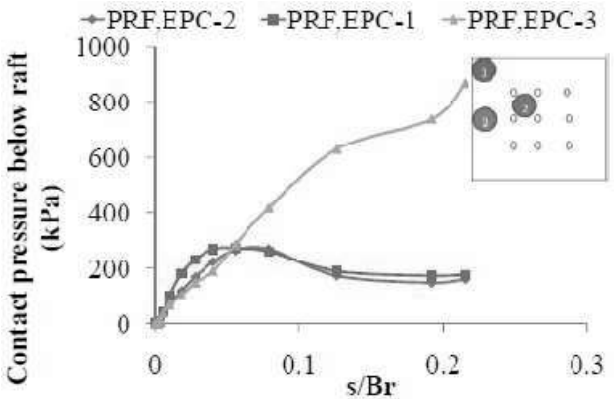

Figure 5-153 : Contact pressure distribution below raft for different location of earth pressure cells vs. relative settlement characteristics *(I_d = 60%; S = 7d; pile group = 3 × 3; L/d ratio of pile = 30; d = 9.7 mm)*

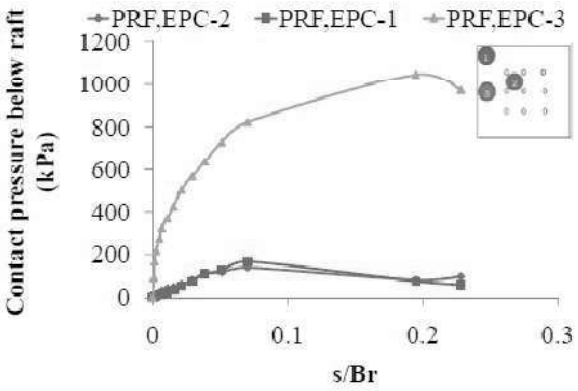

Figure 5-154 : Contact pressure distribution below raft for different location of earth pressure cells vs. relative settlement characteristics *(I_d = 80%; S = 7d; pile group = 3 × 3; L/d ratio of pile = 30; d = 9.7 mm)*

5.3.3.3.3 Load Sharing Mechanism

Figure 5-155 to Figure 5-157 display the load settlement behaviour of a piled raft with different spacing of piles, along with the load shared by pile group (*LSPG*) and raft (*LSR*) at varying relative densities of the sand bed. The results indicate that in PRF with *3d*, *5d*, and *7d* spacing, the *LSPG* was more than the *LSR* for most settlements at an I_d = 40%. At an I_d = 60%, the *LSPG* was more than the *LSR* in PRF with *3d* and *5d* spacing, whereas, in the case of *7d* spacing, the *LSPG* was more than the *LSR* from 0 mm to 9.5 mm settlements but lesser afterward. For an I_d of 80%, the *LSPG* of PRF with *3d* and *5d* spacing was more significant than the *LSR* from 0 to 2 mm and 0 to 16 mm settlement, respectively, after which the *LSR* was more than the *LSPG*. For PRF with *7d* spacing, the *LSPG* was more than the *LSR* for all settlements at 80% relative density of sand.

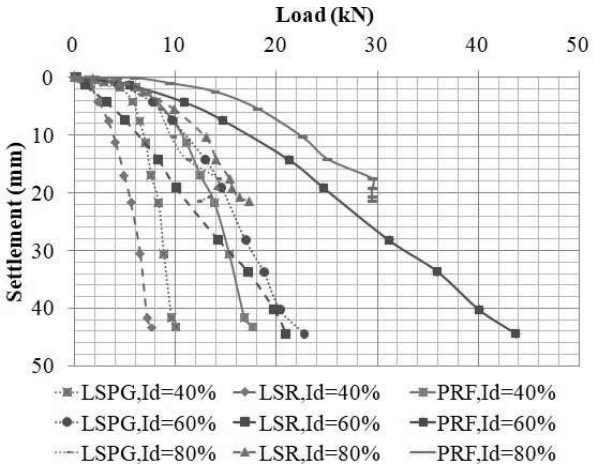

Figure 5-155 : Load settlement characteristics of piled raft and Load sharing by pile group and raft at different relative densities of sand *(S = 3d; d = 9.7 mm; pile group = 3 × 3; L/d ratio = 30)*

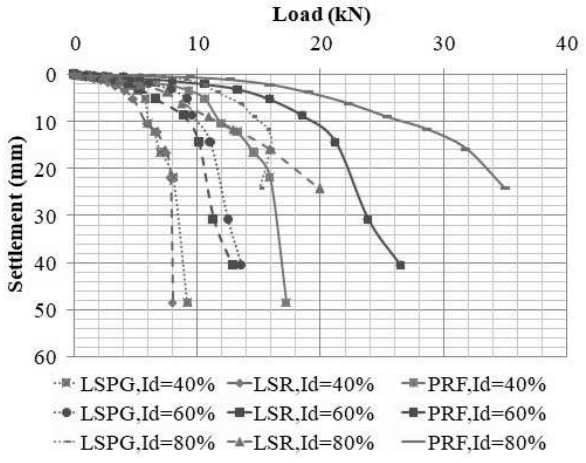

Figure 5-156 : Load settlement characteristics of piled raft and Load sharing by pile group and raft at different relative densities of sand *(S = 5d; d = 9.7 mm; pile group = 3 × 3; L/d ratio = 30)*

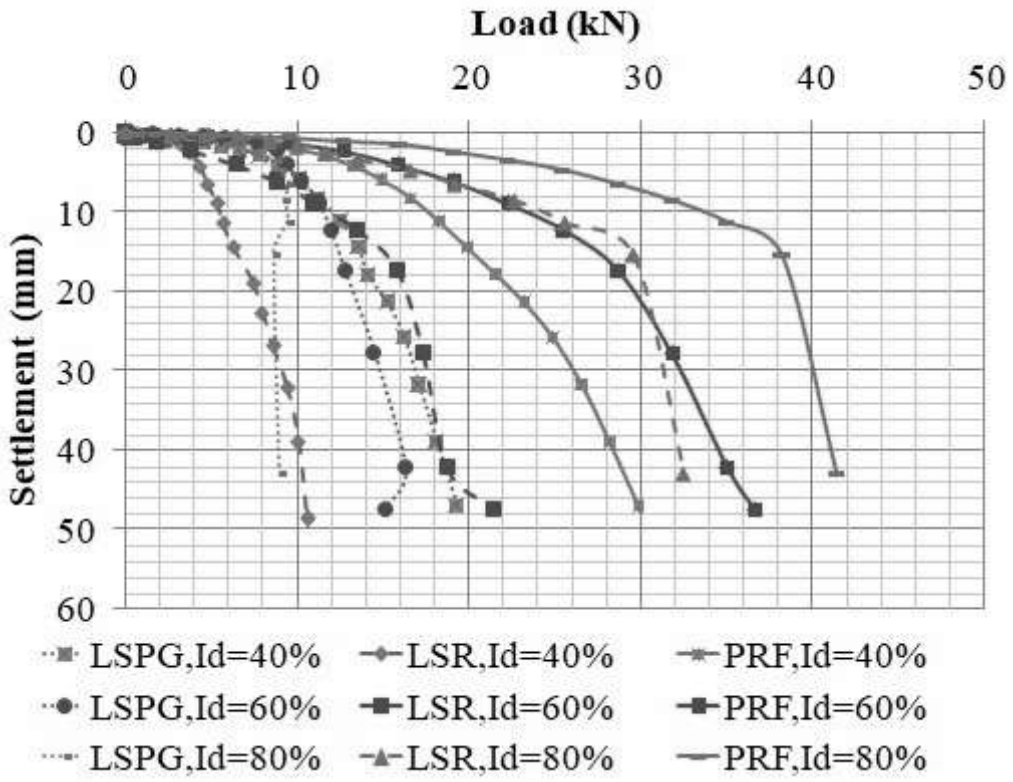

Figure 5-157 : Load settlement characteristics of piled raft and Load sharing by pile group and raft at different relative densities of sand *(S=7d; d=9.7mm; pile group = 3 × 3; L/d ratio = 30)*

Figure 5-159 to Figure 5-163 depict the *LSPG* and *LSR* at *IYL* and *FYL* of the piled raft foundation with different spacing between piles at different relative densities of the sand bed. The *LSR* and *LSPG* at Initial Yield Load (*IYL*) and Final Yield Load (*FYL*) for PRF with *3d* and *5d* spacing increased as the relative density of the sand increased. The *LSPG* at *IYL* for PRF with *7d* spacing increased with an increase in relative density from 40% to 60% but decreased with an increase in relative density from 60% to 80%. The *LSR* at *IYL* and *FYL* of PRF with *7d* spacing increased as the relative density of sand increased. However, the *LSPG* at *FYL* of PRF with *7d* spacing decreased as the relative density of sand increased.

The *LSR* at *IYL* of PRF with *3d* spacing at 60% and 80% relative density of sand increased by 0.83 kN and 4.43 kN, respectively, compared to 40% relative density of sand. i.e., in percentage terms, this represents an increase of 36% and 191%, respectively.The *LSR* at *FYL* of PRF with

3d spacing at 60% and 80% relative density of sand increased by 4.45 kN and 9.77 kN, respectively, compared to 40% relative density of sand. i.e., in percentage terms, this represents an increase of 80% and 175%, respectively.

The *LSPG* at *IYL* of PRF with *3d* spacing at 60% and 80% relative density of sand increased by 1.93 kN and 1.44 kN, respectively, compared to 40% relative density of sand. i.e., in percentage terms, this represents an increase of 34% and 25%, respectively. The *LSPG* at *FYL* of PRF with *3d* spacing at 60% and 80% relative density of sand increased by 6.29 kN and 5.85 kN, respectively, compared to 40% relative density of sand. i.e., in percentage terms, this represents an increase of 76% and 71%, respectively.

The *LSR* at *IYL* of PRF with *5d* spacing at 60% and 80% relative density of sand increased by 0.84 kN and 1.28 kN, respectively, compared to 40% relative density of sand. i.e., in percentage terms, this represents an increase of 20% and 31%, respectively. The *LSR* at *FYL* of PRF with *5d* spacing at 60% and 80% relative density of sand increased by 2.3 kN and 8.03 kN, respectively, compared to 40% relative density of sand. i.e., in percentage terms, this represents an increase of 29% and 102%, respectively.

The *LSPG* at *IYL* of PRF with *5d* spacing at 60% and 80% relative density of sand increased by 1.82 kN and 5.36 kN, respectively, compared to 40% relative density of sand. i.e., in percentage terms, this represents an increase of 35% and 103%, respectively. The *LSPG* at *FYL* of PRF with *5d* spacing at 60% and 80% relative density of sand increased by 3.01 kN and 7.91 kN, respectively, compared to 40% relative density of sand. i.e., in percentage terms, this represents an increase of 37% and 98%, respectively.

The *LSR* at *IYL* of PRF with *7d* spacing at 60% and 80% relative density of sand increased by 5.1 kN and 9.8 kN, respectively, compared to 40% relative density of sand. i.e., in percentage terms, this represents an increase of 135% and 260%, respectively. The *LSR* at *FYL* of PRF with *7d* spacing at 60% and 80% relative density of sand increased by 8.42 kN and 22.15 kN, respectively, compared to 40% relative density of sand. i.e., in percentage terms, this represents an increase of 113% and 297%, respectively.

The *LSPG* at *IYL* of PRF with *7d* spacing at 60% and 80% relative density of sand increased by 2.41 kN and 0.9 kN, respectively, compared to 40% relative density of sand. i.e., in percentage terms, this represents an increase of 31% and 11%, respectively. The *LSPG* at *FYL* of PRF with *7d* spacing at 60% and 80% relative density of sand decreased by 1.31 kN and 5.48 kN, respectively, compared to 40% relative density of sand. i.e., in percentage terms, this represents a decrease of 9% and 39%, respectively.

The *LSR* at *IYL* of PRF with *5d* spacing at 40% and 60% relative density of sand increased by 1.79 kN and 1.79 kN, respectively, compared to 3d spacing. i.e., in percentage terms, this represents an increase of 77% and 57%, respectively. The *LSR* at *IYL* of PRF with *5d* spacing at 80% relative density of sand decreased by 1.36 kN compared to 3d spacing. i.e., in percentage it was 20%. The *LSR* at *IYL* of PRF with 7d spacing at 40%, 60%, and 80% relative density of sand increased by 1.46 kN, 5.72 kN, and 6.82 kN, respectively, compared to *3d* spacing between piles. i.e., in percentage terms, this represents an increase of 63%, 182%, and 101%, respectively.

The *LSPG* at *IYL* of PRF with *5d* spacing at 40% and 60% relative density of sand decreased by 0.56 kN and 0.67 kN, respectively, compared to *3d* spacing. i.e., in percentage terms, this represents a decrease of 10% and 9%, respectively. The *LSPG* at *IYL* of PRF with *5d* spacing at 80% relative density of sand increased by 3.36 kN compared to *3d* spacing. i.e., in percentage it was 47%. The *LSPG* at *IYL* of PRF with *7d* spacing at 40%, 60%, and 80% relative density of sand increased by 2.1 kN, 2.57 kN, and 1.55 kN, respectively, compared to *3d* spacing between piles. i.e., in percentage terms, this represents an increase of 36%, 33%, and 22%, respectively.

The *LSR* at *FYL* of PRF with *5d* spacing at 40% , 60% and 80% relative density of sand increased by 2.27 kN, 0.12 kN and 0.53 kN, respectively, compared to *3d* spacing. i.e., in percentage terms, this represents an increase of 41%, 1% and 3%, respectively. The *LSR* at *FYL* of PRF with *7d* spacing at 40%, 60%, and 80% relative density of sand increased by 1.86 kN, 5.83 kN, and 14.25 kN, respectively, compared to *3d* spacing between piles. i.e., in percentage terms, this represents an increase of 33%, 58%, and 93%, respectively.

The *LSPG* at *FYL* of PRF with *5d* spacing at 40% and 60% relative density of sand decreased by 0.20 kN and 3.48 kN, respectively, compared to *3d* spacing. i.e., in percentage terms, this represents a decrease of 2% and 24%, respectively. The *LSPG* at *FYL* of PRF with *5d* spacing at 80% relative density of sand increased by 1.86 kN compared to *3d* spacing. i.e., in percentage it was 13%. The *LSPG* at *FYL* of PRF with *7d* spacing at 40% relative density of sand increased by 5.85 kN, compared to *3d* spacing between piles. i.e., in percentage terms, this represents an increase of 71%. The *LSPG* at *FYL* of PRF with *7d* spacing at 60% and 80% relative density of sand decreased by 1.75 kN and 5.48 kN, respectively, compared to *3d* spacing. i.e., in percentage terms, this represents a decrease of 12% and 39%, respectively.

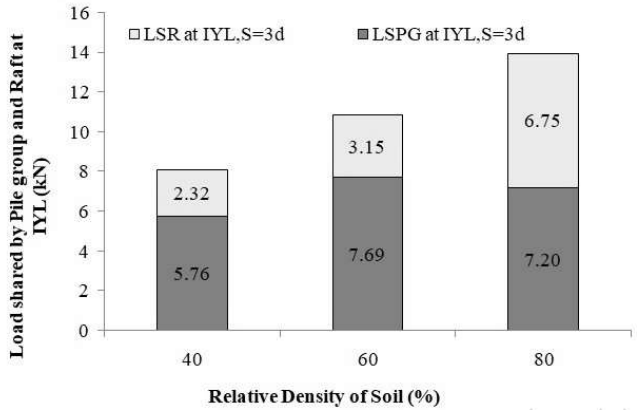

Figure 5-158 : Load shared by pile group and raft at *IYL* of piled raft foundation *(S = 3d; d = 9.7 mm; pile group = 3 × 3; L/d ratio = 30)*

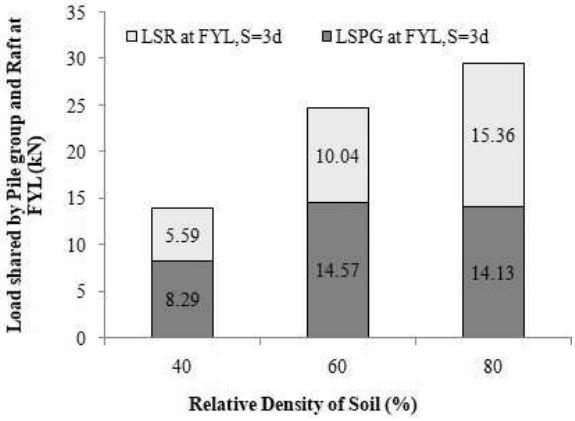

Figure 5-159 : Load shared by pile group and raft at *FYL* of piled raft foundation *(S = 3d; d = 9.7 mm; pile group = 3 × 3; L/d ratio = 30)*

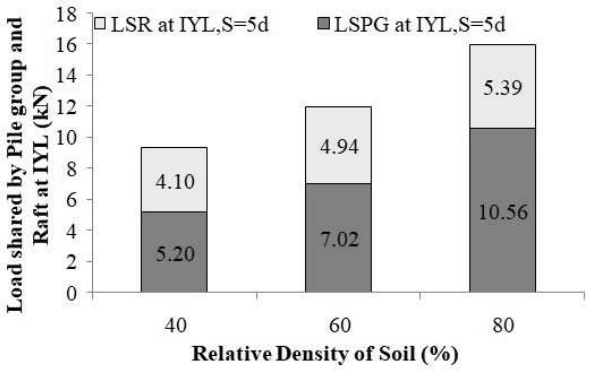

Figure 5-160 : Load shared by pile group and raft at *IYL* of piled raft foundation *(S = 5d; d = 9.7 mm; pile group = 3 × 3; L/d ratio = 30)*

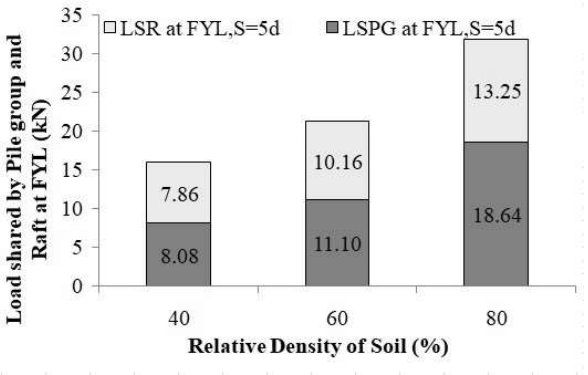

Figure 5-161 : Load shared by pile group and raft at *FYL* of piled raft foundation *(S = 5d; d = 9.7 mm; pile group = 3 × 3; L/d ratio = 30)*

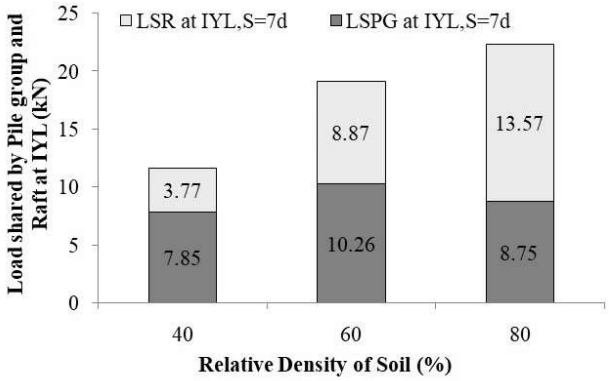

Figure 5-162 : Load shared by pile group and raft at *IYL* of piled raft foundation *(S = 7d; d = 9.7 mm; pile group = 3 × 3; L/d ratio = 30)*

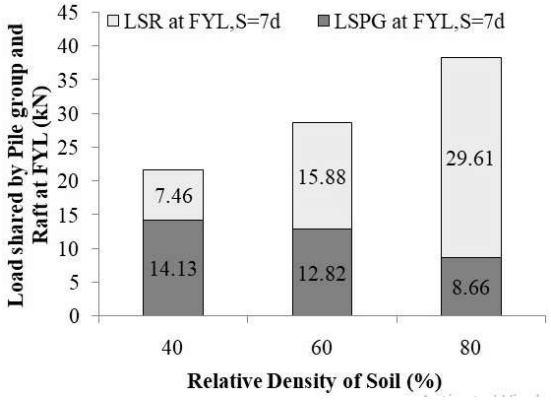

Figure 5-163 : Load shared by pile group and raft at *FYL* of piled raft foundation *(S = 7d; d = 9.7 mm; pile group = 3 × 3; L/d ratio = 30)*

Figure 5-164 to Figure 5-172 show the percentage load shared by pile group (% *LSPG*) and raft (% *LSR*) in piled raft with different spacing between piles vs. different relative settlements at different relative densities of the sand bed. In PRF with *3d* spacing, the % *LSPG* and % *LSR* became equal at relative settlement (s/B_r) = 0.13 and 0.016 for I_d = 60% and 80%, respectively,

while at I_d = 40%, the % *LSPG* was more than % *LSR* at all relative settlements. In PRF with *5d* spacing, the % *LSPG* and % *LSR* became equal at relative settlement (s/B_r) = 0.05 for I_d = 40%, while at I_d = 60% and 80%, the % *LSPG* was more than % *LSR* at all relative settlements. In the case of PRF with *7d* spacing and I_d = 40%, the % *LSPG* was more than % *LSR* at all relative settlements. The % *LSPG* and % *LSR* were equal at relative settlement (s/B_r) = 0.04 for PRF with *7d* spacing at 60% relative density. In the case of PRF with *7d* spacing and I_d = 80%, the % *LSPG* was less than % *LSR* at all relative settlements.

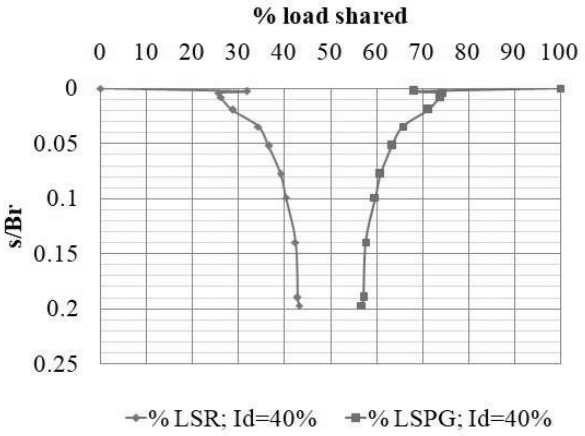

Figure 5-164 : Percentage load shared by pile group (% *LSPG*) and raft (% *LSR*) in piled raft at different relative settlement *(S = 3d; I_d = 40%;d = 9.7 mm; pile group = 3 × 3; L/d ratio = 30)*

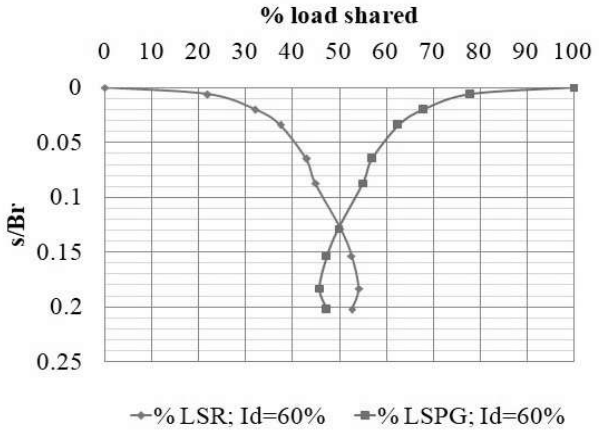

Figure 5-165 : Percentage load shared by pile group (% *LSPG*) and raft (% *LSR*) in piled raft at different relative settlement *(S = 3d; I_d = 60%; d = 9.7 mm; pile group = 3 × 3; L/d ratio = 30)*

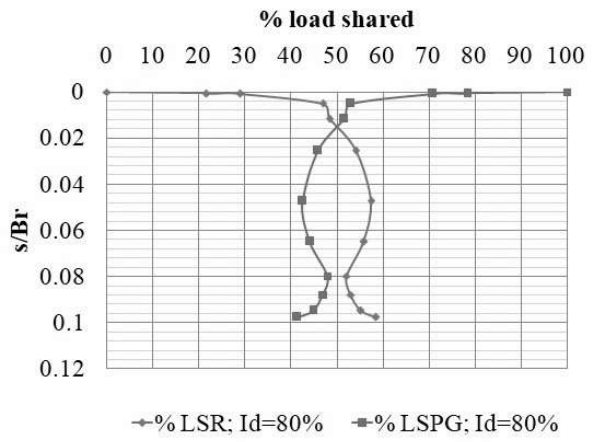

Figure 5-166 : Percentage load shared by pile group (% *LSPG*) and raft (% *LSR*) in piled raft at different relative settlement *(S = 3d; I_d = 80%; d = 9.7 mm; pile group = 3 × 3; L/d ratio = 30)*

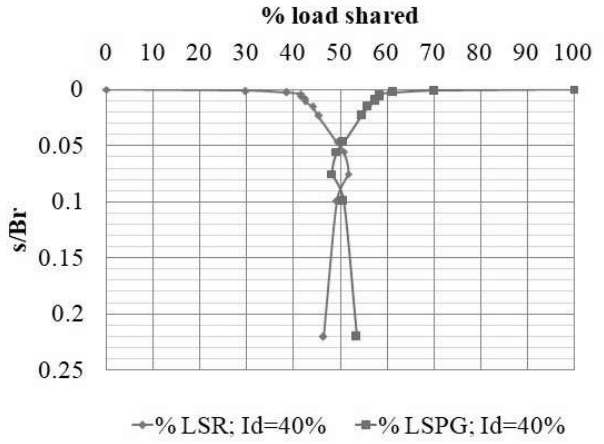

Figure 5-167 : Percentage load shared by pile group (% *LSPG*) and raft (% *LSR*) in piled raft at different relative settlement *(S = 5d; I_d = 40%; d = 9.7 mm; pile group = 3 ×3; L/d ratio = 30)*

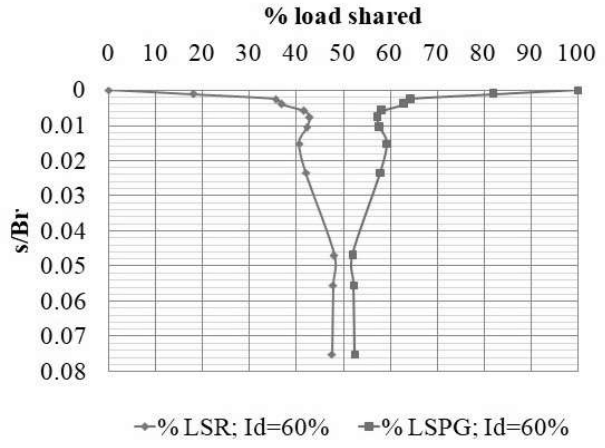

Figure 5-168 : Percentage load shared by pile group (% *LSPG*) and raft (% *LSR*) in piled raft at different relative settlement *(S = 5d; I_d = 60%; d = 9.7 mm; pile group = 3 × 3; L/d ratio = 30)*

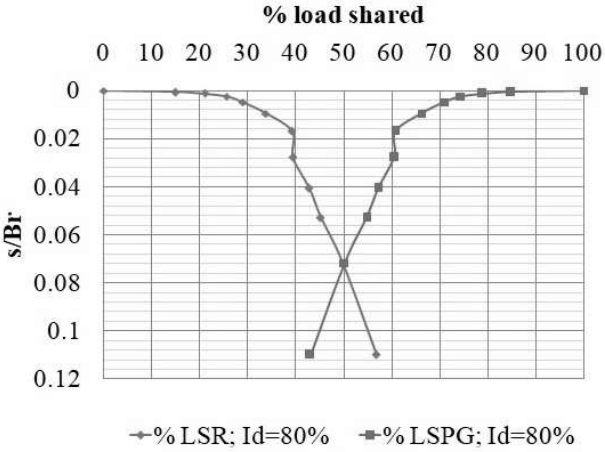

Figure 5-169 : Percentage load shared by pile group (% *LSPG*) and raft (% *LSR*) in piled raft at different relative settlement *(S = 5d; I_d = 80%; d = 9.7 mm; pile group = 3 ×3; L/d ratio = 30)*

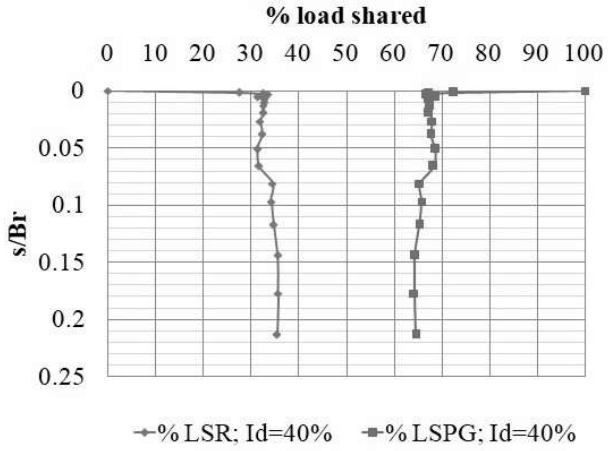

Figure 5-170 : Percentage load shared by pile group (% *LSPG*) and raft (% *LSR*) in piled raft at different relative settlement *(S = 7d; I_d = 40%; d = 9.7 mm; pile group = 3 × 3; L/d ratio = 30)*

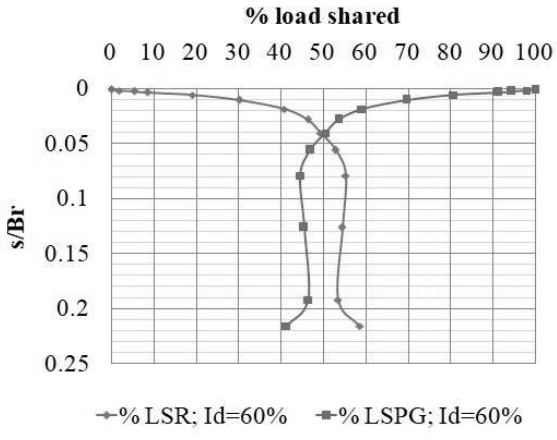

Figure 5-171 : Percentage load shared by pile group (% *LSPG*) and raft (% *LSR*) in piled raft at different relative settlement *(S = 7d; I_d = 60%; d = 9.7 mm; pile group = 3 × 3; L/d ratio = 30)*

5.3.3.3.4 Piled Raft Coefficient (α_p)

Figure 5-173 to Figure 5-175 illustrate the relationship between the piled raft coefficient (α_p) and the settlement characteristics of piled raft foundations with different pile spacing and relative densities of the sand bed. The results show that α_p decreases as the spacing between piles (s/B_r) increases. Moreover, the relative density of the sand bed has a significant effect on the α_p value of PRF with *7d* spacing between piles.

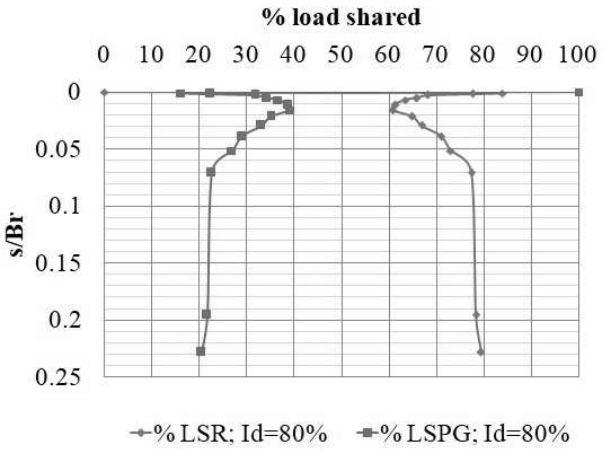

Figure 5-172 : Percentage load shared by pile group (% *LSPG*) and raft (% *LSR*) in piled raft at different relative settlement *(S = 7d; I_d = 80%; d = 9.7 mm; pile group = 3 × 3; L/d ratio = 30)*

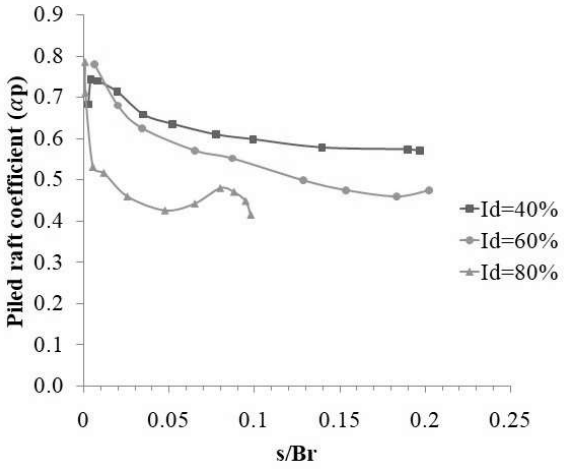

Figure 5-173 : Piled raft coefficient (α_p) vs. relative settlement characteristics of piled raft foundation at different relative densities of sand bed *(S = 3d; d = 9.7 mm; pile group = 3 × 3; L/d ratio of pile = 30)*

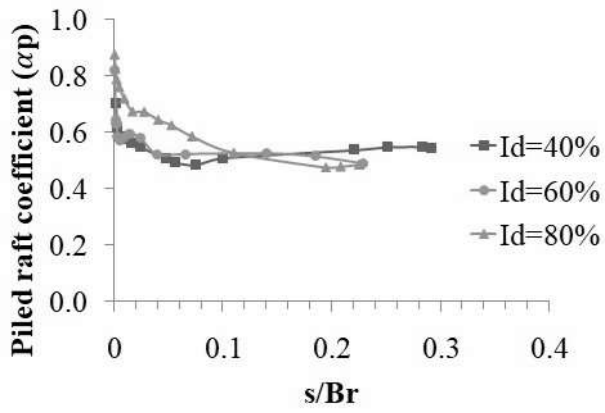

Figure 5-174 : Piled raft coefficient (α_p) vs. relative settlement characteristics of piled raft foundation at different relative densities of sand bed *(S = 5d; d = 9.7 mm; pile group = 3 × 3; L/d ratio of pile = 30)*

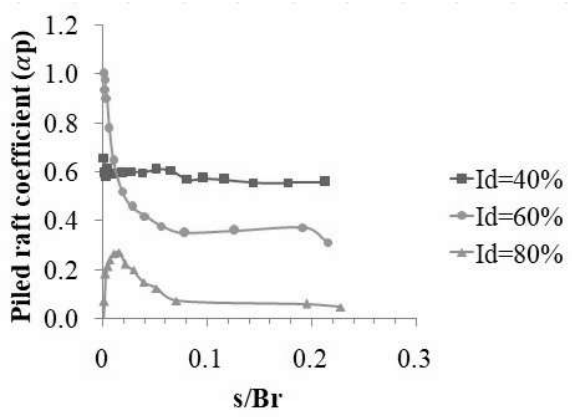

Figure 5-175 : Piled raft coefficient (α_p) vs. relative settlement characteristics of piled raft foundation at different relative densities of sand bed *(S = 7d; d = 9.7 mm; pile group = 3 × 3; L/d ratio of pile = 30)*

5.3.3.3.5 Settlement Reduction Ratio (SRR) and Load Improvement Ratio (LIR)

Table 5-40 shows the Settlement Reduction Ratio *(SRR)* of PRF with different spacing between piles at various load levels and 40% relative densities of the sand bed. The *SRR* ranged from 3% to 47%, 22% to 52%, and 42% to 78%, with *3d*, *5d*, and *7d* spacing between piles, respectively.

Table 5-40 Settlement reduction ratio of PRF with different spacing between piles at different load levels and 40% relative densities of the sand bed

I_d (%)	Load(kN)	Settlement (mm)				Settlement reduction ratio (%)		
		UPR	PRF *(S=3d)*	PRF *(S=5d)*	PRF *(S=7d)*	PRF *(S=3d)*	PRF *(S=5d)*	PRF *(S=7d)*
40	2.5	0.77	0.62	0.53	0.45	19	31	42
	5	2.48	1.30	1.19	0.79	47	52	68
	10	8.45	8.20	4.29	2.22	3	49	74
	12.5	14.22	17.30	11.09	3.60	-22	22	75
	15	27.11	28.91	18.04	5.96	-7	33	78

Table 5-41 displays the settlement reduction ratio *(SRR)* of PRF for various pile spacings, load levels, and 60% relative densities of the sand bed. With *3d*, *5d*, and *7d* pile spacing, the range of *SRR* was 0% to 23%, 48% to 59%, and 46% to 68%, respectively.

Table 5-41 Settlement reduction ratio of PRF with different spacing between piles at different load levels and 60% relative densities of the sand bed

I_d (%)	Load(kN)	Settlement (mm)				Settlement reduction ratio (%)		
		UPR	PRF *(S=3d)*	PRF *(S=5d)*	PRF *(S=7d)*	PRF *(S=3d)*	PRF *(S=5d)*	PRF *(S=7d)*
60	2.5	0.62	0.62	0.32	0.33	0	48	46
	5	1.62	1.25	0.66	0.62	23	59	62
	10	4.42	3.91	1.85	1.43	12	58	68
	12.5	6.13	5.71	2.79	2.24	7	54	64
	15	8.54	7.81	4.48	3.58	9	48	58

Table 5-42 shows the settlement reduction ratio *(SRR)* of PRF, taking into account different spacing between piles, various load levels, and 80% relative densities of the sand bed. The *SRR* ranged from 34% to 78%, 65% to 72%, and 47% to 72%, with *3d*, *5d*, and *7d* spacing between piles, respectively. It also observed that in PRF with *3d* and *5d* spacing, the *SRR* was initially lower and increased with an increase in load up to a certain point. After that, it decreased with further load increases. On the other hand, in PRF with *7d* spacing, the *SRR*increased with an increase in load.

The load improvement ratio *(LIR)* of PRF with different spacing between piles at different load levels and 40% relative densities of the sand bed is shown in Table 5-43. The range of *LIR* for PRF with *3d*, *5d*, and *7d* spacing was found to be 0.93 to 1.09, 1.07 to 1.35, and 1.59 to 1.83, respectively. It can be observed that the *LIR* is maximum at 5.5 mm settlement among all settlements considered in this analysis.

Table 5-42 Settlement reduction ratio of PRF with different spacing between piles at different load levels and 80% relative densities of the sand bed

I_d (%)	Load (kN)	Settlement (mm)				Settlement reduction ratio (%)		
		UPR	PRF *(S=3d)*	PRF *(S=5d)*	PRF *(S=7d)*	PRF *(S=3d)*	PRF *(S=5d)*	PRF *(S=7d)*
80	2.5	0.28	0.12	0.10	0.15	57	66	47
	5	0.65	0.14	0.19	0.27	78	70	59
	10	2.07	1.28	0.58	0.65	38	72	68
	12.5	3.41	2.07	0.99	1.09	39	71	68
	15	4.99	3.29	1.76	1.40	34	65	72

Table 5-43 Load improvement ratio of PRF with different spacing between piles at different load levels and 40% relative densities of the sand bed

I_d (%)	Settlement (mm)	Load (kN)				Load improvement ratio (%)		
		UPR	PRF *(S=3d)*	PRF *(S=5d)*	PRF *(S=7d)*	PRF *(S=3d)*	PRF *(S=5d)*	PRF *(S=7d)*
40	5.5	7.96	8.71	10.72	14.56	1.09	1.35	1.83
	11	11.33	10.94	12.44	18.17	0.97	1.10	1.60
	16.5	13.18	12.29	14.61	20.93	0.93	1.11	1.59
	22	13.72	13.91	15.95	23.51	1.01	1.16	1.71
	27.5	15.22	14.78	16.23	25.38	0.97	1.07	1.67

The load improvement ratio *(LIR)* of PRF with different spacing between piles at different load levels and 60% relative densities of the sand bed is shown in Table 5-44. The range of *LIR* for PRF with *3d*, *5d*, and *7d* spacing was found to be 1.05 to 1.52, 1.08 to 1.38, and 1.40 to 1.58,

respectively. It can be observed that the *LIR* increases with settlements in the case of PRF with *3d* spacing, while in the case of PRF with *5d* and *7d* spacing, the *LIR* decreases with an increase in settlements up to 16.5 mm, and after that, it increases.

Table 5-44 Load improvement ratio of PRF with different spacing between piles at different load levels and 60% relative densities of the sand bed

I_d (%)	Settlement (mm)	Load (kN)				Load improvement ratio		
		UPR	PRF *(S=3d)*	PRF *(S=5d)*	PRF *(S=7d)*	PRF *(S=3d)*	PRF *(S=5d)*	PRF *(S=7d)*
60	5.5	11.69	12.24	16.14	18.07	1.05	1.38	1.55
	11	17.06	18.05	19.68	24.27	1.06	1.15	1.42
	16.5	20.08	22.77	21.61	28.14	1.13	1.08	1.40
	22	20.84	26.68	22.50	30.11	1.28	1.08	1.44
	27.5	20.15	30.62	23.39	31.79	1.52	1.16	1.58

The load improvement ratio *(LIR)* of PRF with different spacing between piles at different load levels and 80% relative densities of the sand bed is shown in Table 5-44. The range of *LIR* for PRF with *3d*, *5d*, and *7d* spacing was found to be 1.01 to 1.21, 1.08 to 1.36, and 1.23 to 1.71, respectively. It can be observed that at I_d = 80%, in PRF with *3d* , *5d* and *7d* spacing, the *LIR* decreases with an increase in settlements up to 22 mm, and after that, it increases.

Table 5-45 Load improvement ratio of PRF with different spacing between piles at different load levels and 80% relative densities of the sand bed

I_d (%)	Settlement (mm)	Load(kN)				Load improvement ratio		
		UPR	PRF (S=3d)	PRF (S=5d)	PRF (S=7d)	PRF (S=3d)	PRF (S=5d)	PRF (S=7d)
80	5.5	15.78	18.07	21.53	26.93	1.14	1.36	1.71
	11	22.62	22.99	27.97	34.73	1.02	1.24	1.54
	16.5	27.92	28.07	32.16	38.38	1.01	1.15	1.37
	22	31.81	30.18	34.24	39.02	0.95	1.08	1.23
	27.5	31.30	37.72	35.19	39.66	1.21	1.12	1.27

5.3.3.3.6 Comparison between Predicted and Experimental Values of IYL and FYL

Table 5-46 represents the efficiency factor of raft (C_1) and pile group (C_2) in PRF with different spacing between piles calculated as mentioned in 5.3.3.1.6. Table 5-47 represents the efficiency factors of the raft (C_1) , and pile group (C_2) in PRF with different spacing between piles calculated from the proposed equations (5-14) to (5-15) and percentage variations in *IYL* determined from proposed equation (5-16) with respect to experimental *IYL*. The percentage variations in the predicted *IYL* from experimental *IYL* are observed to be in the range of -59% to +56%, and in most of the cases, it is found to be less than 20%. Figure 5-176 represents the comparison of *IYL* of piled raft foundation with different spacing between piles at different relative densities of sand bed found from experimental results and calculated from the proposed equation (5-16). Table 5-48 shows the percentage variations in *FYL* of PRF with different spacing between piles determined from the proposed equation (5-19) with respect to experimental *FYL*. The range of percentage variation in predicted *FYL* as compared to experimental *FYL* is found to be less than 20% in most cases except for PRF, with *3d* spacing at 40% relative density and *7d* spacing at 80% relative density of the sand bed. Figure 5-177 represents the comparison of *FYL* of piled raft foundation with different spacing between piles at different relative densities of sand bed found from experimental results and calculated from the proposed equation.

The range of the piled raft efficiency at *IYL* varied from 0.9 to 1.02, 1.06 to 1.34, and 1.20 to 1.69 at pile spacings of *3d*, *5d*, and *7d*. This indicates that the efficiency of the piled raft at *IYL* increased as the spacing between piles increased from *3d* to *7d* at 40% relative density, while at 60% and 80% relative density the maximum and minimum efficiency of the piled raft at *IYL* was found to be at *5d* and *3d* spacing respectively.

Similarly, the range of the piled raft efficiency at *FYL* was found to be 0.86 to 0.96, 0.95 to 1.06, and 1.17 to 1.47 at pile spacings of *3d*, *5d*, and *7d*. This indicates that the efficiency of the piled raft at *FYL* increased with an increase in spacing between piles from *3d* to *7d*.

Table 5-46 Efficiency factor of raft (C_1), efficiency factor of pile group (C_2), and efficiency of PRF at *IYL* (β_1) with different spacing between piles

Spacing between piles	I_d **(%)**	***IYL*** **(kN)**	***LSR*** **in PRF at *IYL* (kN)**	***LSP*** ***G*** **in PRF at *IYL* (kN)**	**Piled raft coefficient (α_p)**	**Settlement s_i at *IYL* (mm)**	B_r **(mm)**	s/B_r	$(P_r)_{s_i}$ **(kN)**	$(P_{sp})_{s_i}$ **(kN)**	$(P_{pg})_{s_i}$ **(kN)**	C_1	C_2	β_1
3d	40	8.07	2.32	5.76	0.71	4.28	220	0.01	6.91	0.02	1.01	0.336	5.680	1.02
	60	10.84	3.15	7.69	0.71	4.38	220	0.02	9.93	0.31	2.11	0.317	3.651	0.90
	80	13.95	6.75	7.20	0.52	2.53	220	0.01	11.00	0.22	3.28	0.614	2.194	0.98
5d	40	9.30	4.10	5.20	0.56	5.15	220	0.02	7.68	0.05	1.10	0.534	4.721	1.06
	60	11.96	4.94	7.02	0.59	3.11	220	0.01	7.74	0.33	1.42	0.638	4.928	1.30
	80	15.94	5.39	10.56	0.66	2.07	220	0.01	10.00	0.24	1.93	0.538	5.471	1.34
7d	40	11.63	3.77	7.85	0.68	2.88	220	0.02	6.23	0.16	0.65	0.606	12.109	1.69
	60	19.13	8.87	10.26	0.54	6.20	220	0.01	15.09	0.42	1.81	0.588	5.659	1.13
	80	22.32	13.57	8.75	0.39	3.46	220	0.02	15.09	0.52	3.57	0.899	2.454	1.20

Table 5-47 Efficiency factor of raft (C_1), and efficiency factor of pile group (C_2) in PRF with different spacing between piles calculated from proposed equations and percentage variations in *IYL* determined from proposed equations with respect to experimental *IYL*

Spacing between piles	***I_d* (%)**	***IYL* (kN)**	***S/d***	***B_r/L_r***	***L/d***	***n***	***s/B_r***	**C_1**	**C_2**	***IYL*-EXP (kN)**	***IYL*-PROPOSED EQUATION (kN)**	**% Variations in predicted *IYL* as compared to *IYL*-EXP**
3d	40	8.07	3	1	30	9	0.02	0.209	6.212	8.07	7.74	-4
	60	10.84	3	1	30	9	0.02	0.320	5.302	10.84	14.35	32
	80	13.95	3	1	30	9	0.01	0.247	5.882	13.95	22.02	58
5d	40	9.30	5	1	30	9	0.02	0.418	4.612	9.30	8.29	-11
	60	11.96	5	1	30	9	0.01	0.379	4.875	11.96	9.88	-17
	80	15.94	5	1	30	9	0.01	0.337	5.180	15.94	13.36	-16
7d	40	11.63	7	1	30	9	0.01	0.328	5.245	11.63	5.44	-53
	60	19.13	7	1	30	9	0.03	1.058	1.859	19.13	19.34	1
	80	22.32	7	1	30	9	0.02	0.787	2.733	22.32	21.62	-3

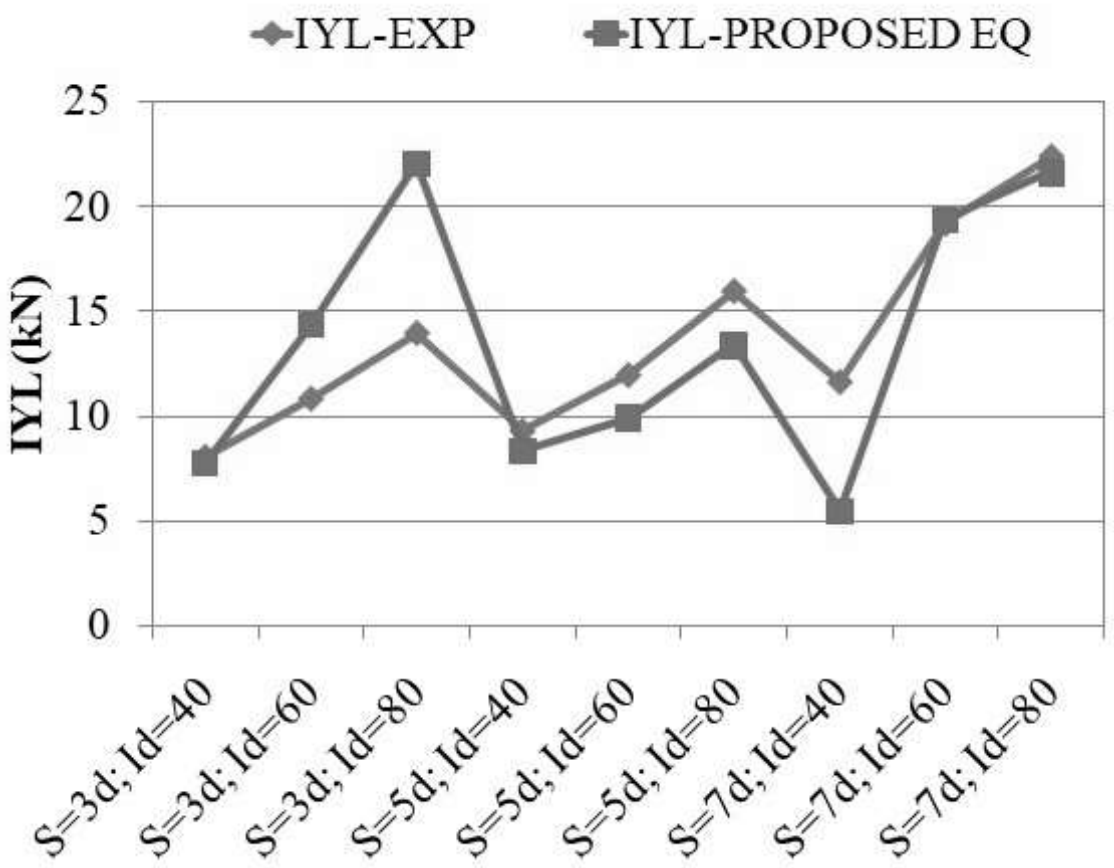

Figure 5-176 : Comparison of *IYL* of piled raft foundation with different spacing between piles at different relative density of sand bed found from experimental results and calculated from proposed equation

Table 5-48 Percentage variations in *FYL* of PRF with different spacing between piles determined from proposed equations with respect to experimental *FYL* and efficiency of PRF at *FYL* (β_2)

Spacing between piles	I_d **(%)**	***FYL* (kN)**	***LSR* at FYL**	***LSPG* at FYL**	α_p	**Settlement (mm) at FYL**	B_r	s/B_r	C_3	C_4	Qur **(kN)**	Qu,pg **(kN)**	***FYL* –EXP (kN)**	***FYL* - PROPOSED EQUATION (kN)**	**% Variations in predicted FYL as compared to FYL-EXP**	β_2
3d	40	13.88	9.32	4.56	0.33	21.78	220	0.10	0.398	2.116	13.25	1.27	13.88	7.97	-43	0.96
	60	20.84	9.17	11.67	0.56	16.72	220	0.08	0.405	2.049	20.3	3.29	20.84	14.95	-28	0.88
	80	29.49	13.37	16.13	0.55	17.56	220	0.08	0.426	1.859	28.69	5.67	29.49	22.76	-23	0.86
5d	40	15.94	7.86	8.08	0.51	21.81	220	0.10	0.664	3.525	13.25	1.74	15.94	14.92	-6	1.06
	60	21.26	10.16	11.10	0.52	14.30	220	0.06	0.663	3.537	20.3	1.97	21.26	20.43	-4	0.95
	80	31.89	13.25	18.64	0.58	15.77	220	0.07	0.697	3.208	28.69	3.11	31.89	29.97	-6	1.00
7d	40	21.59	7.46	14.13	0.57	17.86	220	0.08	0.911	5.127	13.25	1.48	21.59	19.68	-9	1.47
	60	28.70	15.88	12.82	0.35	17.40	220	0.08	0.950	4.734	20.3	2.17	28.70	29.57	3	1.28
	80	38.27	29.61	8.66	0.38	15.50	220	0.07	0.974	4.514	28.69	4.11	38.27	46.48	21	1.17

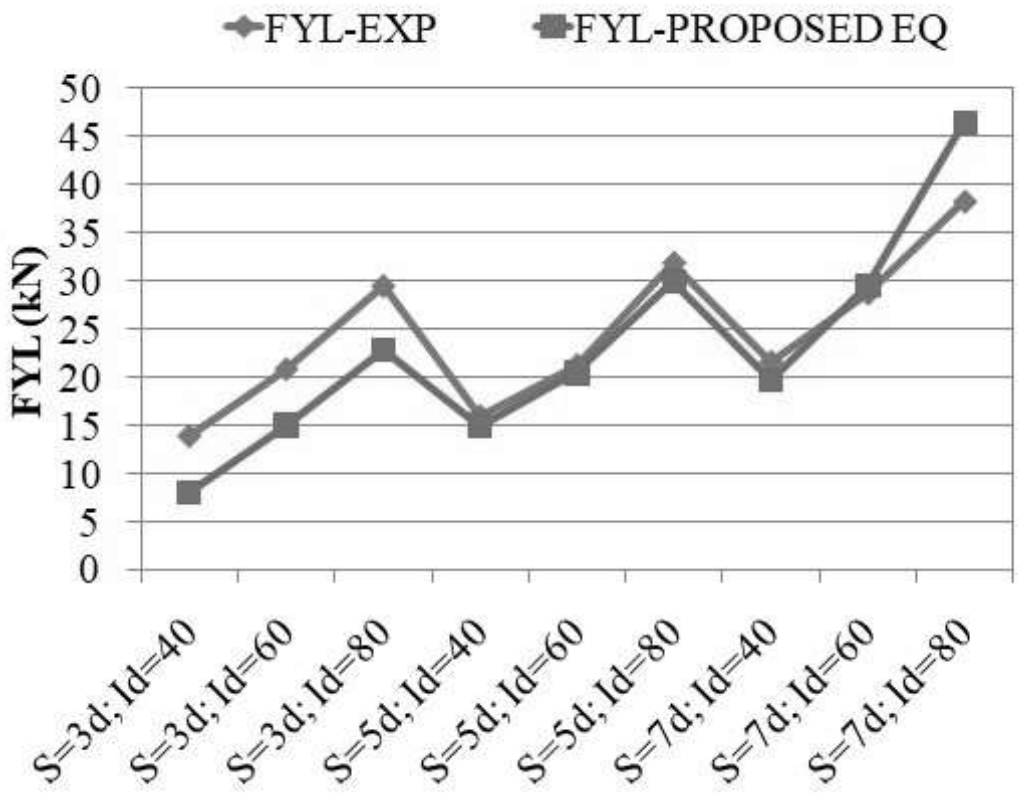

Figure 5-177 : Comparison of *FYL* of piled raft foundation with different spacing between piles at different relative density of sand bed found from experimental results and calculated from proposed equation

5.3.3.3.7 Comparison between Predicted and Experimental Values of $(k_{pr})_p$

Table 5-49 displays the primary stiffness of piled raft foundations $(k_{pr})_p$ with varying spacing between piles in PRF. Table 5-49 and Figure 5-178 show the variations in experimental $(k_{pr})_p$ and determined from the proposed equation (5-22).

The results show that the $(k_{pr})_p$ increased in all cases with an increase in the relative density of sand. The $(k_{pr})_p$ of PRF with *3d* spacing increased by 109% and 289% at 60% and 80% relative

density, respectively, compared to 40% relative density. The $(k_{pr})_p$ of PRF with *5d* spacing increased by 51% and 105% at 60% and 80% relative density, respectively, compared to 40% relative density. The $(k_{pr})_p$ of PRF with *7d* spacing increased by 42% and 88% at 60% and 80% relative density, respectively, compared to the 40% relative density of sand. The $(k_{pr})_p$ of PRF with *5d* spacing increased by 96%, 42%, and 3% at I_d = 40%, I_d = 60%, and I_d = 80%, respectively, compared to *3d* spacing. The $(k_{pr})_p$ of PRF with *7d* spacing increased by 54%, 45%, and 41% at I_d = 40%, I_d = 60%, and I_d = 80%, respectively, compared to *3d* spacing.

Table 5-49 Variations in primary stiffness of PRF $(k_{pr})_p$ with different spacing between piles (experimental) and determined from the proposed equation

Spacing between piles	**Relative density of sand (%)**	B_r **(m)**	**TLP (m)**	**Primary stiffness of PRF** $(k_{pr})_p$ **in kN/m (Experimental)**	**Secondary Stiffness of PRF** $(k_{pr})_s$ **in kN/m**	**Initial stiffness of UPR** (k_{ri}) **(kN/m)**	**Initial stiffness of PG** $(k_{pg})_i$ **(Experimental)**	**Primary stiffness of PRF** $(k_{pr})_p$ **in kN/m (Proposed equation)**	**% variation in** $(k_{pr})_p$ **calculated from proposed eq. and** $(k_{pr})_p$ **- EXP.**
3d	40	0.22	2.619	1743.67	315.97	2321.44	266.59	3065.672	76
	60	0.22	2.619	3636.62	704.68	3585.12	785.53	4958.992	36
	80	0.22	2.619	6786.95	1162.50	5331.36	2105.29	7676.131	13
5d	40	0.22	2.619	3412.76	354.90	2321.44	166.14	2979.283	-13
	60	0.22	2.619	5147.66	812.17	3585.12	184.27	4441.908	-14
	80	0.22	2.619	6982.18	1259.84	5331.36	302.45	6125.687	-12
7d	40	0.22	2.619	5262.22	593.20	2321.44	315.01	3107.312	-41
	60	0.22	2.619	7489.01	1313.46	3585.12	563.58	4768.116	-36
	80	0.22	2.619	9873.06	1601.48	5331.36	2260.30	7809.436	-21

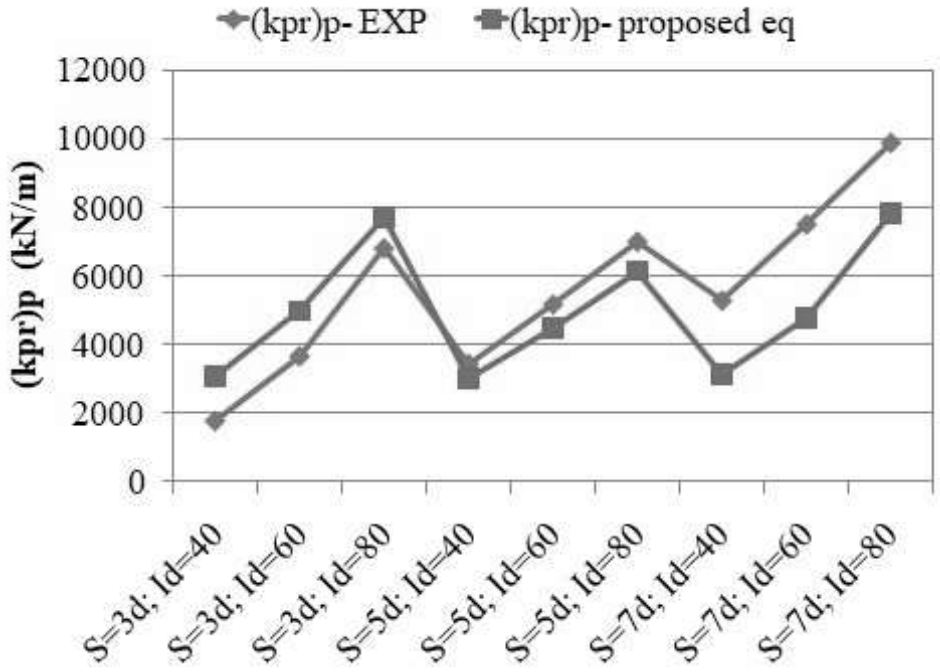

Figure 5-178 : Comparison of primary stiffness of PRF $(k_{pr})_p$ with different spacing between piles at different relative density of sand bed found from experimental results and calculated from proposed equation

5.3.3.3.8 Comparison between Predicted and Experimental Values of $(k_{pr})_s$

Table 5-50 and Figure 5-179 represent the variations in secondary stiffness of PRF $(k_{pr})_s$ with different *L/d* ratios of the pile (experimental) and determined from the proposed equation (5-23).

The secondary stiffness $(k_{pr})_s$ of PRF with *3d* spacing increased by 123% and 268% at 60% and 80% relative density, respectively, compared to 40% relative density. The secondary stiffness $(k_{pr})_s$ of PRF with *5d* spacing increased by 129% and 255% at 60% and 80% relative density,

respectively, compared to 40% relative density. The secondary stiffness $(k_{pr})_s$ of PRF with *7d* spacing increased by 121% and 170% at 60% and 80% relative density, respectively, compared to 40% relative density. The $(k_{pr})_s$ of PRF with *5d* spacing increased by 12%, 15%, and 8% at I_d = 40%, I_d = 60%, and I_d = 80%, respectively, compared to *3d* spacing. The $(k_{pr})_s$ of PRF with *7d* spacing increased by 67%, 62%, and 27% at I_d = 40%, I_d = 60%, and I_d = 80%, respectively, compared to *3d* spacing.

Table 5-50 Variations in secondary stiffness of PRF $(k_{pr})_s$ with different spacing between piles (experimental) and determined from the proposed equation

Spacing between piles	**I_d (%)**	**Secondary Stiffness of Piled Raft $(k_{pr})_s$ in kN/m**	**k_{ri} (kN/m)**	**$(k_{pr})_s$ in kN/m predicted from eq. (5-23)**	**% variation in predicted $(k_{pr})_s$ from experimental $(k_{pr})_s$**
3d	40	315.97	2321.44	646.99	105
	60	704.68	3585.12	972.33	38
	80	1162.50	5331.36	1306.36	12
5d	40	354.90	2321.44	646.99	82
	60	812.17	3585.12	972.33	20
	80	1259.84	5331.36	1306.36	4
7d	40	593.20	2321.44	646.99	9
	60	1313.46	3585.12	972.33	-26
	80	1601.48	5331.36	1306.36	-18

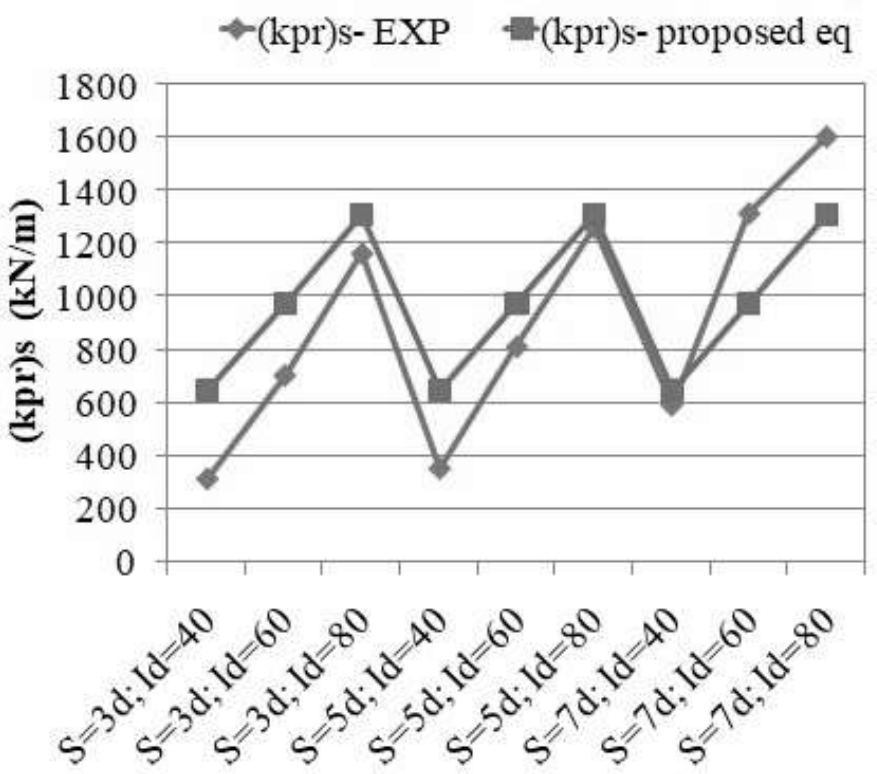

Figure 5-179 : Comparison of secondary stiffness of PRF $(k_{pr})_s$ with different spacing between piles at different relative density of sand bed found from experimental results and calculated from proposed equation

5.3.3.4 Configuration of Piles

5.3.3.4.1 Load Settlement Characteristics

Figure 5-180 to Figure 5-182 show how load settlement characteristics of piled raft foundations with different pile configurations behave Tri-linearly at I_d = 60%. Figure 5-183 shows the *IYL* and *FYL* obtained from the Tri-linear behaviour of PRF with different configurations. Figure 5-184 shows the load settlement characteristics of piled raft foundations with different pile configurations. The *IYL* and *FYL* were highest for *CF-9* and lowest for *CF-7*, indicating that the *IYL* and *FYL* depends on the length of piles in PRF, as *CF-9* had long piles and *CF-7* had short piles. The group of configurations with nearly the same *IYL* value was (*CF-2, CF-7*), (*CF-3, CF-6*), and (*CF-4, CF-5, CF-8*). *CF-2* and *CF-7* had larger numbers of small piles at the periphery of the pile group. *CF-3* and *CF-6* had the same number of long piles. The *IYL* in decreasing order

according to the configuration was *CF-9*, *CF-1*, *CF-8*, *CF-4*, *CF-5*, *CF-6*, *CF-3*, *CF-2*, and *CF-7*. In *CF-9*, *CF-1*, and *CF-4*, most of the periphery piles were long piles; in *CF-8*, *CF-5*, and *CF-6*, most of the periphery piles were medium piles; and in *CF-2*, *CF-3*, and *CF-7*, most of the periphery piles were short piles, which shows that the *IYL* of PRF is also depends on the arrangement of the piles. Higher, moderate, and lower *IYL* were observed in the PRF with long piles, medium piles, and short piles, respectively, nearer to the periphery of the raft. The percentage increment in *IYL* for *CF-1* to *CF-9* as compared to *CF-7* was 50%, 6%, 14%, 40%, 39%, 21%, 0%, 53%, and 88%, respectively.

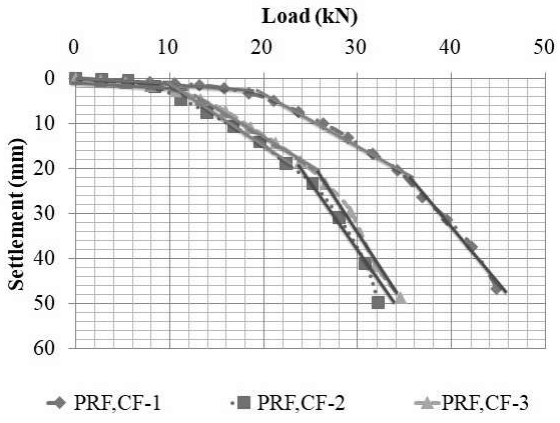

Figure 5-180 : Load settlement characteristics of piled raft foundation with different configurations of piles *(L/d ratio of pile =10, 20, and 30; I_d = 60%; S = 5d ;d = 9.7 mm; pile group = 5 × 5; CF-1 to CF-3)*

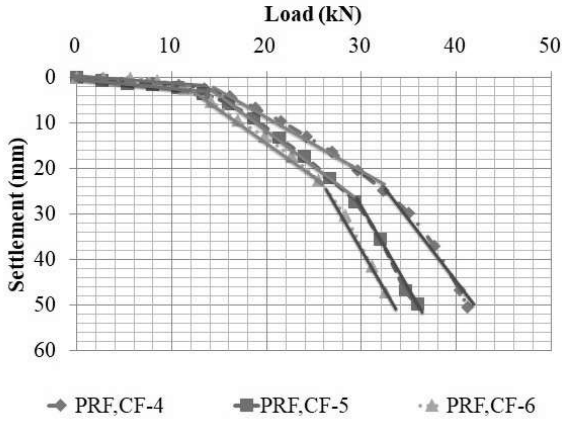

Figure 5-181 : Load settlement characteristics of piled raft foundation with different configurations of piles *(L/d ratio of pile =10, 20, and 30; I_d = 60%; S= 5d ;d = 9.7 mm; pile group = 5 × 5; CF-4 to CF-6)*

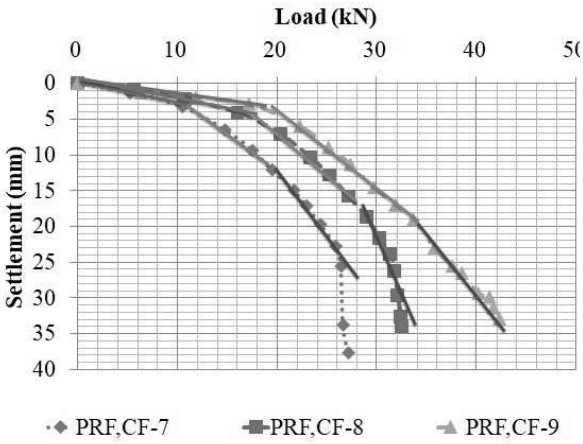

Figure 5-182 : Load settlement characteristics of piled raft foundation with different configurations of piles *(L/d ratio of pile =10, 20, and 30; I_d = 60%; S = 5d ; d = 9.7 mm; pile group = 5 × 5; CF-7 to CF-9)*

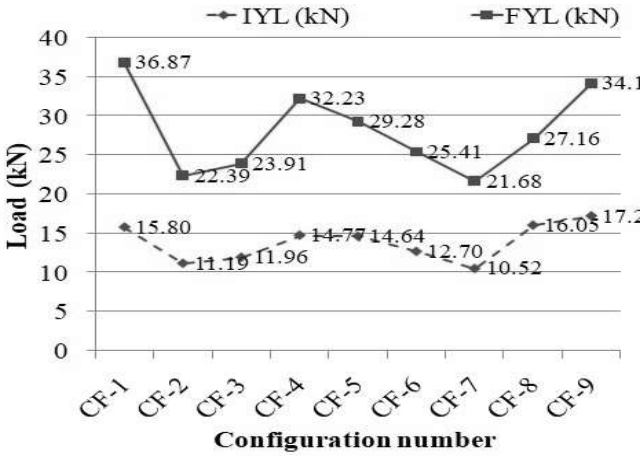

Figure 5-183 : Initial yield load (*IYL*) and Final yield load (*FYL*) of piled raft foundation with different pile configurations *(L/d ratio of pile =10, 20, and 30; I_d = 60%; S = 5d ; d = 9.7 mm; pile group = 5 × 5; CF-1 to CF-9)*

5.3.3.4.2 Contact Pressure Distribution beneath Raft of PRF

The variations in contact pressure beneath the raft in PRF were shown in Figure 5-185 to Figure 5-190. The variations in earth pressure cell readings with respect to relative settlement were studied for *CF-1* to *CF-6* configurations, and the following observations were made: 1. The pattern of contact pressure distribution was found to be the same for the groups of configurations (*CF-1, CF-4*), and (*CF-5, CF-6*) during the initial loading stage. 2. The contact pressure distribution for *CF-1*, *CF-2* and *CF-4* was maximum at the center, intermediate at the side, and minimum at the corner of model PRF. For *CF-3*, the values of contact pressures were maximum at the center, intermediate at the corner, and minimum at the side of the model raft. In *CF-5*, initially, the contact pressure at the corner and the side was equal and minimum at the center up to s/B_r = 0.04; afterward, it was more at the side than at the corner. For *CF-6*, the contact pressure was maximum at the side, intermediate at the corner, and minimum at the center of the model PRF up to s/B_r = 0.06; after that, it changed its behaviour.

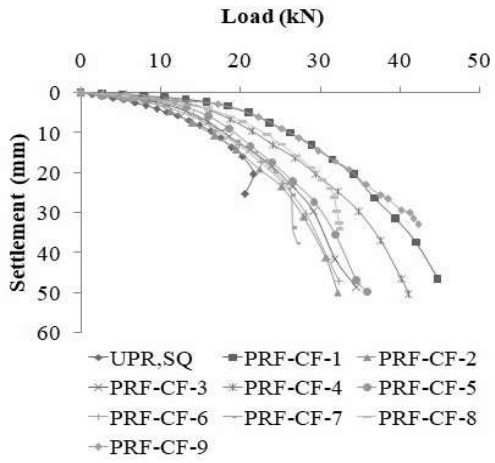

Figure 5-184 : Load settlement characteristics of piled raft foundation with different configurations of piles *(L/d ratio of pile = 10, 20, and 30; I_d = 60%; S = 5d ; d = 9.7 mm; pile group = 5 × 5)*

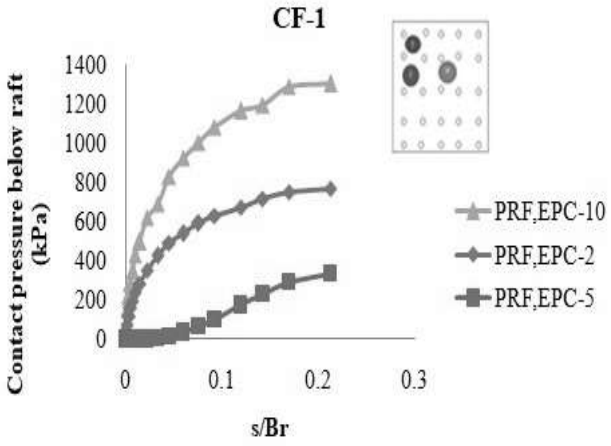

Figure 5-185 : Contact pressure distribution below raft for different location of earth pressure cells vs. relative settlement characteristics *(L/d ratio of pile = 10, 20, and 30; I_d = 60%; S = 5d ; d = 9.7 mm; pile group = 5 × 5; configuration of piles = CF-1)*

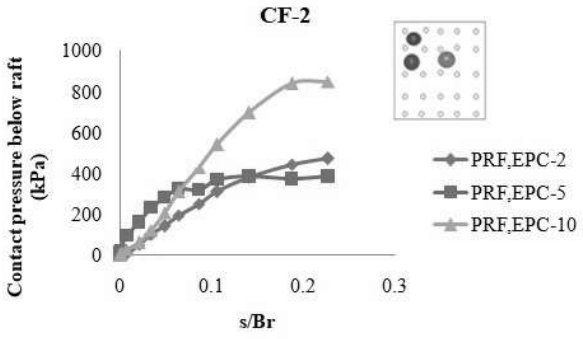

Figure 5-186 : Contact pressure distribution below raft for different location of earth pressure cells vs. relative settlement characteristics *(L/d ratio of pile = 10, 20, and 30; I_d = 60%; S = 5d ; d = 9.7 mm; pile group = 5 x 5; configuration of piles = CF-2)*

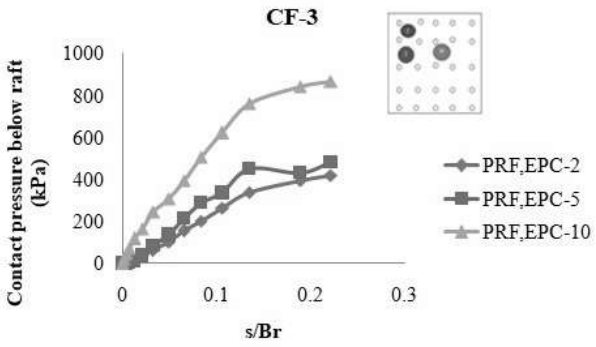

Figure 5-187 : Contact pressure distribution below raft for different location of earth pressure cells vs. relative settlement characteristics *(L/d ratio of pile = 10, 20, and 30; I_d = 60%; S = 5d ; d = 9.7 mm; pile group = 5 x 5; configuration of piles = CF-3)*

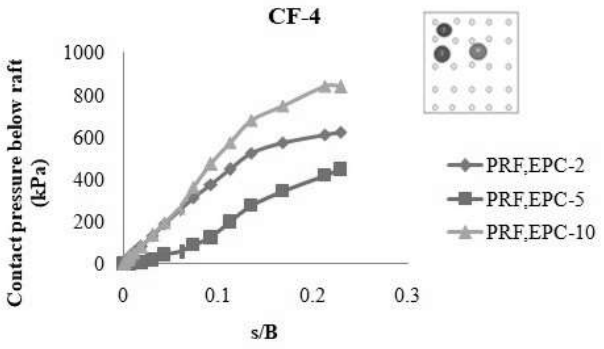

Figure 5-188 : Contact pressure distribution below raft for different location of earth pressure cells vs. relative settlement characteristics *(L/d ratio of pile = 10, 20, and 30; I_d = 60%; S = 5d ; d = 9.7 mm; pile group = 5 × 5; configuration of piles = CF-4)*

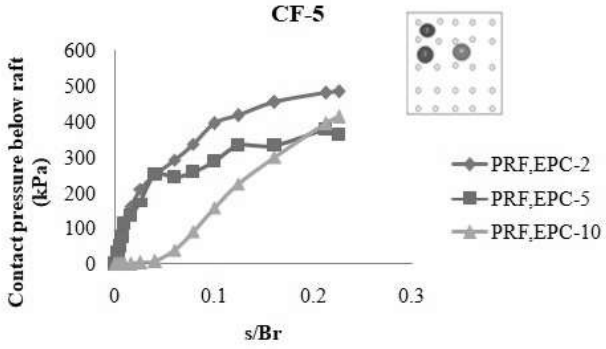

Figure 5-189 : Contact pressure distribution below raft for different location of earth pressure cells vs. relative settlement characteristics *(L/d ratio of pile = 10, 20, and 30; I_d = 60%; S = 5d ; d = 9.7 mm; pile group = 5 × 5; configuration of piles = CF-5)*

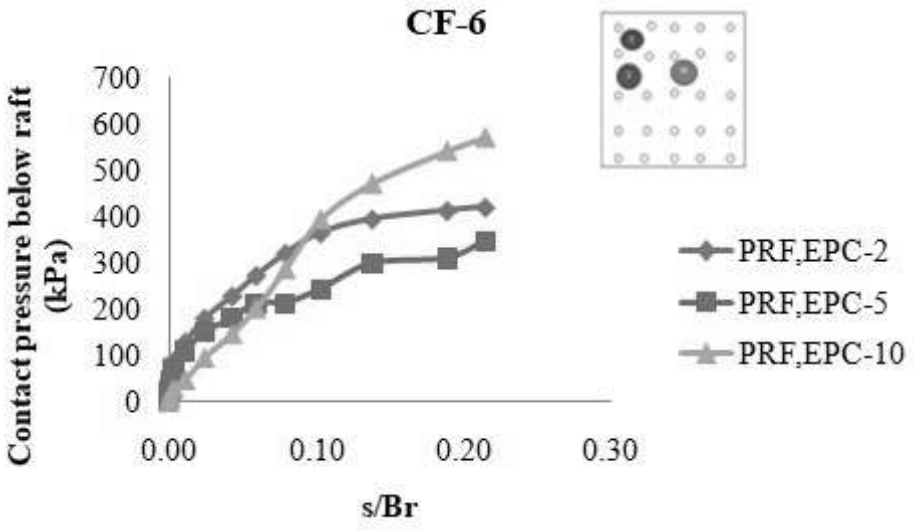

Figure 5-190 : Contact pressure distribution below raft for different location of earth pressure cells vs. relative settlement characteristics *(L/d ratio of pile = 10, 20, and 30; I_d = 60%; S = 5d ; d = 9.7 mm; pile group = 5 x 5; configuration of piles = CF-6)*

5.3.3.4.3 Load Sharing Mechanism

Figure 5-191 to Figure 5-193 demonstrate the load settlement characteristics of piled raft and load shared by pile group and raft with different configurations of piles at I_d = 60%. The results show that the *LSPG* was almost the same in the Piled Raft Foundation (PRF) with *CF-1* and *CF-2*. CF-3 indicates a higher *LSPG* than *CF-1* and *CF-2*. The pattern of *LSPG* obtained was almost the same in the case of *CF-3* and *CF-4*. The *LSPG* was less than *LSR* at all settlements in *CF-7*, while in *CF-8*, it was more than *LSR* up to 7 mm settlement. After that, *LSR* was more than *LSPG*. In the case of *CF-9*, the *LSPG* was more than *LSR* at all settlement levels.

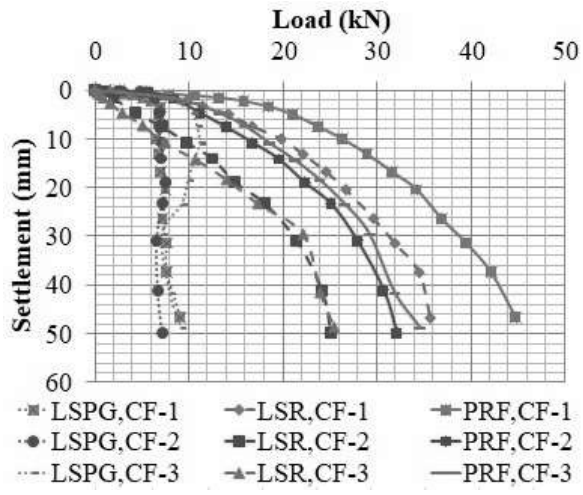

Figure 5-191 : Load settlement characteristics of piled raft and Load sharing by pile group and raft with different configuration of piles *(L/d ratio of pile = 10, 20, and 30; I_d = 60%; S = 5d; d = 9.7 mm ; Pile group = 5 × 5; configuration of piles = CF-1, CF-2, CF-3)*

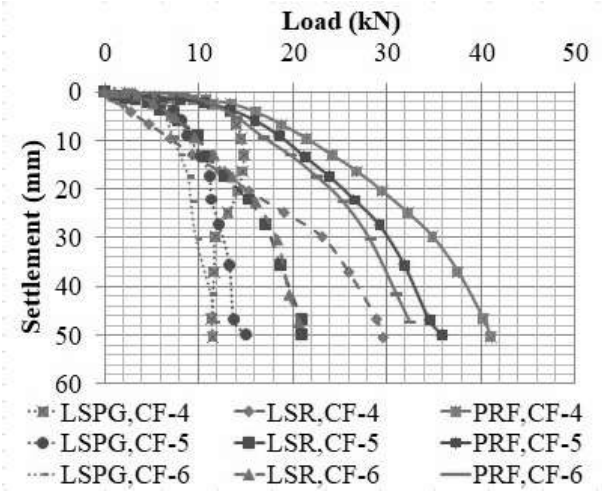

Figure 5-192 : Load settlement characteristics of piled raft and Load sharing by pile group and raft with different configuration of piles *(L/d ratio of pile = 10, 20, and 30; I_d = 60%; S = 5d; d = 9.7 mm ; Pile group = 5 × 5; configuration of piles = CF-4, CF-5, CF-6)*

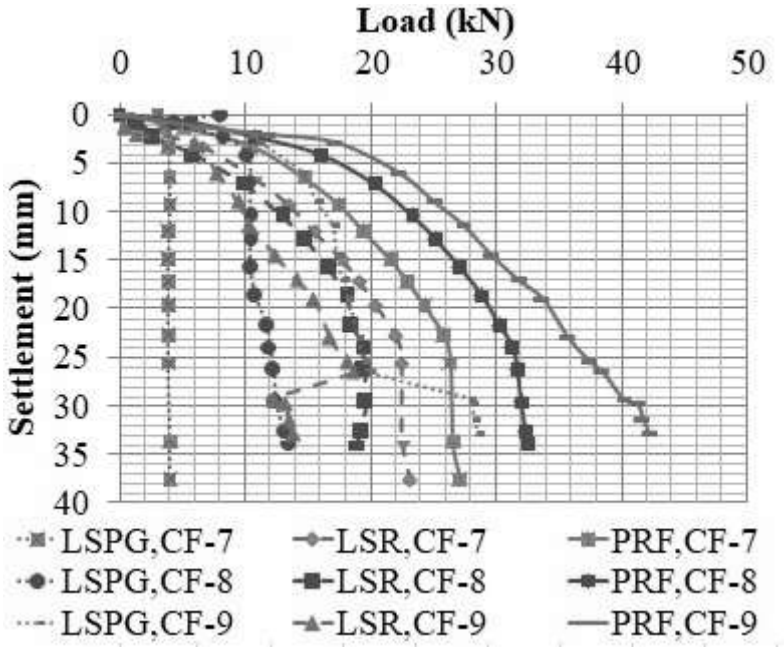

Figure 5-193 : Load settlement characteristics of piled raft and Load shared by pile group and raft with different configuration of piles *(L/d ratio of pile = 10, 20, and 30; I_d = 60%; S = 5d; d = 9.7 mm ; Pile group = 5 × 5; configuration of piles = CF-7, CF-8, CF-9)*

The load shared by piles and raft in the model piled-raft foundation at Initial Yield Load (*IYL*) and Final Yield Load (*FYL*) are presented in Figure 5-194 and Figure 5-195, respectively. The *LSPG* was higher than the *LSR* in all configurations at *IYL* except *CF-1* and *CF-7*. The reason for the lower contribution of piles at *IYL* in *CF-7* may be the length of the piles (all the piles were short), and in *CF-1*, it may be the confinement of sand below the raft due to the arrangement of long piles at the periphery of the pile group. The *LSR* was higher than the *LSPG* at *FYL* in all configurations. The differences in *LSPG* at *FYL* and *LSPG* at *IYL* were negligible in all configurations.

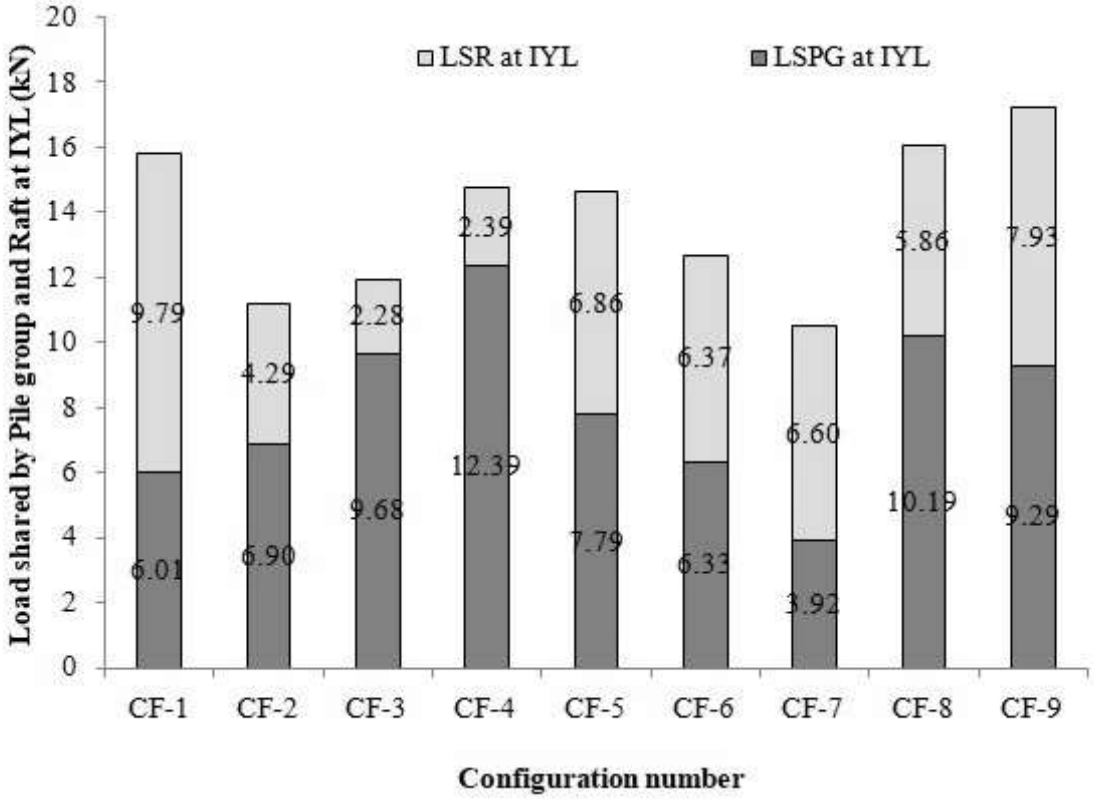

Figure 5-194 : Load shared by pile group and raft at *IYL* of piled raft foundation for configuration of piles at 60% relative density of sand bed *(S = 5d; L/d ratio of pile = 10, 20, and 30; configuration of piles = CF-1 to CF-9; pile group = 5 × 5)`*

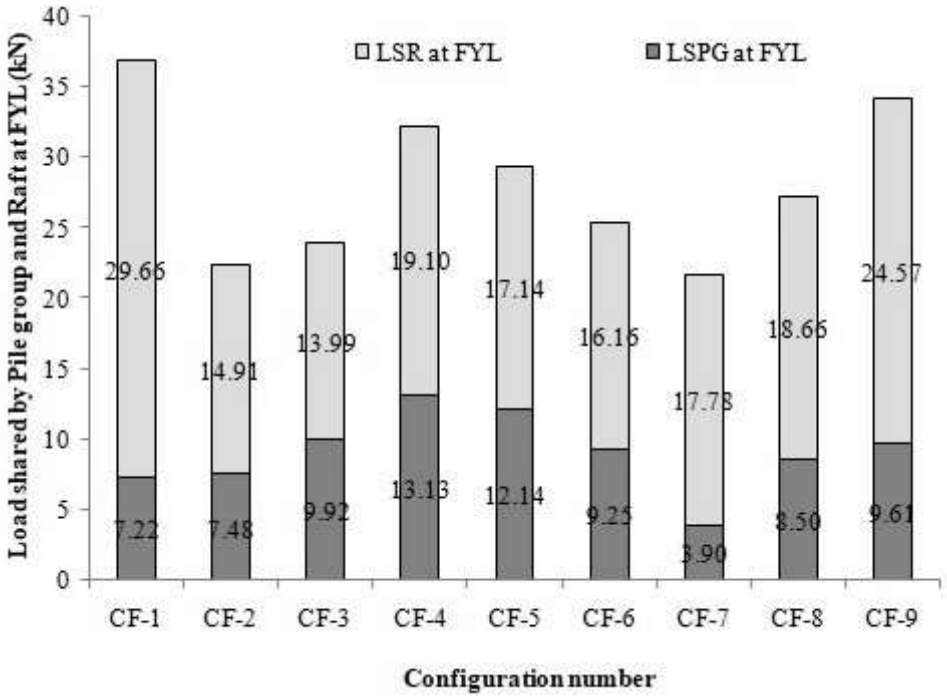

Figure 5-195 : Load shared by pile group and raft at *FYL* of piled raft foundation for configuration of piles at 60% relative density of sand bed *(S = 5d; L/d ratio of pile = 10, 20, and 30; configuration of piles = CF-1 to CF-9; pile group = 5× 5)*

Figure 5-196 to Figure 5-204 depict the percentage load shared by pile group (% *LSPG*) and raft (% *LSR*) in piled rafts with different pile configurations at different relative settlements. It observed that for all configurations, the % *LSPG* decreased with increased relative settlement(s/B_r), and the % *LSR* increased with an increase in s/B_r. In the case of *CF-1*, the % *LSPG* was less than 50% at all relative settlements. The % *LSPG* and % *LSR* were equal at s/B_r = 0.03, 0.065, 0.09, 0.03, 0.02, 0.01 and 0.03 in piled raft with *CF-2*, *CF-3*, *CF-4*, *CF-5*, *CF-6*, *CF-7* and *CF-8* respectively. In the case of PRF with *CF-9*, the % *LSPG* was more than 50% at all s/B_r values.

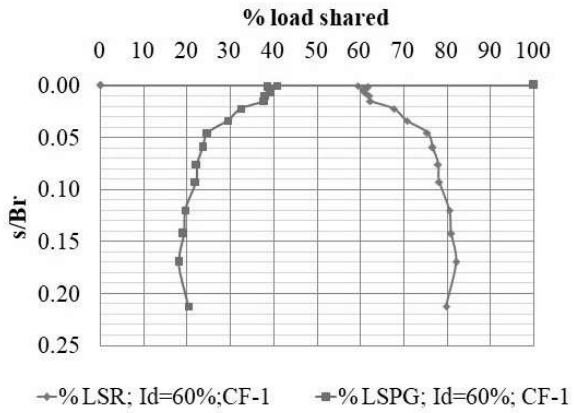

Figure 5-196 : Percentage load shared by pile group (% *LSPG*) and raft (% *LSR*) in piled raft at different relative settlement *(S = 5d; I_d = 60%; d = 9.7 mm; pile group = 5× 5; L/d ratio of pile = 10, 20 and 30; CF-1)*

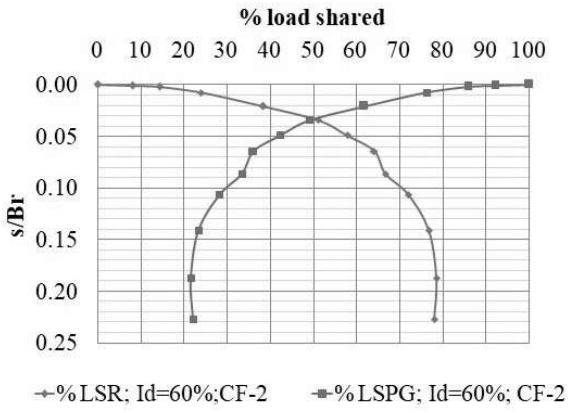

Figure 5-197 : Percentage load shared by pile group (% *LSPG*) and raft (% *LSR*) in piled raft at different relative settlement *(S = 5d; I_d = 60%; d = 9.7 mm; pile group = 5 × 5; L/d ratio of pile = 10, 20 and 30; CF-2)*

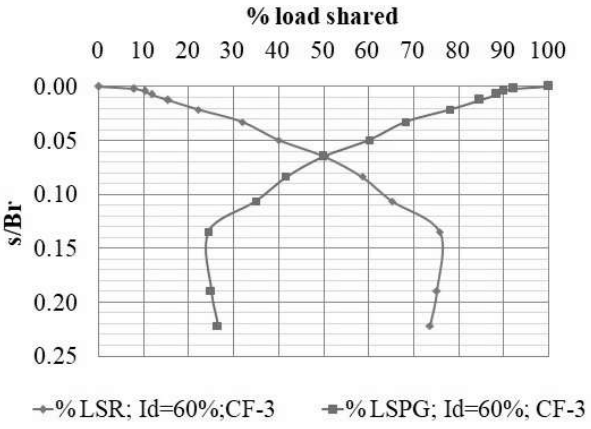

Figure 5-198 : Percentage load shared by pile group (% *LSPG*) and raft (% *LSR*) in piled raft at different relative settlement *(S = 5d; I_d = 60%; d = 9.7 mm; pile group = 5 ×5; L/d ratio of pile = 10 and 30; CF-3)*

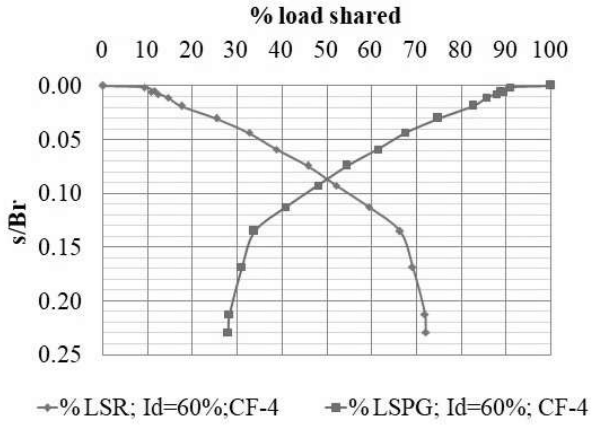

Figure 5-199 : Percentage load shared by pile group (% *LSPG*) and raft (% *LSR*) in piled raft at different relative settlement *(S = 5d; I_d = 60%; d = 9.7 mm; pile group = 5 × 5; L/d ratio of pile = 10 and 30; CF-4)*

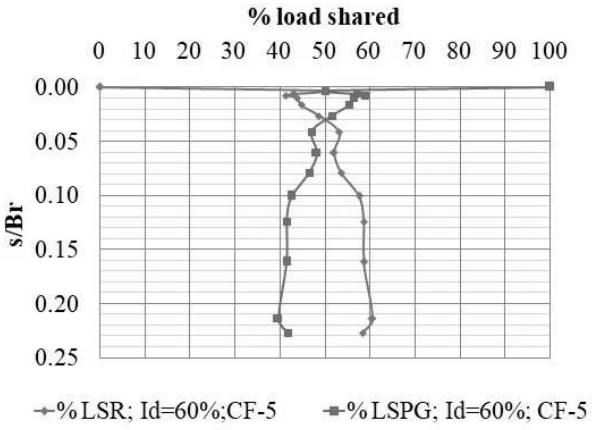

Figure 5-200 : Percentage load shared by pile group (% *LSPG*) and raft (% *LSR*) in piled raft at different relative settlement *(S = 5d; I_d = 60%; d = 9.7 mm; pile group = 5 × 5; L/d ratio of pile = 10, 20 and 30; CF-5)*

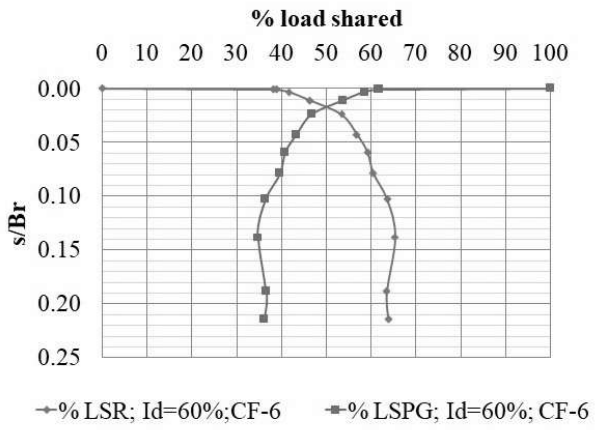

Figure 5-201 : Percentage load shared by pile group (% *LSPG*) and raft (% *LSR*) in piled raft at different relative settlement *(S = 5d; I_d = 60%; d = 9.7 mm; pile group = 5 × 5; L/d ratio of pile = 10, 20 and 30; CF-6)*

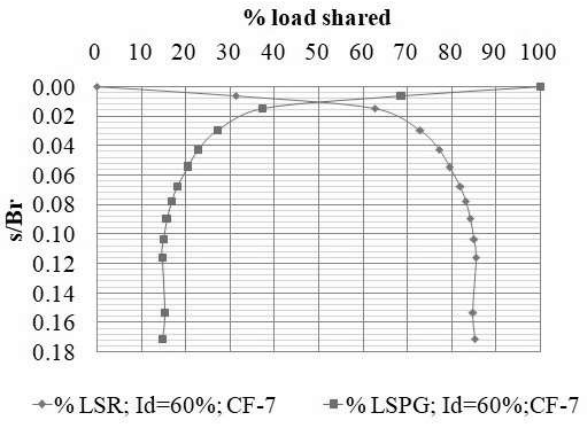

Figure 5-202 : Percentage load shared by pile group (% *LSPG*) and raft (% *LSR*) in piled raft at different relative settlement *(S = 5d; I_d = 60%; d = 9.7 mm; pile group = 5 × 5; L/d ratio of pile = 10; CF-7)*

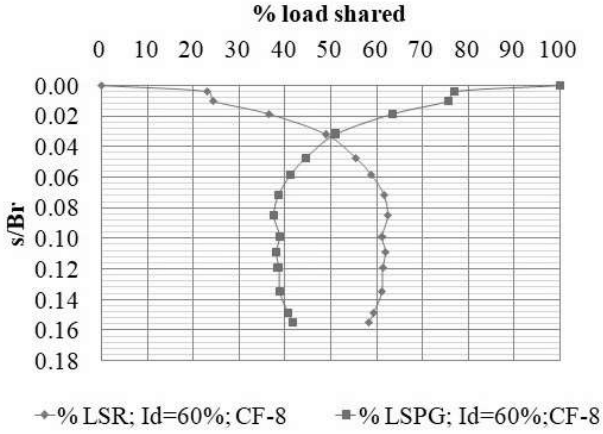

Figure 5-203 : Percentage load shared by pile group (% *LSPG*) and raft (% *LSR*) in piled raft at different relative settlement *(S = 5d; I_d = 60%; d = 9.7 mm; pile group = 5 × 5; L/d ratio of pile = 20; CF-8)*

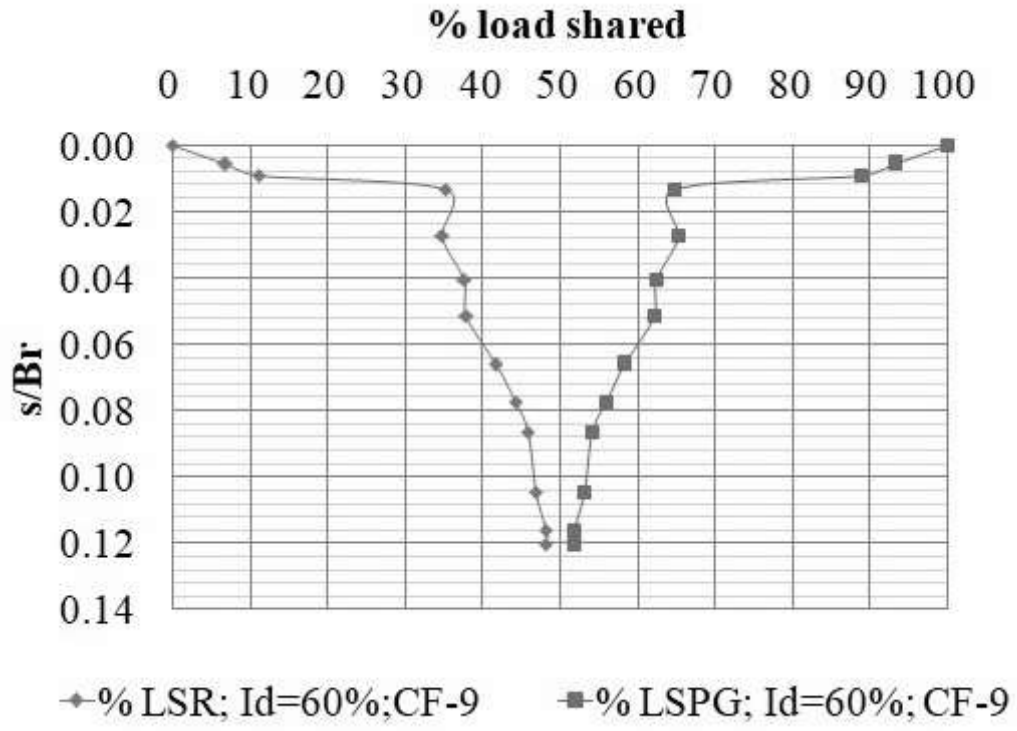

Figure 5-204 : Percentage load shared by pile group (% *LSPG*) and raft (% *LSR*) in piled raft at different relative settlement *(S = 5d; I_d = 60%; d = 9.7 mm; pile group = 5 × 5; L/d ratio of pile = 30; CF-9)*

5.3.3.4.4 Piled Raft Coefficient (α_p)

Figure 5-205 illustrate the relationship between the piled raft coefficient (α_p) and the settlement characteristics of piled raft foundations with different pile configuration and 60% relative density of the sand bed. The piled raft coefficient was decrease with the increase in relative settlement. The decreament in the piled raft coefficient was rapid initially up to *IYL* and then gentle up to *FYL*, after which it remained almost constant. The range of relative settlement (s/B_r) for different configurations was 0.01 to 0.02 for *IYL* and 0.07 to 0.12 for *FYL*.

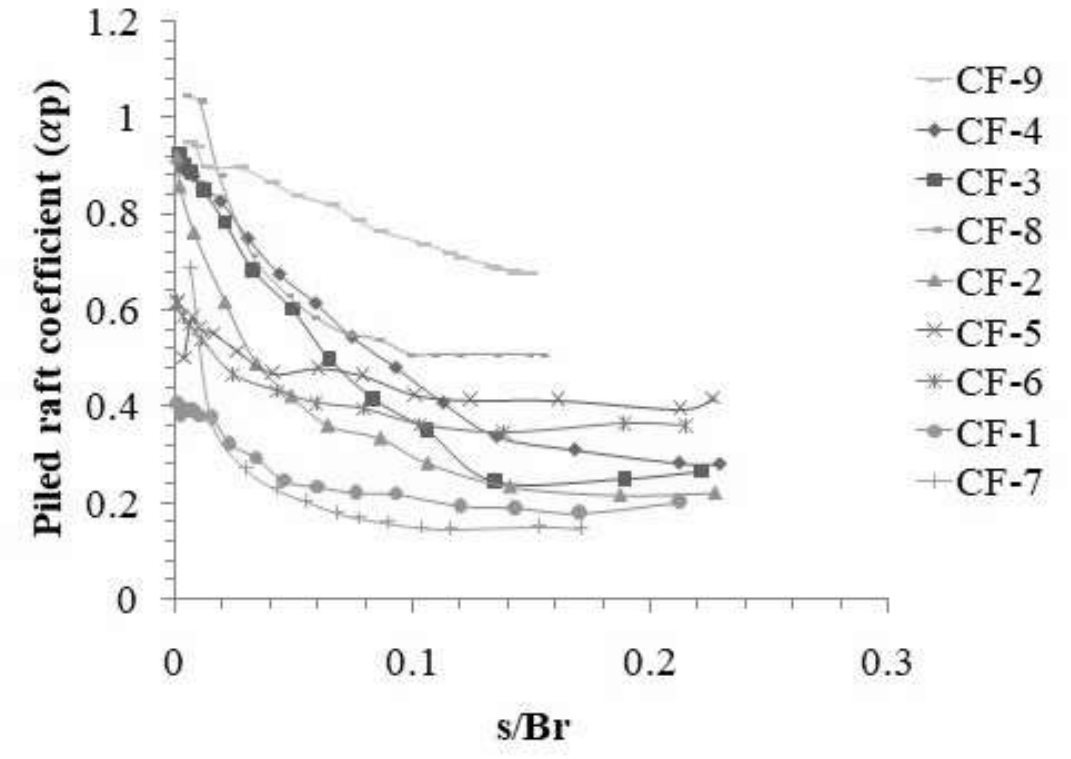

Figure 5-205 : Piled raft coefficient (α_p) vs. relative settlement characteristics of piled raft foundation at different configuration of piles *(I_d = 60%; S = 5d; L/d ratio of pile = 30; configuration of piles = CF-1 to CF-9; pile group = 5 × 5)*

5.3.3.4.5 Settlement Reduction Ratio (SRR) and Load Improvement Ratio (LIR)

The range of settlement reduction ratio of PRF with configuration *CF-1*, *CF-2*, *CF-3*, *CF-4*, *CF-5*, *CF-6*, *CF-7*, *CF-8*, and *CF-9* was found to be 76% to 87%, 0.35% to 72%, 26% to 46%, 46% to 62%, -18% to 53%, 23% to 91%, -6% to 30%, 39% to 56%, 17% to 76% respectively. The range of load improvement ratio *(LIR)*of PRF with configuration *CF-1*, *CF-2*, *CF-3*, *CF-4*, *CF-5*, *CF-6*, *CF-7*, *CF-8*, and *CF-9* was found to be 1.57 to 1.86, 1.0 to 1.33, 1.10 to 1.41, 1.32 to 1.67, 1.16 to 1.46,1.07 to 1.35, 1.1 to 1.31, 1.37 to 1.58, 1.57 to 1.94 respectively. i.e. maximum load improvement was observed in *CF-9* and *CF-1*, while minimum load improvement was observed in *CF-7* and *CF-2* compared to UPR.

Table 5-51 Settlement reduction ratio of PRF with different configuration of piles at different load levels and 60% relative densities of the sand bed

I_d (%)	Load (kN)	Settlement (mm)										Settlement reduction ratio (%)								
		UPR	**PRF *(CF-1)***	**PRF *(CF-2)***	**PRF *(CF-3)***	**PRF *(CF-4)***	**PRF *(CF-5)***	**PRF *(CF-6)***	**PRF *(CF-7)***	**PRF *(CF-8)***	**PRF *(CF-9)***	**PRF *(CF-1)***	**PRF *(CF-2)***	**PRF *(CF-3)***	**PRF *(CF-4)***	**PRF *(CF-5)***	**PRF *(CF-6)***	**PRF *(CF-7)***	**PRF *(CF-8)***	**PRF *(CF-9)***
60	2.5	0.62	0.08	0.17	0.43	0.30	0.73	0.12	0.66	0.38	0.51	87	72	30	52	-18	81	-6	39	17
	5	1.62	0.39	0.40	0.87	0.87	1.25	0.15	1.31	0.75	1.02	76	76	46	46	23	91	19	54	37
	10	4.42	1.04	3.40	2.46	1.53	2.07	1.63	3.09	2.06	1.79	76	23	44	65	53	63	30	53	59
	12.5	6.13	1.40	6.00	4.10	2.18	3.18	3.65	4.79	2.88	2.15	77	2	33	64	48	41	22	53	65
	15	8.54	1.98	8.51	6.35	3.46	5.01	6.60	6.76	3.75	2.55	77	0.35	26	59	41	23	21	56	70

Table 5-52 Load improvement ratio of PRF with different configuration of piles at different load levels and 60% relative densities of the sand bed

I_d (%)	Settlement (mm)	Load(kN)										Load improvement ratio								
		UPR	PRF *(CF-1)*	PRF *(CF-2)*	PRF *(CF-3)*	PRF *(CF-4)*	PRF *(CF-5)*	PRF *(CF-6)*	PRF *(CF-7)*	PRF *(CF-8)*	PRF *(CF-9)*	PRF *(CF-1)*	PRF *(CF-2)*	PRF *(CF-3)*	PRF *(CF-4)*	PRF *(CF-5)*	PRF *(CF-6)*	PRF *(CF-7)*	PRF *(CF-8)*	PRF *(CF-9)*
60	5.5	11.69	21.65	12.02	14.13	17.53	15.59	14.25	13.43	18.02	21.44	1.85	1.03	1.21	1.50	1.33	1.22	1.15	1.54	1.83
	11	17.06	27.18	16.98	18.68	22.59	19.87	18.18	18.70	23.81	27.05	1.59	1.00	1.10	1.32	1.16	1.07	1.10	1.40	1.59
	16.5	20.08	31.45	20.94	22.68	26.97	23.38	22.01	22.59	27.58	31.44	1.57	1.04	1.13	1.34	1.16	1.10	1.13	1.37	1.57
	22	20.84	34.95	24.29	25.84	30.52	26.53	25.07	25.49	30.43	35.26	1.68	1.17	1.24	1.46	1.27	1.20	1.22	1.46	1.69
	27.5	20.15	37.49	26.70	28.33	33.69	29.33	27.19	26.46	31.90	39.12	1.86	1.33	1.41	1.67	1.46	1.35	1.31	1.58	1.94

5.3.3.4.6 Comparison between Predicted and Experimental Values of Primary Stiffness of PRF $(k_{pr})_p$ and Secondary Stiffness of PRF $(k_{pr})_s$

Table 5-53 displays the experimental and predicted values of the primary stiffness of PRF $(k_{pr})_p$ and secondary stiffness of PRF $(k_{pr})_s$. In present parameter study, the initial stiffness of pile groups was calculated using Fleming's equation since experiments were not conducted on only pile groups with configuration *CF-1* to *CF-6*. The primary stiffness of PRF $(k_{pr})_p$ was predicted using equation (5-22), which utilized the initial stiffness of pile groups, calculated using Fleming's equation. The differences between the experimental and predicted values of the secondary stiffness of PRF $(k_{pr})_s$ are minimal.

Table 5-53 Primary Stiffness of Piled Raft $(k_{pr})_p$ in kN/m and Secondary Stiffness of Piled Raft $(k_{pr})_s$ in kN/m with different configuration of piles

Configuration no.	**Relative density of sand (%)**	**Total Length of piles (m)**	**Primary Stiffness of Piled Raft $(k_{pr})_p$ in kN/m**	**Secondary Stiffness of Piled Raft $(k_{pr})_s$ in kN/m**	**Initial stiffness of UPR (k_{ri}) (kN/m)**	**Initial stiffness of PG $(k_{pg})_i$ (kN/m) (Fleming)**	**Primary stiffness of PRF $(k_{pr})_p$ in kN/m (Proposed equation)**	**Secondary Stiffness of Piled Raft $(k_{pr})_s$ in kN/m (Proposed equation)**
CF-1	60	6.305	8240.006	971.24	3585.12	824.68	4992.66	972.33
CF-2	60	3.395	2031.55	903.31	3585.12	238.68	4488.70	972.33
CF-3	60	4.171	5001.50	891.75	3585.12	488.78	4703.78	972.33
CF-4	60	5.529	6286.254	878.62	3585.12	715.63	4898.87	972.33
CF-5	60	5.335	4946.92	697.70	3585.12	436.94	4659.20	972.33
CF-6	60	4.365	3781.84	746.35	3585.12	635.06	4829.59	972.33
CF-7	60	2.425	2769.20	811.40	3585.12	25.70	4305.54	972.33
CF-8	60	4.85	3164.36	857.71	3585.12	264.04	4510.51	972.33
CF-9	60	7.275	5981.83	954.38	3585.12	960.87	5109.78	972.33

5.3.3.4.7 Comparison between Predicted and Experimental Values of IYL and FYL

The experiments on only pile groups with different configurations were not conducted in this study, so for predicting the load taken by only pile groups at the settlement s_i, was calculated as below.

$$P_{pg_{s_i}} = \frac{Q_{u,pg}}{2} \tag{5-28}$$

where,

$P_{pg_{s_i}}$ = Load taken by only pile group (kN) corresponding to the settlement of PRF at *IYL* i.e.s_i

$Q_{u,pg}$= Estimated ultimate load of only pile group (kN) with different configurations of piles using equation (5-29).

Table 5-54 represents the efficiency factors of the raft (C_1) , and pile group (C_2) in PRF with different configurations of piles calculated from proposed equations (5-14) and (5-15), percentage variations in *IYL* determined from proposed equation (5-16) with respect to experimental *IYL*. The value of $P_{pg_{s_i}}$ calculated from equation (5-28) has been used in equation (5-16) for predicting *IYL* of PRF with different configurations of piles.The variations in the predicted *IYL* and experimental *IYL* were found to be less than 15% in most of the cases considered in this study.

Table 5-54 Efficiency factors of the raft (C_1) , and pile group (C_2) in PRF with different configuration of piles calculated from proposed equations and percentage variations in *IYL* determined from proposed equations with respect to experimental *IYL*

Configuration no.	***IYL*-EXP (KN)**	**settlement at *IYL*, s_i (mm)**	**Numbers of Long Piles (nL_1)**	**Numbers of Medium Piles (nL_2)**	**Numbers of Short Piles (nL_3)**	**Total Length of piles (mm) (nL)**	**B_r (mm)**	**$(P_r)_{s_i}$ (kN)**	**$(P_{pg})_{s_i}$ (kN)**	**C_1**	**C_2**	***IYL*-PROPOSED EQUATION**	**% Variations**
CF-1	15.80	2.19	16	8	1	6305	220	6.15	2.31	0.64	3.35	13.63	-14
CF-2	11.19	4.64	1	8	16	3395	220	10.38	0.65	0.73	2.95	9.98	-11
CF-3	11.96	3.70	9	0	16	4171	220	8.77	1.16	0.72	3.01	10.65	-11
CF-4	14.77	3.32	16	0	9	5529	220	8.09	1.94	0.85	2.48	12.90	-13
CF-5	14.64	4.71	4	12	9	4365	220	10.51	1.73	0.95	2.14	14.66	0
CF-6	12.70	3.86	9	12	4	5335	220	9.04	1.17	0.96	2.14	11.77	-7
CF-7	10.52	3.28	0	0	25	2425	220	8.04	0.16	0.37	4.93	3.97	-62
CF-8	16.05	4.12	0	25	0	4850	220	9.48	1.34	0.93	2.23	12.52	-22
CF-9	17.22	2.90	25	0	0	7275	220	7.39	2.93	0.98	2.07	14.82	-14

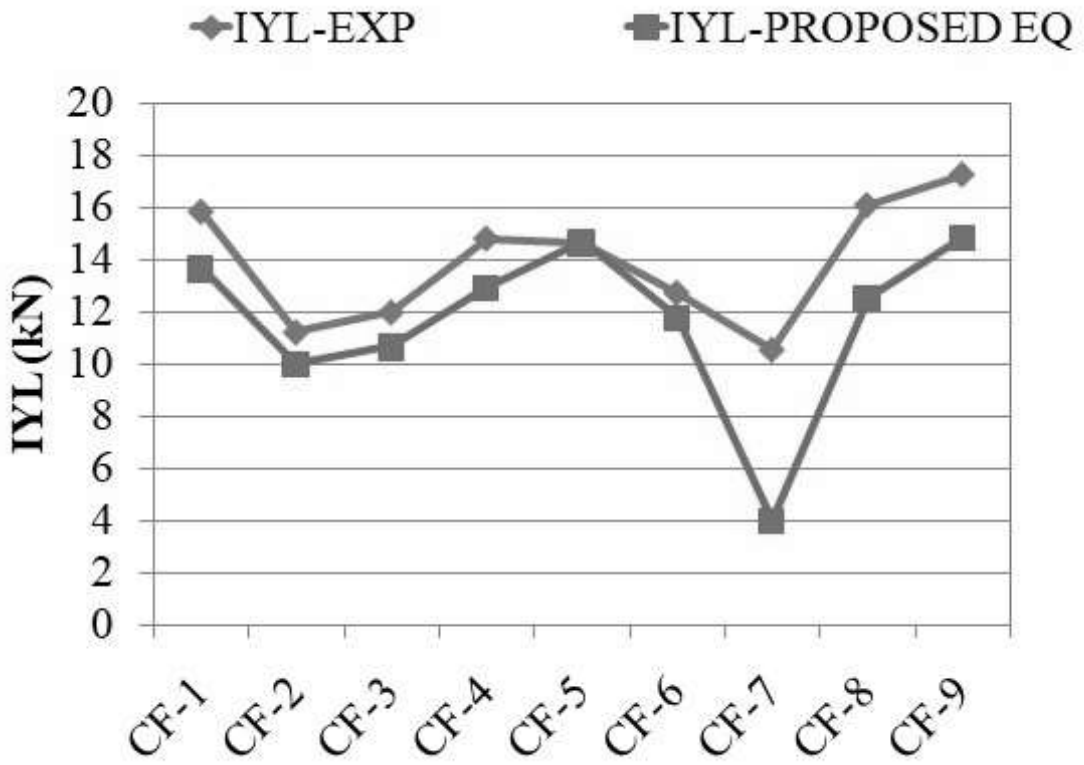

Figure 5-206 : Comparison of *IYL* of piled raft foundation with different spacing between piles at different relative density of sand bed found from experimental results and calculated from proposed equation

Because experiments on only pile groups with different configurations were not carried out in this study, the ultimate load taken by only pile groups with different configurations was calculated as per equation (5-29) and was used in equation (5-19) to calculate the *FYL* of PRF with different pile configurations. Table 5-55 demonstrates that the most of the anticipated value of *FYL* using equations (5-19) and (5-29) is varied by less than 15% from the experimental value of *FYL*.

$$Q_{u,pg} = \left(Q_{u,sp}\right)_{L_1} \times nL_1 \times \eta_1 + \left(Q_{u,sp}\right)_{L_2} \times nL_2 \times \eta_2 + \left(Q_{u,sp}\right)_{L_3} \times nL_3 \times \eta_3 \quad (5\text{-}29)$$

where,

$Q_{u,pg}$= Estimated ultimate load of only pile group with different configurations of piles (kN)

$\left(Q_{u,sp}\right)_{L_1}$ = Ultimate load of a single long pile (kN)

nL_1 = number of long piles in configuration

η_1 = Efficiency of pile group with long piles

$\left(Q_{u,sp}\right)_{L_2}$ = Ultimate load of a single medium pile (kN)

nL_2 = number of medium piles in configuration

η_2 = Efficiency of pile group with medium piles

$\left(Q_{u,sp}\right)_{L_3}$ = Ultimate load of a single short pile (kN)

nL_3 = number of short piles in configuration

η_3 = Efficiency of pile group with short piles

Table 5-55 Variations in *FYL* with different configurations of pile (experimental) and determined from the proposed equation

Configuration no.	***FYL*-EXP. (kN)**	**Numbers of Long Piles (nL_1)**	**Numbers of Medium Piles (nL_2)**	**Numbers of Short Piles (nL_3)**	**Total Length of piles (mm) (nL)**	**B_r in mm**	**Q_{ur} (kN)**	**$Q_{u,sp}$ (L_1) (kN)**	**$Q_{u,sp}$ (L_2) (kN)**	**$Q_{u,sp}$ (L_3) (kN)**	**$Q_{u,pg}$ (kN)**	**C_3**	**C_4**	***FYL*-PROPOSED EQUATION (kN)**	**% Variations**
CF-1	36.87	16	8	1	6305	220	25.45	0.131	0.086	0.012	5.78	0.63	3.86	35.21	-5
CF-2	22.39	1	8	16	3395	220	25.45	0.131	0.086	0.012	1.63	0.61	4.16	19.14	-15
CF-3	23.91	9	0	16	4171	220	25.45	0.131	0.086	0.012	2.90	0.61	4.12	24.39	2
CF-4	32.23	16	0	9	5529	220	25.45	0.131	0.086	0.012	4.84	0.63	3.95	31.82	-1
CF-5	29.28	4	12	9	4365	220	25.45	0.131	0.086	0.012	4.32	0.63	3.92	29.68	1
CF-6	25.41	9	12	4	5335	220	25.45	0.131	0.086	0.012	2.93	0.62	4.06	24.42	-4
CF-7	21.68	0	0	25	2425	220	25.45	0.131	0.086	0.012	0.41	0.60	4.24	13.97	-36
CF-8	27.16	0	25	0	4850	220	25.45	0.131	0.086	0.012	3.35	0.61	4.12	26.25	-3
CF-9	34.19	25	0	0	7275	220	25.45	0.131	0.086	0.012	7.34	0.64	3.81	40.89	20

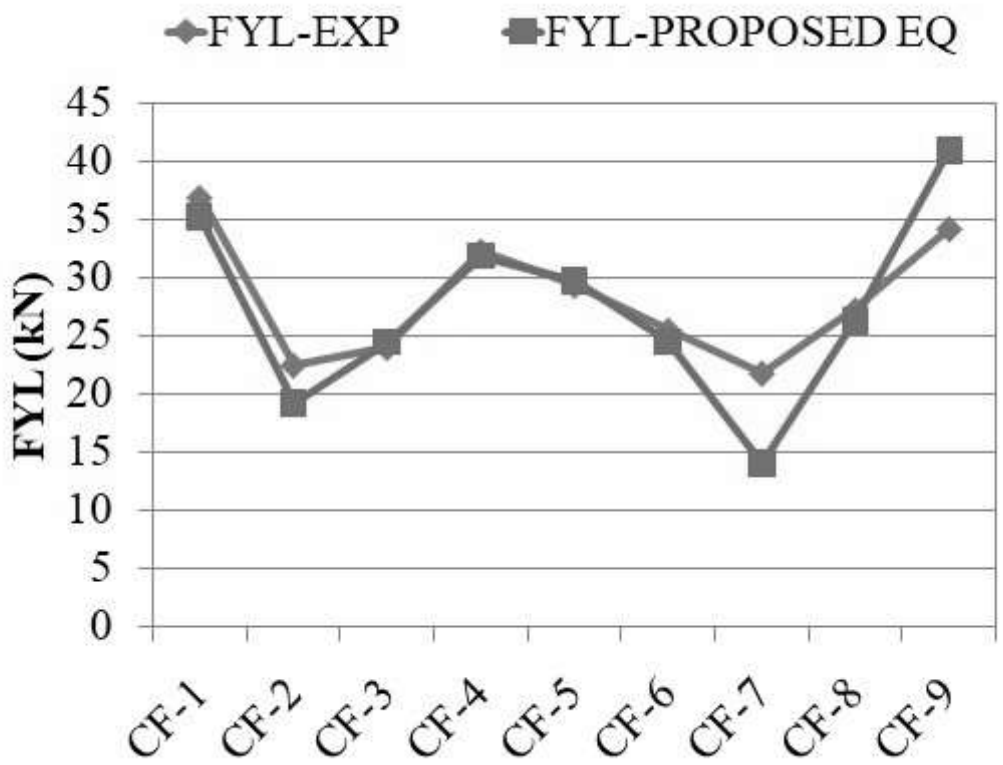

Figure 5-207 : Comparison of *FYL* of piled raft foundation with different spacing between piles at different relative density of sand bed found from experimental results and calculated from proposed equation

5.3.3.5 Soil-Pile Friction

5.3.3.5.1 Load Settlement Characteristics and Load Sharing Mechanism at 40% Relative Density

Figure 5-208 represents the load settlement characteristics of piled raft foundation with different soil pile friction angles at I_d = 40%. It observed that the load-carrying capacity of PRF increased as the soil pile friction angle increased (δ_0 to δ_3). The load settlement characteristics of PRF with soil-pile friction angles δ_2 and δ_3 were quite similar. Figure 5-209 to Figure 5-212 depict the load settlement characteristics of piled raft and load shared by pile group and raft with soil pile friction angle (δ_0 to δ_3) at 40% relative density of sand bed. It observed that at δ_0 = 22.4°, the *LSPG* was slightly higher than *LSR* at most settlement levels. The *LSPG* was more than the *LSR* at all settlement levels for PRF with δ_1= 24.36°,δ_2 = 25.8°, and δ_3 = 27.1°. i.e., the effect of soil pile friction was less significant on load settlement characteristics of PRF and more significant on load sharing characteristics of PRF at I_d = 40%.

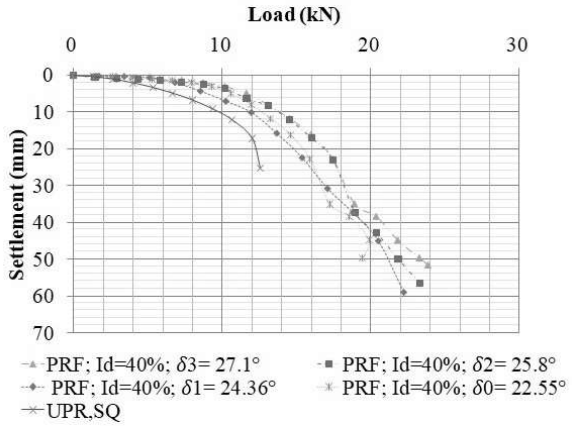

Figure 5-208 : Load settlement characteristics of piled raft foundation with different soil pile friction in sand *(L/d ratio of pile = 30; I_d = 40%; d = 9.7 mm)*

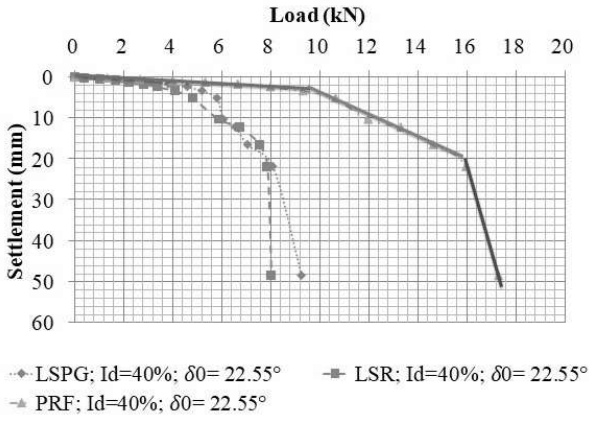

Figure 5-209 : Load settlement characteristics of piled raft and Load shared by pile group and raft with soil pile friction angle δ_0 = 22.4° at 40% relative density of sand bed *(S = 5d; L/d ratio of pile = 30; pile group = 3 × 3)*

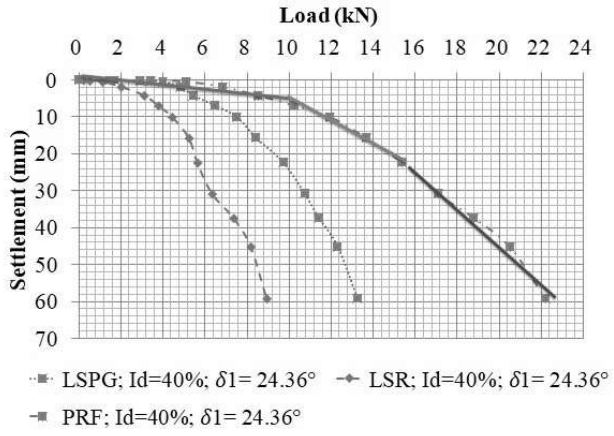

Figure 5-210 : Load settlement characteristics of piled raft and Load shared by pile group and raft with soil pile friction angle δ_1 = 24.36° at 40% relative density of sand bed *(S = 5d; L/d ratio of pile = 30; pile group = 3 × 3)*

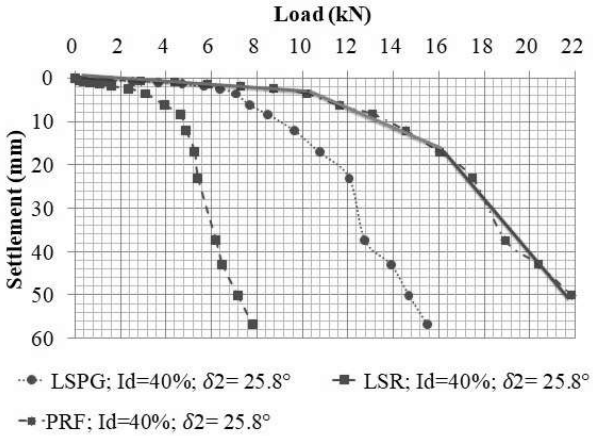

Figure 5-211 : Load settlement characteristics of piled raft and Load shared by pile group and raft with soil pile friction angle δ_2 = 25.8° at 40% relative density of sand bed *(S = 5d; L/d ratio of pile = 30; pile group = 3 × 3)*

Figure 5-213 depicts the Initial yield load (*IYL*) and Final yield load (*FYL*) of piled raft foundation at different soil pile friction angles at I_d = 40%. It can be observed that the *IYL* and *FYL* increases with increase in soil pile friction anlge but the amount of increment is very less.

The value of *IYL* is observed to be increased by 0.1 kN, 0.9 kN, and 1.62 kN at δ_1 = 24.36° , δ_2 = 25.8° , and δ_3 = 27.1° respectively as compared to at δ_0 = 22.4°.i.e. in percentage it was 1%, 10% and 17% respectively. The value of *FYL* is observed to be increased by 0.1 kN, 0.76 kN, and 1.47 kN at δ_1 = 24.36° , δ_2 = 25.8° , and δ_3 = 27.1° respectively as compared to at δ_0 = 22.4°.i.e. in percentage it was 1%, 5% and 10% respectively.

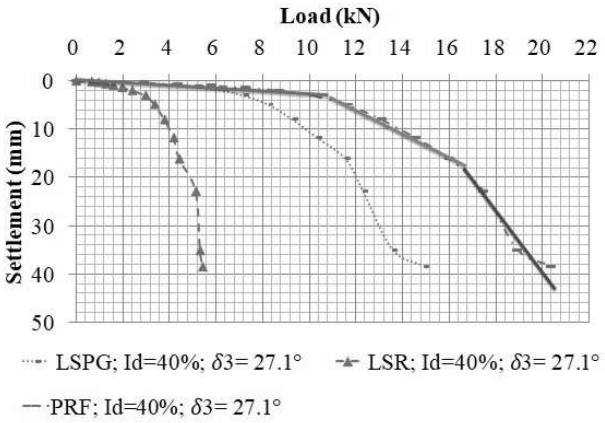

Figure 5-212 : Load settlement characteristics of piled raft and Load shared by pile group and raft with soil pile friction angle δ_3= 27.1° at 40% relative density of sand bed *(S = 5d; L/d ratio of pile = 30; pile group = 3 × 3)*

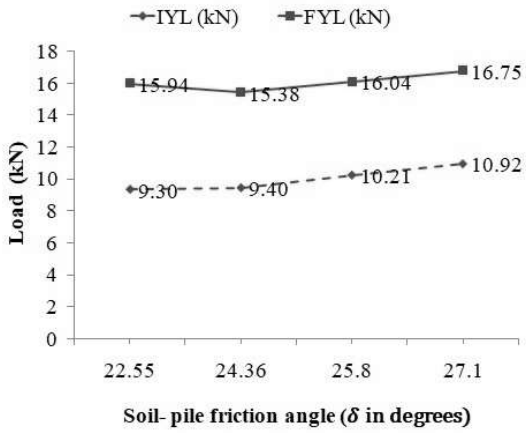

Figure 5-213 : Initial yield load (*IYL*) and Final yield load (*FYL*) of piled raft foundation at different soil pile friction angles *(S = 5d; I_d = 40%; L/d ratio of pile = 30)*

Figure 5-214 to Figure 5-215 represents the load shared by pile group and raft at *IYL* and *FYL* of the piled raft foundation, respectively, for different soil pile friction angles at 40% relative density of the sand bed. It can be noticed that the *LSPG* at *IYL* and *FYL* increases as the soil pile friction angle increases. The value of *LSR* at *IYL* is observed to be decreased by 0.66 kN, 0.98 kN and 0.92 kN at δ_1= 24.36° , δ_2 = 25.8° , and δ_3 = 27.1° respectively as compared to at δ_0 = 22.4°.i.e. in percentage it was 16%, 24% and 22% respectively. The value of *LSPG* at *IYL* is observed to be increased by 0.76 kN, 1.88 kN and 2.54 kN at δ_1= 24.36° , δ_2 = 25.8° , and δ_3 = 27.1° respectively as compared to at δ_0 = 22.4°.i.e. in percentage it was 15%, 36% and 49% respectively.

The value of *LSR* at *FYL* decreased by 2.21 kN, 2.59 kN, and 3.07 kN at δ_1 = 24.36°, δ_2 = 25.8°, and δ_3 = 27.1° respectively as compared to at δ_0 = 22.4°. i.e., in percentage it was 28%, 33% and 39% respectively. The value of *LSPG* at *FYL* increased by 1.65 kN, 2.69 kN, and 3.87 kN at δ_1 = 24.36°, δ_2 = 25.8°, and δ_3 = 27.1° respectively as compared to at δ_0 = 22.4°. i.e., in percentage it was 20%, 33% and 48% respectively.

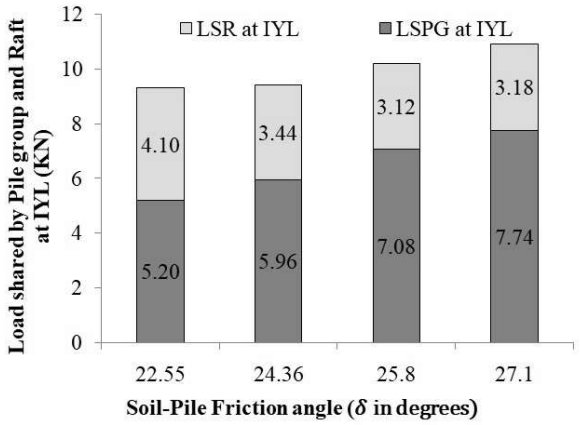

Figure 5-214 : Load shared by pile group and raft at *IYL* of piled raft foundation for different soil pile friction angle at 40% relative density of sand bed *(S = 5d; I_d = 40%; L/d ratio of pile = 30; Pile group = 3 × 3)*

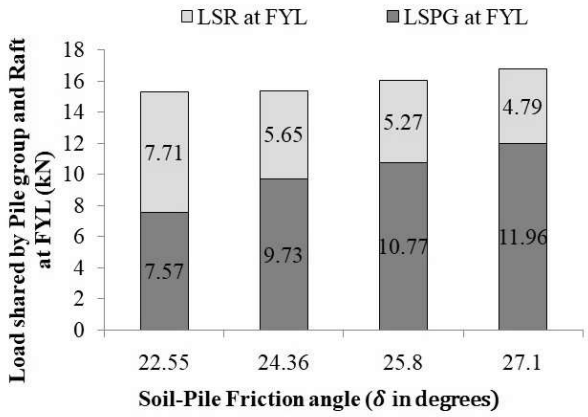

Figure 5-215 : Load shared by pile group and raft at *FYL* of piled raft foundation for different soil pile friction angle at 40% relative density of sand bed *(S = 5d; I_d = 40%; L/d ratio of pile = 30; Pile group = 3 × 3)*

Figure 5-216 to Figure 5-219 represent the percentage load shared by pile group (% *LSPG*) and raft (% *LSR*) in a piled raft with different soil pile friction angle Vs. relative settlement at I_d = 40% . It can observed that the % *LSPG* and % *LSR* became equal at s/B_r = 0.05, and after that, %*LSPG* decreased up to s/B_r = 0.09 and then it again increased by the minimal amount for PRF with δ_0 = 22.5° at I_d = 40%. The % *LSPG* was more than the % *LSR* in PRF with δ_1 = 24.36°, δ_2 = 25.8°, δ_3= 27.1° at I_d = 40%. The % *LSPG* and the % *LSR* in PRF with δ_1 = 24.36° and δ_2 = 25.8° were more or less the same, while with δ_3 = 27.1° the %*LSPG* decreases up to s/B_r = 0.0007 and then increased upto s/B_r = 0.004 and after that it became more or less constant.

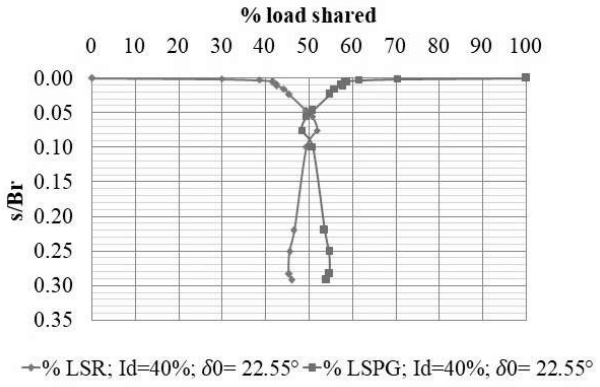

Figure 5-216 : Percentage load shared by pile group (% *LSPG*) and raft (% *LSR*) in piled raft at different relative settlement *(S = 5d; I_d = 40%; d = 9.7 mm; pile group = 5 × 5; L/d ratio of pile = 30; δ_0 = 22.5°)*

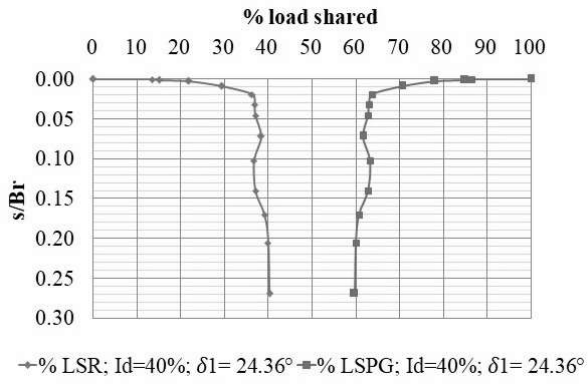

Figure 5-217 : Percentage load shared by pile group (% *LSPG*) and raft (% *LSR*) in piled raft at different relative settlement *(S = 5d; I_d = 40%; d = 9.7 mm; pile group = 5 × 5; L/d ratio of pile = 30; δ_1= 24.36°)*

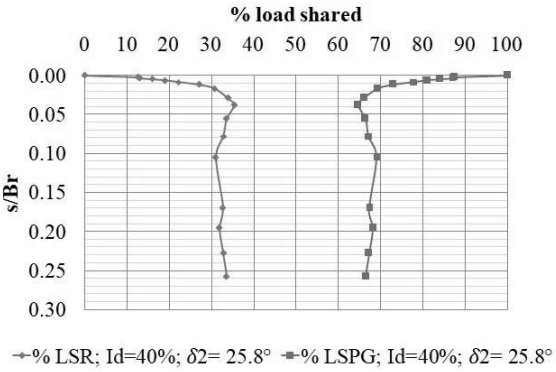

Figure 5-218 : Percentage load shared by pile group (% *LSPG*) and raft (% *LSR*) in piled raft at different relative settlement *(S = 5d; I_d = 40%; d = 9.7 mm; pile group = 5 × 5; L/d ratio of pile = 30; δ_2 = 25.8°)*

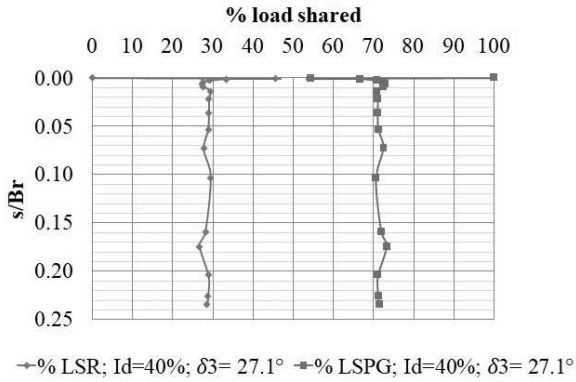

Figure 5-219 : Percentage load shared by pile group (% *LSPG*) and raft (% *LSR*) in piled raft at different relative settlement *(S = 5d; I_d = 40%; d = 9.7 mm; pile group = 5 × 5; L/d ratio of pile = 30; δ_3 = 27.1°)*

Figure 5-220 represents piled raft coefficient *(α_p)* vs. relative settlement characteristics of piled raft foundation with different soil pile friction at I_d = 40%. It was observed that the α_p decreased

with the relative settlement of PRF, and the maximum and minimum α_p were with δ_3 = 27.1° and δ_0 = 22.5° respectively.

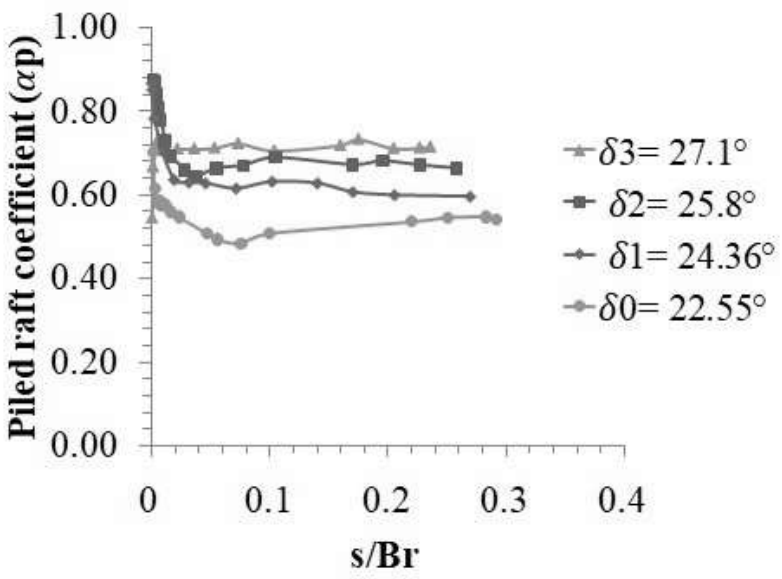

Figure 5-220 : Piled raft coefficient (α_p) vs. relative settlement characteristics of piled raft foundation at different soil pile friction *(S = 5d; I_d = 40%; L/d ratio of pile =30; Pile group = 3 × 3)*

5.3.3.5.2 Load Settlement Characteristics and Load Sharing Mechanism at 60% Relative Density

Figure 5-221 represents the load settlement characteristics of piled raft foundations with different soil pile friction angles in sand bed with I_d = 60%. It was observed that the load-carrying capacity of PRF increased as the soil pile friction angle increased (δ_0 to δ_3). The load settlement characteristics of PRF with soil-pile friction angle δ_1 and δ_2 were similar. Figure 5-222 to Figure 5-225 depicts the load settlement characteristics of piled raft and Load shared by pile group and raft with soil pile friction angle (δ_0 to δ_3) at 60% relative density of sand bed. It was observed that for δ_0 = 24.5°, and δ_2 = 26.58°, the *LSPG* was more than the *LSR* at all settlement levels. For δ_1 = 25.7°, the *LSPG* was more than the *LSR* up to 5mm settlement and after that, the *LSR* was more than the *LSPG* of PRF. For δ_3 = 28.62°, the *LSPG* was more than the *LSR* for the range

of settlement 0 to 8.45 mm and 26.54 mm to 48.70 mm settlement, and in the remaining portion, the *LSPG* was less than the *LSR*.

The value of *IYL* increased by 0.59 kN, 1.93 kN, and 1.98 kN at $\delta_1 = 25.7°$, $\delta_2 = 26.58°$, and $\delta_3 = 28.62°$ respectively as compared to at $\delta_0 = 24.5°$. i.e., in percentage it was 5%, 16% and 17% respectively. The value of *FYL* was observed to be increased by 0.19 kN, 1.39 kN, and 2.21 kN at $\delta_1 = 25.7°$, $\delta_2 = 26.58°$, and $\delta_3 = 28.62°$ respectively, as compared to at $\delta_0 = 24.5°$, i.e., in percentage it was 1%, 7% and 10% respectively.

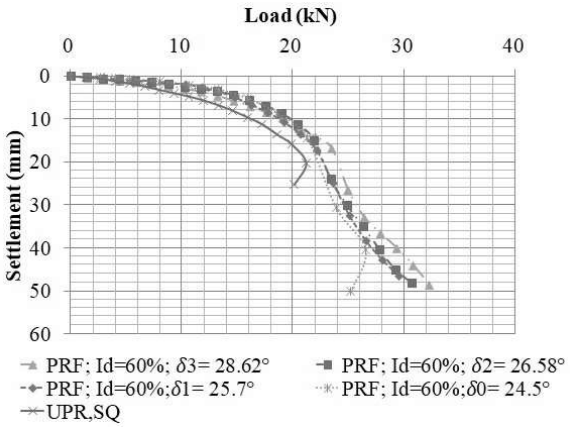

Figure 5-221 : Load settlement characteristics of piled raft foundation with different soil pile friction in sand *(L/d ratio of pile = 30; I_d = 60%; d = 9.7 mm)*

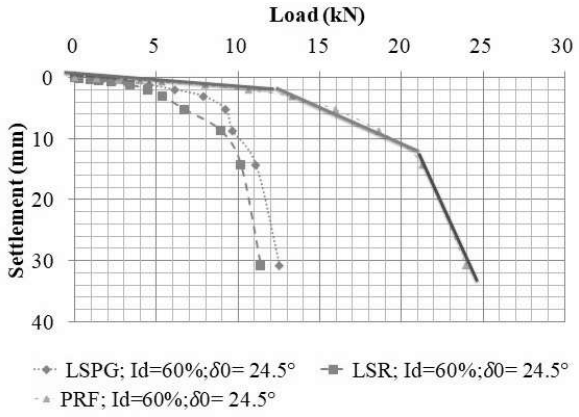

Figure 5-222 : Load settlement characteristics of piled raft and Load shared by pile group and raft with soil pile friction angle $\delta_0 = 24.5°$ at 60% relative density of sand bed *(S = 5d; L/d ratio of pile = 30; pile group = 3 × 3)*

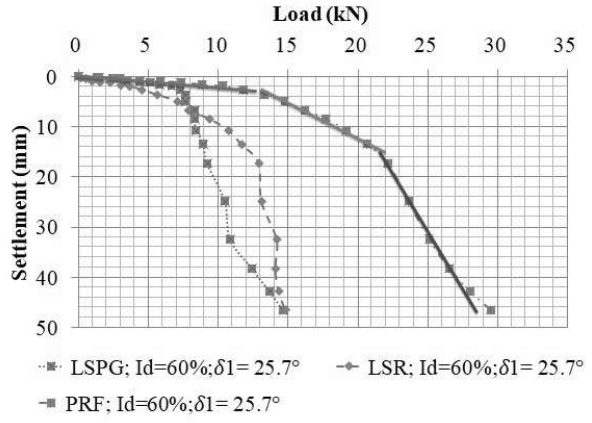

Figure 5-223 : Load settlement characteristics of piled raft and Load shared by pile group and raft with soil pile friction angle δ_1 = 25.7° at 60% relative density of sand bed *(S = 5d; L/d ratio of pile = 30; pile group = 3 × 3)*

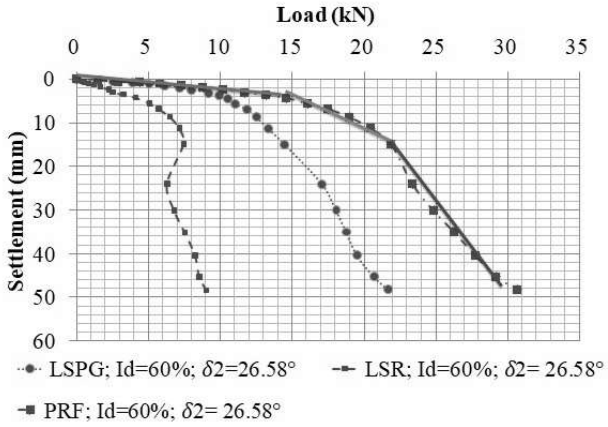

Figure 5-224 : Load settlement characteristics of piled raft and Load shared by pile group and raft with soil pile friction angle δ_2 = 26.58° at 60% relative density of sand bed *(S = 5d; L/d ratio of pile = 30; pile group = 3 × 3)*

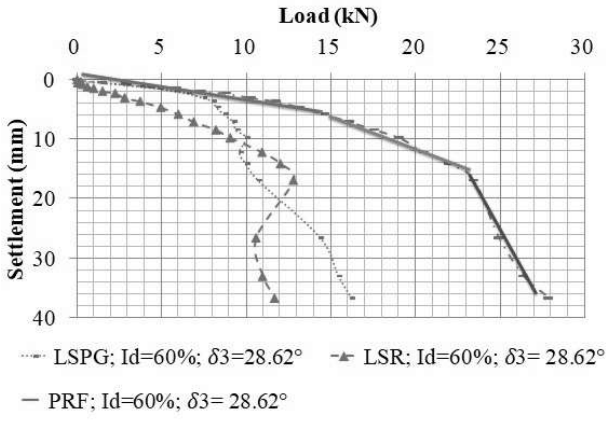

Figure 5-225 : Load settlement characteristics of piled raft and Load shared by pile group and raft with soil pile friction angle δ_3 = 27.1° at 60% relative density of sand bed *(S = 5d; L/d ratio of pile = 30; pile group = 3 x 3)*

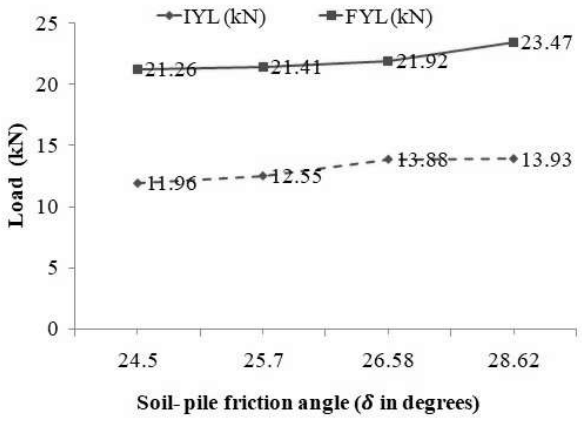

Figure 5-226 : Initial yield load (*IYL*) and Final yield load (*FYL*) of piled raft foundation at different soil pile friction angles *(S = 5d; I_d = 60%; L/d ratio of pile = 30)*

Figure 5-227 to Figure 5-228 represent the load shared by pile group (*LSPG*) and raft (*LSR*) at *IYL* and *FYL* of the piled raft foundation, respectively, for different soil pile friction angles at 60% relative density of the sand bed. It noticed that the *LSPG* at *IYL* increased as the soil pile friction angle increased from $\delta_0 = 24.5°$ to $\delta_2 = 26.58°$, but it decreased as the soil pile friction angle increased from $\delta_2 = 26.58°$ to $\delta_3 = 27.1°$. It noticed that the *LSPG* at *FYL* decreased as the soil pile friction angle increased from $\delta_0 = 24.5°$ to $\delta_1 = 25.7°$ and $\delta_2 = 26.58°$ to $\delta_3 = 27.1°$, but it increased as the soil pile friction angle increased from $\delta_1 = 25.7°$ to $\delta_2 = 26.58°$.

The value of *LSR* at *IYL* increased by 0.14 kN, decreased by 1.28 kN, and increased by 0.53 kN at $\delta_1 = 24.36°$, $\delta_2 = 25.8°$, and $\delta_3 = 27.1°$ respectively, as compared to at $\delta_0 = 22.4°$, i.e., in percentage it was increased by 3%, decreased by 26% and increased by 11% respectively. The value of *LSPG* at *IYL* increased by 0.45 kN, 3.2 kN, and 1.45 kN at $\delta_1 = 25.7°$, $\delta_2 = 26.58°$, and $\delta_3 = 28.62°$ respectively, as compared to at $\delta_0 = 24.5°$. i.e., in percentage it was 6%, 46%, and 21% respectively.

The following are the changes in the value of *LSR* and *LSPG* at *FYL* at different soil pile friction angles. As compared to the value at $\delta_0 = 22.4°$, the value of *LSR* increased by 21% at $\delta_1 = 24.36°$, decreased by 27% at $\delta_2 = 25.8°$, and increased by 26% at $\delta_3 = 27.1°$. On the other hand, the value of *LSPG* decreased by 18% at $\delta_1 = 25.7°$, increased by 31% at $\delta_2 = 26.58°$, and decreased by 4% at $\delta_3 = 28.62°$, as compared to the value at $\delta_0 = 24.5°$. The changes in the value of *LSR* and *LSPG* at *FYL* were 2.15 kN, 2.73 kN, 2.63 kN, and 2.00 kN, 3.39 kN, and 0.42 kN, respectively.

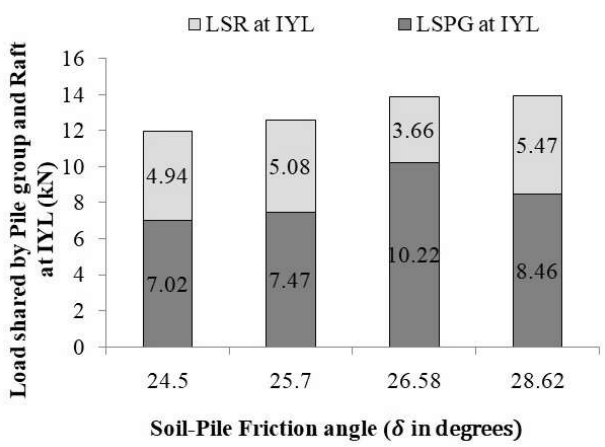

Figure 5-227 : Load shared by pile group and raft at *IYL* of piled raft foundation for different soil pile friction angle at 60% relative density of sand bed *(S = 5d; I_d = 60%; L/d ratio of pile = 30; Pile group = 3 × 3)*

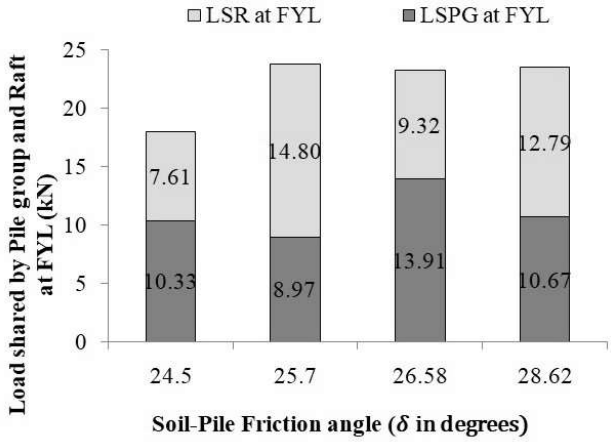

Figure 5-228 Load shared by pile group and raft at *FYL* of piled raft foundation for different soil pile friction angle at 60% relative density of sand bed *(S = 5d; I_d = 60%; L/d ratio of pile = 30; Pile group = 3 × 3)*

Figure 5-229 to Figure 5-232 represent the percentage load shared by pile group (% *LSPG*) and raft (% *LSR*) in a piled raft with different soil pile friction angle Vs. relative settlement at I_d = 60% . It observed that the % *LSPG* was more than 50% at all relative settlements for PRF with δ_0 = 24.5° and δ_2 = 26.58°, at I_d = 60%. The % *LSPG* was more than 50% from s/B_r = 0 to 0.03, and after that, it was less than 50% in PRF with δ_1 = 25.7° at I_d = 60%. The % *LSPG* and the % *LSR* in PRF with δ_3= 26.58° were equal at s/B_r = 0.05 and s/B_r = 0.09, and then it increased up to s/B_r = 0.12, and after that it became more or less constant.

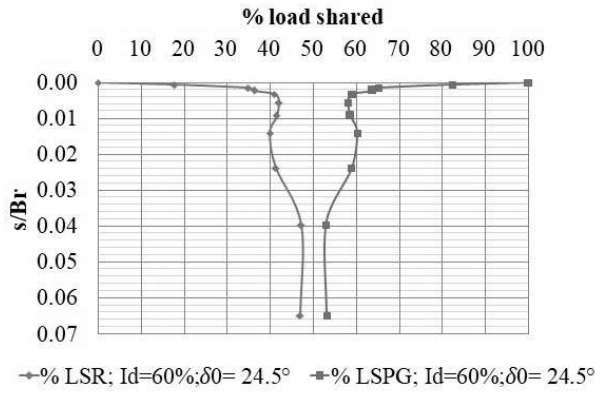

Figure 5-229 : Percentage load shared by pile group (% *LSPG*) and raft (% *LSR*) in piled raft at different relative settlement *(S = 5d; I_d = 60%; d = 9.7 mm; pile group = 3 × 3; L/d ratio of pile = 30; δ_0 = 24.5°)*

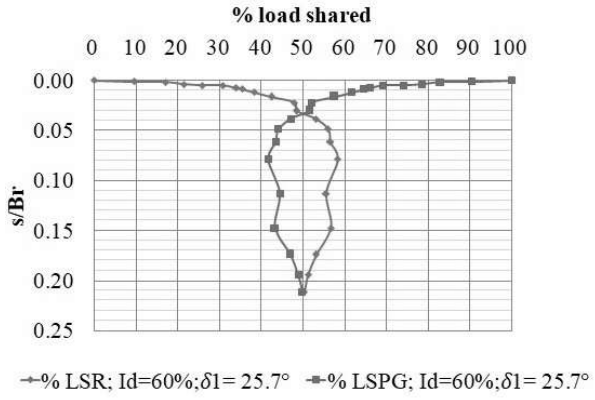

Figure 5-230 : Percentage load shared by pile group (% *LSPG*) and raft (% *LSR*) in piled raft at different relative settlement *(S = 5d; I_d = 60%; d = 9.7 mm; pile group = 3 × 3; L/d ratio of pile = 30; δ_1= 25.7°)*

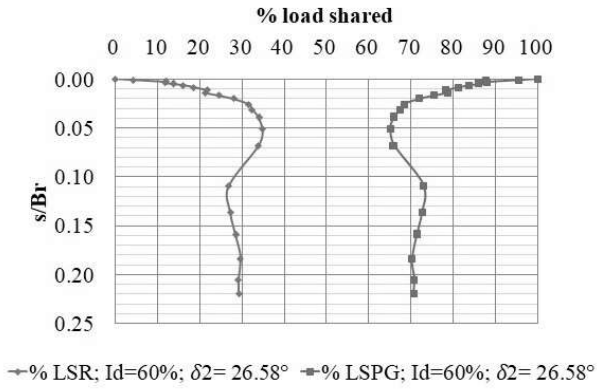

Figure 5-231 : Percentage load shared by pile group (% *LSPG*) and raft (% *LSR*) in piled raft at different relative settlement *(S = 5d; I_d = 60%; d = 9.7 mm; pile group = 3 × 3; L/d ratio of pile = 30; δ_2 = 26.58°)*

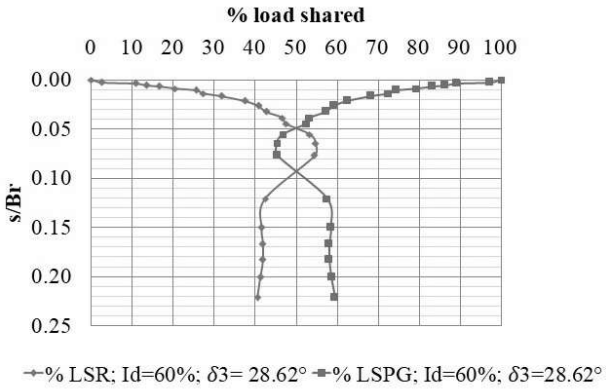

Figure 5-232 : Percentage load shared by pile group (% *LSPG*) and raft (% *LSR*) in piled raft at different relative settlement *(S = 5d; I_d = 60%; d = 9.7 mm; pile group = 3 × 3; L/d ratio of pile = 30; δ_3 = 26.58°)*

Figure 5-233 shows the relationship between the piled raft coefficient (α_p) and the relative settlement characteristics of a piled raft foundation with varying soil pile friction at I_d = 60% . The results indicate that as the relative settlement of the PRF increases, the α_p decreases. The maximum and minimum α_p values were observed at δ_2= 26.58° and δ_1= 25.7°, respectively.

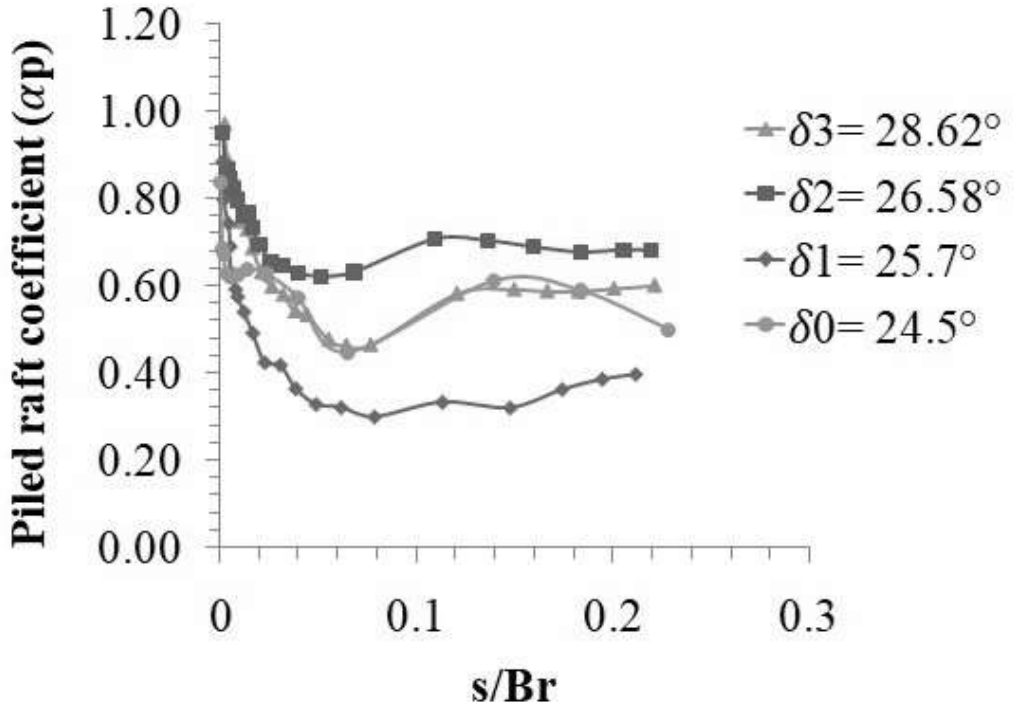

Figure 5-233 : Piled raft coefficient (α_p) vs. relative settlement characteristics of piled raft foundation at different soil pile friction *(S = 5d;I_d = 60%; L/d ratio of pile = 30; Pile group = 3 × 3)*

5.3.3.5.3 Load Settlement Characteristics and Load Sharing Mechanism at 80% Relative Density

Figure 5-234 represents the load settlement characteristics of piled raft foundations with different soil pile friction in sand bed at I_d = 80%. It can observed that the load-carrying capacity of PRF increased as the soil pile friction angle increased (δ_0 to δ_3). Figure 5-235 to Figure 5-238 depicts the load settlement characteristics of piled raft and load shared by pile group and raft with soil

pile friction angle (δ_0 to δ_3) at 80% relative density of sand bed. It can observed that at δ_0 = 26.3°, the *LSPG* was less than the *LSR* at all settlement levels, while at δ_1= 27.41°, δ_2 = 28.22°, and δ_3 = 30.04°, the *LSPG* was more than the *LSR* at all settlement. i.e., the effect of soil pile friction was less significant on load settlement characteristics of PRF but more significant on load sharing characteristics of PRF at I_d = 80%.

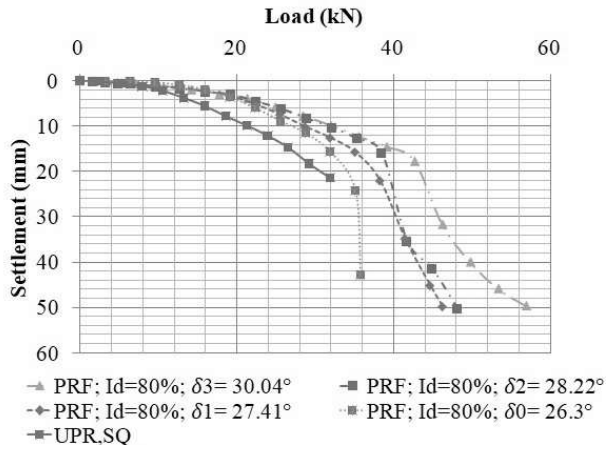

Figure 5-234 : Load settlement characteristics of piled raft foundation with different soil pile friction in sand *(L/d ratio of pile = 30; I_d = 80%; d = 9.7 mm)*

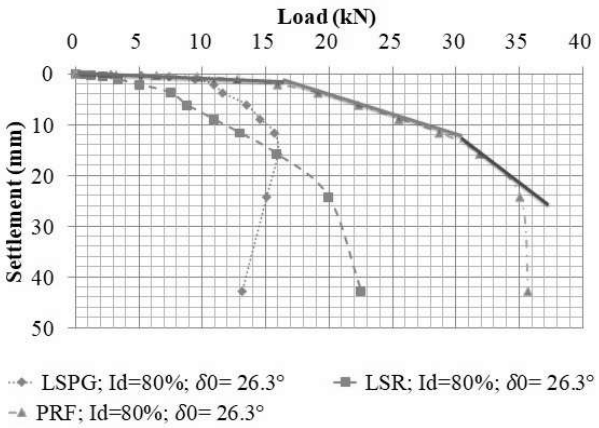

Figure 5-235 : Load settlement characteristics of piled raft and Load shared by pile group and raft with soil pile friction angle δ_0 = 26.3° at 80% relative density of sand bed *(S = 5d; L/d ratio of pile = 30; pile group = 3 × 3)*

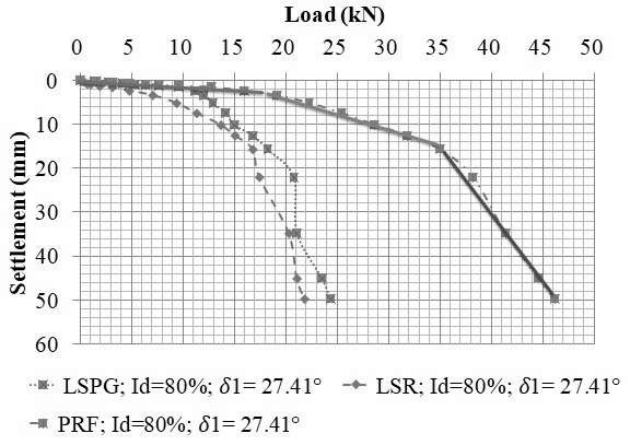

Figure 5-236 : Load settlement characteristics of piled raft and Load shared by pile group and raft with soil pile friction angle δ_1 = 27.41° at 80% relative density of sand bed *(S = 5d; L/d ratio of pile = 30; pile group = 3 × 3)*

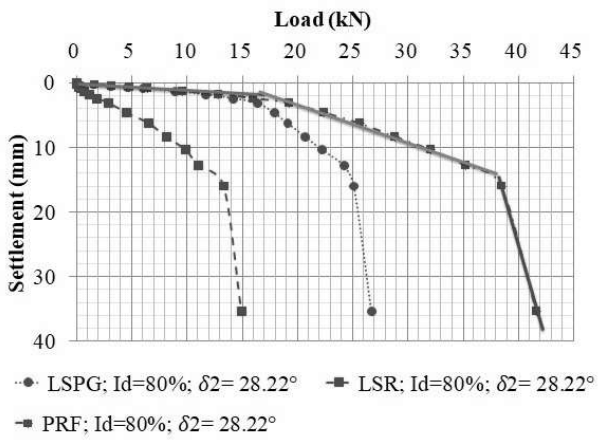

Figure 5-237 : Load settlement characteristics of piled raft and Load shared by pile group and raft with soil pile friction angle δ_2 = 28.22° at 80% relative density of sand bed *(S = 5d; L/d ratio of pile = 30; pile group = 3 × 3)*

Figure 5-239 depicts the Initial yield load (*IYL*) and Final yield load (*FYL*) of the piled raft foundation at different soil pile friction angles at I_d = 80%. It observed that the *IYL* and *FYL* increased with an increase in soil pile friction angle, but the increment was negligible.

The value of *IYL* increased by 1.58 kN, 3.30 kN, and 5.38 kN at δ_1 = 27.41°, δ_2 = 28.22°, and δ_3 = 30.04° respectively, as compared to at δ_0 = 26.3°, i.e., in percentage it was 10%, 21% and 34% respectively. The value of *FYL* increased by 3.17 kN, 6.60 kN, and 10.76 kN at δ_1 = 27.41°, δ_2 = 28.22°, and δ_3 = 30.04° respectively as compared to at δ_0 = 26.3°, i.e., in percentage it was 10%, 21% and 34% respectively.

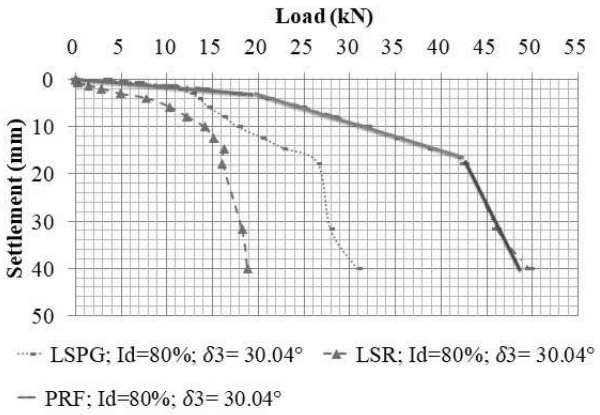

Figure 5-238 : Load settlement characteristics of piled raft and Load shared by pile group and raft with soil pile friction angle δ_3 = 30.04° at 80% relative density of sand bed *(S= 5d; L/d ratio of pile = 30; pile group = 3 × 3)*

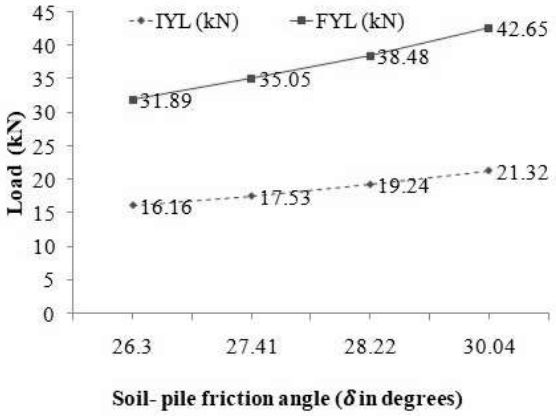

Figure 5-239 : Initial yield load (*IYL*) and Final yield load (*FYL*) of piled raft foundation at different soil pile friction angles *(S = 5d; I_d = 80%; L/d ratio of pile = 30)*

Figure 5-240 to Figure 5-241 represents the load shared by the pile group and raft at *IYL* and *FYL* of piled raft foundation for different soil pile friction angles at 80% relative density of sand bed. It observed that the *LSPG* at *IYL* and *FYL* increased as the soil pile friction angle increased except at *IYL* for δ_3.

The *LSR* value at *IYL* was found to have increased by 0.53 kN at δ_1 = 27.41°, decreased by 2.5 kN at δ_2 = 28.22°, and increased by 2.41 kN at δ_3 = 30.04°, compared to its value at δ_0 = 26.3°. i.e., an increase of 10%, a decrease of 46%, and an increase of 45%, respectively. Similarly, the *LSPG* value at *IYL* increased by 1.06 kN, 5.79 kN, and 2.97 kN at δ_1 = 27.41°, δ_2 = 28.22°, and δ_3 = 30.04° respectively, compared to its value at δ_0 = 26.3°. i.e., an increase of 10%, 55%, and 28%, respectively.

The value of *LSR* at *FYL* increased by 0.9 kN, decreased by 2.56 kN, and increased by 0.2 kN at δ_1 = 27.41°, δ_2 = 28.22°, and δ_3 = 30.04° respectively, as compared to at δ_0 = 26.3°, i.e., in percentage it was increased by 6%, decreased by 16% and increased by 1% respectively. The

value of *LSPG* at *FYL* increased by 2.27 kN, 9.16 kN, and 10.57 kN at $\delta_1 = 27.41°$, $\delta_2 = 28.22°$, and $\delta_3 = 30.04°$ respectively, as compared to at $\delta_0 = 26.3°$, i.e., in percentage it was increased by 14%, 57% and 66% respectively.

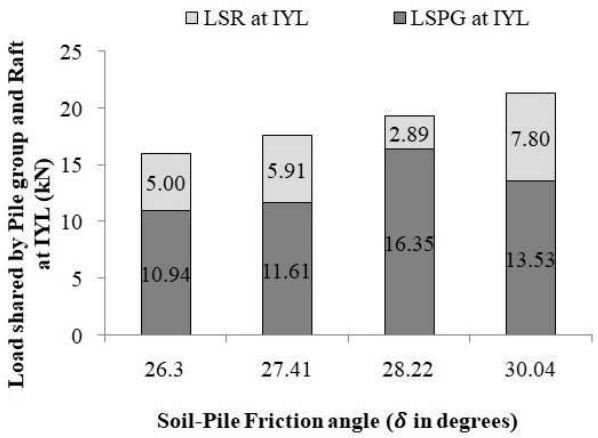

Figure 5-240 : Load shared by pile group and raft at *IYL* of piled raft foundation for different soil pile friction angle at 80% relative density of sand bed *(S = 5d; I_d = 80%; L/d ratio of pile = 30; Pile group = 3 × 3)*

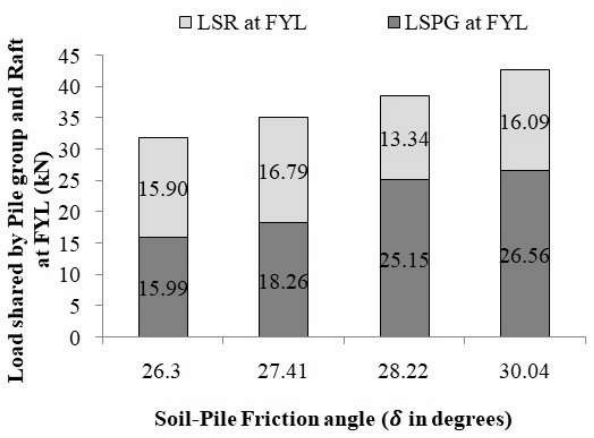

Figure 5-241 : Load shared by pile group and raft at *FYL* of piled raft foundation for different soil pile friction angle at 80% relative density of sand bed *(S = 5d; I_d = 80%; L/d ratio of pile = 30; Pile group = 3 × 3)*

Figure 5-242 to Figure 5-245 represent the percentage load shared by the pile group (% *LSPG*) and raft (% *LSR*) in a piled raft with different soil pile friction angle Vs. relative settlement at I_d = 80%. It can observed that the % *LSPG* and % *LSR* became equal at $s/B_r = 0.07$, and after that, % *LSPG* was decreasing for PRF with $\delta_0 = 26.3°$ at $I_d = 80\%$. The % *LSPG* was more than the % *LSR* in PRF with $\delta_1 = 27.41°$, $\delta_2 = 28.22°$, $\delta_3 = 30.04°$ at $I_d = 80\%$. The % *LSPG* and the % *LSR* in PRF with $\delta_1 = 27.41°$ and $\delta_2 = 28.22°$ were more or less the same, while with $\delta_3 = 30.04°$ the % *LSPG* was decreasing up to $s/B_r = 0.045$ and then increasing up to $s/B_r = 0.08$ and after that, it becomes more or less constant.

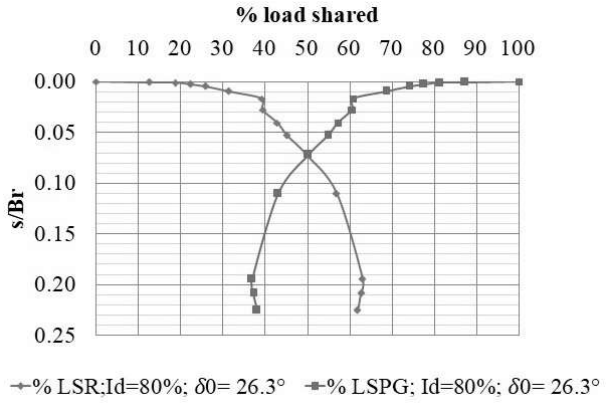

Figure 5-242 : Percentage load shared by pile group (% *LSPG*) and raft (% *LSR*) in piled raft at different relative settlement *(S = 5d; I_d = 80%; d = 9.7 mm; pile group = 3 × 3; L/d ratio of pile = 30; δ_0= 26.3°)*

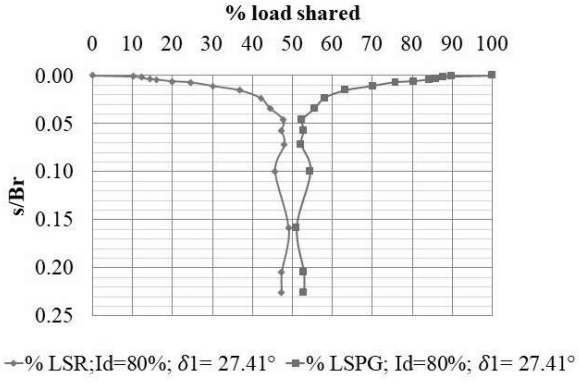

Figure 5-243 : Percentage load shared by pile group (% *LSPG*) and raft (% *LSR*) in piled raft at different relative settlement *(S = 5d; I_d = 80%; d = 9.7 mm; pile group = 3 × 3; L/d ratio of pile = 30; δ_1= 27.41°)*

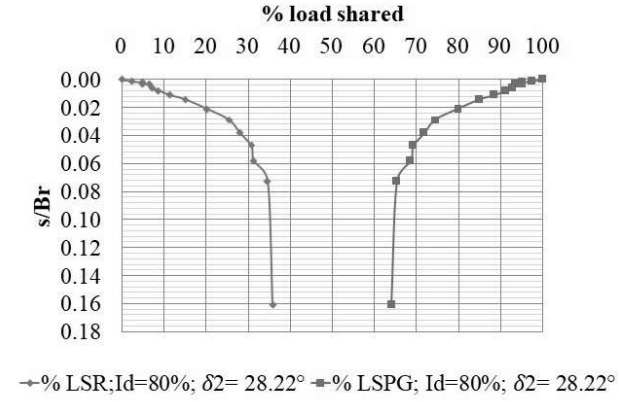

Figure 5-244 : Percentage load shared by pile group (% *LSPG*) and raft (% *LSR*) in piled raft at different relative settlement *(S = 5d; I_d = 80%; d = 9.7 mm; pile group = 3 × 3; L/d ratio of pile = 30; δ_2= 28.22°)*

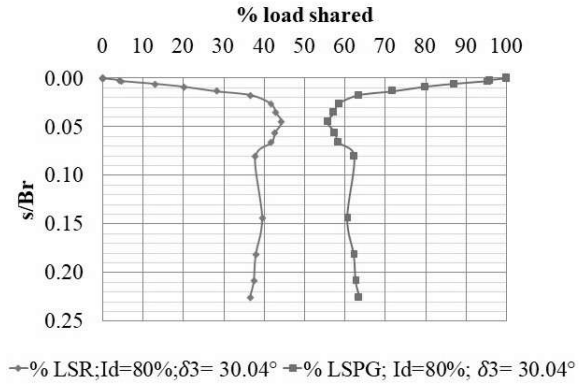

Figure 5-245 : Percentage load shared by pile group (% *LSPG*) and raft (% *LSR*) in piled raft at different relative settlement *(S = 5d; I_d = 80%; d = 9.7 mm; pile group = 3 × 3; L/d ratio of pile = 30; δ_3= 30.04°)*

Figure 5-246 displays the piled raft coefficient (α_p) about the settlement characteristics of piled raft foundations with varying soil pile friction when I_d is at 80%. The results indicate that α_p decreases as the relative settlement of PRF increases. The highest and lowest values of α_p were found at δ_2= 28.22° and δ_0= 26.3°, respectively.

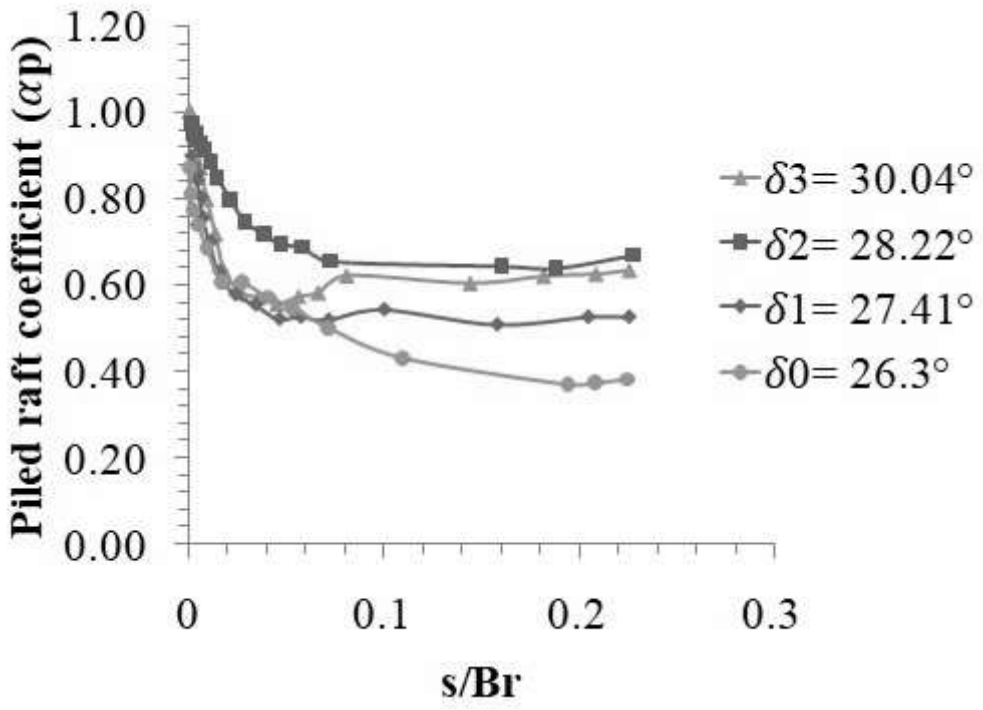

Figure 5-246 : Piled raft coefficient (α_p) vs. relative settlement characteristics of piled raft foundation at different soil pile friction *(S = 5d;I_d = 80%; L/d ratio of pile = 30; Pile group = 3 × 3)*

5.3.3.5.4 Settlement Reduction Ratio (SRR) and Load Improvement Ratio (LIR)

Table 5-56 shows the settlement reduction ratio of PRF *(SRR)* with different soil-pile friction angles at different load levels and 40% relative densities of the sand bed. It can be observed that the range of *SRR*at δ_0 = 22.55° is 41% to 60%, at δ_1 = 24.36° is 31% to 81%, at δ_2 = 25.8° is 22% to 71%, and at δ_3 = 27.1° is 57% to 75%.

Table 5-56 Settlement reduction ratio of PRF with different soil-pile friction angles at different load levels and 40% relative densities of the sand bed

I_d (%)	Load (kN)	Settlement (mm)					Settlement reduction ratio (%)			
		UPR	PRF (δ_0= 22.55°)	PRF (δ_1= 24.36°)	PRF (δ_2= 25.8°)	PRF (δ_3= 27.1°)	PRF (δ_0= 22.55°)	PRF (δ_1= 24.36°)	PRF (δ_2= 25.8°)	PRF (δ_3= 27.1°)
40	2.5	0.90	0.53	0.22	0.70	0.29	41	76	22	68
	5	2.97	1.19	0.56	1.16	0.75	60	81	61	75
	10	10.73	4.29	6.62	3.48	2.88	60	38	68	73
	12.5	25.30	11.09	11.88	7.45	6.68	56	53	71	74
	15	30.36	18.04	20.96	13.60	13.06	41	31	55	57

Table 5-57 shows the settlement reduction ratio of PRF *(SRR)*with different soil-pile friction angles at different load levels and 60% relative densities of the sand bed. It can be observed that the range of *SRR*at δ_0 = 24.5° is 48% to 59%, at δ_1 = 25.7°is 38% to 57%, at δ_2 = 26.58° is 14% to 45%, and at δ_3 = 28.62° is 3% to 34%.

Table 5-58 shows the settlement reduction ratio of PRF *(SRR)*with different soil-pile friction angles at different load levels and 80% relative densities of the sand bed. It can be observed that the range of *SRR* at δ_0 = 26.3° is 55% to 68%, at δ_1= 27.41°is 3% to 48%, at δ_2 = 28.22°° is 6% to 46%, and at δ_3 = 30.04° is 10% to 47%.

Table 5-57 Settlement reduction ratio of PRF with different soil-pile friction angles at different load levels and 60% relative densities of the sand bed

I_d (%)	Load (kN)	Settlement (mm)					Settlement reduction ratio (%)			
		UPR	PRF (δ_0= 24.5°)	PRF (δ_1= 25.7°)	PRF (δ_2= 26.58°)	PRF (δ_3= 28.62°)	PRF (δ_0= 24.5°)	PRF (δ_1= 25.7°)	PRF (δ_2= 26.58°)	PRF (δ_3= 28.62°)
60	2.5	0.62	0.32	0.37	0.53	0.60	48	41	14	3
	5	1.62	0.66	1.01	0.93	1.30	59	38	42	20
	10	4.42	1.85	1.91	2.41	2.91	58	57	45	34
	12.5	6.13	2.79	3.12	3.41	4.17	54	49	44	32
	15	8.54	4.48	5.26	4.71	6.10	48	38	45	29

Table 5-58 Settlement reduction ratio of PRF with different soil-pile friction angles at different load levels and 80% relative densities of the sand bed

I_d (%)	Load (kN)	Settlement (mm)					Settlement reduction ratio (%)			
		UPR	PRF (δ_0= 26.3°)	PRF (δ_1= 27.41°)	PRF (δ_2= 28.22°)	PRF (δ_3= 30.04°)	PRF (δ_0= 26.3°)	PRF (δ_1= 27.41°)	PRF (δ_2= 28.22°)	PRF (δ_3= 30.04°)
80	2.5	0.28	0.10	0.21	0.20	0.19	66	27	29	33
	5	0.65	0.19	0.48	0.47	0.44	70	26	27	33
	10	2.07	0.58	1.38	1.37	1.20	72	33	34	42
	12.5	3.41	0.99	1.56	1.72	1.66	71	54	50	51
	15	4.99	1.76	2.16	2.22	2.20	65	57	56	56

Table 5-59 shows load improvement ratio of PRF *(LIR)*with different soil-pile friction angles at different settlement levels and 40% relative densities of the sand bed. The range of *LIR* observed to be 1.19 to 1.51 at δ_0 = 22.55°, 1.18 to 1.31 at δ_1 = 24.36°, 1.32 to 1.58 at δ_2 = 25.8°, and 1.33 to 1.68 at δ_3 = 27.1°.

Table 5-59 Load improvement ratio of PRF with different soil-pile friction angles at different settlement levels and 40% relative densities of the sand bed

I_d (%)	Settlement (mm)	Load(kN)					Load improvement ratio			
		UPR	PRF (δ_0= 22.55°)	PRF (δ_1= 24.36°)	PRF (δ_2= 25.8°)	PRF (δ_3= 27.1°)	PRF (δ_0= 22.55°)	PRF (δ_1= 24.36°)	PRF (δ_2= 25.8°)	PRF (δ_3= 27.1°)
40	5.5	7.11	10.72	9.31	11.24	11.95	1.51	1.31	1.58	1.68
	11	10.12	12.44	12.24	14.13	14.28	1.23	1.21	1.40	1.41
	16.5	11.76	14.61	13.86	15.86	16.10	1.24	1.18	1.35	1.37
	22	12.25	15.95	15.27	17.23	17.30	1.30	1.25	1.41	1.41
	27.5	13.59	16.23	16.41	17.94	18.03	1.19	1.21	1.32	1.33

Table 5-60 shows load improvement ratio of PRF *(LIR)*with different soil-pile friction angles at different settlement levels and 60% relative densities of the sand bed. The range of *LIR* observed to be 1.08 to 1.38 at δ_0 = 24.5°, 1.09 to 1.30 at δ_1= 25.7°, 1.10 to 1.36 at δ_2 = 26.58°, and 1.16 to 1.25 at δ_3 = 28.62°.

Table 5-61 shows load improvement ratio of PRF *(LIR)* with different soil-pile friction angles at different settlement levels and 80% relative densities of the sand bed. The range of *LIR* observed to be 1.08 to 1.75 at δ_0 = 26.3°, 1.20 to 1.97 at δ_1= 27.41°, 1.24 to 2.01 at δ_2 = 28.22°, and 1.38 to 2.24 at δ_3 = 30.04°.

Table 5-60 Load improvement ratio of PRF with different soil-pile friction angles at different settlement levels and 60% relative densities of the sand bed

I_d (%)	Settlement (mm)	Load(kN)					Load improvement ratio			
		UPR	PRF (δ_0= 24.5°)	PRF (δ_1= 25.7°)	PRF (δ_2= 26.58°)	PRF (δ_3= 28.62°)	PRF (δ_0= 24.5°)	PRF (δ_1= 25.7°)	PRF (δ_2= 26.58°)	PRF (δ_3= 28.62°)
60	5.5	11.69	16.14	15.20	15.88	14.28	1.38	1.30	1.36	1.22
	11	17.06	19.68	19.33	20.29	19.81	1.15	1.13	1.19	1.16
	16.5	20.08	21.61	21.84	22.17	23.26	1.08	1.09	1.10	1.16
	22	20.84	22.50	23.06	23.06	24.25	1.08	1.11	1.11	1.16
	27.5	20.15	23.39	24.13	24.23	25.15	1.16	1.20	1.20	1.25

Table 5-61 Load improvement ratio of PRF with different soil-pile friction angles at different settlement levels and 80% relative densities of the sand bed

I_d (%)	Settlement (mm)	Load(kN)					Load improvement ratio			
		UPR	PRF (δ_0= 26.3°)	PRF (δ_1= 27.41°)	PRF (δ_2= 28.22°)	PRF (δ_3= 30.04°)	PRF (δ_0= 26.3°)	PRF (δ_1= 27.41°)	PRF (δ_2= 28.22°)	PRF (δ_3= 30.04°)
80	5.5	15.78	21.53	22.72	24.13	24.25	1.36	1.44	1.53	1.54
	11	22.62	27.97	29.78	32.92	33.54	1.24	1.32	1.46	1.48
	16.5	27.92	32.16	35.45	38.58	41.22	1.15	1.27	1.38	1.48
	22	31.74	34.24	38.23	39.49	43.73	1.08	1.20	1.24	1.38
	27.5	20.15	35.19	39.61	40.40	45.13	1.75	1.97	2.01	2.24

5.3.3.5.5 Primary Stiffness of PRF $(k_{pr})_p$ and Secondary Stiffness of PRF $(k_{pr})_s$

Table 5-62 represents Primary Stiffness of Piled Raft $(k_{pr})_p$ *i*n kN/m and Secondary Stiffness of Piled Raft $(k_{pr})_s$ in kN/m with different soil-pile friction angles at different relative density of sand bed. It was found that at 40%, 60% and 80% relative density of sand the primary stiffness of piled raft $(k_{pr})_p$ decreased with increase in soil-pile friction angle while the secondary stiffness of piled raft $(k_{pr})_s$ was increased. At 40% relative density, the $(k_{pr})_p$ was decreased by 13%, 14% and 33% at δ_1 = 24.36°, δ_2 = 25.8°, δ_3 = 27.1° as compared to at δ_0 = 24.5° while $(k_{pr})_s$ was increased by 15%, 22% and 21% respectively. At 60% relative density, the $(k_{pr})_p$ was decreased by 11%, 31% and 35% at δ_1 = 25.7°, δ_2 = 26.5°, δ_3 = 28.6° as compared to at δ_0 = 24.5° while $(k_{pr})_s$ was increased by 2%, 4% and 22% respectively. At 80% relative density, the $(k_{pr})_p$ was decreased by 15%, 10% and 26% at δ_1 = 27.41°, δ_2 = 28.22°, δ_3 = 30.04° as compared to at δ_0 = 26.3° while $(k_{pr})_s$ was increased by 2%, 13% and 19% respectively. The primary stiffness of Piled Raft $(k_{pr})_p$ with soil-pile friction angle δ_0, δ_1, δ_2, δ_3 at 60% relative density of sand was increased by 51%, 55%, 21%, 45%, respectively, compared to 40% relative density of sand, while for secondary stiffness of piled raft $(k_{pr})_s$ it was 129%, 104%, 95%, and 129% respectively.

The primary stiffness of Piled Raft $(k_{pr})_p$ with soil-pile friction angle δ_0, δ_1, δ_2, δ_3 at 80% relative density of sand was increased by 36%, 28%, 77%, 55%, respectively, compared to 40% relative density of sand, while for secondary stiffness of piled raft $(k_{pr})_s$ it was 55%, 55%, 69%, and 51% respectively.

Table 5-62 Primary Stiffness of Piled Raft $(k_{pr})_p$ in kN/m and Secondary Stiffness of Piled Raft $(k_{pr})_s$ in kN/m with different soil-pile friction angles

Soil-pile friction angle	**Relative density of sand (%)**	**Primary Stiffness of Piled Raft $(k_{pr})_p$ in kN/m**	**Secondary Stiffness of Piled Raft $(k_{pr})_s$ in kN/m**
δ_0 = 22.55°	40	3865	389
δ_1 = 24.36°		2971	407
δ_2 = 25.8°		2924	432
δ_3 = 27.1°		2291	431
δ_0 = 24.5°	60	5148	812
δ_1 = 25.7°		4595	829
δ_2 = 26.58°		3547	842
δ_3= 28.62°		3321	989
δ_0 = 26.3°	80	6982	1064
δ_1 = 27.41°		6900	1215
δ_2 = 28.22°		6269	1421
δ_3 = 30.04°		5163	1497

5.3.3.6 Shape of Pile

5.3.3.6.1 Load Settlement Characteristics

Figure 5-247 to Figure 5-249 represent the tri-linear behaviour of the load settlement curve of model square piled raft with different shapes of piles at 40%, 60%, and 80% relative density of

sand bed, respectively. From this tri-linear behaviour, the obtained values of *IYL* and *FYL* are shown in Figure 5-250 to Figure 5-252. It observed that *IYL* and *FYL* of PRF with all shapes of piles increased as the relative density of the sand bed increased. The lowest value of *IYL* and *FYL* was in PRF with the HSQ pile and highest with the H pile.

The initial yield load (*IYL*) for the H pile increased by 2.69 kN and 10.27 kN at 60% and 80% relative density, respectively, compared to a sand bed with 40% relative density. This increase represents a percentage increase of 26% and 100%, respectively. Similarly, the final yield load (*FYL*) of the H pile increased by 3.6 kN and 14.07 kN at 60% and 80% relative densities, respectively, compared to the sand bed's 40% relative density. It represents a percentage increase of 21% and 84%, respectively, compared to the 40% relative density of the sand bed.

The *IYL* of the HC pile increased by 1.41 kN and 7.96 kN at 60% and 80% relative density, respectively, compared to the sand bed's 40% relative density, i.e., by 54% and 303%. The *FYL* of the HC pile increased by 4.79 kN and 15.35 kN at 60% and 80% relative density, respectively, compared to the 40% relative density of the sand bed, i.e., in percentages of 31% and 99%.

The *IYL* of the HSQ pile increased by 4.23 kN and 9.21 kN at 60% and 80% relative density, respectively, compared to the sand bed's 40% relative density, i.e., in percentages 70% and 153%. The *FYL* of the H pile increased by 5.62 kN and 13.42 kN at 60% and 80% relative density, respectively, compared to the 40% relative density of the sand bed, i.e., in percentages of 46% and 110%.

At a relative density of 40% of the sand bed, the initial yield load (*IYL*) of PRF with H and HC pile increased by 4.28 kN and 4.28 kN, respectively, compared to the HSQ pile. This increase represents a 71% improvement for both H and HC piles. At a relative density of 60% of the sand bed, the *IYL* of PRF with H and HC pile increased by 2.75 kN and 1.46 kN, respectively, compared to the HSQ pile. This increase represents a 27% improvement for the H pile and a 14% improvement for the HC pile. At a relative density of 80% of the sand bed, the *IYL* of PRF with H and HC pile increased by 5.34 kN and 3.03 kN, respectively, compared to the HSQ pile. This increase represents a 35% improvement for the H pile and a 20% improvement for the HC pile.

At a relative density of 40% of the sand bed, the final yield load (*FYL*) of PRF with H and HC pile increased by 4.58 kN and 3.25 kN, respectively, compared to the HSQ pile. This increase represents a 76% and 54% improvement for H and HC piles. At a relative density of 60% of the sand bed, the *FYL* of PRF with H and HC pile increased by 2.57 kN and 2.42 kN, respectively, compared to the HSQ pile. This increase represents a 25% improvement for the H pile and a 24% improvement for the HC pile. At a relative density of 80% of the sand bed, the *IYL* of PRF with H and HC pile increased by 5.24 kN and 5.18 kN, respectively, compared to the HSQ pile. This increase represents a 34% improvement for both H pile and HC pile.The effect of the shape of piles was found to be significant at 40% relative density of the sand bed compared to 60% and 80% relative density of sand. For PRF, the preferred shape of the pile in descending order can be taken as H pile, HC pile, and HSQ pile.

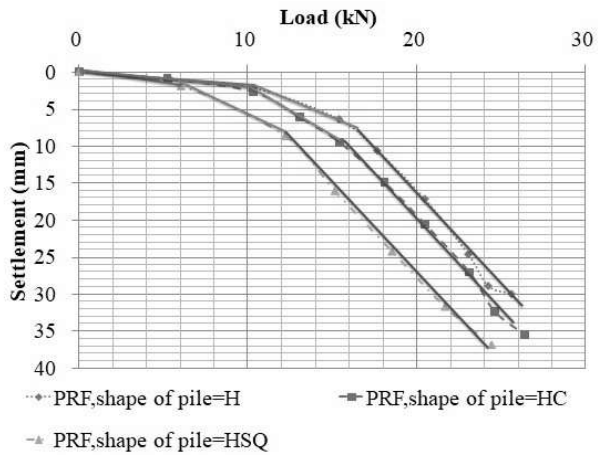

Figure 5-247 : Load settlement characteristics of model square piled raft with different shape of piles at 40% relative density of sand bed *(S = 5d; d = 16 mm; pile group = 3 × 3; L of pile = 300 mm)*

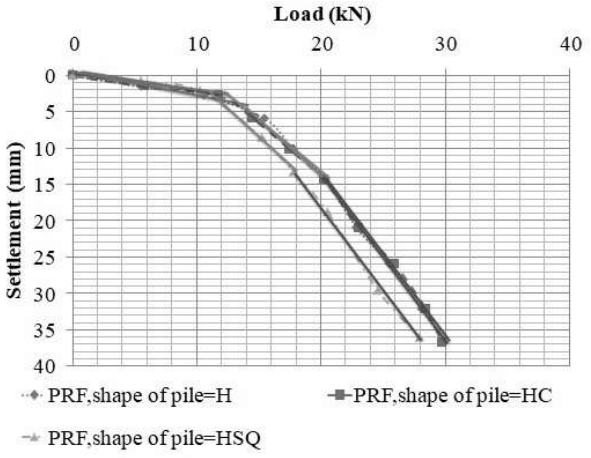

Figure 5-248 : Load settlement characteristics of model square piled raft with different shape of piles at 60% relative density of sand bed *(S = 5d; d = 16 mm; pile group = 3 × 3; L of pile = 300 mm)*

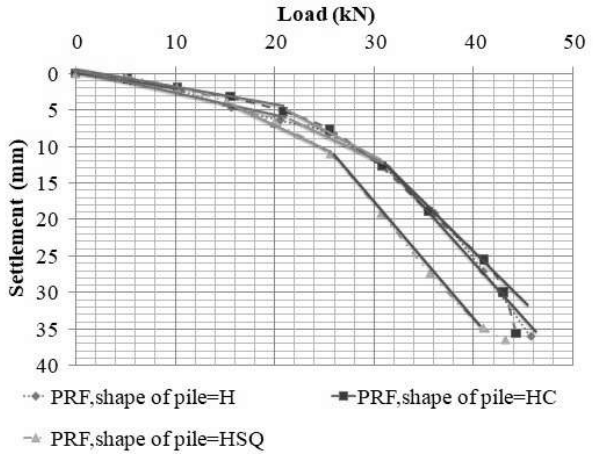

Figure 5-249 : Load settlement characteristics of model square piled raft with different shape of piles at 80% relative density of sand bed *(S = 5d; d = 16 mm; pile group = 3 × 3; L of pile = 300 mm)*

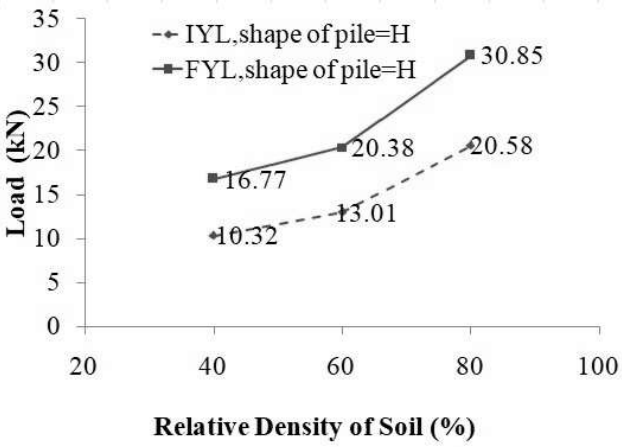

Figure 5-250 : Initial yield load (*IYL*) and Final yield load (*FYL*) of piled raft foundation with H pile at different relative density of sand bed *(S = 5d; d = 16 mm; pile group = 3× 3; L of pile = 300 mm)*

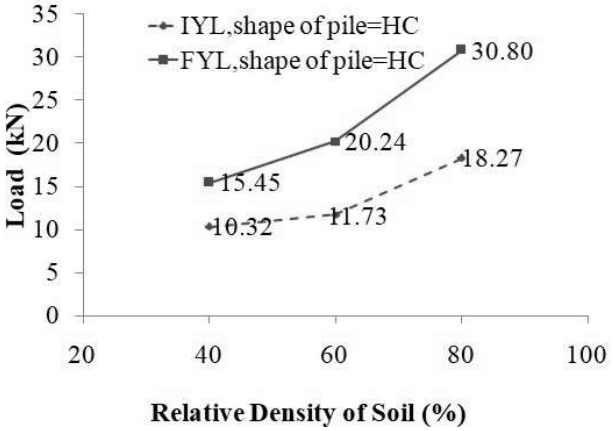

Figure 5-251 : Initial yield load (*IYL*) and Final yield load (*FYL*) of piled raft foundation with HC pile at different relative density of sand bed *(S = 5d; d = 16 mm; pile group = 3 × 3; L of pile = 300 mm)*

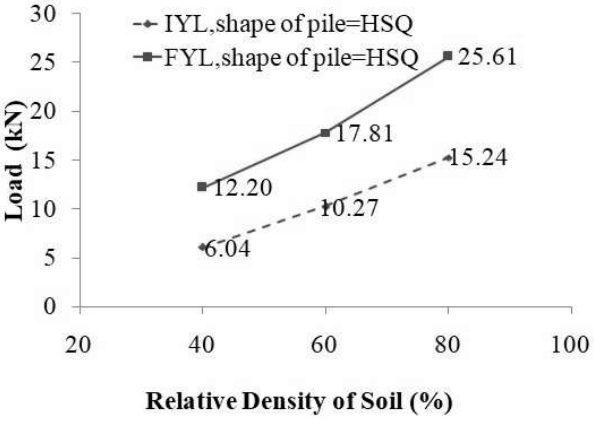

Figure 5-252 : Initial yield load (*IYL*) and Final yield load (*FYL*) of piled raft foundation with HSQ pile at different relative density of sand bed *(S = 5d; d = 16 mm; pile group = 3 × 3; L of pile = 300 mm)*

Figure 5-253 to Figure 5-255 show the load settlement characteristics of different foundation types (pile group, unpiled raft, and piled raft) with various pile shapes at different relative densities of the sand bed. The observed trend is that as the relative density of sand increases, the load-carrying capacity of these foundation types also increases. The load-carrying capacity of only the pile group was less than UPR and PRF with all spacing and at all relative densities.

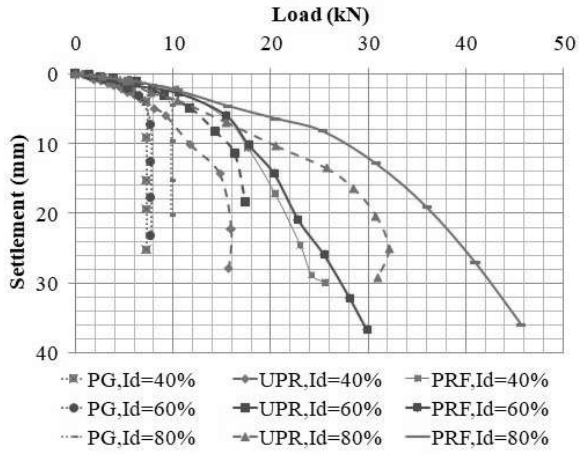

Figure 5-253 : Load settlement characteristics of only pile group, unpiled raft, and piled raft foundation with H pile at different relative density of sand bed *(S = 5d; d = 16 mm; pile group = 3 × 3; L of pile = 300 mm)*

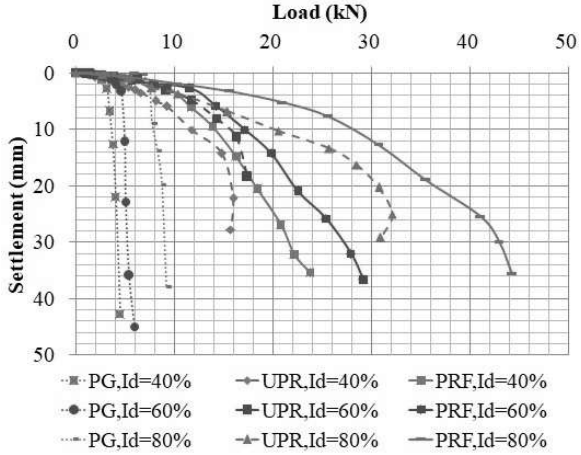

Figure 5-254 : Load settlement characteristics of only pile group, unpiled raft, and piled raft foundation with HC pile at different relative density of sand bed *(S = 5d; d = 16 mm; pile group = 3 × 3; L of pile = 300 mm)*

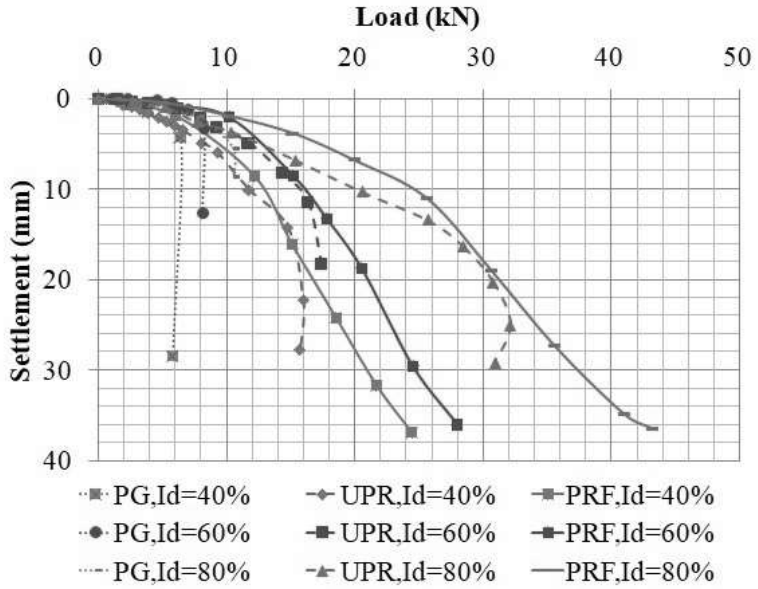

Figure 5-255 : Load settlement characteristics of only pile group, unpiled raft, and piled raft foundation with HSQ pile at different relative density of sand bed *(S = 5d; d = 16 mm; pile group = 3 × 3; L of pile = 300 mm)*

5.3.3.6.2 Settlement Reduction Ratio (SRR) and Load Improvement Ratio (LIR)

Table 5-63 represents the settlement reduction ratio of PRF with different shapes of piles at different load levels and 40% relative densities of the sand bed. The range of *SRR*for PRF with H pile was 48% to 71%, with HC pile 51% to 64%, and HSQ pile 0% to 32%. It also observed that the settlement reduction ratio increased with an increase in load up to a certain point (10 kN for H and HC pile; 5 kN for HSQ pile), and after that, it decreased for some zone of settlement (around 15 mm) and then increased again with settlement (Figure 5-253 to Figure 5-255).

Table 5-63 Settlement reduction ratio of PRF with different shape of piles at different load levels and 40% relative densities of the sand bed

I_d (%)	Load(kN)	Settlement (mm)				Settlement reduction ratio (%)		
		UPR	PRF (H)	PRF (HC)	PRF (HSQ)	PRF (H)	PRF (HC)	PRF (HSQ)
40	2.5	0.94	0.49	0.46	0.79	48	51	16
	5	2.34	0.98	0.92	1.58	58	61	32
	10	7.11	2.08	2.59	6.25	71	64	12
	12.5	11.09	3.97	5.41	9.41	64	51	15
	15	15.52	6.06	8.88	15.3	61	43	1

Table 5-64 represents the settlement reduction ratio of PRF with different shapes of piles at different load levels and 60% relative densities of the sand bed. The range of *SRR* for PRF with H pile was 4% to 39%, with HC pile 1% to 38%, and HSQ pile 11% to 46%. It also observed that the settlement reduction ratio increased with an increase in load up to a certain point (15 kN for H pile; 12.5 kN for HC pile; 10 kN for HSQ pile), and after that, it decreased for some zone of settlement (around 15 mm) and then increased again with settlement (Figure 5-253 to Figure 5-255).

Table 5-64 Settlement reduction ratio of PRF with different shape of piles at different load levels and 60% relative densities of the sand bed

I_d (%)	Load (kN)	Settlement (mm)				Settlement reduction ratio (%)		
		UPR	PRF (H)	PRF (HC)	PRF (HSQ)	PRF (H)	PRF (HC)	PRF (HSQ)
60	2.5	0.37	0.35	0.36	0.33	4	1	11
	5	0.83	0.80	0.82	0.65	4	2	22
	10	3.70	2.56	2.34	1.98	31	37	46
	12.5	5.83	3.97	3.60	4.96	32	38	15
	15	9.26	5.61	6.64	8.21	39	28	11

Table 5-65 represents the settlement reduction ratio of PRF with different shapes of piles at different load levels and 80% relative densities of the sand bed. The range of *SRR*for PRF with H pile was 4% to 39%, with HC pile 4% to 53%, and HSQ pile 21% to 48%. It also observed that the settlement reduction ratio increased with an increase in load up to a certain point (10 kN for the H pile, 15 kN for the HC pile, and 10 kN for the HSQ pile). After that, the *SRR*decreased for some zones of settlement (around 20 mm) and then increased again with settlement (as shown in Figure 5-253 to Figure 5-255).

Table 5-66 represents the load improvement ratio *(LIR)*and efficiency of PRF (β) with different shapes of piles at different settlement levels and 40% relative densities of the sand bed. The range of *LIR* for PRF with H piles, HC piles, and HSQ piles were 1.33 to 1.63, 1.24 to 1.48, and 1.01 to 1.26, respectively. It observed that the *LIR* of PRF with H, HC, and HSQ piles decreased with settlement up to 16.5 mm, and after that, it increased. The efficiency of PRF (β) with H piles, HC piles, and HSQ piles were found in the range of 1 to 1.11, 0.99 to 1.17, and 0.61 to 0.91, respectively. These results indicate that at 40% relative density, PRF with H and HC piles are more efficient than PRF with HSQ piles.

Table 5-65 Settlement reduction ratio of PRF with different shape of piles at different load levels and 80% relative densities of the sand bed

I_d (%)	Load (kN)	Settlement (mm)				Settlement reduction ratio (%)		
		UPR	PRF (H)	PRF (HC)	PRF (HSQ)	PRF (H)	PRF (HC)	PRF (HSQ)
80	2.5	0.31	0.30	0.30	0.25	4	4	21
	5	0.95	0.88	0.68	0.49	8	28	48
	10	3.57	2.17	1.87	1.87	39	48	48
	12.5	5.06	3.19	2.49	2.83	37	51	44
	15	6.62	4.31	3.10	3.81	35	53	42

Table 5-67 represents the load improvement ratio *(LIR)*and efficiency of PRF (β) with different shapes of piles at different settlement levels and 60% relative densities of the sand bed. The range of *LIR* for PRF with H piles, HC piles, and HSQ piles were 1.14 to 1.5, 1.12 to 1.52, and 1.03 to 1.37, respectively. It observed that the *LIR* of PRF with H, HC, and HSQ piles decreased with settlement up to 11 mm, and after that, it increased. The efficiency of PRF (β) with H piles, HC piles, and HSQ piles were found in the range of 0.76 to 1.23, 0.83 to 1.17, and 0.63 to 0.94, respectively. These results indicate that at 60% relative density, PRF with H and HC piles are more efficient than PRF with HSQ piles.

Table 5-68 represents the load improvement ratio *(LIR)*and efficiency of PRF (β) with different shapes of the piles at different settlement levels and 80% relative densities of the sand bed. The range of *LIR* for PRF with H piles, HC piles, and HSQ piles were 1.19 to 1.37, 1.18 to 1.62, and 1.02 to 1.35, respectively. It observed that the *LIR* of PRF with H, HC, and HSQ piles decreased with settlement up to 16.5 mm, and after that, it increased. The efficiency of PRF (β) with H piles, HC piles, and HSQ piles were found in the range of 0.86 to 0.99, 0.95 to 1.03, and 0.55 to 0.75, respectively. These results indicate that at 80% relative density, PRF with H and HC piles are more efficient than PRF with HSQ piles.

Table 5-66 Load improvement ratio and efficiency of PRF with different shape of piles at different settlement levels and 40% relative densities of the sand bed

I_d (%)	Settlement (mm)	Load (kN)				Load improvement ratio			Load (kN)			Efficiency of piled raft (β)		
		UPR	PRF (H)	PRF (HC)	PRF (HSQ)	PRF (H)	PRF (HC)	PRF (HSQ)	PG(H)	PG(HC)	PG(HSQ)	(H)	(HC)	(HSQ)
40	5.5	8.77	14.33	12.58	9.32	1.63	1.43	1.06	5.06	3.37	6.44	1.04	1.04	0.61
	11	12.44	17.82	16.18	13.13	1.43	1.30	1.06	5.01	3.71	6.29	1.02	1.00	0.70
	16.5	15.14	20.20	18.80	15.32	1.33	1.24	1.01	5.08	3.91	6.15	1.00	0.99	0.72
	22	15.95	22.16	21.11	17.60	1.39	1.32	1.10	4.02	4.05	6.00	1.11	1.06	0.80
	27.5	15.73	23.85	23.28	19.90	1.52	1.48	1.26	8.01	4.16	5.86	1.00	1.17	0.92

Table 5-67 Load improvement ratio and efficiency of PRF with different shape of piles at different settlement levels and 60% relative densities of the sand bed

I_d (%)	Settlement (mm)	Load (kN)				Load improvement ratio (%)			Load (kN)			Efficiency of piled raft (β)		
		UPR	PRF (H)	PRF (HC)	PRF (HSQ)	PRF (H)	PRF (HC)	PRF (HSQ)	PG(H)	PG(HC)	PG(HSQ)	(H)	(HC)	(HSQ)
60	5.5	12.24	14.83	14.14	12.91	1.21	1.15	1.05	7.24	4.71	8.25	0.76	0.83	0.63
	11	16.08	18.33	18.04	16.58	1.14	1.12	1.03	2.27	4.97	8.19	1.00	0.86	0.68
	16.5	17.13	21.20	21.15	19.41	1.24	1.23	1.13	1.87	5.05	8.13	1.12	0.95	0.77
	22	17.42	23.41	23.61	21.75	1.34	1.36	1.25	1.66	5.09	8.08	1.23	1.05	0.85
	27.5	17.42	26.18	26.53	23.81	1.50	1.52	1.37	9.19	5.20	8.03	0.98	1.17	0.94

Table 5-68 Load improvement ratio and efficiency of PRF with different shape of piles at different settlement levels and 80% relative densities of the sand bed

I_d (%)	Settlement (mm)	Load (kN)				Load improvement ratio (%)			Load (kN)			Efficiency of piled raft (β)		
		UPR	PRF (H)	PRF (HC)	PRF (HSQ)	PRF (H)	PRF (HC)	PRF (HSQ)	PG(H)	PG(HC)	PG(HSQ)	(H)	(HC)	(HSQ)
80	5.5	13.21	18.10	21.44	17.88	1.37	1.62	1.35	7.82	7.68	10.55	0.86	1.03	0.75
	11	21.73	28.78	28.97	25.59	1.32	1.33	1.18	7.31	8.02	13.37	0.99	0.97	0.73
	16.5	28.55	33.95	33.64	29.08	1.19	1.18	1.02	7.40	8.52	20.06	0.94	0.91	0.60
	22	31.27	37.88	38.08	32.42	1.21	1.22	1.04	10.67	8.83	26.74	0.90	0.95	0.56
	27.5	31.45	41.23	41.92	35.67	1.31	1.33	1.13	13.34	8.98	33.43	0.92	1.04	0.55

5.3.3.6.3 Primary Stiffness of PRF $(k_{pr})_p$ and Secondary Stiffness of PRF $(k_{pr})_s$

Table 5-49 represents the values of the primary stiffness of piled raft $(k_{pr})_p$ in kN/m and the secondary stiffness of piled raft $(k_{pr})_s$ in kN/m with different shapes of piles. It was observed that the values of the secondary stiffness of piled raft $(k_{pr})_s$ were less than the primary stiffness of piled raft $(k_{pr})_p$. The primary stiffness of piled raft $(k_{pr})_p$ with H pile increased by 38% and 49% at 60% and 80% relative density of sand, compared to 40%. The secondary stiffness of piled raft $(k_{pr})_s$ with H pile increased by 23% and 44% at 60% and 80% relative density of sand, compared to I_d = 40%. The primary stiffness of piled raft $(k_{pr})_p$ with HC pile increased by 32% and 50% at 60% and 80% relative density of sand, compared to I_d = 40%. The secondary stiffness of piled raft $(k_{pr})_s$with HC pile increased by 5% and 41% at 60% and 80% relative density of sand, compared to I_d = 40%. The primary stiffness of piled raft $(k_{pr})_p$ with HSQ pile increased by 16% and 145% at 60% and 80% relative density of sand, compared to I_d = 40%. The secondary stiffness of piled raft $(k_{pr})_s$with HSQ pile increased by 36% and 83% at 60% and 80% relative density of sand, compared to I_d = 40%.

The primary and secondary stiffness of piled raft systems with different types of piles (H, HC, and HSQ) under varying soil densities is discussed below.

At 40% relative density of sand, compared to the HSQ pile, the primary stiffness of piled raft $(k_{pr})_p$ increased by 71% with the H pile and 54% with the HC pile. At 60% relative density of sand, the primary stiffness of piled raft $(k_{pr})_p$ increased by 104% with the H pile and 75% with the HC pile, compared to the HSQ pile. At 80% relative density of sand, the primary stiffness of piled raft $(k_{pr})_p$ increased by 24% with the H pile and 7% with the HC pile, compared to the HSQ pile.

For the secondary stiffness of piled raft systems, at 40% relative density of sand, compared to the HSQ pile, the $(k_{pr})_s$ increased by 64% with the H pile and 75% with the HC pile. At 60% relative density of sand, the $(k_{pr})_s$ increased by 48% with the H pile and 35% with the HC pile, compared to the HSQ pile. At 80% relative density of sand, the $(k_{pr})_s$ increased by 17% with the H pile and 3% with the HC pile, compared to the HSQ pile.

Table 5-69 Primary Stiffness of Piled Raft $(k_{pr})_p$ in kN/m and Secondary Stiffness of Piled Raft $(k_{pr})_s$ in kN/m with different shape of piles

Shape of pile	**Relative density of sand**	**Primary Stiffness of Piled Raft $(k_{pr})_p$ in kN/m**	**Secondary Stiffness of Piled Raft $(k_{pr})_s$ in kN/m**
H	40	2195.33	649.99
	60	3023.41	802.45
	80	4491.67	1157.28
HC	40	1968.05	695.99
	60	2594.18	728.66
	80	3900.04	1025.19
HSQ	40	1280.26	396.59
	60	1480.94	540.59
	80	3633.34	991.80

5.3.4 Prototype Piled Raft Foundation-Numerical Study

An extensive study was conducted to investigate the impact of a pile foundation in the field. The study focused on two configurations pattern: square and radial or circular, with the piles having different length-to-diameter (*L/d*) ratios of 10, 20, and 30. The investigation specifically targeted a 60% relative density of sand. The primary objective of the study was to obtain crucial data such as load settlement curves, settlement reduction ratios *(SRR)*, initial yield loads (*IYL*), final yield loads (*FYL*), load sharing between pile/pile group (LSP/*LSPG*) and raft (*LSR*) in PRF, and load distribution among the piles.

5.3.4.1 Load Settlement Characteristic

Load settlement characteristic obtained for all the configuration of pile and for individual square and circular pattern is shown in Figure 5-256, Figure 5-257, and Figure 5-258 respectively.

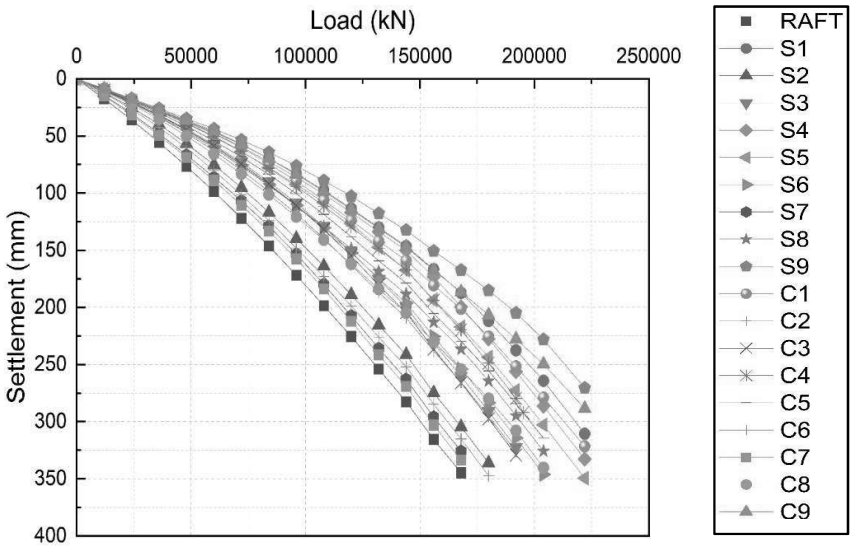

Figure 5-256 Load settlement curve for all configuration pile

From the primary observation of combined load settlement curve for both the square and circular patterns, some conclusions were made regarding the settlement behaviour.

The minimum settlement was observed in the *S9* configuration, followed by *C9*, *S1*, *C1*, *S4*, *S5*, *C4*, *C5*, *C8* and *S8*. On the other hand, the maximum settlement was observed in the *C7*, *S7*, *C2*, *S2*, *C3*, and *S3* configurations, listed in descending order.

Upon analyzing the individual load settlement curves of the square and circular patterns, several conclusions can be drawn. The maximum settlement at a particular load was observed in the *S7* configuration, followed by *S2*, *S3*, *S6*, *S8*, *S5*, *S4*, and *S1*. The minimum settlement was found in the *S9* configuration. However, an interesting observation was made in the *S8* configuration, where its load settlement curve started crossing with those of *S3* and *S6* at 96000 kN and completely crossed both line at a load of 120000 kN leading reduced settlement at higher load in comparison to *S3* and *S6* configuration. This crossing phenomenon was unique compared to the other configurations, which maintained a consistent trend from the initial to the final load.

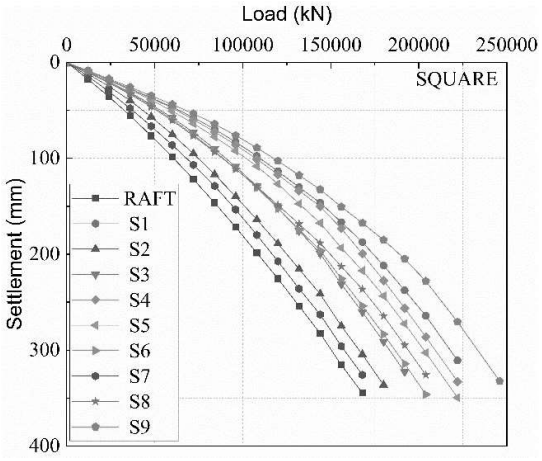

Figure 5-257 : Load settlement curve for all configurations of pile in square pattern

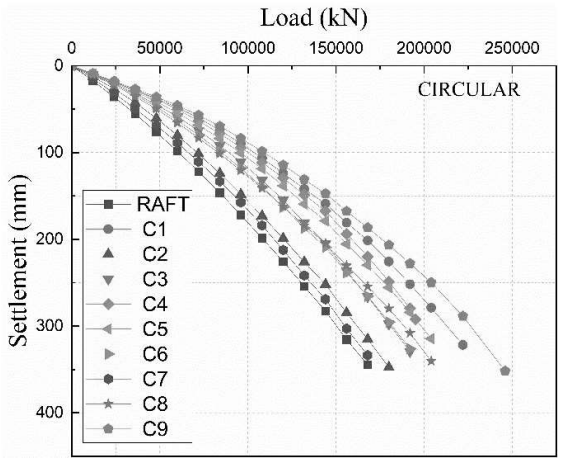

Figure 5-258 : Load settlement curve for all configurations of pile in circular pattern

Similarly, when examining the load settlement curve of the circular pattern, it displayed a similar trend to the square pattern. The maximum settlement was observed in the *C7* configuration, followed by *C2*, *C3*, *C6*, *C8*, *C5*, *C4*, and *C1*. The configuration *C9* exhibited the minimum settlement. Additionally, a crossing point was observed between the load

settlement curves of *C8* with *C3* and *C6* which started at a load of 120000 kN and completely surpassed *C3* and *C6*, resulting in lower settlement values at a load of about 140000 kN.

5.3.4.2 IYL and FYL

By analyzing the Tri-linear pattern in the load settlement curve for various configurations (Figure 5-259 to Figure 5-264), the Initial Yield Load (*IYL*) and Final Yield Load (*FYL*) were determined.

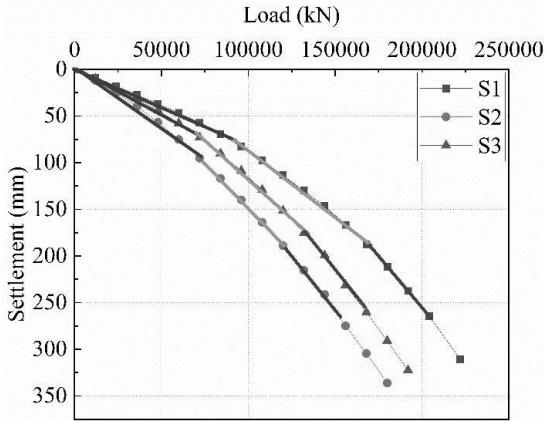

Figure 5-259 : Tri-linear load settlement behaviour of PRF for *S1*, *S2* and *S3*

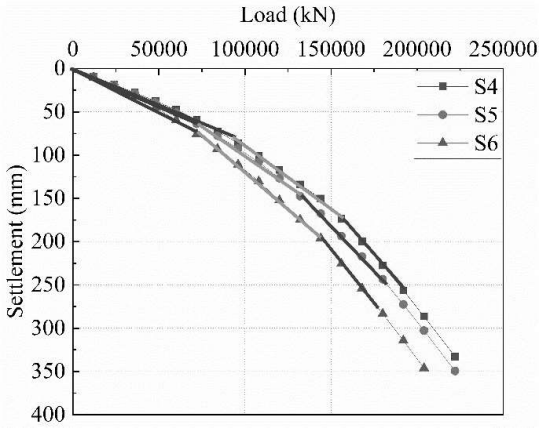

Figure 5-260 : Tri-linear load settlement behaviour of PRF for *S3*, *S4* and *S5*

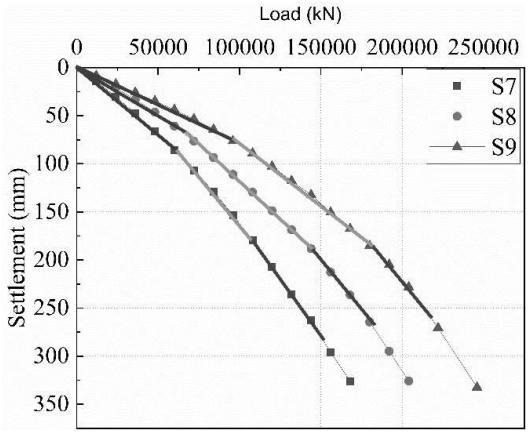

Figure 5-261 : Tri-linear load settlement behaviour of PRF for *S7*, *S8* and *S9*

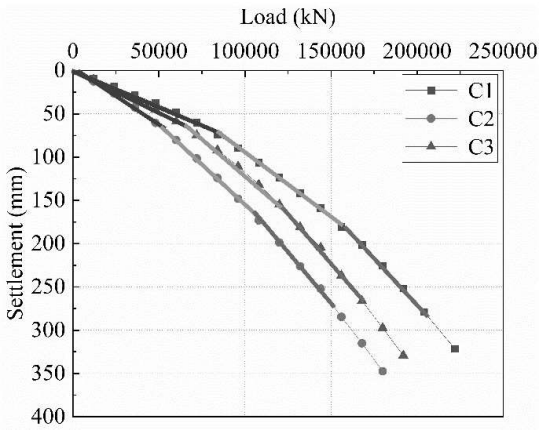

Figure 5-262 : Tri-linear load settlement behaviour of PRF for *C1*, *C2* and *C3*

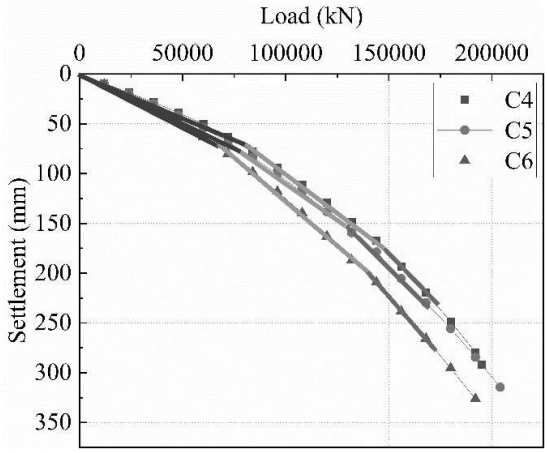

Figure 5-263 : Tri-linear load settlement behaviour of PRF for *C4*, *C5* and *C6*

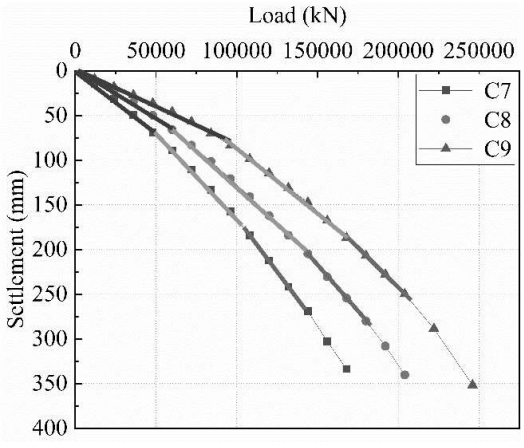

Figure 5-264 : Tri-linear load settlement behaviour of PRF for *C7*, *C8* and *C9*

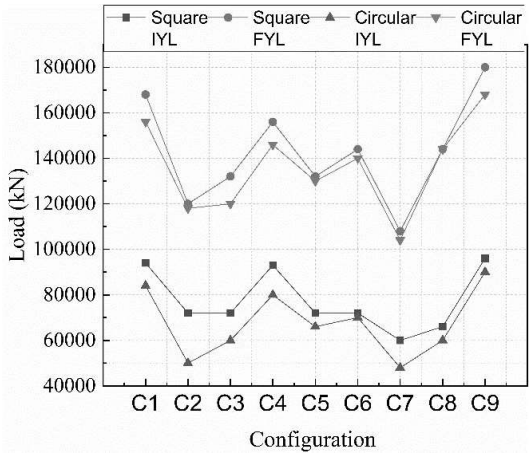

Figure 5-265 : *IYL* and *FYL* for square and circular pattern of piles in Piled-Raft Foundation

The obtained results for different configurations are as follows:

The *IYL* and *FYL* for the configurations obtained were for *S1*, 94000 kN and 168000 kN, *S2*: 72000 kN and 120000 kN, *S3*: 72000 kN and 130000 kN, *S4*: 93000 kN and 156000 kN, *S5*: 72000 kN and 132000 kN, *S6*:72000 kN and 144000 kN, *S7*: 60000 kN and 108000 kN, *S8*: 660000 kN and 144000 kN, *S9*: 96000 kN and 18000 kN respectively. In prototype study the configurations in square pattern *S1*, *S2*, *S3*, *S4*, *S5*, *S6*, *S7*, *S8*, and *S9* represents the configurations in experimental model study *CF-1*, *CF-2*, *CF-3*, *CF-4*, *CF-5*, *CF-6*, *CF-7*, *CF-8*, and *CF-9* respectively. The changes in *IYL* and *FYL* with respect to configurations

were found similar in prototype and experimental study except for *CF-6* (Figure 5-183 and Figure 5-265).

In case of the circular pattern also the *IYL* and *FYL* are as follows: *C1*: 84000 kN and 156000 kN, *C2*: 50000 kN and 102000 kN, *C3*: 66000 kN and 120000 kN, *C4*: 80000 kN and 146000 kN, *C5*: 66000 kN and 130000 kN, *C6*: 70000 kN and 140000 kN, *C7*: 48000 kN and 104000 kN, *C8*: 60000 kN and 144000 kN, *C9*: 90000 kN and 168000 kN respectively.

The *IYL* in decreasing order according to the configuration was *CF-9*, *CF-1*, *CF-8*, *CF-4*, *CF-5*, *CF-6*, *CF-3*, *CF-2*, and *CF-7*.

5.3.4.3 Settlement Reduction Ratio (SRR) and Load Improvement Ratio (LIR)

Based on the settlement reduction ratio versus load figure, it was observed that the *S9* configuration had the maximum reduction, followed by *S1*, *C9*, and *C1*. Additionally, at the *IYL*, the settlement reduction ratio of *S4* was lower than *S1* and *C9*, but at the *FYL*, it surpassed them. The configuration with the least settlement reduction was *C7*, followed by *S7*, *C2*, and *S2*.

S5 and *C4* showed a similar trend in settlement reduction, but the *IYL* and *FYL* values for *C4* were higher than *S5*.

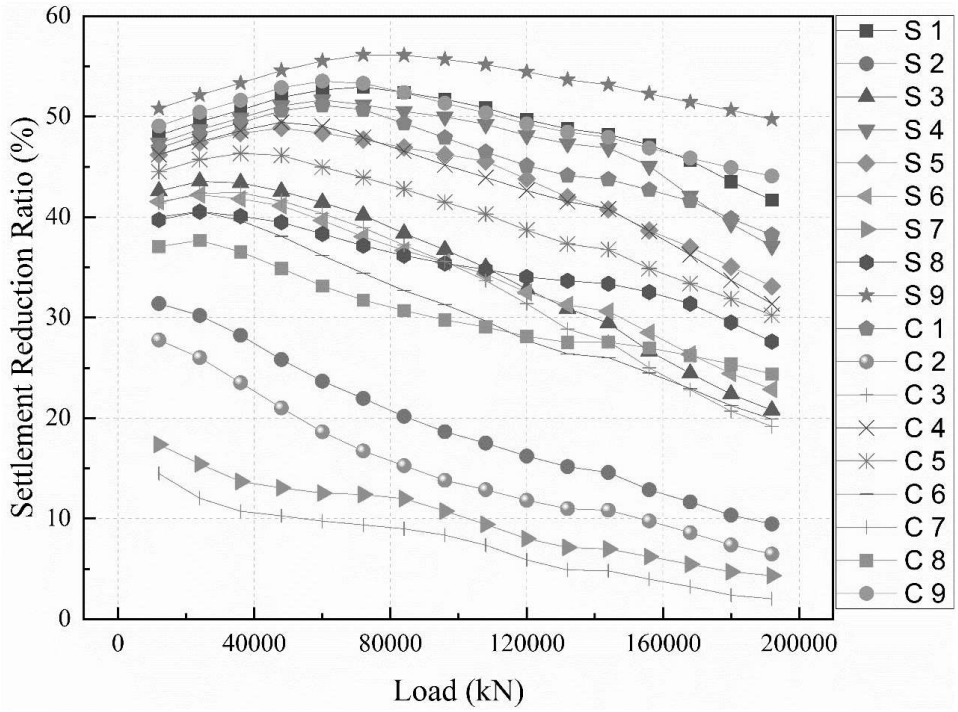

Figure 5-266 : Settlement reduction ratio for all configuration of pile in a Piled-Raft Foundation

Another observation was that the settlement reduction ratio of *S6* and *C3* was greater than *C8* at the *IYL*, but at the *FYL*, *C8* had more settlement reduction compared to *S6* and *C3*. A notable difference was observed in the behaviour of the *C3* and *S3* configurations, which was opposite to the trend observed in other cases. The *C3* configuration had much greater settlement reduction than the *S3* configuration. Additionally, in the *S3* configuration, there was a lower settlement reduction value at the initial yield load compared to *C8* and *C6*, but at the final yield load, *S3* had a higher value compared to *C8* and *C6*.

5.3.4.4 Load Sharing Mechanism

The study also aimed to investigate the load sharing between the piles and the raft at both the initial yield load and final yield load for all pile configurations. It was generally observed that at the initial yield load, the piles carried a greater portion of the load compared to the raft. However, at the final yield load, there was a reduction in the load-carrying capacity of the piles. The pattern of load sharing between pile and raft at *IYL* and *FYL* with different

configurations was observed similarly in the case of the prototype study and experimental study except in *CF-1* or *S1* (Figure 5-194 and Figure 5-267, Figure 5-195 and Figure 5-268).

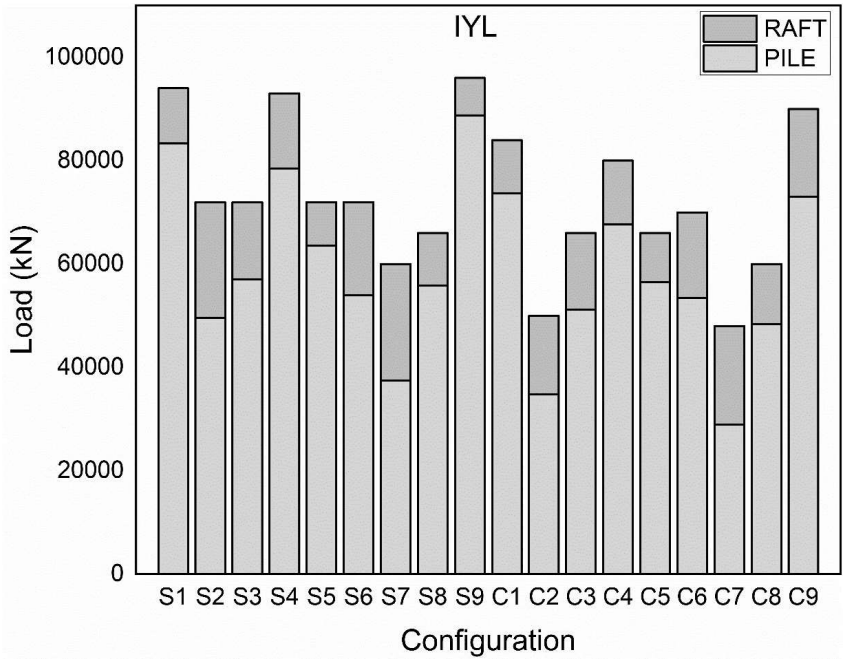

Figure 5-267 : Load Sharing between Pile and Raft at *IYL*

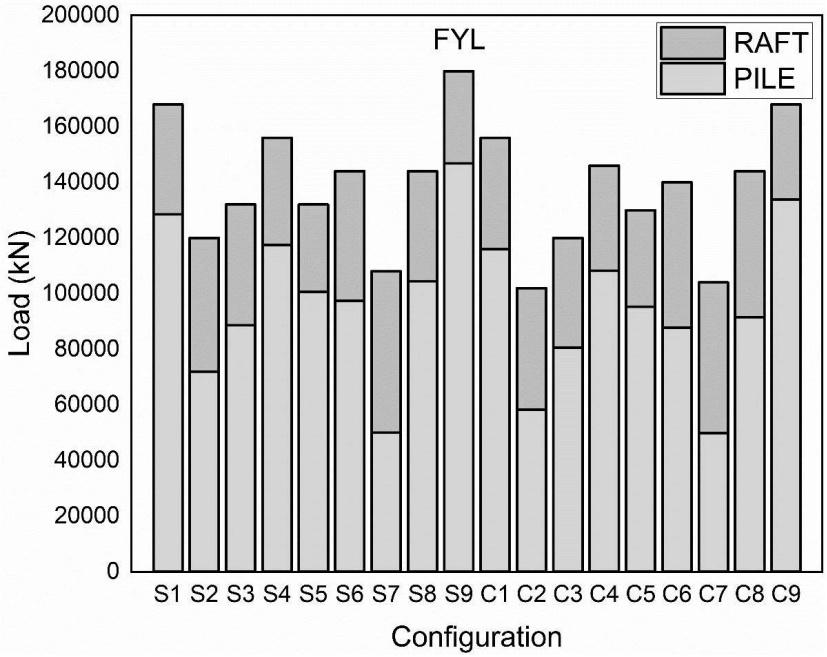

Figure 5-268 : Load Sharing between Pile and Raft at *FYL*

Furthermore, it was observed that the maximum load was shared by the piles in the *S9* configuration, followed by *C9*, *S1*, and *C1*. The load shared by the piles ranged from 85% to 93% at the initial yield load and from 75% to 82% at the final yield load. In contrast, for the *C7* configuration, the load shared by the piles was around 60% at the initial yield load and lower than 50% at the final yield load. Similar trends were observed in the *S7* configuration, where the values were 63% and 47% respectively. Based on these observations, it can be concluded that PRF with shorter piles, the load taken by pile less and raft also has a significant role in load sharing, while longer piles carry a greater share of the load compared to the raft.

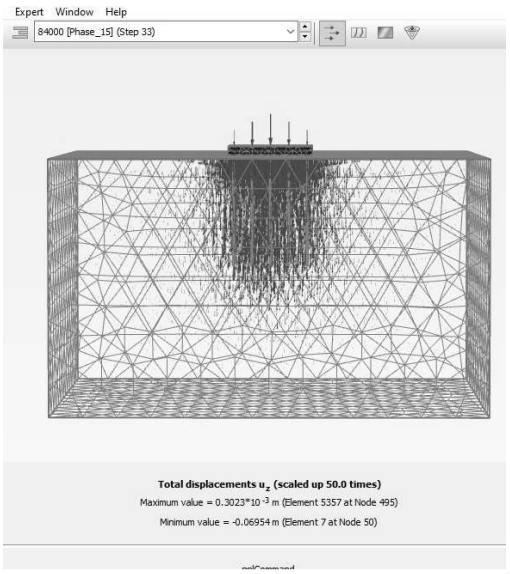

Figure 5-269 Stressed Zone at Lower Load *(P=84000 kN in S8 Configuration)*

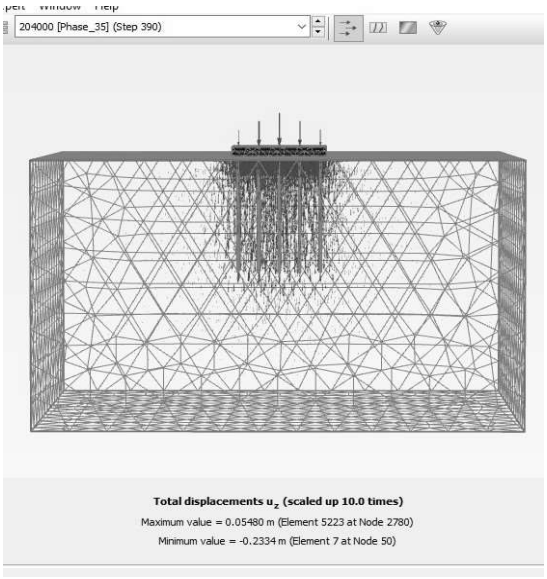

Figure 5-270 Stressed Zone at Higher Load *(P=204000 kN in S8 Configuration)*

The Figure 5-269 and Figure 5-270 shows that at lower loads the plastic points can be observed uniform throughout the structure of PRF whereas as the load increase the concentration of plastic points are found nearer to raft indicating the load sharing is increased by raft than that of pile.

From the analysis of the Figure 5-269 and Figure 5-270, it can be observed that there is a decrease in the load sharing of the pile as the settlement increases, regardless of the configuration. Additionally, another observation is the relationship between settlement and

the width of the raft, expressed as the s/B_r ratio called relative settlement of PRF. At the initial yield load, the s/B_r ratio ranges between 0.004 and 0.007, while at the final yield load, it lies between 0.012 and 0.016 for all configurations.

Table 5-70 Values at Initial Yield Load at square pattern

Configuration	***IYL* (kN)**	**PRF Settlement (mm)**	**RAFT Settlement (mm)**	***SRR***	***% LSPG***	***% LSR***	***s/B_r***
S1	94000	80.77	167.63	51.81	88.65	11.34	0.0059
S2	72000	95.16	121.93	21.95	68.87	31.12	0.0069
S3	72000	90.20	121.93	26.02	79.22	20.77	0.0066
S4	93000	82.61	165.50	50.08	84.40	15.59	0.0060
S5	72000	63.78	121.93	47.69	88.28	11.71	0.0046
S6	72000	75.53	121.93	38.05	74.90	25.09	0.0055
S7	60000	86.18	98.536	12.53	62.37	37.63	0.0063
S8	66000	68.70	110.23	37.67	84.55	15.44	0.0050
S9	96000	76.16	171.88	55.68	92.48	7.510	0.0055

Table 5-71 Values at Final Yield Load at square pattern

Configuration	***FYL* (kN)**	**PRF Settlement (mm)**	**RAFT Settlement (mm)**	***SRR***	***% LSPG***	***% LSR***	***s/B_r***
S 1	168000	187.38	344.72	45.64	76.47	23.52	0.013
S2	120000	188.94	225.49	16.21	59.98	40.01	0.013
S 3	132000	175.54	254.06	30.90	67.13	32.86	0.012
S 4	156000	147.44	315.49	53.26	75.31	24.68	0.010
S 5	132000	147.44	254.06	41.96	76.24	23.75	0.010
S 6	144000	196.05	282.65	30.63	67.64	32.35	0.014
S 7	108000	179.90	198.61	9.421	46.27	53.72	0.013
S 8	144000	188.37	282.65	33.35	72.56	27.43	0.013
S 9	180000	185.17	375.07	50.62	81.58	18.41	0.013

Table 5-72 Values at Initial Yield Load at circular pattern

Configuration	*IYL* (kN)	PRF Settlement (mm)	RAFT Settlement (mm)	*SRR*	*% LSPG*	*% LSR*	s/B_r
C1	84000	74.17	146.35	49.31	87.71	12.28	0.0054
C2	50000	63.74	80.20	20.52	69.53	30.46	0.0046
C3	66000	66.62	110.23	39.56	77.55	22.44	0.0048
C4	80000	73.31	138.21	46.95	84.52	15.47	0.0053
C5	66000	61.29	110.23	44.39	85.57	14.42	0.0045
C6	70000	77.12	118.03	34.65	76.33	23.66	0.0056
C7	48000	68.68	76.543	10.26	60.27	39.72	0.0050
C8	60000	65.88	98.53	33.14	80.65	19.34	0.0048
C9	90000	76.68	159.11	51.80	81.17	18.82	0.0056

Table 5-73 Values at Final Yield Load at circular pattern

Configuration	*FYL* (kN)	PRF Settlement (mm)	RAFT Settlement (mm)	*SRR*	*% LSPG*	*% LSR*	s/B_r
C1	156000	180.76	315.49	42.70	74.41	25.58	0.013
C2	102000	160.60	185.25	13.30	57.22	42.77	0.012
C3	120000	154.76	225.49	31.36	67.15	32.84	0.011
C4	146000	171.70	288.12	40.40	74.12	25.87	0.013
C5	130000	155.74	249.30	37.52	73.30	26.69	0.011
C6	140000	201.76	273.12	26.12	62.66	37.33	0.015
C7	104000	175.18	189.70	7.653	47.91	52.08	0.013
C8	144000	204.78	282.65	27.54	63.59	36.40	0.015
C9	168000	186.64	344.72	45.85	79.62	20.37	0.014

5.3.4.4.1 Load Distribution between Piles in Square pattern

A detailed study was conducted using Plaxis 3D to analyze the load distribution among individual piles. The axial forces acting on each pile were carefully examined. Taking into account the symmetry of the structure and the arrangement of the piles, by finding the axial forces on the nine piles, the load distribution within each pile was calculated with respect to the total load shared by all the piles at the initial and final yield loads. Figure 5-271 to Figure 5-288 illustrates the comparison of the load carried by each pile at the initial and final yield

loads for different pile configurations in square pattern whereas Figure 5-289 to Figure 5-306 shows the same for circular pattern.

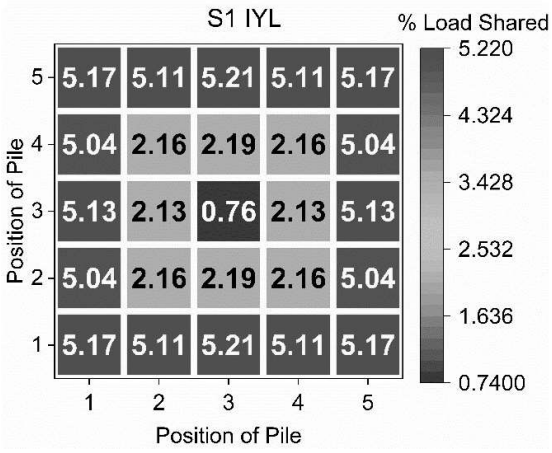

Figure 5-271 : Load Distribution between piles at *IYL* in *S1* configuration

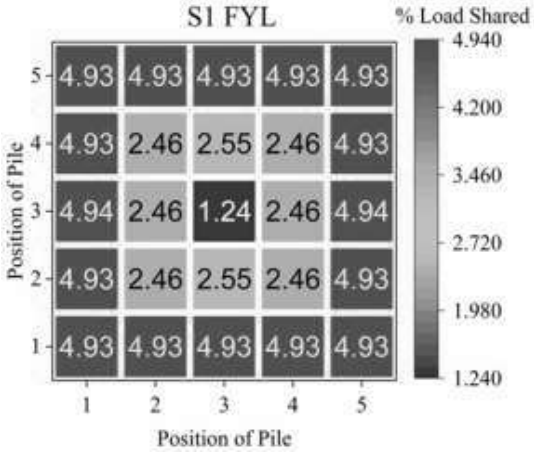

Figure 5-272 : Load Distribution between piles at *FYL* in *S1* configuration

In the case of *S1* configuration, it was observed that the outer longer piles carried a greater proportion of the total load shared by piles compared to the center shorter pile. The outer piles accounted for approximately 5.17% of the total load shared by all the piles, while the center pile carried less than 1% of the load. Additionally, the piles with a length-to-diameter (*L/d*) ratio of 20 contributed around 2.1% to the total load shared by the piles. At the final yield load, changes in load distribution were observed. The load shared by the outer peripheral pile decreased slightly from 5.1%to 4.94%, while the load carried by the center pile increased from 0.76% to 1.24%. Furthermore, the intermediate piles with an *L/d* ratio of 20 experienced an increase in load sharing from 2.16% to 2.46%. These observations indicate variations in load distribution among the different piles within the *S1* configuration at both the *IYL* and *FYL*.

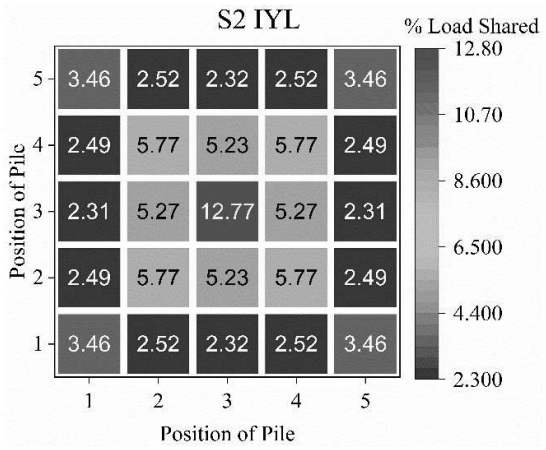

Figure 5-273 : Load Distribution between piles at *IYL* in *S2* configuration

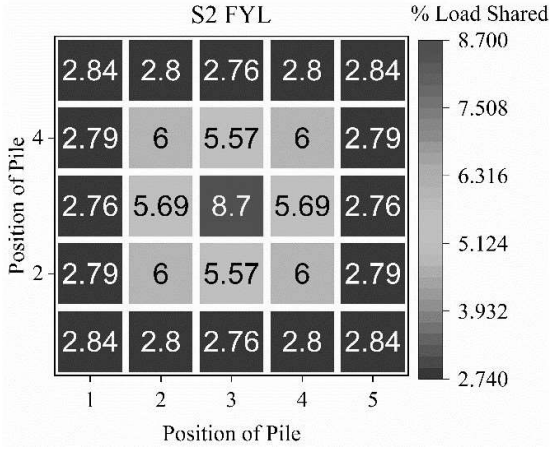

Figure 5-274 : Load Distribution between piles at *FYL* in *S2* configuration

In the *S2* configuration, it was observed that the central longer pile carried a significant portion of the load compared to the shorter piles with an *L/d* ratio of 10 located at the outer periphery of the piled raft foundation. The load shared by the shorter piles ranged from approximately 2.3% to 3.46% at the *IYL*. At the *FYL*, changes in load distribution were observed. The load carried by the outer peripheral piles decreased from 3.46% to 2.84%. Similarly, the load shared by the central longer pile decreased from 12.77% to 8.7%. In contrast, the medium pile with an *L/d* ratio of 20 experienced an increase in load sharing, ranging from 5.77% to approximately 6%. It was also noted that in the *S2* configuration, the corner piles located at the outer periphery carried about 1% more load compared to the edge piles. However, at *FYL*, all the piles within outer periphery of the configuration shared a relatively similar load.

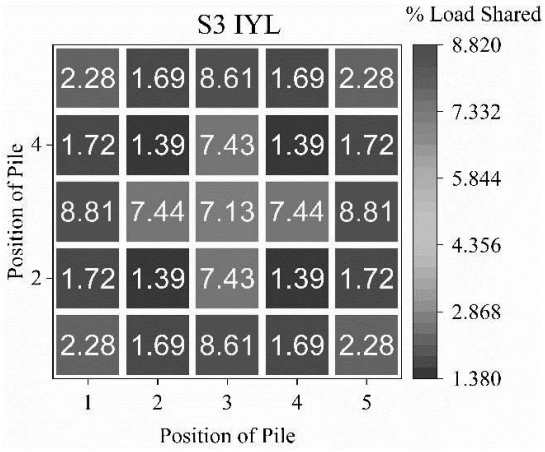

Figure 5-275 : Load Distribution between piles at *IYL* in *S3* configuration

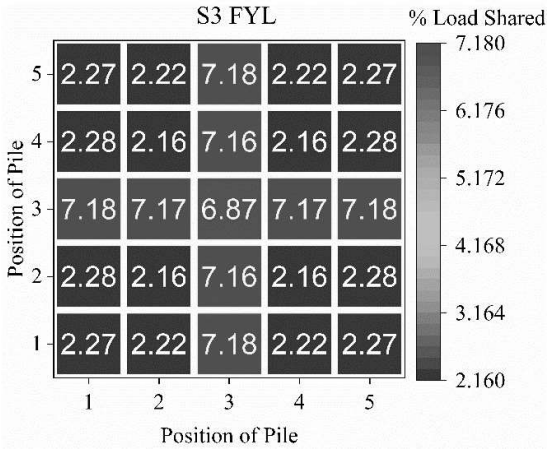

Figure 5-276 : Load Distribution between piles at *FYL* in *S3* configuration

In the *S3* configuration, it was observed that the longer piles with an *L/d* ratio of 30 carried the majority of the load, accounting for approximately 8.61% to 7.13% of the total load shared by the piles, both at the initial yield load (*IYL*) and the final yield load (*FYL*). On the other hand, the shorter piles contributed only around 2% of the total load at *IYL*. This trend remained consistent at the *FYL* as well. The only difference was a slight decrease in the load carried by the central shorter pile, resulting in a slightly lower value.

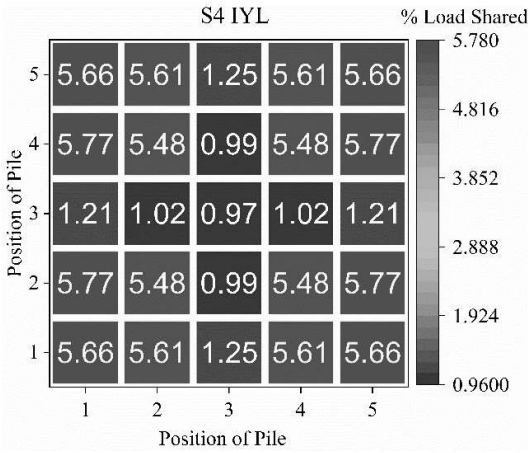

Figure 5-277 : Load Distribution between piles at *IYL* in *S4* configuration

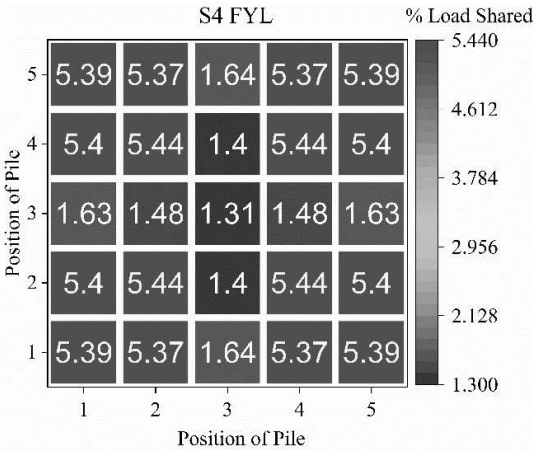

Figure 5-278 : Load Distribution between piles at *FYL* in *S4* configuration

In the *S4* configuration, it was observed that the longer piles carried the majority of the load, while the shorter piles contributed only around 1% of the total load at both the initial and

final yield loads. However, a slight difference was noticed at the final yield load, where the central shorter pile took a slightly higher load of 1.31%, compared to at the initial yield load of 0.97%.

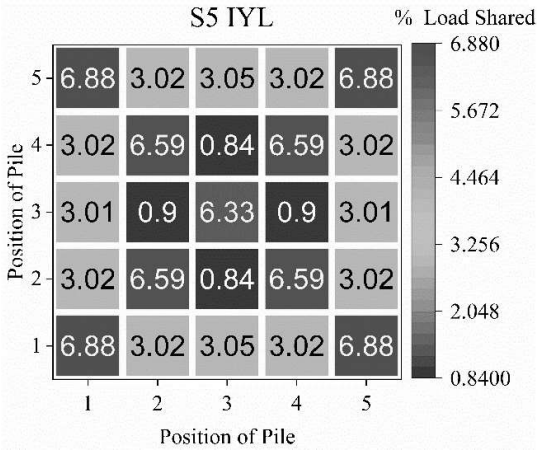

Figure 5-279 : Load Distribution between piles at *IYL* in *S5* configuration

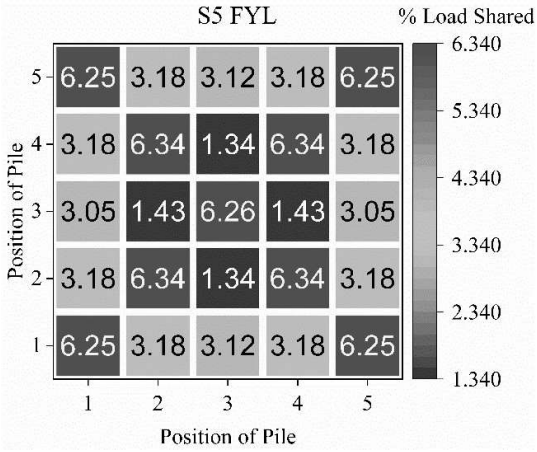

Figure 5-280 : Load Distribution between piles at *FYL* in *S5* configuration

In the *S5* configuration, it was observed that the longer piles, arranged diagonally, carried approximately 6-7% of the load both at the *IYL* and *FYL*. The piles with an *L/d* ratio of 20 accounted for around 3% of the total load. Each shorter piles, with an *L/d* ratio of 10, contributed approximately 1% of the total load.

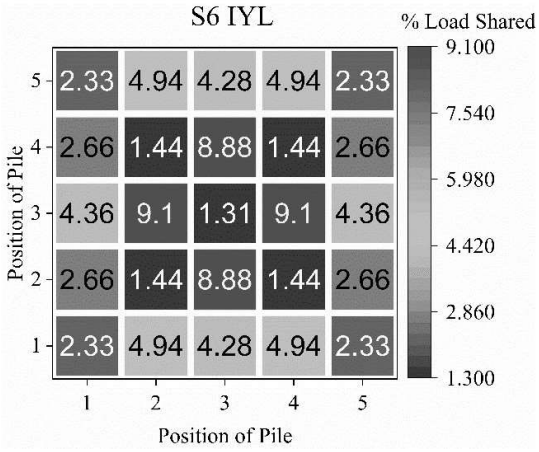

Figure 5-281 : Load Distribution between piles at *IYL* in *S6* configuration

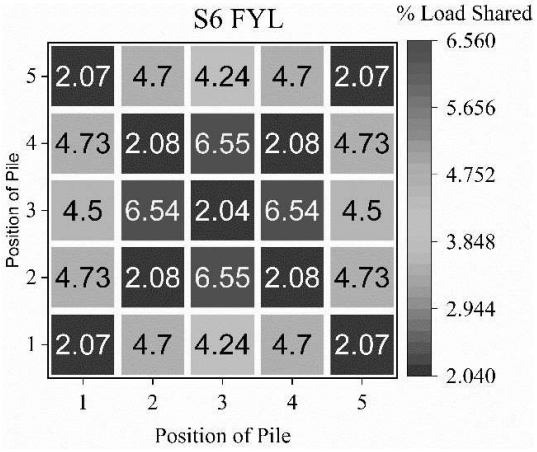

Figure 5-282 : Load Distribution between piles at *FYL* in *S6* configuration

In the *S6* configuration, it is observed that the four longer piles carried a significant portion of the load compared to the total load shared by the piles, accounting for approximately 9%. On the other hand, the shorter piles only contributed around 1-2% of the total load. The piles with an *L/d* ratio of 20 carried approximately 4% of the total load.

During the *FYL*, there was a decrease in the load carried by the longer piles from 9.1% to 6.54%. However, the load carried by the shorter piles showed a slight increase, with approximately 0.5% more load compared to the initial yield load.

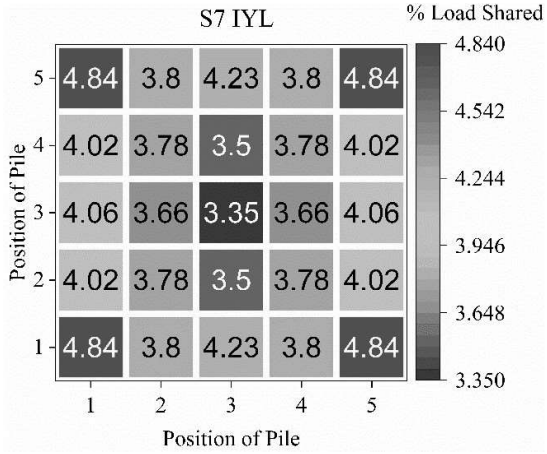

Figure 5-283 : Load Distribution between piles at *IYL* in *S7* configuration

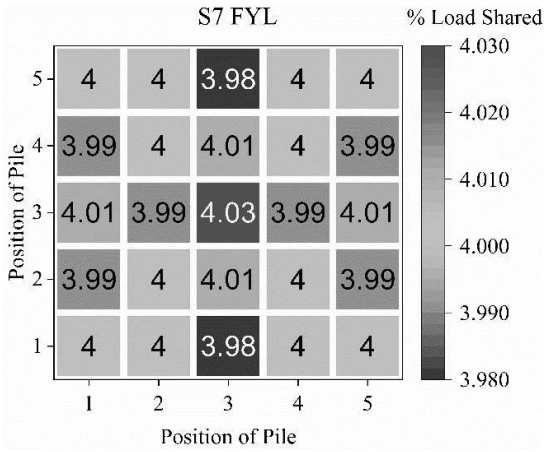

Figure 5-284 : Load Distribution between piles at *FYL* in *S7* configuration

In the *S7* configuration, the total load shared by the piles accounted for approximately 62.37% of the total load at *IYL* whereas at *FYL* it was 46.27%. The central pile contributed 3.35% of the load, while each pile in the outer peripheral carried around 4-5% of the load. It was observed that the load carried by the corner piles at the outer periphery was significantly greater, amounting to approximately 4.84%.

During the *FYL*, the load carried by the central pile increased from 3.35% to 4.03%. However, there was a decrease in the load carried by the corner piles at the outer periphery, which reduced from 4.84% to 4%.

Ningombam et al. (2016) in an elastic analysis of a piled-raft foundation found that at lower pile spacing (*S/d*<7), the corner pile bears the heaviest loads, followed by the edge pile and then the central pile, whereas at wider spacing (*S/d*>8.2), the corner pile bears the least load followed by the edge pile. In *S7* at *IYL* same pattern was observed.

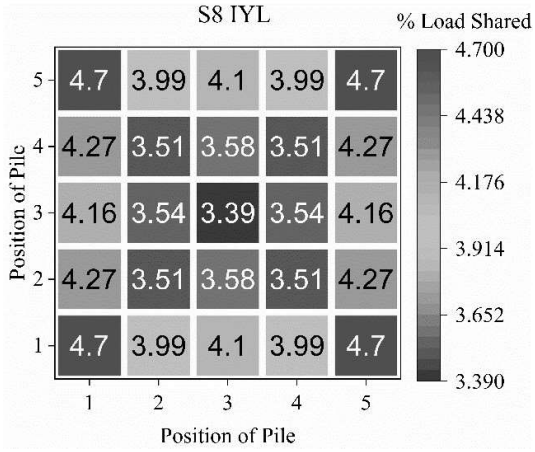

Figure 5-285 : Load Distribution between piles at *IYL* in *S8* configuration

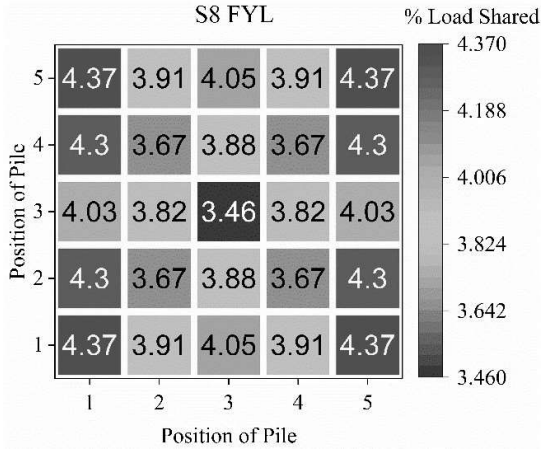

Figure 5-286 : Load Distribution between piles at *FYL* in *S8* configuration

In *S8* configuration also similar distribution of the load among piles was observed from that of *S7* configuration but the load taken by piles to that of raft was greater about 25% when compared *S7* configuration.

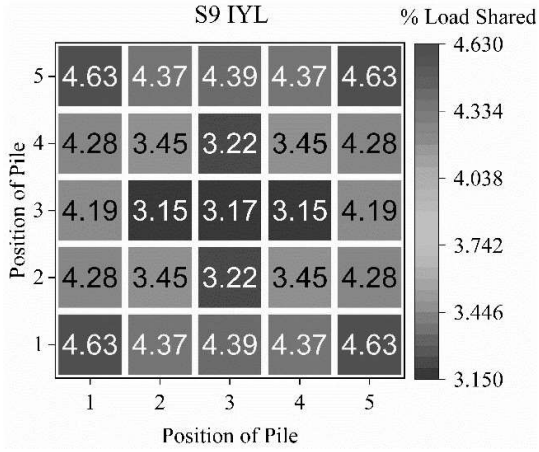

Figure 5-287 : Load Distribution between piles at *IYL* in *S9* configuration

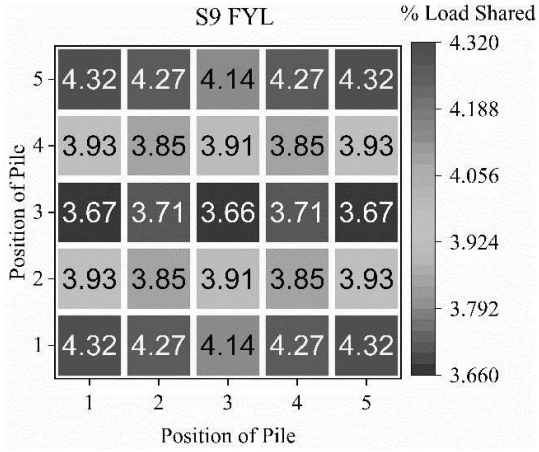

Figure 5-288 : Load Distribution between piles at *FYL* in *S9* configuration

In the *S9* configuration, with all 25 piles as longer pile, it was observed that the piles located at the outer periphery carried a greater load compared to the inner piles. The load shared by the outer piles accounted for approximately 4.62% to 4.28% of the total load, while the inner piles carried around 3.17% of the load. Additionally, a slight difference in load distribution was observed between the corner piles and the side piles within the outer periphery piles, with the corner piles carrying a slightly higher load.

In the *FYL* also a similar trend in load distribution was observed. The load carried by the central pile increased from 3.17% to 3.6%, while the load carried by the outer peripheral pile decreased by approximately 0.3%.

5.3.4.4.2 Load Distribution between Piles in Circular pattern

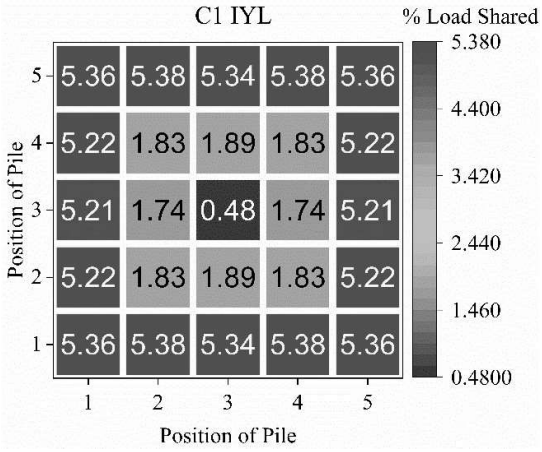

Figure 5-289 : Load Distribution between piles at *IYL* in *C1* configuration

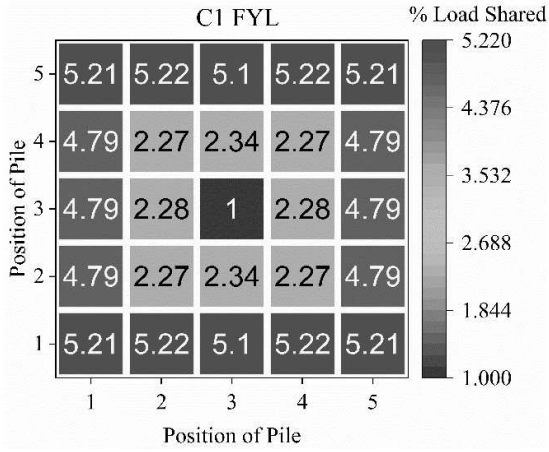

Figure 5-290 : Load Distribution between piles at *FYL* in *C1* configuration

In the *C1* configuration, it was observed that the shorter central pile carried a lesser load compared to that in square configuration. Both at the beginning and end of the loading process, the longer outer pile in the *C1* configuration carried a higher load than the central shorter pile, with a load of up to 5.36%. These outer periphery longer piles carried greater load than what was observed in the square configuration. Similarly, at *FYL*, it was observed that the central pile in the *C1* configuration tends to carry a higher load that at *IYL*, while the distribution of load in outer peripheral longer pile decreased from 5.22% to approximately 4.79%, resembling the observations in the square configuration.

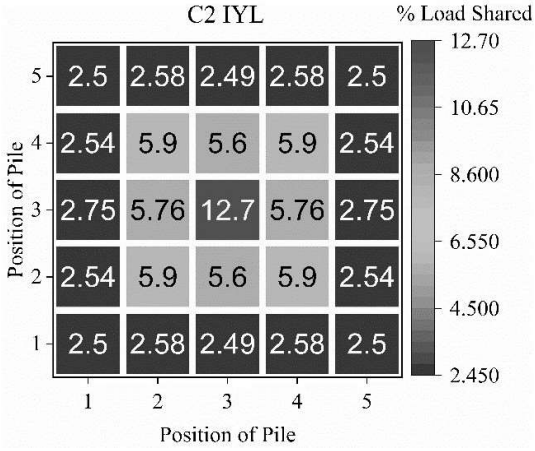

Figure 5-291 : Load Distribution between piles at *IYL* in *C2* configuration

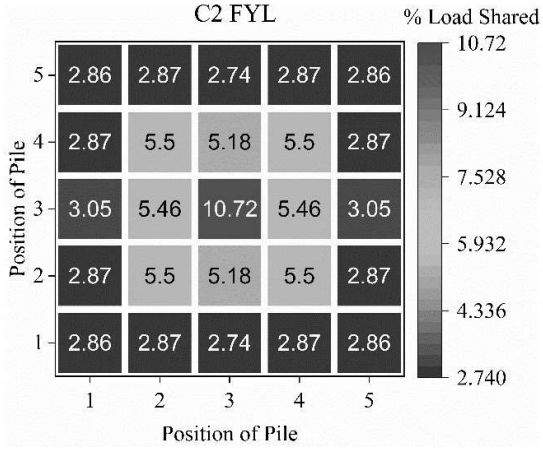

Figure 5-292 : Load Distribution between piles at *FYL* in *C2* configuration

In the *C2* configuration, it was discovered that the central longer pile accounted for approximately 12.7% of the load in both the square and circular configurations at the *IYL*. However, during the *FYL*, these values decreased compared to the *IYL*. Nevertheless, it was observed that the central longer pile in the *C2* configuration carried a load that was approximately 2% greater than what was observed in the square configuration.

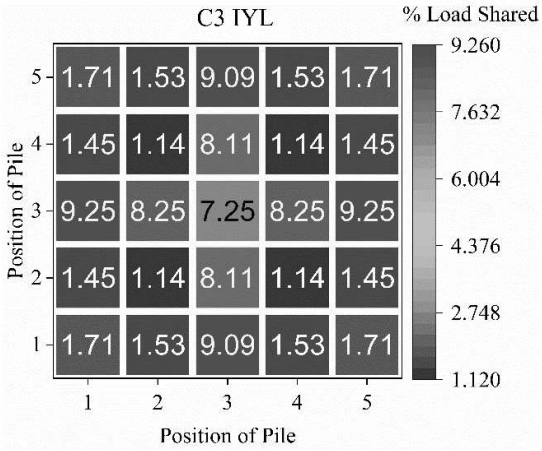

Figure 5-293 : Load Distribution between piles at *IYL* in *C3* configuration

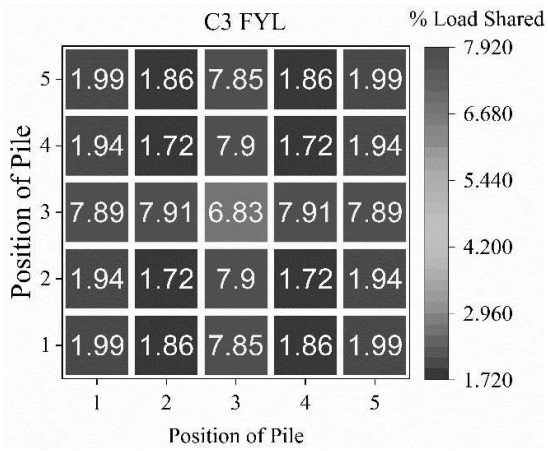

Figure 5-294 : Load Distribution between piles at *FYL* in *C3* configuration

In the *C3* configuration, it was observed that the longer pile carried the majority of the load, ranging from 7.25% to 9.25% during the *IYL*. However, during the *FYL*, the longer pile carried a slightly lower load, ranging from 6.83% to 7.85% compared to *IYL*. On the other

hand, the shorter pile accounted for approximately 1% to 2% of the load during both the *IYL* and *FYL*. Also notable that at *FYL* center pile carried a lower load than *IYL*.

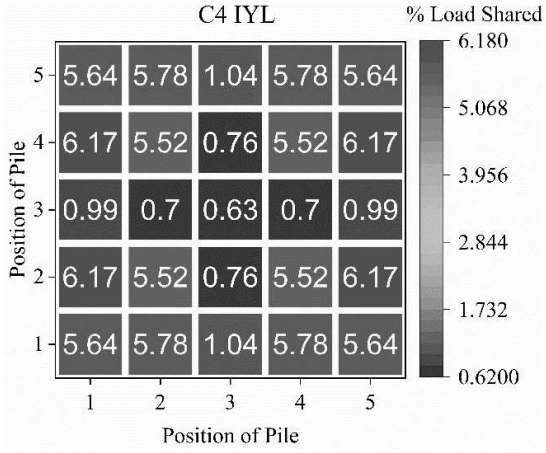

Figure 5-295 : Load Distribution between piles at *IYL* in *C4* configuration

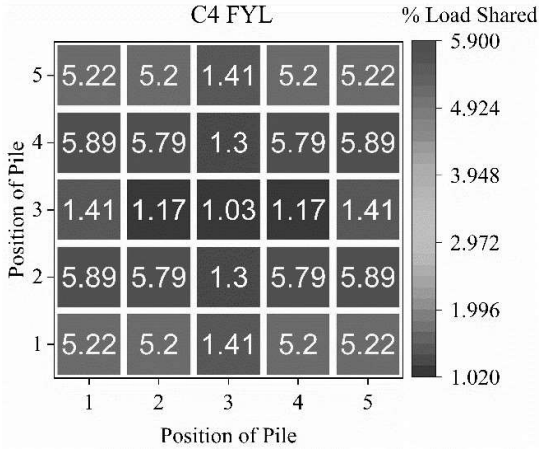

Figure 5-296 : Load Distribution between piles at *FYL* in *C4* configuration

In the *C4* configuration, it was observed that each longer pile carried the majority of the load, accounting for approximately 5.5% to 6% of the total load. In contrast, the shorter pile only carried around 1% of the load, which is lower compared to what was observed in the *C3* configuration.

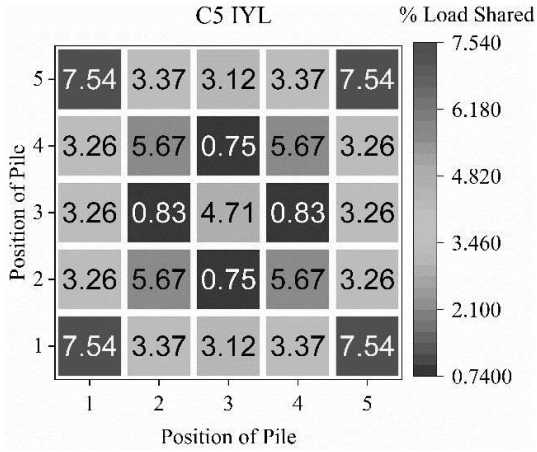

Figure 5-297 : Load Distribution between piles at *IYL* in *C5* configuration

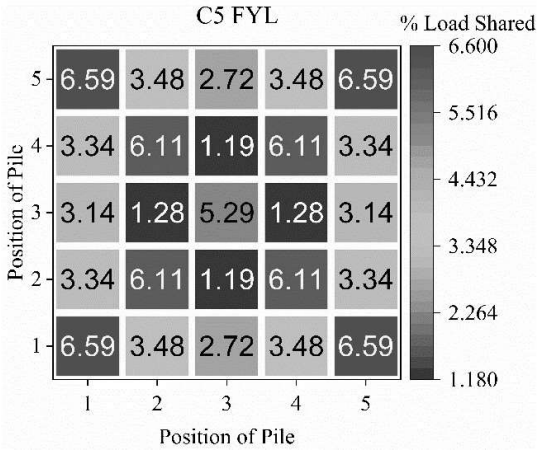

Figure 5-298 : Load Distribution between piles at *IYL* in *C5* configuration

In the *C5* configuration, it was noticed that the longer pile, which was positioned diagonally, carried the majority of the load. Each pile accounted for approximately 4.7% to 7.54% of the total load, while the shorter pile only bore less than 1% of the load. This loading pattern persisted during the *FYL*, although the overall load values decreased. Interestingly, during the *FYL*, the shorter pile carried at the center carried 0.5% more load compared to the *IYL* whereas for other shorter pile it was 1%. Additionally, it was observed that the longer pile located at the extreme corner bore more than 7.5% of the load.

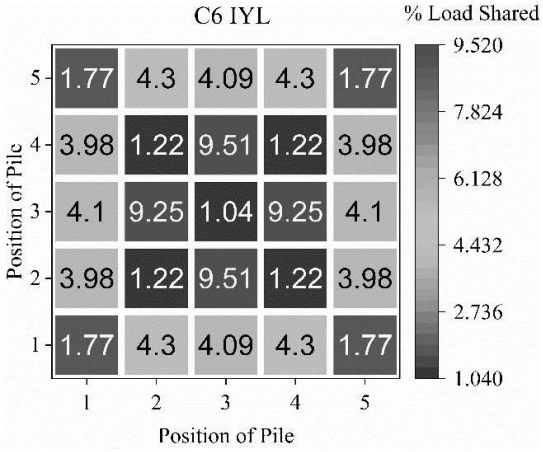

Figure 5-299 : Load Distribution between piles at *IYL* in *C6* configuration

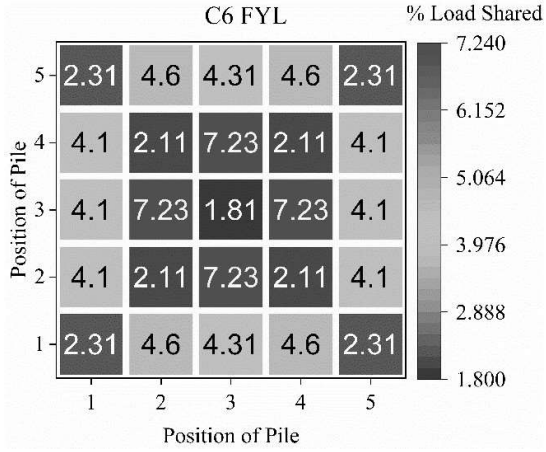

Figure 5-300 : Load Distribution between piles at *FYL* in *C6* configuration

In the *C6* configuration, it was observed that the four longer piles bore the majority of the load, both during the *IYL* and the *FYL*. During the *IYL*, these longer piles carried more than 9% of the load, which was found to be greater than the corresponding *S6* configuration in the square setup. In the *FYL*, although the load shared by the longer piles decreased by 2%, it was still observed that they carried a significant load of approximately 7.2%.

In the *C7* configuration, it was observed that all the piles carried a nearly uniform load, ranging from 3.3% to 4.5%. However, during the initial yield load, the outer piles carried approximately 1% more load compared to the ones located in the middle. At the final yield load, it was found that almost all the piles carried a similar load, around 4%. However, there was an increase in load distribution or sharing at the central pile, from 3.21% to 3.91%, during the final yield load stage.

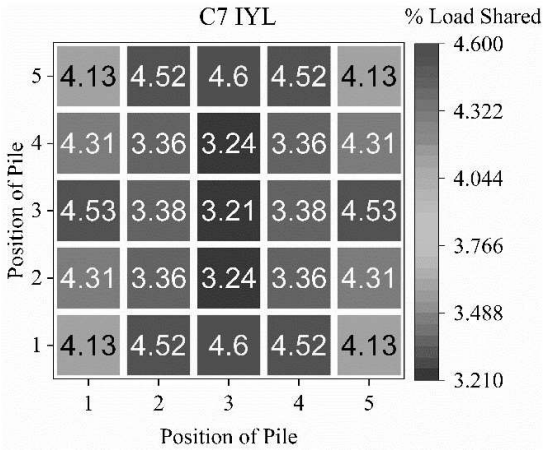

Figure 5-301 : Load Distribution between piles at *IYL* in *C7* configuration

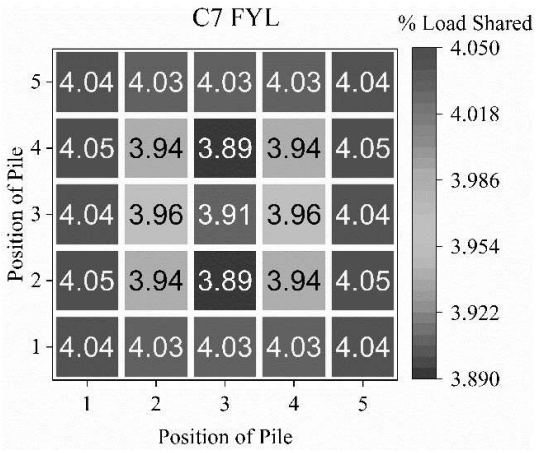

Figure 5-302 : Load Distribution between piles at *FYL* in *C7* configuration

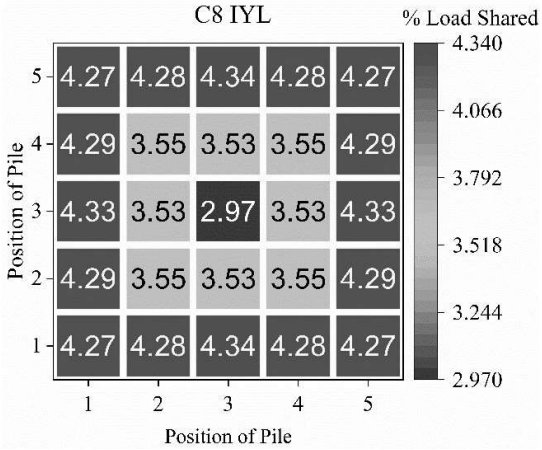

Figure 5-303 : Load Distribution between piles at *IYL* in *C8* configuration

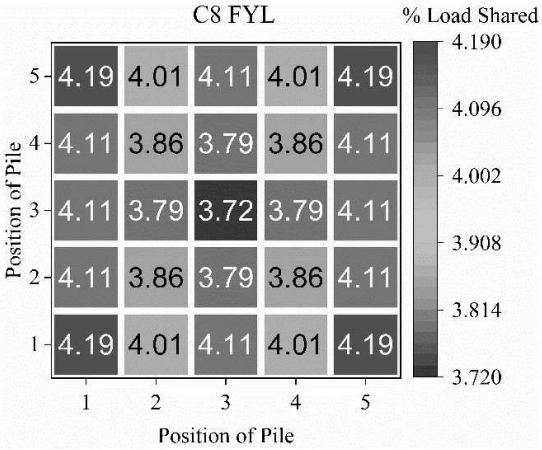

Figure 5-304 : Load Distribution between piles at *FYL* in *C8* configuration

In the *C8* configuration, it was observed that the outer peripheral piles carried a load greater than 4%, while the central pile only bore approximately 3% of the load. As we move from the central pile towards the outer periphery, there was an increase in load sharing among the piles. However, when compared to the *S8* configuration, it was noticed that the central pile in the *C8* configuration carried a load that was nearly 0.5% less. Nevertheless, during the final

yield load, it was observed that the load shared by the central pile in the *C8* configuration was greater than that observed in the *S8* configuration.

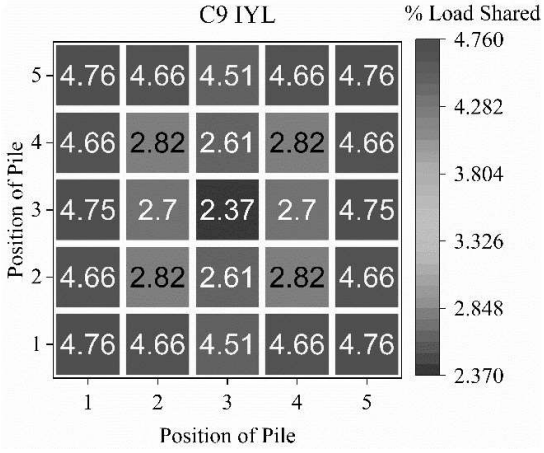

Figure 5-305 : Load Distribution between piles at *IYL* in *C9* configuration

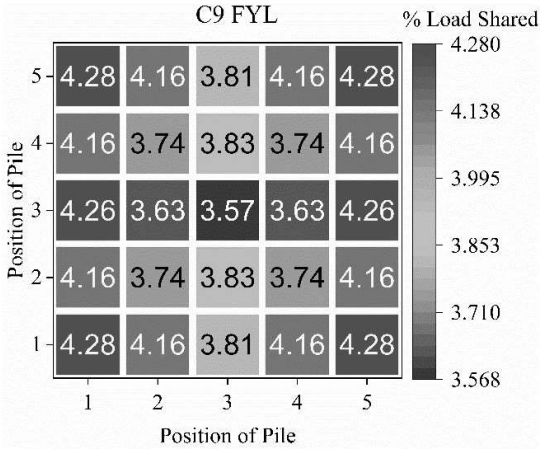

Figure 5-306 : Load Distribution between piles at *FYL* in *C9* configuration

In the *C9* configuration, it was observed that the outer peripheral pile carried more than 4% of the total load shared by the piles, while the central pile carried only 2.37%, which is a lesser load compared to the *S9* configuration. However, during the final yield load, the central pile's load increased to 3.57%, which is closer to what was observed in the *S9* configuration. However, at *IYL*, it was also observed that the outer peripheral pile carried a greater load than the central pile.

5.3.4.5 Stiffness of PRF

The stiffness of each piled-raft configuration was determined by calculating the initial slope of the load-settlement curve. This stiffness value was then compared with the results obtained from the PDR (Poulos- Davis- Randolph) method and the Method by Clancy. The comparison of the stiffness values obtained from these different methods is presented in the Figure 5-307.

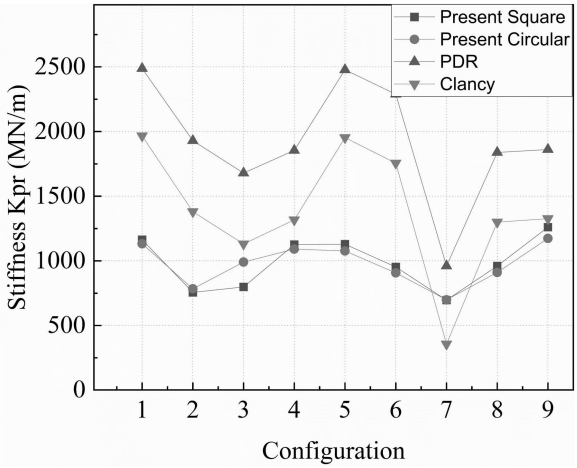

Figure 5-307 : Comparison of Stiffness with PDR and Clancy

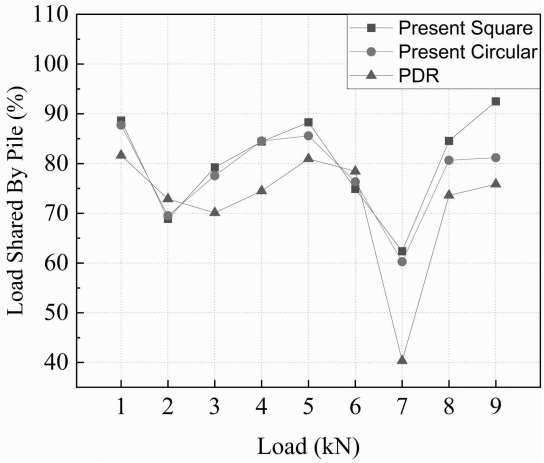

Figure 5-308 : Comparison of Load Shared by pile with PDR

When comparing the stiffness of the pile foundation in various configurations to the results obtained from the PDR method, differences ranging from 27% to 60% were observed. The smallest difference was seen in the *C7* configuration (27%), while the largest difference was found in the *C6* configuration. When examining the load shared by the pile, the difference was approximately 10% in all configurations except in *C7* which was 48%, with the smallest difference observed in the *C6* configuration (around 3%) and the largest difference in the *C4* configuration i.e. 13%.

For the square configuration of the pile foundation, the difference in stiffness ranged from 27% to 60%. The minimum difference was found in the *S7* configuration, while the maximum difference was observed in the *S2* configuration. In the *S9* configuration, the difference was 32%. When comparing the load shared by the pile, the range was between 3% and 53%, with the highest value in the *C7* configuration and the lowest in the *C6* configuration; in all configurations the difference was found less than 16% except in *S7* which was found to be 53%.

When comparing the stiffness of the piled raft foundation with square configuration to the results obtained from the Clancy method, the differences ranged from 5% to 82%. The smallest difference was found in the *S9* configuration (5%), while the largest difference was

observed in the *S6* configuration (84%). In the *S3*, *S4*, and *S8* configurations, the difference ranged from 14% to 40%, while in the *S1*, *S2*, *S5*, and *S6* configurations, it was nearly 50%.

In the case of a circular configuration of piles, the difference in stiffness ranged from 12% to 93%. The smallest difference was observed in the *C9* configuration (12.98%), while the largest difference was found in the *C7* configuration. In the *C3*, *C4*, and *C9* configurations, the difference was less than 20%, while in the *C1*, *C2*, *C5*, *C6*, and *C8* configurations, it ranged from 32% to 70%.

5.4 Discussion:

As suggested by Basuony El-Garhy et al. (2013) the normalized differential settlements decrease with increasing relative raft-soil stiffness (K_{rs}) for different load types and become zero for a rigid raft (K_{rs}> 10). In this study the relative raft-soil stiffness (K_{rs}) for all rafts is greater than 10 so differential settlements are not considered and only average settlement is considered for the analysis. Since the loading was concentric and the shape of raft (except trapezoidal shape) and arrangement of pile group is symmetric, hence differential settlement was not considered and average settlement considered for load settlement characteristics. This is true for rigid raft having relative raft-soil stiffness (K_{rs}) > 10 (Basuony El-Garhy et al. (2013)). In present study minimum value of K_{rs} is about 64.

The load settlement characteristics of trapezoidal and rectangular UPR are found similar at all relative densities of sand i.e. for ultimate bearing carrying capacity of trapezoidal UPR can be calculated using the shape factor formula for rectangular UPR. The ultimate bearing capacity of circular UPR is found to be minimum and maximum for square UPR. These results are consistent with the theory. The ultimate bearing capacity (q_{ult}) and initial tangent stiffness (k_{ri}) all UPR increase with an increase in the relative density of the sand bed, which is evident as an increase in relative density leads to an increase in ϕ values and hence the ultimate bearing capacity. The secant stiffness of square raft and circular raft (k_{sr}) decreases with increase in load because at higher load the average settlements increase due to the plastic deformations. In the linear elastic zone, soil particles do not slide relative to each other under a small stress increment, and the stiffness is at its maximum. The soil stiffness depends on contact interactions, particle packing arrangement, and elastic stiffness of the solids. The

stiffness begins to decrease from the linear elastic value as the applied strains or stresses increase, and the deformation moves into the nonlinear elastic zone and plastic zone.

The secant stiffness of unpiled raft foundation was varying linearly with width of raft, exponentially with relative density of sand and in terms of power with load. This relation was formed as equation (5-10), which is valid up to safe load on unpiled raft. The secant stiffness of square and circular rafts at different loads obtained from the experimental study, and the proposed equation is almost the same. It also matches with the results of Vakili (2015) on square UPR by deviation of less than 18%.

The total load shared by raft in UPR calculated as described in section 5.2.7 was matches well with the total load applied on UPR.

Due to block action, the load carrying capacity of pile group with 3d spacing has maximum load carrying capacity amongst *3d*, *5d* and *7d* spacing. At 40% relative density, the load carrying capacity was decreased as the spacing of pile increased. At 60% and 80% relative density, the load carrying capacity of pile group was decreased as the spacing of pile increased from *3d* to *5d* and after that it was increased at *7d* spacing. This is attributed to block action at *3d* spacing, individual pile pressure bulb overlapping at *5d* spacing and full individual action of piles at *7d* spacing. The initial tangent stiffness of pile group ($(k_{pg})_i$) increased with increase in relative density of sand and *L/d* ratio of piles in pile group. The initial tangent stiffness of pile group ($(k_{pg})_i$) obtained from experimental results and same value calculated using Fleming's relation are coming nearer to same except in spacing criteria at I_d = 80%.

The load settlement characteristics of piled raft foundation in all most all the cases were tri-linear in nature where in the first yielding was denoted as initial yield load (*IYL*) and second yielding was denoted as final yield load (*FYL*), however after that also some residual capacity was observed in many cases. The *IYL* and *FYL* of piled raft foundation (PRF) with different shape of raft were increased with increase in relative density of sand and the minimum and maximum values of *IYL* and *FYL* were found in PRF with circular raft and square raft respectively. The behaviour of piled raft in respect to load carrying capacity was consistent with that of unpiled raft provided same pile group was being used. The load-carrying capacity

of a piled raft with a square raft is often higher because the square shape distributes the load more evenly across the piles. This result in better load transfer efficiency compared to other shapes like circular, rectangular, or trapezoidal rafts, which might concentrate the load unevenly, leading to lower overall capacity.

Increasing the spacing between piles in a piled raft system can lead to an increase in load-carrying capacity (*IYL* and *FYL*) due to several factors. Increasing the spacing between piles allows for a more uniform distribution of loads across the raft. With wider spacing, each pile supports a larger area of the raft, reducing the load per unit area and minimizing stress concentrations. This results in a more efficient load transfer mechanism and higher overall load-carrying capacity. When piles are spaced further apart, there is less interaction between adjacent piles. This can reduce the potential for negative interference effects such as pile group settlement, which can occur when piles are closely spaced. By minimizing pile interaction, the individual capacity of each pile is better utilized, contributing to an increase in the overall load-carrying capacity of the piled raft system. Increasing the spacing between piles allows for the development of soil arching effects between the piles. Soil arching occurs when the soil between piles redistributes loads in response to applied loads, resulting in increased load-bearing capacity of the soil mass between the piles. Wider pile spacing promotes the development of more pronounced soil arching effects, which can contribute to higher load-carrying capacity. Widening the spacing between piles can help reduce settlement of the raft system by distributing loads over a larger area of soil. This can result in lower overall settlement under applied loads, enhancing the structural performance and load-carrying capacity of the piled raft system. Overall, increasing the spacing between piles in a piled raft system from *3d* to *5d* and *5d* to *7d* enhances load distribution, reduces pile interaction, promotes soil arching effects, minimizes settlement, and improves structural efficiency, all of which contribute to an increase in the load-carrying capacity of the system.

While increasing the roughness of the pile surface to improve soil-pile friction angle, the increment in load-carrying capacity of a piled raft system (*IYL* and *FYL*) may not always be significant due to several reasons: Increasing the roughness of the pile surface may initially lead to a significant increase in friction between the soil and the pile. However, beyond a certain point, the increase in friction may not result in a proportional increase in load-carrying

capacity. This is because the additional frictional resistance may not be effectively utilized or transferred to support additional loads. The load-carrying capacity of a piled raft system is influenced by the properties of the surrounding soil. If the soil is already well-compacted, further increasing the roughness of the pile surface may not significantly enhance frictional resistance or improve load transfer between the soil and the pile. In some cases, increasing friction between the soil and pile surface may result in localized stress concentrations or differential settlement, rather than improving overall load distribution within the raft system. This can limit the effectiveness of increasing pile roughness in enhancing load-carrying capacity.

The H-shaped piles typically offer better structural efficiency compared to hollow square-shaped piles due to their geometry. The H-shaped piles have a higher moment of inertia compared to hollow square piles with the same cross-sectional area, which enhances their ability to resist bending and shear forces. This can result in higher load-carrying capacity. Square piles (HSQ) may have higher load-carrying capacities in pile groups on sand due to increased surface area and resistance against lateral movement, circular piles (HC) are often preferred in piled raft systems on sand due to their symmetric load distribution, reduced risk of corner effects, and resistance against rotational forces.

In the present investigation, the load settlement curves were found towards extreme right that of PRF, left of them were UPR and towards extreme left those of pile group (PG). i.e. PRF carries highest load and pile group carries least load.

Stiffness of sandy soil increases with the increase in confining pressure. As confining pressure is at the region under center of a foundation is highest, the stiffness will be also greatest at this region and hence the contact pressure will be higher in this region. Thus in the regions near periphery of foundation the stiffness will be smaller and contact pressure will also be smaller hence in the present investigation the contact pressure of raft measured by EPC located nearer to the center was higher than the EPC at side or corner of UPR. The contact pressure of raft in PRF measured by EPC in one quadrant of 3×3 pile group or between two piles within pile group was higher than other locations in PRF with all shapes of raft at all the relative densities of sand which shows that in PRF due to confinement of sand between adjacent piles the contact pressure was found to be maximum. In all most all cases

the % load shared by the pile group (% *LSPG*) was higher compared to % load shared by raft (% *LSR*) up to the initial range of relative settlement (s/B_r) and gradually it decreased. The reason behind this may be that the pile reaches at ultimate capacity at lower settlement compared to raft.

Piled raft coefficient (α_p) was decreased rapidally with increase in s/B_r upto s/B_r = 0.01 to 0.07 and after that it remained more or less constant. The results are in good agreement with those obtained by Lee et al. (2015) based on numerical modeling of piled raft foundations. As the load-carrying capacity of smaller-diameter piles is mobilized earlier than that of the larger raft, the values of α_p are higher initially and then decrease non-linearly with increasing settlement.

The ratio of load shared by raft (*LSR*) to the load of unpiled raft at the same settlement corresponding to the *IYL* ($(P_r)_{s_i}$) was found less than 1 and the ratio of load shared by pile group (*LSPG*) to the load of only pile group at the same settlement corresponding to the *IYL* $\left(P_{pg}\right)_{s_i}$ was found greater than 1 in most of the cases. i.e. it represents increasing pile skin friction caused by increase in confining stresses within the soil by raft pressure due to contact of raft (pile cap) with sand (Long 1993; Frankeet al. 2000; Katzenbach et al. 2000). The effect of increasing confining stress may differ depending on stress level and location of piles within the raft. The *LSPG* at *FYL* was found to be more than the *LSPG* at *IYL* of PRF with long piles and/or at medium dense to dense sand formation, whereas the *LSPG* at *FYL* was found to be less than the *LSPG* at *IYL* of PRF with short piles and/or at 40% relative density of sand in majority of the cases. This may be attributed to the mechanism of shear failure, for shorter piles the failure starts underneath the raft directly and contribution of pile will be questionable (Figure 5-310) and for longer piles the failure mechanisms may be like as shown in Figure 5-309. Additionally, it was noted that, for the same raft area and at the same spacing ($S = 5d$), the PRF with nine long piles (L/d = 30) outperformed the PRF with twenty-five small piles (L/d = 10). Different possible failure mechanisms for piled rafts are shown in Figure 5-309 to Figure 5-311.

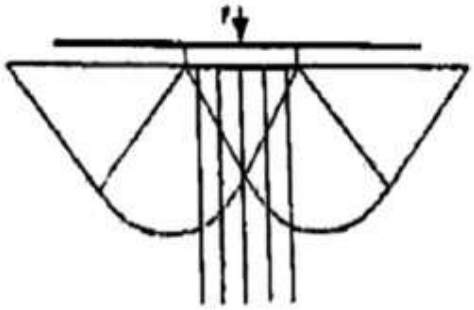

Figure 5-309 Few long piles with relatively large spacing

(Piles acting as dowels and vertical supports)

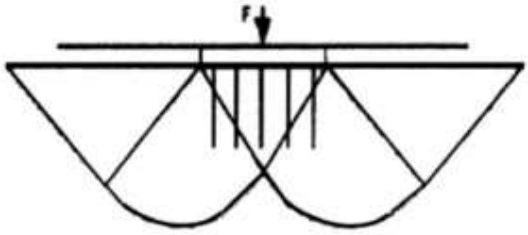

Figure 5-310 Few short piles with relatively large spacing

(Contribution of the piles on the total bearing capacity is questionable)

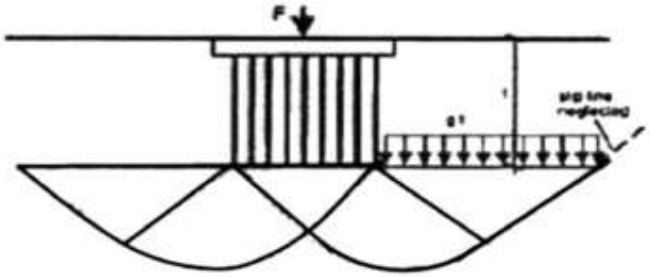

Figure 5-311 Large number of piles with relatively small spacing

(Block failure with free flow at the pile base area)

The majority values of primary stiffness $(k_{pr})_p$ of the present experimental results and predicted from **omeman (2012)** method was varied by less than 20% in case of PRF with 3×3 pile group while the variation is quite large in case of PRF with 5×5 pile group. The equations (5-14) to (5-23) proposed for predicting *IYL*, *FYL*, $(k_{pr})_p$ and $(k_{pr})_s$ respectively and in most of the cases the predicted values were vary by less than 25% of the experimental values.

The range of efficiency of piled raft (β) at *IYL* was found to be 0.9 to 2.08 in PRF with different shape of raft, different *L/d* ratio of piles and with different spacing between piles. The efficiency of piled raft at *IYL* was found to be less than 1in most of the PRF with *3d* spacings, small piles and/or at 60% to 80% relative density of sand. The range of efficiency of piled raft (β) at *FYL* was found to be 0.78 to 1.54 in PRF with different shape of raft, different *L/d* ratio of piles and with different spacing between piles. In a dense sand condition, the mobilization of friction on a pile surface may not be significant but the outer piles starts bending due to the lateral movement of soil with initiation of general shear failure condition (Figure 5-312 and Figure 5-313). This bending of the piles reduces axial capacity of pile. The ultimate result would be the efficiency of piled raft at *FYL* is somewhat less than efficiency of piled raft at *IYL* in most of the cases. The larger efficiency of piled raft is attributed to unfavorable distortion mechanism that would develop in soil, causes higher strength of soil to be mobilized.

Figure 5-312 : Pile bending in PRF with short piles (*L/d=10 at* I_d*=60%*) after test

Figure 5-313 : Pile bending in PRF with medium piles (*L/d=20 at* I_d*=60%*) after test

The settlement reduction ratio of PRF with circular raft, square and trapezoidal raft was found minimum at 80% relative density of sand while in PRF with rectangular raft it was minimum at 60% and 80% relative density for initial loading. The range of Load improvement ratio *(LIR)* remains almost constant from beginning to just prior to failure of circular and trapezoidal UPR. At all relative density of sand, the settlement reduction ratio and load improvement ratio was found minimum with piles having *L/d* =10 and maximum with *L/d* = 30. It may be due to increase in skin friction resistance of pile with increase in length of pile. In the study of the spacing, at 40% and 80% relative density of sand the settlement reduction ratio was found maximum with *7d* spacing and minimum with *3d* spacing. At 80% relative density of sand the settlement reduction ratio was found maximum with *5d* spacing at initial loading. At all relative densities of sand the load improvement ratio *(LIR)* of PRF with different spacings was found maximum with *7d* spacing and minimum with *3d* spacing. The maximum settlement reduction ratio was found in PRF with *CF-1* configuration, this may be due to the longer piles in peripherial potion of PRF which resist the movement of sand particles from center to outer side of raft and provides highest confinment to sand bed. In *CF-2* and *CF-6*, the settlement reduction ratio increased with initial loading and decreased rapidally with increase in load, this may be due to movement of sand particles from center of raft to outward side of raft due to less confinement because in both configurations smaller piles were in the pheripherial portion and longer piles in central portion of PRF. i.e., the effect of PRF is predominant within initial loading (upto 5 kN load) and after 5 kN load the PRF with *CF-2* and *CF-6* configuration will behave similar to UPR. The load improvement ratio *(LIR)* of PRF was found maximum with *CF-9* and *CF-1* and it is

found minimum with *CF-2*. In soil-pile friction angle study, the load improvement ratio of PRF with different soil pile friction angles considered in this study are found to be more or less same at a particular relative density of sand. In the study of shape of piles the *LIR* was found maximum with H pile and minimum with HSQ pile at all relative densities of sand.

5.5 Suggested Design Methodology for Piled Raft Foundation

Three primary steps are proposed as part of a logical design process for piled rafts: **(1)** An initial phase to determine whether utilizing a piled raft and the quantity of piles needed to meet design specifications.

A simplified design approach for a piled raft footing in sand involves the following steps: **Step 1:** Decide permissible settlement for the foundation.

Step 2: Adopt a suitable size of raft for the proposed multistory building/ structure. Calculate the loading on the raft and determine settlement of the raft and bearing capacity of the raft by the codal provision.

Step 3: If the obtained settlement is less than the permissible settlement of raft and bearing capacity criteria is satisfied then carry out structural design of raft and design is complete and no piles are required.

Step 4: If settlement is beyond permissible limit and/or bearing capacity criteria not satisfied then piles are needed.

Estimate the load carried by the piles (P_{piles})

$$P_{piles} = P_{total} - P_{raft} \quad (5\text{-}30)$$

where, P_{total} represents the total applied load on foundation. P_{raft} = 0.4 to 0.7 times the ultimate load capacity of the raft.

Step 5: Calculate the number of piles *n* using the formula

$$n = P_{piles} / P_s \tag{5-31}$$

where, P_s represents the safe capacity of a single pile.

Step 6: locate the piles below column in PRF and at suitable location by adjusting suitable spacing between piles.

Step 7: predict the load settlement curve of unpiled raft, and pile group by using known methods.

Step 8: the initial yield load (*IYL*) of PRF can be predicted by trial and error method as discussed below.

(i) Take any trial settlement at which the relative settlement (s/B_r) should be less than 0.01 and calculate C_1 , C_2 from formula. Also take $(P_r)_{s_i}$ and $\left(P_{pg}\right)_{s_i}$ corresponding to the considered settlement from the load settlement curve of unpiled raft, and pile group.

(ii) Calculate *IYL* at considered settlement using formula of *IYL*.

(iii) Calculate the primary stiffness of PRF $\left(k_{pr}\right)_p$ as a ratio of *IYL* to the corresponding settlement. If this value matches with the primary stiffness of PRF $\left(k_{pr}\right)_p$calculated from proposed equation (5-22) then it is ok otherwise repeat the same procedure till the value matches.

Step 9: The finial yield load (*FYL*) of PRF can be predicted by trial and error method as discussed below.

(i) Take any trial settlement at which the relative settlement (s/B_r) should be in the range of 0.01 to 0.07 and calculate C_3, C_4 from formula. Also calculate ultimate load on UPR and pile group (PG) from predicted load –settlement curves of UPR and PG.

(ii) Calculate *FYL* at considered settlement using formula of *FYL*.

(iii) Calculate the secondary stiffness of PRF $(k_{pr})_s$ as a ratio of difference in *FYL* and *IYL* to the difference in corresponding settlement. If this value matches with the secondary stiffness of PRF $(k_{pr})_s$ calculated from proposed equation (5-23) then it is ok otherwise repeat the same procedure till the value matches.

Step 10: Calculate safe load on PRF by dividing the *FYL* with a factor of safety. Estimate the settlement of PRF at safe load either by using primary stiffness of PRF $(k_{pr})_p$ if safe load is less than *IYL*, if safe load is more than *IYL* then settlement s = *IYL*/ $(k_{pr})_p$ + (Safe load – *IYL*)/ $(k_{pr})_s$.

Step 11: If the above settlement is less than permissible limit then preliminary design of piled raft is over. If the above settlement is more than the permissible settlement then increase the number of piles or increase the length of piles and repeate the same procedure till this criteria satisfied.

(2) A second phase to determine the locations and overall qualities of the piles that are needed when column loadings are present. A pile beneath the column may be required in at least four situations: If the maximum moment in the raft below the column exceeds the allowable value for the raft, the maximum shear in the raft below the column exceeds the allowable value for the raft, the maximum contact pressure below the raft exceeds the allowable design value for the soil, and the maximum local settlement below the column exceeds the allowable value. The maximum values of moment in the raft, shear in the raft, contact pressure, local settlement below the column can be calculated as discussed in chapter 2 using equation (2-31) to (2-43).

(3) The final detailed design step, which determines the ideal quantity, positioning, and configuration of the piles and computes the precise distributions of settlement, shear, and bending moment in the raft, as well as the loads and moments of the piles.

5.5.1 Illustrative Example:

Carry out a preliminary design for a piled raft foundation based on the following conditions:

i) The design load of the superstructure on the foundation is 70 MN.

ii) The permissible settlement of the foundation is 75 mm.

iii) The dimensions of the raft are 13.608 m × 13.608 m × 1.5 m.

Assume the diameter of the pile is 0.6 m and the length of the pile is 12 m. Use the provided load-settlement curve for both the single pile and the unpiled raft foundation. The properties of the foundation soil are as follows:

Table 5-74 Properties of foundation soil

Relative Density, I_d (%)	60
Soil Density, γ (kN/m^3)	16.8
Modulus of elasticity of sand, E_s (kPa)	33889
Friction Angle (ϕ)	35°
Poisson Ratio (μ)	0.298
Cohesion, c (kN/m^2)	0

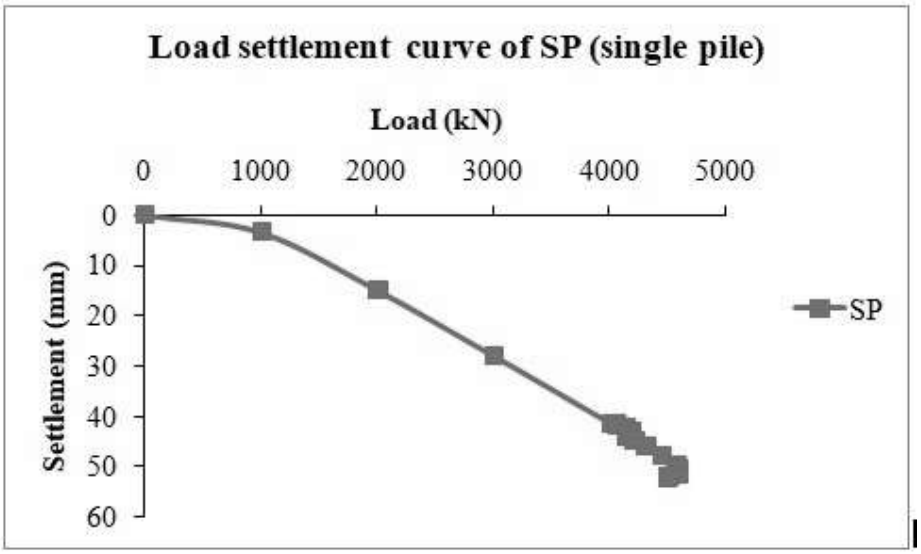

Figure 5-314 : Load settlement curve of single pile

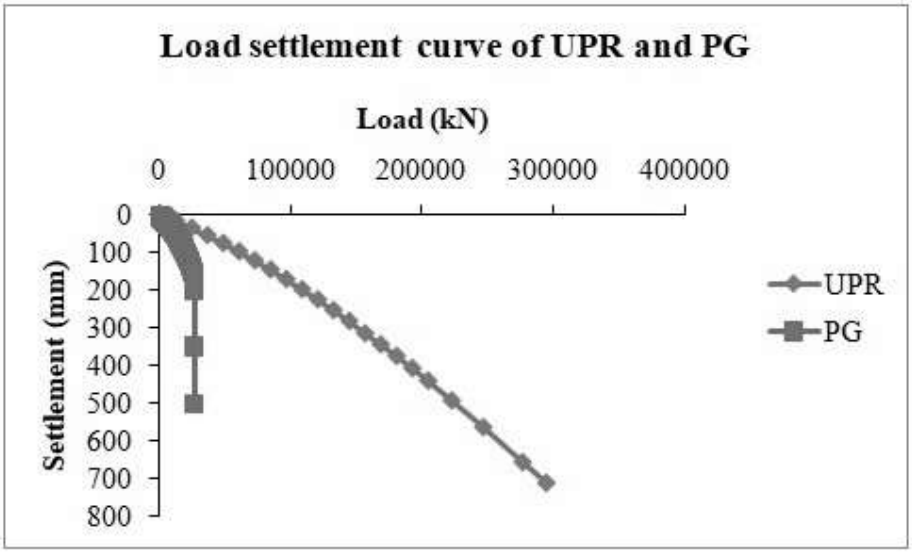

Figure 5-315 : Load settlement curve of unpiled raft and pile group

Solution:

Step 1: Decide permissible settlement for the foundation.

Permissible settlement for the foundation $s_p = 75\ mm$

Step 2: Adopt a suitable size of raft for the proposed multistory building/ structure. Calculate the loading on the raft and determine settlement of the raft and bearing capacity of the raft by the codal provision.

Adopt size of raft = 13.608 m × 13.608 m × 1.5 m.

Design load from the super structure P_{total} = 70 MN

Settlement of raft at design load, $s_r = qB_r\,(1-\mu^2) * \frac{I}{E}$

$$s_r = 123.92\ mm$$

Ultimate load capacity of the raft from load settlement curve of UPR, Q_{ur} = 78952.128 kN

Step 3: If the obtained settlement is less than the permissible settlement of raft and bearing capacity criteria is satisfied then carry out structural design of raft and design is complete and no piles are required.

$s_r > s_p$, only raft foundation is not sufficient so piles are required as settlement reducer

Step 4: If settlement is beyond permissible limit and/or bearing capacity criteria not satisfied then piles are needed.

Estimate the load carried by the piles (P_{piles})

$$P_{piles} = P_{total} - P_{raft} \qquad (5\text{-}32)$$

where, P_{total} represents the total applied load on foundation. P_{raft} = 0.4 to 0.7 times the ultimate load capacity of the raft.

P_{total} = 70000 kN

P_{raft} = 0.4 × Q_{ur} = 31580.85 kN

P_{piles} = 38419.149 kN

Step 5: Calculate the number of piles *n* using the formula

$$n = P_{piles} / P_s \quad (5\text{-}33)$$

where, P_s represents the safe capacity of a single pile.

As per IS: 2911 (part 1/Sec 2) : 2010, the ultimate load carrying capacity of single pile = 4424.11 kN, which is nearer to the value observed from load settlement curve of single pile.

P_s = 4424.11/2.5 =1769.64 kN

n = 21.7

Step 6: locate the piles below column in PRF and at suitable location by adjusting suitable spacing between piles.

Spacing between piles = 5d = 5 × 0.6 = 3 m

Step 7: predict the load settlement curve of unpiled raft, and pile group by using known methods.

Refer Figure 5-315 for this step

Step 8: the initial yield load (IYL) of PRF can be predicted by trial and error method as discussed below.

(i) Take any trial settlement at which the relative settlement (s/B_r) should be less than 0.01 and calculate C_1 , C_2 from formula. Also take $(P_r)_{s_i}$ and $\left(P_{pg}\right)_{s_i}$ corresponding to the considered settlement from the load settlement curve of unpiled raft, and pile group.

Take $\frac{s_i}{B_r}$ = 0.0056, s_i = 76.21 mm

Take n = 25, I_d = 60, $S/_d$ = 5, $B_r/_{L_r}$ = 1, $L/_d$ = 20

$$C_1 = 0.00033 * n * I_d * S/_d * B_r/_{L_r} * L/_d * s_i/_{B_r}$$

$$C_2 = 8.375 * e^{\left(-0.000175 * n * I_d * S/_d * B_r/_{L_r} * L/_d * s_i/_{B_r}\right)}$$

C_1= 0.277

C_2 = 7.229

$(P_r)_{s_i}$ = 47812.56 kN

$\left(P_{pg}\right)_{s_i}$ = 14800 kN

(ii) Calculate *IYL* at considered settlement using formula of *IYL*.

$$IYL = C_1 * (P_r)_{s_i} + C_2 * \left(P_{pg}\right)_{s_i}$$

IYL = 120258.6 kN

(iii) Calculate the primary stiffness of PRF $\left(k_{pr}\right)_p$ as a ratio of IYL to the corresponding settlement. If this value matches with the primary stiffness of PRF $\left(k_{pr}\right)_p$calculated from proposed equation (5-22) then it is ok otherwise repeat the same procedure till the value matches.

$\left(k_{pr}\right)_p$ = *IYL*/ s_i = 1577890 kN/m

Take k_{ri} = 692403 kN/m and $(k_{pg})_i$ = 1472429 kN/m calculated using Fleming's equation and k_{p1} = 294485.8 kN/m

$(k_{pr})_p$ calculated from proposed equation (5-22) = 1463438 kN/m

Here the variation in $(k_{pr})_p$ values matches with 7% variation so adopt *IYL* = 120258.6 kN

Step 9: The finial yield load (*FYL*) of PRF can be predicted by trial and error method as discussed below.

(i) Take any trial settlement at which the relative settlement (s/B_r) should be in the range of 0.01 to 0.07 and calculate C_3, C_4 from formula. Also calculate ultimate load on UPR and pile group (PG) from predicted load –settlement curves of UPR and PG.

Take $s/B_r = 0.014$, *corresponding settlement* = 190.512 mm

$$C_3 = 0.119 * \frac{S}{d} * \frac{B_r}{L_r} * e^{\left(0.0083 * I_d * {}^{1}/_{n} * {}^{L}/_{d} * {}^{S}/_{B_r}\right)}$$

$$C_4 = 0.871 * \frac{S}{d} * \frac{B_r}{L_r} * e^{\left(-0.016 * I_d * {}^{1}/_{n} * {}^{L}/_{d} * {}^{S}/_{B_r}\right)}$$

C_3 = 0.598328

C_4 = 4.308426

Q_{ur} = 78952.128 kN

$Q_{u,pg}$ = 23400 kN

(ii) Calculate FYL at considered settlement using formula of FYL

$$FYL = C_3 * Qur + C_4 * Qu, pg$$

FYL = 148056.4 kN

(iii) Calculate the secondary stiffness of PRF $(k_{pr})_s$ as a ratio of difference in *FYL* and *IYL* to the difference in corresponding settlement. If this value matches with the secondary stiffness of PRF $(k_{pr})_s$ calculated from proposed equation (5-23) then it is ok otherwise repeat the same procedure till the value matches.

$(k_{pr})_s$ = a ratio of difference in *FYL* and *IYL* to the difference in corresponding settlement = 15199.16 kN/m

$(k_{pr})_s$ calculated from proposed equation (5-23) = 13384.85 kN/m

here the both values of $(k_{pr})_s$ are matches well with 11 % variation

Step 10: Calculate safe load on PRF by dividing the *FYL* with a factor of safety. Estimate the settlement of PRF at safe load either by using primary stiffness of PRF $(k_{pr})_p$ if safe load is less than *IYL*, if safe load is more than *IYL* then settlement *s* = *IYL*/ $(k_{pr})_p$ + (Safe load – *IYL*)/ $(k_{pr})_s$.

Take FOS = 2

Safe load = *FYL*/FOS = 74028.21 kN < *IYL* = 120258.6 kN

the settlement of PRF at safe load = Safe load/ $(k_{pr})_p$ = 50.27 mm < 75 mm

Step 11: If the above settlement is less than permissible limit then preliminary design of piled raft is over. If the above settlement is more than the permissible settlement then increase the number of piles or increase the length of piles and repeat the same procedure till this criteria satisfied.

50.27 mm < 75 mm then preliminary design of piled raft is over.

5.6 Concluding Remarks

Uptill now many researches have been done for predicting load carrying capacity of piled raft. The procedure of which are very complex and not fully justifiable. Akinmusuru (1980), Liu et al. (1985) proposed empirical equations (2-1) and (2-2) for the determination of piled raft ultimate carrying capacity based on ultimate capacity of unpiled raft and pile group. In these equations they considered full ultimate capacity of unpiled raft which is questionable because in our study the carrying capacity of raft in piled raft is found to be less than the carrying capacity of unpiled raft. Phung Duc Long (2010) developed equation (2-4) for the carrying capacity of piled raft foundation by considering load efficiency factors in ultimate capacity of unpiled raft and pile group but they suggested the values of load efficiency factors which may be not applicable to in all cases of piled raft foundations. They also suggested a practical procedure of design of piled footing in sand in which the load shared by piles in piled raft can be calculated as total load on piled raft minus the load on unpiled raft without causing excessive settlement. i.e. full contribution of raft had been taken which is not true. The load settlement response of any foundation is very important and as per Polous (2001), the load settlement curve of piled raft foundation is tri-linear and till date many researches on piled raft foundation has been done but no such studies are found in literature. For present study, 15 experiments on model unpiled raft foundation (UPR), 18 experiments on model single pile (SP), 27 experiments on model pile groups (PG), and 60 experiments on model piled raft foundation (PRF) have been performed. Experimental results have been validated by numerical analysis also and additionally prototype PRF with 18 configurations has been analyzed numerically by using PLAXIS 3D software. In the present investigation most of the results of load settlement characteristics were fall in the category of tri-linear characteristic as suggested by Polous (2001). The present study focused on the rigirous analysis of this tri-linear load settlement characteristics of piled raft foundation with emphasis on initial yield load (*IYL*), final yield load (*FYL*), primary stiffness of piled raft $\left(k_{pr}\right)_p$, and secondary stiffness of piled raft $\left(k_{pr}\right)_s$. The analytical equations are developed for predicting these above parameters using load settlement characteristics of pile group and only raft (UPR) which are helpful for preliminary design of piled raft foundation which assist for further detailed design procedure implimenting computer as suggested by Polous (2001). From the

results, it was found that the load carrying capacity of raft decreases in piled raft on sand compared to unpiled raft, the load carrying capacity of pile group increases in piled raft on sand compared to only pile group. Square shape of raft gives best performance in PRF compared to other shapes of raft with equal contact area, however the performance of PRF with rectangular and trapezoidal raft is nearer to square raft. As per this study, Circular raft in PRF is least preferable. The performance of PRF improves with increase in length of piles as compared to increase in number of short piles. It also increases by locating longer piles in the outer side of square pile group closer to the periphery of the raft compared to shorter piles. There is no use to provide small piles (L/d = 10) in PRF on sand because there is no improvement in load carrying capacity of unpiled raft by providing small piles in PRF. Steel H pile is most suitable for piled raft compared to open ended hollow circular and hollow square pile with same cross sectional area. The load settlement curve of piled raft foundation can be predicted by using load settlement characteristics of pile group and only raft (UPR).